To the Graduate Council:

I am submitting herewith a dissertation written by Robert Eric Johnson entitled "Petrogenesis of Carbonate Lithofacies Along an Evolving Paleozoic Shelf, Lower Chickamauga Group and Equivalents, Middle Ordovician, Northeastern Tennessee." I have examined the final copy of this dissertation for form and content and recommend that it be accepted in partial fulfillment of the requirements for the degree of Doctor of Philosophy, with a major in Geology.

Kenneth R. Walker

Kenneth R. Walker, Major Professor

We have read this dissertation
and recommend its acceptance:

Karla C. Mira

Richard W. Arnseth

E Kreisa

Accepted for the Council:

Lou Minkel

Vice Provost
and Dean of The Graduate School

PETROGENESIS OF CARBONATE LITHOFACIES ALONG AN EVOLVING PALEOZOIC SHELF, LOWER CHICKAMAUGA GROUP AND EQUIVALENTS, MIDDLE ORDOVICIAN, NORTHEASTERN TENNESSEE

A Dissertation

Presented for the

Doctor of Philosophy

Degree

The University of Tennessee, Knoxville

Robert Eric Johnson

March 1988

This dissertation is dedicated to my family
whose constant support made its completion possible.

ACKNOWLEDGEMENTS

I wish to express my gratitude to my doctoral advisor, Dr. Kenneth R. Walker, for inviting me to join the PhD. program in the Department of Geological Sciences, suggesting the thesis topic, and offering helpful comments which lead to its completion. I would also like to thank Dr. Richard W. Arnseth, whose comments at various stages of this research concerning analytical methods and data interpretation helped considerably. Dr's. Kula C. Misra and Earl Wehry also provided input on analytical procedures used in this study, and suggestions on the final draft of this work. The following individuals provided technical assistance and/or access to equipment during the course of this investigation: Dr. Otto Kopp, Department of Geological Sciences, UT (XRD); Richard Williams, Department of Biological Sciences, UT (SEM); Dr. C. Steven Hasse, Environmental Sciences Divison, ORNL (cathodoluminescence). Newman Smith, Greg Jernigan and Linclon Foreman served as valuable field assistants. Dr. Frank McKinney (Appalachian State University) generously shared his knowledge of nicholsonellid bryozoans. Discussions with Dr. Philip Sandberg (University of Illinois) on the petrography and geochemistry of micrites contributed to ideas presented in Chapter 2.

During my matriculation at The University of Tennessee,

numerous students have contributed, either academically or nonacademically, to the completion of this dissertation. Since brevity is required, I wish to offer special thanks to the following individuals: Charles Lutz, Jim Weber, James Wedekind, Anita Cristil, Lincoln Foreman, Tom Helms, Steve Knapp, and John Simonson.

Field, petrographic and geochemical work was supported by the Appalachian Basin Industrial Associates, The University of Tennessee Department of Geological Sciences Discretionary Fund, and a Texaco Scholarship.

ABSTRACT

Petrography, cathodoluminescence and elemental geochemistry offer insights concerning the petrogenesis of Middle Ordovician shelf limestones (Chickamauga Group and equivalents).

Shelf micrites and slope calcisiltites have textures similar to Holocene calcite-dominated matrix precursors. Fine grained carbonates are interpreted to be the breakdown products of Mg-calcite skeletons. Trace element compositions of micrites form a trend connecting Mg-calcite lime mud and micrites lithified during meteoric diagenesis. Slope calcisiltites have elemental concentrations which indicate Sr retention during lithification. A calcite-dominated micrite precursor offers an additional mechanism for matrix dolomitization in shelf sequences.

Skeletal components exhibit four distinct styles of preservation: 1) skeletal molds occluded by calcite spar; 2) skeletons preserved as replacement spar or replacement-cement mosaics; 3) skeletons with excellent microstructure retention as ferroan or nonferroan calcite; 4) microcrystalline components preserved as nonferroan calcite. Comparison with characteristics of other carbonates indicates Middle Ordovician particles in groups (1) and (2) were originally aragonite, and those in groups (3) and (4) were calcite/Mg-calcite. Marine cements occur

as fibrous calcite rims, microdolomite-bearing syntaxial overgrowths and microcrystalline calcite, and are interpreted as originally Mg-calcite. Constituent particle analysis indicates the original shelf sediments consisted primarily of magnesian calcite.

Samples were grouped into six geochemical facies based on lithologic and elemental data. Peritidal limestones and outer shelf limestones are depleted in whole-rock Sr, Fe and Mn relative to argillaceous limestones and deep-water limestones; drowned limestones comprise a separate group substantially enriched in Fe and Mn. The regional and stratigraphic distribution of geochemical facies reflect the complex interaction of depositional and diagenetic factors.

Basinal shales appear to have influenced the diagenesis of equivalent limestones. Diagenetic reactions in shales are interpreted to have added Mn and Fe, and removed Mg from interbedded slope limestones. Drowned carbonates encountered these metal-rich fluids migrating in response to fluid potential gradients. Anoxic marine waters were the source of metals in syndepositional oxide deposits in shelf-margin limestones. Deep burial diagenesis of outer shelf facies included the introduction of basin-derived saline brines. Burial history analysis indicates movement of waters through porous zones during the Middle Paleozoic.

TABLE OF CONTENTS

CHAPTER		PAGE
1.	INTRODUCTION	1
	Depositional Model for the Middle Ordovician in the Southern Appalachians	1
	Purpose of the Study	5
	Geologic Setting	6
	Methods of Study	14
	Geochemistry of Ancient Carbonates: A Prologue	16
2.	PETROGENESIS OF MICRITE/DOLOMICRITE AND CALCISILTITE FROM THE MIDDLE ORDOVICIAN CHICKAMAUGA GROUP AND EQUIVALENTS, EAST TENNESSEE	19
	Introduction	19
	Genesis of Holocene Platform Muds and Periplatform Oozes	21
	Petrography of Shelf Micrites and Slope Calcisiltites	22
	Elemental Geochemistry of Shelf Micrites	41
	Geochemistry of Slope Calcisiltites	60
	Summary of Micrite and Calcisiltite Petrogenesis	67
	Discussion	67
3.	ORIGINAL MINERALOGY OF SEDIMENTARY FACIES ALONG AN EARLY PALEOZOIC CARBONATE SHELF (MIDDLE ORDOVICIAN), EAST TENNESSEE	81
	Introduction	81
	Skeletal Allochems	82
	Discussion of Interpreted Skeletal Mineralogies	114
	Non-skeletal Allochems	127
	Synsedimentary Cements	139
	Original Mineralogy of Sedimentary Facies	152

4. CARBONATE GEOCHEMICAL FACIES IN A RAMP-TO-SHELF TRANSITION, MIDDLE ORDOVICIAN, EAST TENNESSEE 163

Introduction 163
Methods 164
Carbonate Geochemical Facies 166
Interpretation of Geochemical Facies Distribution 175

5. SHELF LIMESTONE - SHALE BASIN INTERACTION DURING EARLY AND LATE DIAGENESIS: AN EXAMPLE FROM THE MIDDLE ORDOVICIAN OF EAST TENNESSEE . 200

Introduction 200
Clay Mineralogy of Shales from the Sevier Basin 201
Geochemical Classification of Slope Lithofacies, Sevier Basin 212
Slope Lithofacies 215
Bathymetrically-Displaced Ramp/Shelf and Foreslope Deposits 237
Carbonate Shelf Lithofacies 246

6. SUMMARY AND CONCLUSIONS 306

LIST OF REFERENCES 311

APPENDICES 341

A. DESCRIPTIONS OF STRATIGRAPHIC SECTIONS 342
B. PROCEDURE FOR ATOMIC ABSORPTION ANALYSIS OF OF LIMESTONES, ALLOCHEMS AND MATRIX 363
C. DERIVATION OF STRONTIUM AND MAGNESIUM CONCENTRATIONS FOR LIME MUDS AND THEIR LITHIFICATION PRODUCTS 374
D. X-RAY DIFFRACTION ANALYSIS OF SHALES 381
E. CONSTITUENT PARTICLE ANALYSIS 384
F. INTERPRETED ORIGINAL SEDIMENT MINERALOGY 387

VITA 391

LIST OF TABLES

TABLE		PAGE
2.1.	Trace element composition of Middle Ordovician shelf micrites	51
2.2.	Elemental geochemistry of tidal flat dolomicrite	74
3.1.	Interpreted original mineralogy of bryozoa from the Middle Ordovician lower Chickamauga Group	100
3.2.	Summary of interpreted mineralogy of biotic components and ooids from selected Paleozoic ages	126
3.3.	Petrography of peloids from the lower Chickamauga Group and equivalents	130
4.1.	Geochemical and lithologic variables used to characterize samples for Q-mode cluster analysis	169
4.2.	Summary of geochemical facies	171
4.3.	Mean trace element composition of drowned (Mosheim) and shelf (Five Oaks) carbonate tidal flat lithofacies	195
4.4.	Diagenetic features of basal onlap tidal facies	197
5.1.	Mineral composition of Middle Ordovician shales and tectonostratigraphic analogues	205
5.2.	Mean detrital modes (%) of sandstones from the Blount clastic wedge and Cenozoic convergent margin analogues	207
5.3.	Trace element analyses of slope limestone beds (Whitesburg Fm.), Middle Ordovician Sevier Basin	231
5.4.	Trace element composition of coarsely crystalline equant calcite cements from the Holston Formation	277

5.5. Stratigraphic units and their respective thicknesses used in constructing burial curves 303

B.1. Sample weights prior to acid dissolution 366

B.2. Summary of trace element data and method acceptability 368

B.3. Trace element composition of Ordovician skeletal allochems 373

C.1. Mineralogy and elemental composition of mud-contributing marine organisms 377

D.1. Summary of mineralogical data on Sevier Basin shales 383

LIST OF FIGURES

FIGURE		PAGE
1.1.	Series of sediment distribution maps superposed on the palinspastic base of Roeder and Witherspoon (1978)	4
1.2.	Generalized temporal relationships of early Middle Ordovician strata in the Valley and Ridge Province, northeastern Tennessee	7
1.3.	Stratigraphic cross-sections from northwest (left) to southeast (right) of Middle Ordovician rocks in northeastern Tennessee ..	9
1.4.	Dominant lithofacies and depositional environments of the lower Chickamauga Group and equivalents	11
1.5.	Locality map showing area studied and locations of sections	12
2.1.	SEM photomicrographs of Middle Ordovician shelf micrites	23
2.2.	Grain size histograms of micritic matrix including (A) and excluding (B) microspar cement	26
2.3.	SEM photomicrographs of Middle Ordovician micrites	28
2.4.	SEM photomicrographs of intercrystalline mineral aggregations in shelf mircrites	30
2.5.	Thin section and SEM photomicrographs of slope calcisiltites	34
2.6.	Grain size histogram of calcisiltite from the Whitesburg Formation	36
2.7.	SEM photomicrographs of lightly etched Plio-Pleistocene aragonite-dominated (A) and calcite-dominated (B) micrite precursors	39
2.8.	Thin section photomicrographs of bored skeletal grains from shallow-water limestones	44

2.9. Trace element stabilization 'trends' for hypothetical calcite- and aragonite-dominated lime muds 48

2.10. Strontium and magnesium concentration of Ordovician shelf micrites plotted with respect to calculated compositional end members of originally aragonitic and calcitic muds 52

2.11. Trace element equilibration diagrams for shelf micrites (after Brand and Veizer, 1980) 55

2.12. Elemental geochemistry of Ordovician micrites compared with other Phanerozoic micrites and botryoidal cements which are interpreted as originally aragonite 57

2.13. Strontium and magnesium concentration of Ordovician slope calcisiltites from the Whitesburg Formation, plotted with respect to the calculated compositional end member for originally calcitic sediment 62

2.14. Elemental geochemistry of Ordovician calcisiltites from this study compared with modern and ancient diagenetic calcites precipitated from deep marine waters 64

2.15. The effects of separate diagenetic histories on Sr and Mg composition of fine grained carbonate sediments 68

2.16. Composition of Ordovician micrites superposed on the diagenetic trends for aragonite (A), calcite (LMC) and magnesian calcite (HMC) constructed by Brand and Veizer (1980) 70

2.17. Strontium and magnesium concentration of Ordovician tidal flat dolomicrites compared to undolomitized Ordovician shelf micrites .. 73

2.18. Iron and magnesium concentration of Ordovician tidal flat dolomicrites 77

2.19. Preliminary hypothetical model for the early dolomitization of tidal mudflats at the base of an onlap sequence 79

3.1. Thin section photomicrographs of calcareous algae 84

3.2. Strontium and magnesium concentration of Ordovician Girvanella-bearing oncoids and contemporaneous micrites 89

3.3. Range of Mg/Sr ratios in fossil and Recent calcareous marine organisms 91

3.4. Thin section and SEM photomicrographs of bryozoans 96

3.5. Thin section and SEM photomicrographs of articulate brachiopods and molluscs 102

3.6. Thin section photomicrographs of arthropods and echinoderms 107

3.7. Summary sketch showing the recognized types of skeletal preservation in Middle Ordovician in eastern Tennessee 115

3.8. Schematic illustration comparing meteoric and burial calcite cement, and clear, intrazooecial spar in nicholsonellid replacement-cement mosaics 118

3.9. Diagenetic textures and fabrics associated with nicholsonellid replacement-cement mosaics 119

3.10. Strontium and magnesium concentration of nicholsonellid replacement-cement mosaics and coarsely crystalline, burial calcite cement . 122

3.11. Model for shallow meteoric- to burial-phreatic diagenesis of originally aragonitic nicholsonellid bryozoans 124

3.12. Thin section photomicrographs of non-skeletal allochems 132

3.13. Criteria for recognizing synsedimentary cements in ancient limestones 141

3.14. Thin section and SEM photomicrographs of interpreted synsedimentary cements 145

3.15. Original mineralogy of Middle Ordovician sedimentary facies (N=120) and Holocene platform, periplatform and pelagic sediments (N=150) 154

3.16. Interpreted original mineralogy of major sedimentary facies suites on the Ordovician ramp and shelf 157

3.17. Cross-shelf variation in marine lithification as reflected by the abundance of interpreted synsedimentary cements 159

4.1. Simplified Q-mode cluster dendogram constructed from S.A.S. "tree diagram" 167

4.2. Cross-sections (see Chapter 1 for comparison) showing the regional distribution of geochemical facies 172

4.3. Compositional fields for geochemical facies based on the elements strontium, manganese, iron and magnesium 174

4.4. Histograms of bulk manganese concentrations for samples separated with respect to inferred paleobathymetry 177

4.5. Plot of bulk manganese versus acid-insoluble residue (IR) for the Lenoir Formation 180

4.6. Plot of bulk manganese versus acid-insoluble residue (IR) for selected samples from each geochemical facies 182

4.7. Numerous brightly luminescent cement zones in echinoderm syntaxial overgrowth calcite from skeletal packstone, lower Lincolnshire Formation 184

4.8. Mean and standard deviation of bulk strontium concentrations in grain- and mud-supported lithologies from the lower Chickamauga Group at the Cedar Springs and Red House Branch localities 188

4.9. Correlation matrix of dominant skeletal allochems, micrite, and bulk strontium in shelf limestones 189

4.10. Plot of bulk strontium versus volume percent of arthropods in shelf limestones 190

4.11. Diagenetic features in onlap tidal flat deposits of the Mosheim Member of the Lenoir Formation and Five Oaks Formation 196

5.1. Representative x-ray diffraction patterns from calcareous shales of the Whitesburg Formation 203

5.2. Transformation of detrital smectite clays during burial 211

5.3. Classification of diagenetic environments after Berner (1981) 213

5.4. Composite stratigraphic section of shelf-to-basin transition from numerous localities in northeastern Tennessee 216

5.5. Deep-water limestones from the Whitesburg and Blockhouse Formations 219

5.6. Frequency histograms which compare manganese and strontium concentrations in uncleaved (SC and MM) and cleaved (DL) limestones of Whitesburg Formation 226

5.7. Plot of strontium versus magnesium concentration in calcisiltites from Silver City (SC) and Martin Mill Pike (MM) localities 228

5.8. Plot of bulk iron versus bulk manganese in calcisiltite beds 229

5.9. Mean and standard deviation of manganese, strontium and magnesium in carbonate silt and neomorphic calcspar fractions in calcisiltite beds 233

5.10. Stratigraphic variation in bulk, acid-soluble manganese and iron from sequences associated with drowning of shallow-water areas during downwarping 238

5.11. Diagrammatic representation of changes in bulk, acid-soluble manganese in the lower 50 meters of the Lenoir Formation at Midway Road (MR), St. Clair (STC), Martin Mill (MM), Silver City (SC) and Douglas Lake (DL) localities 241

5.12. Diagenetic features in bathymetrically-displaced shallow-water deposits of the Lenoir Formation 243

5.13. Generalized cross-section of Ordovician shelf-to-basin transition which depicts probable fluid migration paths during burial of drowned carbonates, and stratigraphic zone of iron and manganese enrichment 247

5.14. Photomicrographs of iron-manganese oxides from the Holston Formation 252

5.15. Close-up of hematite-rich and -poor microlaminations in internal sediments, and inferred fluctuations in respective sediment accumulation rates 255

5.16. Diagrammatic sketch of bryozoan boundstone lithofacies showing diagenetic changes accompanying secondary cavity formation/ enlargement and penecontemporaneous iron and manganese oxide precipitation 258

5.17. Hematitic peloidal sediments in boundstone facies of the Holston Formation 260

5.18. Photomicrographs of compactional fabrics in shelf limestones 267

5.19. Compactional fabrics in shelf limestones 270

5.20. Photomicrographs of deep burial cements in shelf limestones 274

5.21. Photomicrographs which illustrate the fabric interrelationships between luminescent-zoned, precursor prismatic and equant calcite cement, and very dull to non-luminescent baroque dolospar cement (D) 279

5.22. Photomicrographs of deep burial diagenetic features in shelf limestones 282

5.23. Diagenetic histories of outer shelf limestones in the northern part of the study area 285

5.24. Composite schematic diagram showing cross-shelf variations in the relative abundance of deep-burial phases in terms of the percentage of samples containing each phase 287

5.25. Stratigraphic variation in bulk iron and magnesium concentrations in shelf-margin limestones at Red House Branch 290

5.26. Plot comparing the calculated m_{Te}/m_{Ca} ratios of burial waters in equilibrium with deep burial calcite cement (open circles), and published element compositions of deep burial brines 298

5.27. Frequency histogram showing bulk sodium concentrations of shelf-marginal limestones . 300

5.28. Burial history of Middle Ordovician shelf and basinal strata using compacted stratigraphic thicknesses of exposed Paleozoic rocks (see Table 5.5) 302

B.1. Simplified flow diagram showing laboratory sample processing scheme 365

CHAPTER 1

INTRODUCTION

Depositional Model for the Middle Ordovician in the Southern Appalachians

Middle Ordovician (Champlainian) strata in eastern Tennessee include a mixture of carbonate and siliciclastic facies exposed in the foreland thrust belt of the Southern Appalachians. Until the 1970's, investigations of these and time-equivalent rocks in southwestern Virginia dealt primarily with description and/or revision of the regional stratigraphy (Cooper, 1945; Neuman, 1955; Prouty, 1946; Rodgers, 1953). However, flaws existed in these early stratigraphic interpretations. Some workers viewed regional facies as separate formational units which extended over the entire basin (i.e., 'layer-cake stratigraphy'). Also, biostratigraphic correlations were occasionally based on taxanomic groups that were probably facies-controlled.

Over the past fifteen years, Kenneth R. Walker, Thomas

W. Broadhead and their co-workers at the University of Tennessee-Knoxville have developed a dynamic odel which tracks the evolution of the regional facies mosaic during the Middle Ordovician. The essentials of this depositional scenario are presented in Ruppel and Walker (1977, 1984), and Walker et al. (1980).

Temporal variations in regional facies patterns and inferred water depths delimit three 'phases' in the development of the basin which reflect the interplay of tectonic and sedimentary processes. The first stage began with a regional transgression over the exposed Knox Group, which initiated deposition on a shallow-water homoclinal ramp (terminology after Read, 1982) that sloped gently to the southeast. Carbonate ramp facies - represented by the lower Lenoir Formation in southeastern strike belts - have characteristics similar to modern ramps (Ahr, 1973). Based on the facies succession above the unconformity, the paleoenvironments along the ramp consisted of a low-energy tidal flat which passed eastward (seaward) to nearshore algal sand-banks, and an offshore muddy subtidal zone.

Soon after re-establishment of deposition in the basin, a major tectonic downwarping, connected with orogenic activity to the east, caused a portion of the ramp to break and rapidly subside (Shanmugam and Walker, 1983). The high subsidence rates inferred for this event (60-65

cm/1000 yr., Shanmugam and Walker, 1980) produced a relatively steep slope, thereby creating a shelf to the northwest. As a result of the new marine topography, five major environmental zones were developed, each represented by a unique facies package. From northwest to southeast, these zones are: (1) shallow-water, inner carbonate shelf; (2) shelf-edge skeletal sand-bank and foreslope, discontinuous bryozoan reef tract; (3) mixed carbonate-siliciclastic slope; (4) deep-water shale basin; (5) slope that joined the basin with an area of predominately siliciclastic deposition (Times 1 and 2, Figure 1.1). The regional facies distribution in East Tennessee during this second stage resembles the rimmed shelf of Read (1982).

The basin formed by downwarping (i.e., Sevier Basin) soon became the site of turbidite and contourite deposition. The high sedimentation rates associated with turbidite and contourite facies resulted in the rapid infilling of the Sevier Basin, thereby initiating a change in the regional facies distribution (Time 3, Figure 1.1). This third stage is marked by an increase in siliciclastic input to shelf areas previously dominated by carbonate sediments. Mixed carbonate-siliciclastic peritidal deposits of the upper Middle Ordovician Moccasin Formation formed in front of the tectonic highlands to the east. This unit

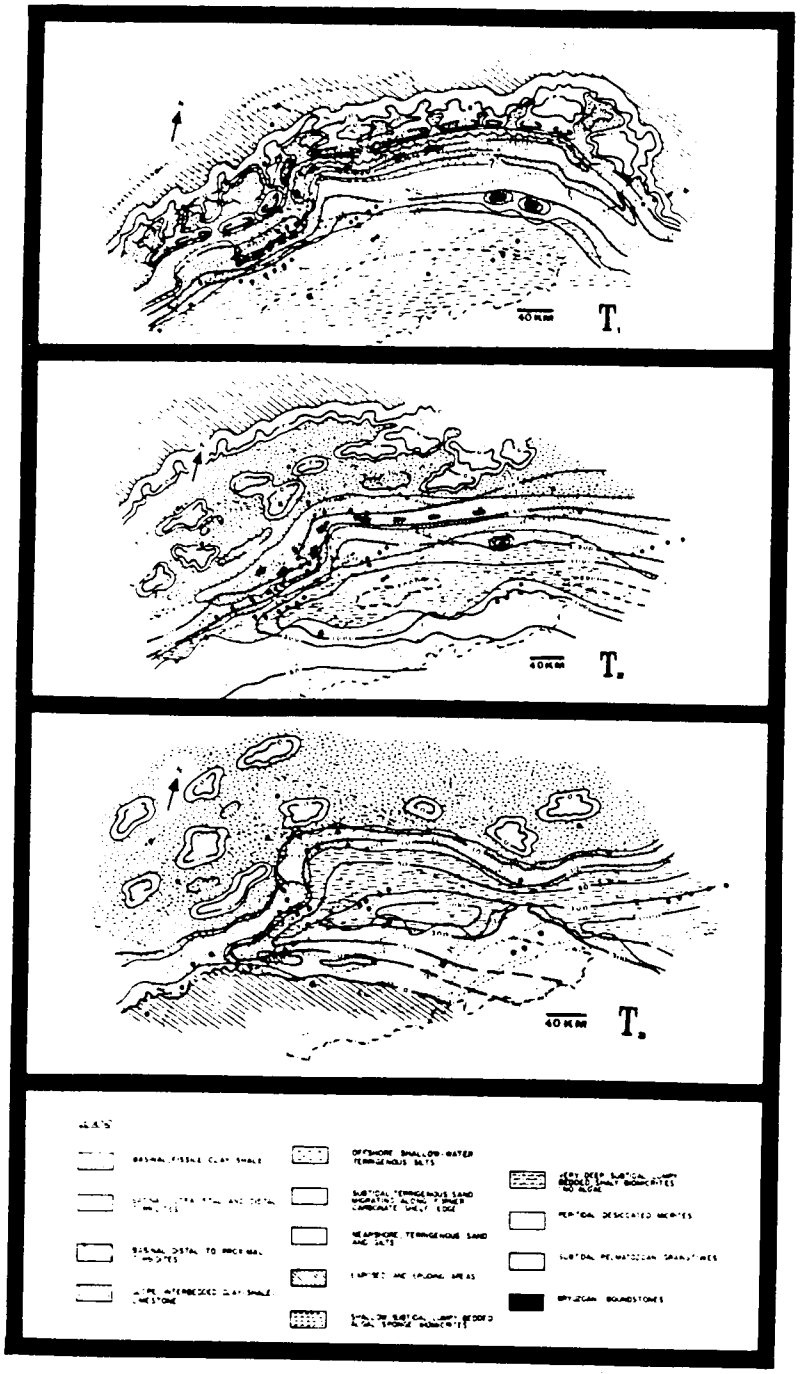


Figure 1.1. Series of sediment distribution maps superposed on the palinspastic base of Roeder and Witherspoon (1978). Time 1 (T_1, earliest) corresponds to time-line 1 in cross-sections of Fig. 1.3, time 2 (T_2) corresponds to time-line 2, and time 3 (T_3, latest) corresponds to time-line 3. From Walker et al. (1980).

marks the culmination of a 'bathymetric reversal' which characterizes the latest phase of sedimentation in the basin (Simonson, 1985).

Purpose of the Study

The overall purpose of this study is to assess minor and trace element geochemistry of carbonate shelf and slope facies in light of their depositional and diagenetic characteristics. Some of the individual aspects this study will address include: (1) mineralogical comparison of Ordovician and Holocene sediments and synsedimentary cements; (2) origin and mineralogy of micrites, and their potential influence on early diagenetic dolomitization in a humid climatic setting; (3) petrogenesis of carbonate shelf and slope facies within an evolving foredeep basin; (4) depositional and diagenetic control on geochemical gradients in a mixed carbonate-siliciclastic basin; and (5) trace element variations in carbonate-dominated facies, and their applicability in tracking changes in the diagenetic system.

Geologic Setting

Stratigraphy of the lower Middle Ordovician overlying the post-Knox unconformity in northeastern Tennessee is shown in Figure 1.2. This stratigraphic interval corresponds to the first and second phases of deposition discussed in the previous section. The upper boundary is the Time 3 isochronous surface of Benedict and Walker (1978). Figure 1.3 depicts the regional stratigraphic relationships for the entire Middle Ordovician sequence. The dominant lithofacies of each unit and the interpreted depositional environment(s) are given in Figure 1.4.

Lower Middle Ordovician strata are extensively exposed within imbricate thrust sheets in the Valley and Ridge Province (Fig. 1.5). A thorough study of the geochemistry of an extensive sequence such as the Middle Ordovician necessitates the collection of a large number of samples representative of the regional facies mosaic. Stratigraphic sections where lithic samples were collected for analysis are indicated in Figure 1.5. The sections located around Knoxville, Tennessee are at Solway Bridge (SB), along Martin Mill Pike(MM), and Douglas Lake(DL). The other sections, located approximately 90 kilometers northeast of Knoxville along strike, consist of exposures at Cedar Springs(CS),

Figure 1.2. Generalized temporal relationships of early Middle Ordovician strata in the Valley and Ridge Province, northeastern Tennessee. Modified from Ruppel and Walker (1984).

NW

SE

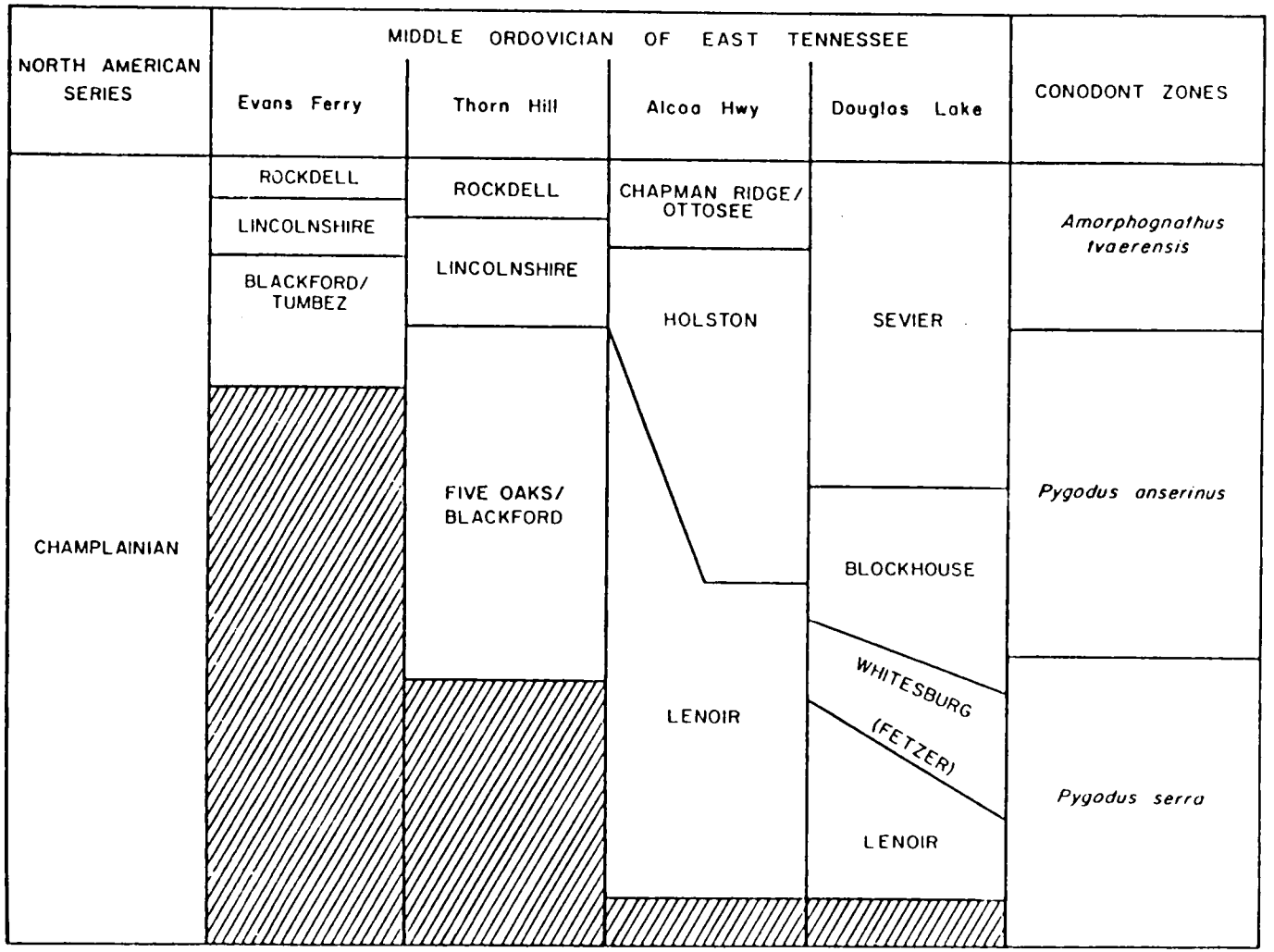
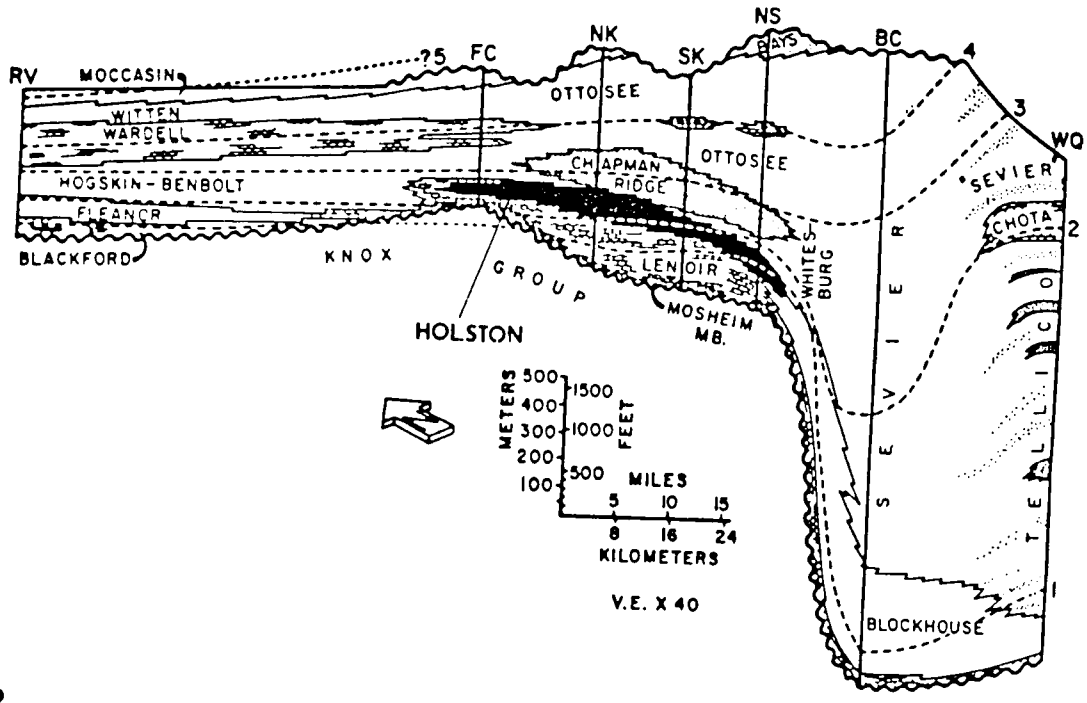
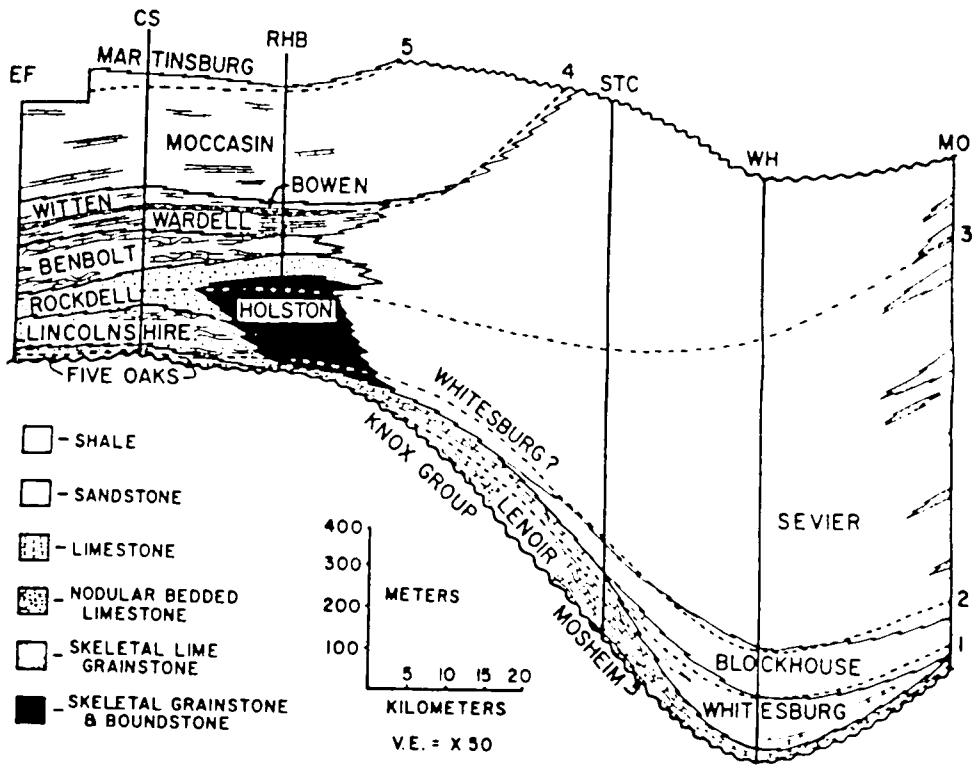

MIDDLE ORDOVICIAN OF EAST TENNESSEE
NORTH AMERICAN SERIES
Evans Ferry
Thorn Hill
Alcoa Hwy
Douglas Lake
CONODONT ZONES
CHAMPLAINIAN
ROCKDELL
LINCOLNSHIRE
BLACKFORD/ TUMBEZ
ROCKDELL
LINCOLNSHIRE
FIVE OAKS/ BLACKFORD
CHAPMAN RIDGE/ OTTOSEE
HOLSTON
LENOIR
SEVIER
BLOCKHOUSE
WHITESBURG
(FETZER)
LENOIR
Amorphognathus tvaerensis
Pygodus anserinus
Pygodus serra

Figure 1.3. Stratigraphic cross-sections from northwest (left) to southeast (right) of Middle Ordovician rocks in northeastern Tennessee. Section A extends from Raccoon Valley (RV) through Knoxville to Wildwood Quadrangle (WQ). Section B extends from Evans Ferry (EF) to Mosheim (MO). Palinspastically restored. A from Walker et al. (1980); B from Ruppel and Walker (1984).

A


RV
MOCCASIN
?5
FC
NK
SK
NS
BAYS
BC
4
3
WQ
OTTOSEE
WITTEN
WARDELL
OTTOSEE
CHAPMAN RIDGE
HOGSKIN - BENBOLT
SEVIER
CHOTA
2
FLEANOR
BLACKFORD
KNOX
GROUP
LENOIR
WHITESBURG
HOLSTON
MOSHEIM MB.
TELLICO
METERS 500 400 300 200 100
1500 1000 500 FEET
MILES 5 10 15
8 16 24 KILOMETERS
V.E. X 40
BLOCKHOUSE
1

B

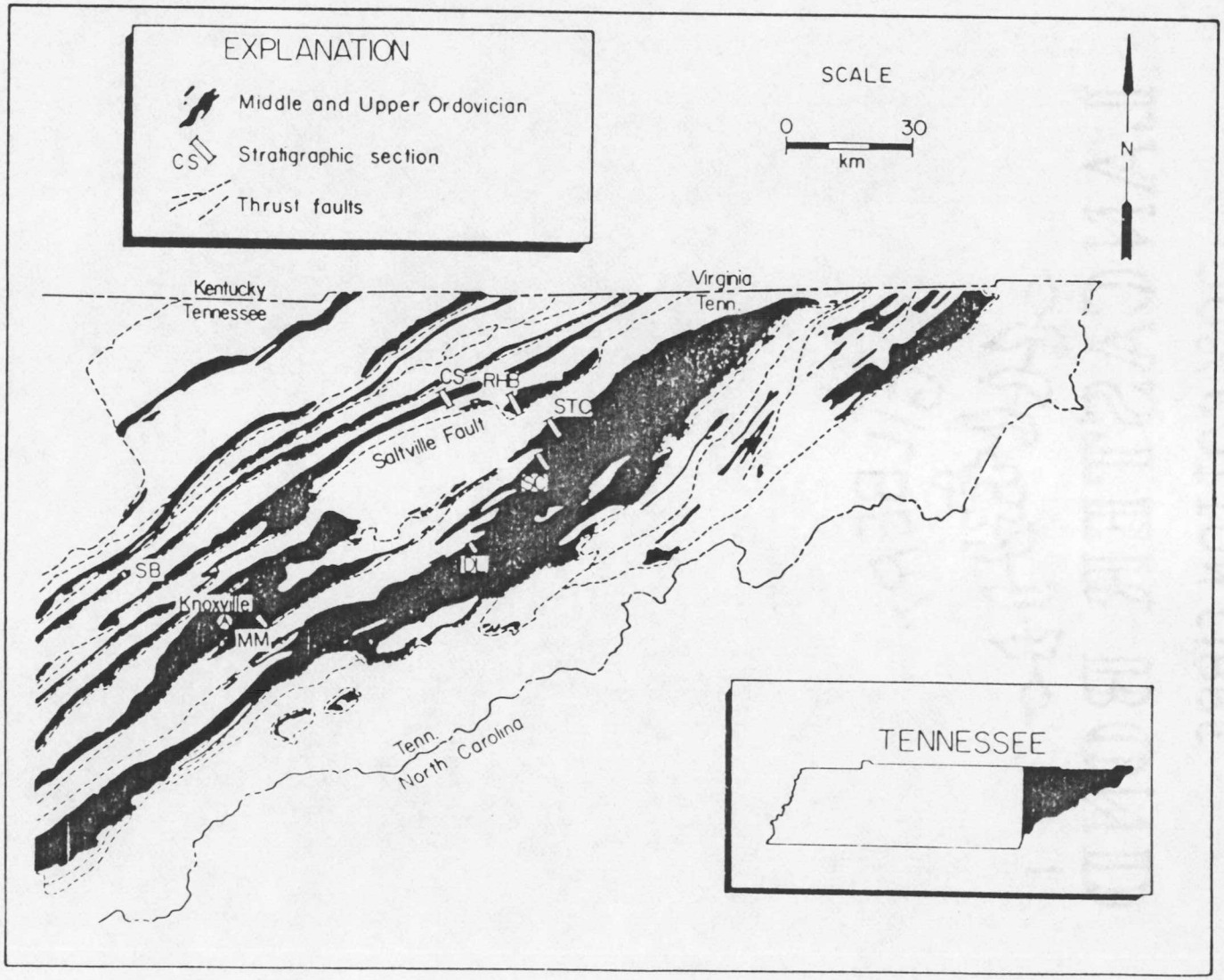

CS
RHB
EF
MARTINSBURG
5
4
STC
WH
MO
MOCCASIN
BOWEN
WITTEN
WARDELL
BENBOLT
ROCKDELL
HOLSTON
LINCOLNSHIRE
FIVE OAKS
3
WHITESBURG?
KNOX GROUP
LENOIR
SEVIER
2
MOSHEIM
BLOCKHOUSE
1
WHITESBURG
- SHALE
- SANDSTONE
- LIMESTONE
- NODULAR BEDDED LIMESTONE
- SKELETAL LIME GRAINSTONE
- SKELETAL GRAINSTONE & BOUNDSTONE
400 300 200 100 METERS
5 10 15 20 KILOMETERS
V.E. = X 50

Unit	Dominant Lithofacies	Depositional Environments
Blackford	Argillaceous lime-dolomitic mudstone; fossiliferous wackestone	Beach ridge, tidal mud-flats and sandflats
Five Oaks	Dolomitic mudstone; peloidal packstone and grainstone	Peritidal; tidal flat
Lincolnshire	Fossiliferous wackestone; echinoderm-bryozoan packstone and grainstone	Shallow to deep subtidal, open marine
Rockdell	Bryozoan wackestone; echinoderm-bryozoan packstone and grainstone	Muddy subtidal sand banks and mud mounds
Holston	Echinoderm grainstone; bryozoan packstone; bryozoan wackestone-boundstone	Shelf-margin reef complex
Benbolt	Fossiliferous wackestone; peloidal packstone and grainstone; lime mudstone; shale	Open shelf, shallow to deep subtidal
Mosheim	Fenestral mudstone; lime mudstone	Low energy tidal flat
Lenoir	Fossiliferous wackestone and packstone	Shallow to deep subtidal, open shelf/ramp
Whitesburg	Fossiliferous wackestone packstone and grainstone; calcisiltite; shale	Shelf-basin transition (slope)
Blockhouse	Graptoliferous clay shale	Starved, deep-water basin
Sevier	Shale; siltstone; fine-grained sandstone	Basin; turbidite and contourite(?) deposition

Modified from Ruppel and Walker (1984)

Figure 1.4. Dominant lithofacies and depositional environments of the lower Chickamauga Group and equivalents.

Figure 1.5. Locality map showing area studied and locations of sections. CS, Cedar Springs; RHB, Red House Branch; STC, St. Clair; SC, Silver City; SB, Solway Bridge; MM, Martin Mill Pike; DL, Douglas Lake.


EXPLANATION
Middle and Upper Ordovician
CS
Stratigraphic section
Thrust faults
SCALE
0
30
km
N
Kentucky
Tennessee
Virginia
Tenn.
CS
RHB
STC
Saltville Fault
SB
Knoxville
MM
Tenn.
North Carolina
TENNESSEE

along Red House Branch (RHB), at St Clair (STC), and Silver City (SC). Previous studies have already provided detailed lithologic and biotic descriptions of each stratigraphic section; however, additional information was collected in the present study. Lithofacies present at SB, RHB, and CS represent shelf deposition which followed formation of the Seiver Basin (phase 2); lithofacies at the remaining sections represent ramp deposition (phase 1) and deep-water (slope and basin) deposition (phase 2).

Methods of Study

Samples of carbonate and siliciclastic lithologies were collected from the respective units at each of the seven sections. Field descriptions of each section are concise due to the emphasis of the study, and the existence of already detailed descriptions. Lithic samples for petrographic and geochemical analysis were selected so as to furnish a representative sampling of lithotypes in each unit, and provide a sufficient degree of stratigraphic control. The diagenetic history of carbonate facies was interpreted from petrographic data obtained by analysis of stained, 5 cm x 8 cm thin sections. Cathodoluminescence

petrography was used on some thin sections to refine cement parageneses, and provide a semi-quantitative measure of Mn through the relative abundance of orange luminescence in calcite (see Sippel and Glover, 1965, Frank et al, 1982). Volume percentages of both depositional and diagenetic constituents were obtained by point count analysis of samples chosen for geochemical analysis. A minimum of 400 points per thin section were counted; errors shown for constituent percentages are from Van der Plas and Tobi (1965). Sample cubes of fine grained depositional matrix (micrite), calcisiltite, skeletal allochems and cements were polished to 0.02 micrometers and etched from 15 to 45 seconds with 50% v/v acetic acid for SEM analysis on an ETEC Autoscan Scanning Electron Microscope. Calcareous shale samples from the Whitesburg Formation were prepared using standard procedures for mineralogical analysis using a Norelco x-ray diffractometer. Samples were crushed and the carbonate fraction removed using a buffered acetic acid solution. The <5 micrometer size fraction was obtained by pipetting, and at least one elutriated slide was prepared for each sample. Further details concerning the mineralogical analysis of shales are given in the Appendix D.

Trace element analysis was performed on bulk samples and individual allochem and matrix components. Microsamples

of the latter were obtained with a Jensen vertical milling machine, or cutting with a rock saw. Analysis of Fe, Mn, Sr, Na, Mg, and Zn in the acid-soluble fraction was by atomic absorption spectrophotometry. (For details of this and other analytical methods, see Appendix B.)

Statistical analysis of petrographic and geochemical data was performed using the Statgraphics package of computer programs available in the Department of Geological Sciences and SAS programs on a VAX 11/780 mainframe computer at the University of Tennessee.

Geochemistry of Ancient Carbonates: A Prologue

Studies of Recent carbonate environments have discerned relationships between sediment mineralogy and chemistry. Seigel (1961) noted an inverse relationship between Sr and Mg in reef and back-reef lagoon sediments of the Florida Keys. Strontium contents increased and magnesium contents decreased in samples collected successively landward from the reef tract. Seigel attributed these concentration gradients to changes in the "mineralogical nature of the organic remains". A correlation between Mg and the coral:coralline algae:mollusc ratio of carbonate sands was

noted by Friedman (1968). Unlike Seigel's study, this work showed that geochemistry may vary even when sediments are dominated by a single carbonate polymorph (aragonite).

Since the dominant polymorphs in bank and bank-derived carbonate sediments are metastable at diagenetic temperatures, pressures and fluid compositions, the original minor and trace element component will be re-partitioned between diagenetic phases and solution. The degree of depletion or enrichment of an element is dependent upon numerous factors which include 1) temperature, 2) kinetics of re-equilibration or precipitation (Lorens, 1981), 3) composition of pore waters, and 4) "openness" of the system or water/rock ratio during diagenesis. Factors 3 and 4 are probably the most important in terms of depletion/enrichment of divalent elements in diagenetic low-Mg calcite. The incorporation of monovalent ions, which substitute interstially or into crystal defects, may be significantly affected by the kinetics of diagenetic processes. Element trends which reflect changing bulk sediment compositions are unlikely to be preserved in diagenetically-stabilized sediments.

Geochemical studies of shelf/platform limestones are numerous in the geologic literature. The more recent studies apply trace elements - in concert with petrographic and isotopic data - to obtain a better understanding of

diagenetic processes in a limited stratigraphic interval (see Wagner and Matthews, 1982, James and Klappa, 1983). The few studies that have been done on different facies within a sedimentary basin are limited in scope, either in the number of elements analyzed or diversity of environments chosen for examination. No study to date has attempted to synthesized trace element geochemistry in light of depositional and diagenetic parameters and conditions in a sequence as complex and wide-spread as that studied here.

CHAPTER 2

PETROGENESIS OF MICRITE/DOLOMICRITE AND CALCISILTITE FROM THE MIDDLE ORDOVICIAN CHICKAMAUGA GROUP AND EQUIVALENTS, EAST TENNESSEE

Introduction

The diagenetic products of carbonate muds have for a long time been recognized as one of the dominant components in Phanerozoic limestones. Even with the extensive study of mudstones and other micritic lithologies, many questions about the deposition and lithification of micrites and other fine grained carbonates remain either unaddresses or incompletely answered. One reason for this state is that data necessary to understand the petrogenesis of micrites must be supplemented by geochemical analyses (trace elements, stable isotopes) of this fraction (see Choquette, 1968; Wiggins, 1986). These data, combined with textures observed using the scanning electron microscope (SEM), offer the necessary tools with which to decipher the origin and diagenesis of lime muds.

The mineralogy of micrite precursors through the Phanerozoic has important implications in terms of understanding the evolution of carbonate rocks, and their original sediments. Such information would permit identifying temporal variations in the relative proportions of aragonite, calcite and magnesian calcite in platform/shelf environments, and perhaps allow for elucidation of the factors controlling these mineralogic fluctations. Wilkinson (1979) determined the dominant sediment-contributing marine organisms during the Paleozoic actively or passively formed skeletons of magnesian calcite not, aragonite as in analogous modern environments. In terms of carbonate diagenesis, the existence of magnesian calcite-dominated micrite precursors may have provided an alternate dolomitization mechanism in platform areas.

As the initial step in understanding the petrogenesis of a carbonate shelf sequence, the original mineralogy and diagenetic history of fine grained carbonates (depositional micrite and calcisiltite) from limestones was examined. A holistic approach was used that combined stratigraphic, petrographic and geochemical data on a limited number of micrite and calcisiltite samples, together with knowledge of paleoenvironments and diagenetic processes.

Genesis of Holocene Platform Muds and Periplatform Oozes

Lime muds accumulating on shallow-water banks, such as the Bahamas Platform, appear to be of biotic origin, particularly in environments lacking hypersaline waters. The proposed sources of these fine sediments include: 1) disarticulated crystallites of calcareous algae and other indigenous organisms (Lowenstam and Epstein, 1957; Stockman et al., 1967; Neumann and Land, 1975); 2) remains of carbonate secreting epibionts on marine vegetation (Nelson and Ginsbuurg, 1986); 3) breakdown of skeletal debris by physical and biological agents (Folk and Robles, 1964; Matthews, 1966); 4) combination of all the above (see Bosence et al., 1985). Mineralogical and geochemical analyses of this sediment fraction show contributions from two sources, high-Sr aragonite and low-Sr magnesian calcite. Low-Sr aragonite precipitated by molluscs is an insignificant mud contributor based on the available data.

The term periplatform ooze was first proposed by Schlanger and James (1978) for the fine calcareous sediments which accumulated in deeper waters adjacent to carbonate platforms. These sediments consist of a mixture of pelagic and bank-derived components. Mineralogical and geochemical

analyses similar to those of bank muds indicate periplatform oozes off the Bahamas Platform are a mixture of shallow-water, high-Sr aragonite, and calcite/Mg-calcite from various sources (Boardman and Neumann, 1984). The bank-derived component dominates these sediments, a consequence of sediment overproduction in bank environments (Neumann and Land, 1975). Carbonate oozes accumulating in other deep-water areas adjacent to the Bahamian escarpement are also dominated by shoal-derived aragonite and magnesian calcite (Schlanger and James, 1978).

Petrography of Shelf Micrite and Slope Calcisiltite

Micrite

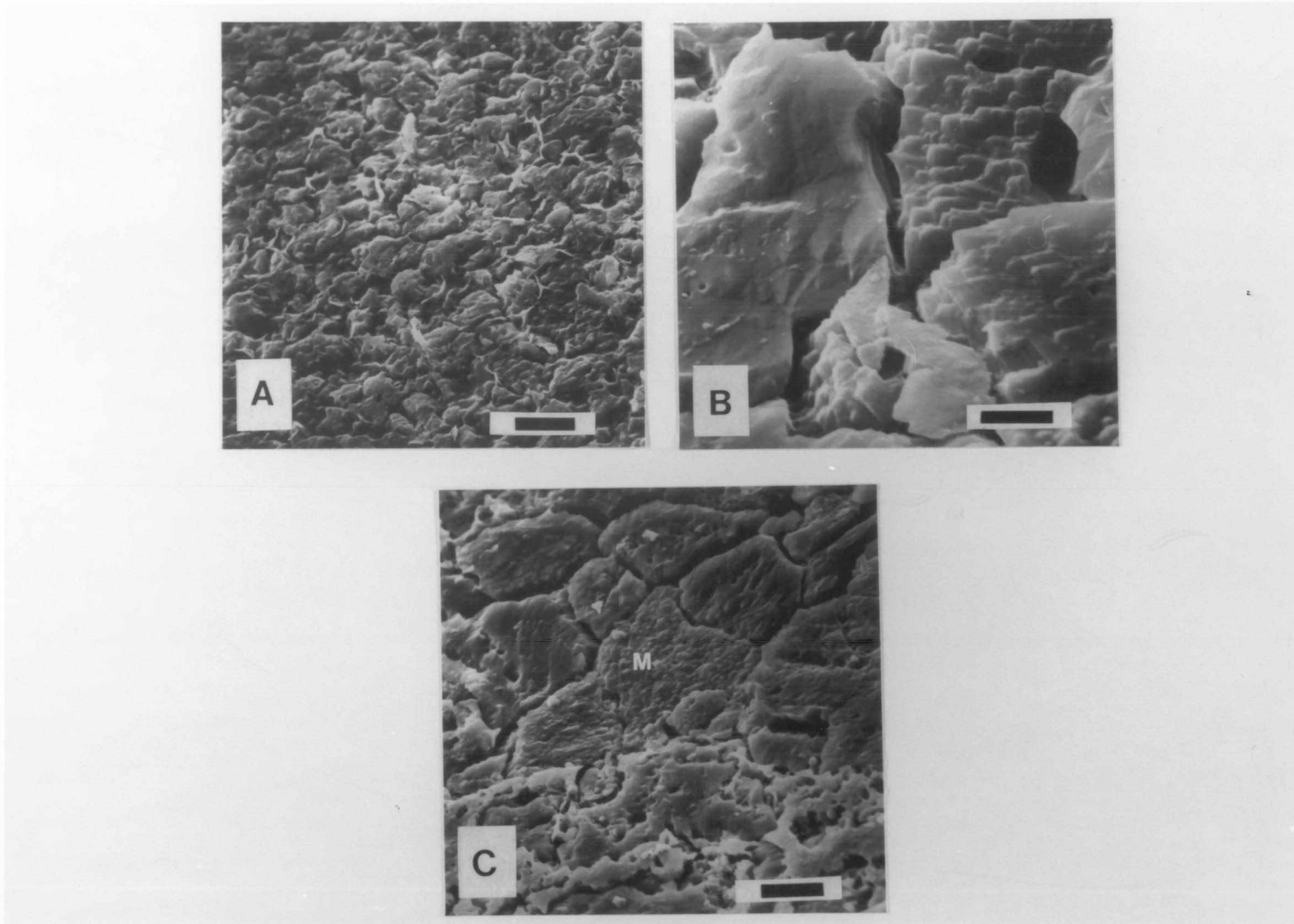
Scanning electron microscopy (SEM) shows that micrites consist of a mosaic of equant to sub-equant grains (Fig. 2.1A and B) regardless of depositional environment. The observed texture is identical to other micrites throughout the Phanerozoic (Folk, 1965; Fisher et al., 1967; Gillot, 1969; Miller, 1986). Individual fibrous and platy grains resulting from the trituration of articulate brachiopod shells (Lobo and Osborne, 1973, Figure 2B and C) were not observed in etched, polished surfaces, even in facies where

Figure 2.1. SEM photomicrographs of Middle Ordovician shelf micrites.

A. Equant to subequant micrite grains from outer shelf mud mound facies. Sample CS53. Scale bar = 6 micrometers.

B. Close-up of crystals which form the micritic portions of shelf limestones. Note the absence of acicular crystal relics and rareity of pits on this etched surface. Sample MMc. Scale bar = 2 micrometers.

C. Relict microporosity (M) which has been occluded by very finely crystalline calcite cement. Note the textural and fabric difference between cement and depositional matrix. Sample MM18. Scale bar = 7 micrometers.


A
B
M
C

this biotic group contributes significantly to the allochem fraction. Acicular textures after acid etching that may suggest an aragonitic lime mud precursor were also absent from samples.

The apparent grain size distribution in the micritic matrix is shown by the frequency histogram in Figure 2.2A. Based on this data it appears shelf micrite possesses a bimodal size distribution, with the dominant mode occurring at around 5 micrometers and a much smaller mode at 10-12 micrometers. The majority of grains in this upper mode constitute patches or clusters of inclusion-poor crystals with planar intercrystalline boundaries, and textures noticeably different from other portions of the matrix (Fig. 2.1C). The textural dissimilarity suggests these crystals may represent low-Mg calcite cement which completely occluded secondary(?) porosity (Steinen, 1978). Size range of microspar cements studied by Stienen approximates the upper size mode from Middle Ordovician samples, and crystals interpreted as cement by other workers. Assuming these "grains" represent void-filling cement and are not the product of mud lithification, they can be excluded from the micrite data set; the modified frequency histogram (Fig. 2.2B) for depositional matrix now exhibits only the single lower size mode (4-6 micrometers).

Grains occasionally possess minor, submicrometer-sized

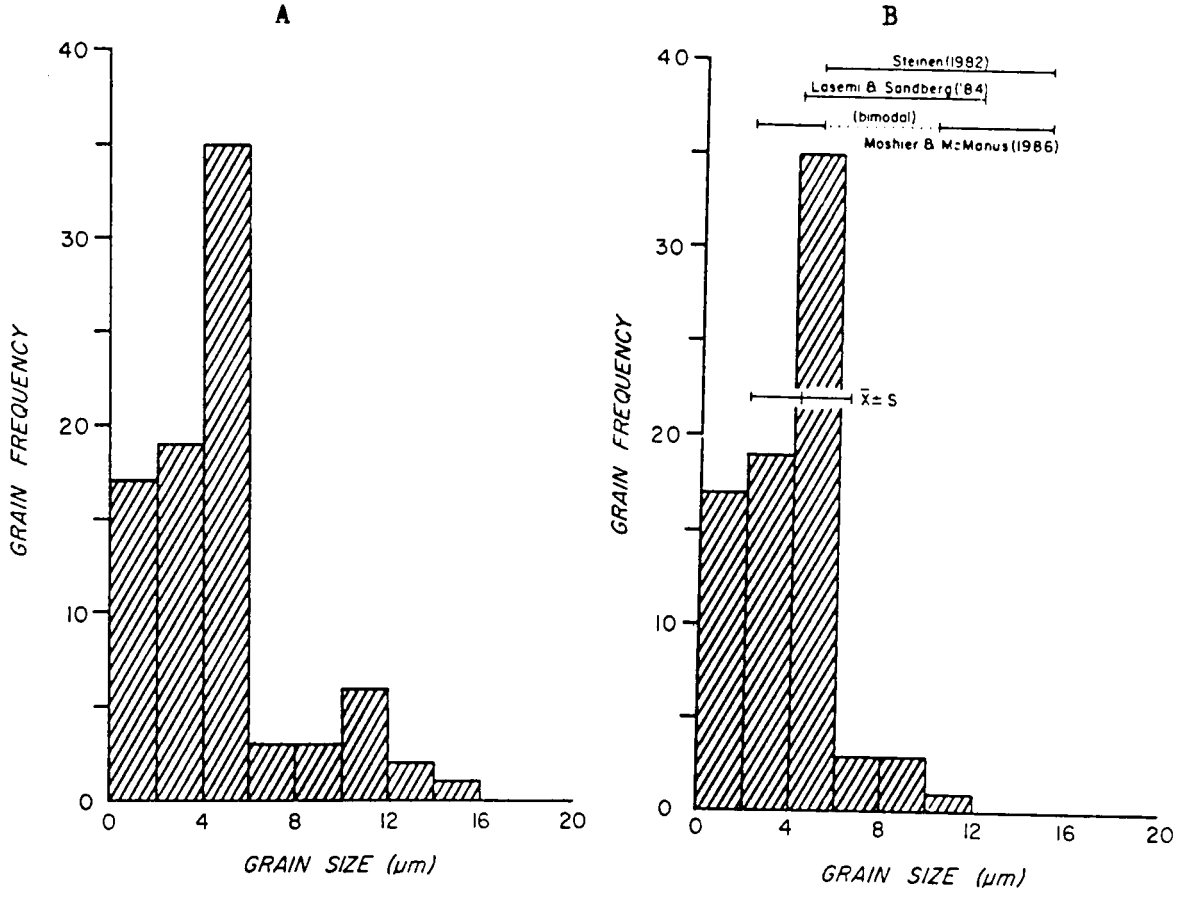


Figure 2.2. Grain size histograms of micritic matrix including (A) and excluding (B) microspar cement. Sizes represent the long dimensions of micrite grains measured directly from SEM photomicrographs. Mean (x) and standard deviation (s) of Middle Ordovician samples together with grain dimensions from studies of aragonite-dominated micrite precursors are shown in B. N = 86.

pits or hollow inclusions. Equant micrite grains from Walsortian mud mounds often contain blocky inclusions which are believed to represent microdolomite inclusions (Miller, 1986). Etched surfaces of Middle Ordovician micrites typically have extremely fine blebs which stand out in micro-relief from the rest of the grain (Fig. 2.1B). These features exhibit a range of sizes and morphologies, none of which resemble rhombic microdolomites. This is not to say microdolomite inclusions are completely absent from these micrites; this inclusion type cannot be discerned with certainty based entirely on morphological criteria.

The most enigmatic feature of the Middle Ordovician micrites are continuous to discontinuous intergranular aggregations which appear resistant to the weak acid etch (Fig. 2.3). This material may form an anastomosing or branching network of varying thickness that surrounds individual micrite grains. This material is ubiquitous among shelf/ramp micrites and is restricted to the depositional matrix (Fig. 2.4A). Identical fabrics were observed in Ordovician limestones from Canada by Gillot (1969), although his "branching aggregations" are not as well developed as in micrites from Tennessee. Gillot (1969) interpreted these aggregations as representing fine grained argillaceous material that was either excluded from enlarging diagenetic calcites during lithification, or

Figure 2.3. SEM photomicrographs of Middle Ordovician shelf micrites.

A. Anastomosing intercrystalline aggregations in tidal flat lime mudstone. Note how this material has higher relief than micrite grains after acid etching. Sample MMc. Scale bar = 1 micrometer.

B. Intercrystalline material in argillaceous limestone which exhibit fabrics different from those in purer limestones. Sample MM18. Scale bar = 6 micrometers.

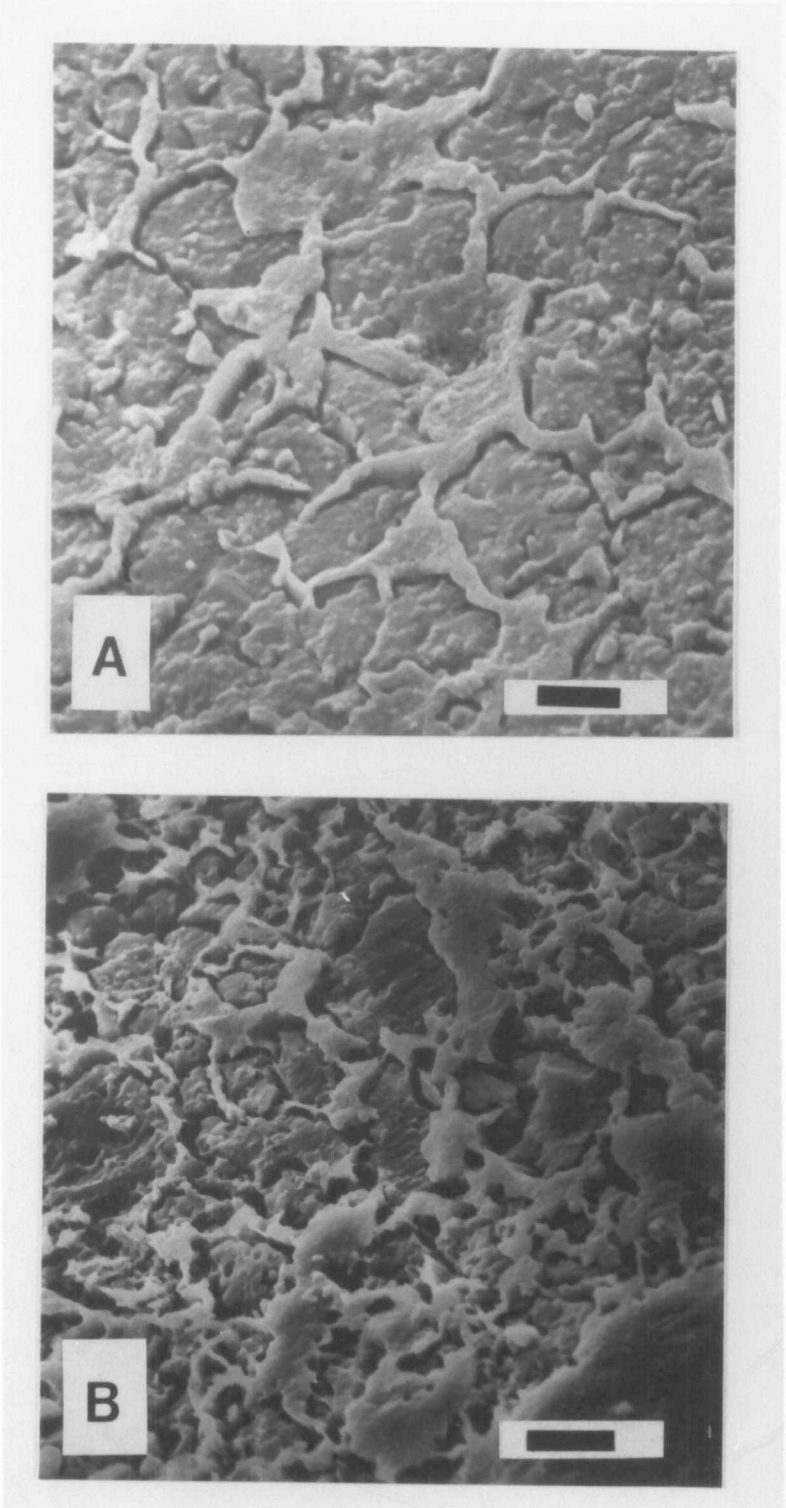

A
B

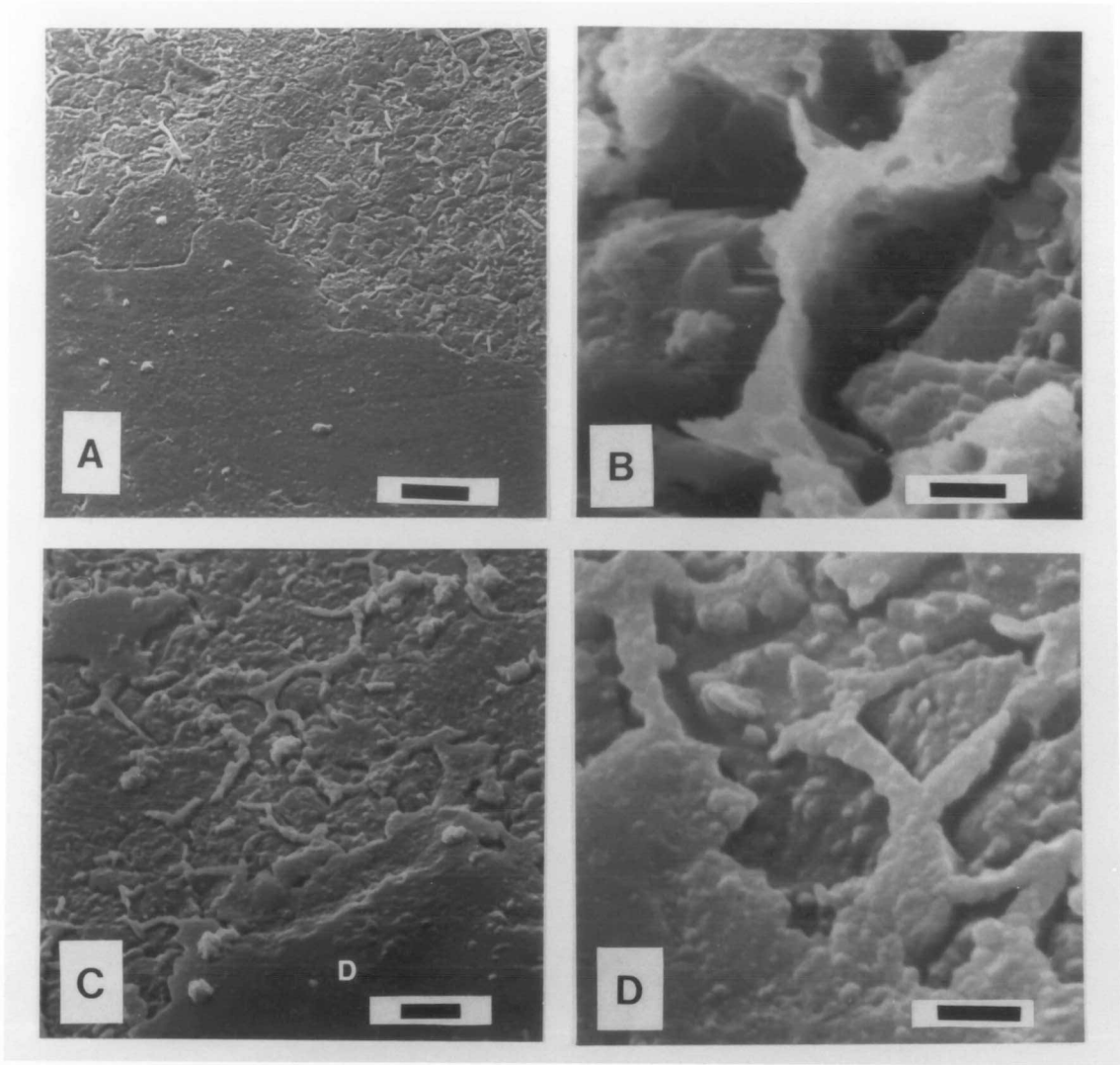
Figure 2.4. SEM photomicrographs of intercrystalline mineral aggregations in shelf micrites.

A. Margin of spar-filled pore showing the restriction of intercrystallinne aggregations to fine grained carbonate matrix. Sample MMc. Scale bar = 5 micrometers.

B. Close-up of intercrystalline material from a highly etched micrite sample. The aggregation appears to be authigenic in origin due to the lack of recognizable detrital grains which may have been excluded during calcite precipitation. Sample MM18. Scale bar = 1 micrometer.

C. Anastomosing intercrystalline aggregations that occur as uninterrupted extensions from a dolomite rhomb (D) in tidal flat lime mudstone. Sample MMc. Scale bar = 2 micrometers.

D. Outer margin of tidal flat dolomite under high magnification, showing the continuous interconnection of intercrystalline aggregations with these diagenetic dolomites. Sample MMc. Scale bar = 1 micrometer.


A
B
C
D
D

formed an open, "rigid" framework soon after deposition but prior to lithification. This interpretation of these aggregations as clays/phyllosilicates is supported by the presence of relatively high (>10% by weight) acid-insoluble residue contents in lithologies possessing this fabric. Even though either hypothesis concerning this fabric is plausible, certain aspects seem difficult to explain simply by the presence of only argillaceous material. The examination of deeply etched surfaces at high magnifications (>10,000x) did not reveal the presence of distinct clay particles (Fig. 2.4B). Also, the aggregations differ from intergranular detrital phyllosilicates identified from other micrites and microspars (see Fisher et al., 1967, Figure 94). Interstitial detrital grains typically do not extend over entire intercrystalline boundaries, and fail to exhibit an anastomosing fabric that completely envelopes grains.

In Middle Ordovician micrites, intergranular aggregations form structurally uniform extensions from dolomite rhombohedra (Fig. 2.4C and D) which resemble "amoeba-shaped dolomite crystals" in supratidal sediments examined by Carballo et al. (1987). Gillot (1969) proposed an interpretation similar to the branching aggregations for such dolomite-micrite contacts. However, the continuity of these intergranular aggregations with associated dolomites is unquestionable, and offers <u>prima facie</u> evidence for a

dolomite origin. This fabric could reflect enrichment of Mg within interstitial fluids during lithification. Since organic matter and clays can fix magnesium via complexation and ion exchange, respectively, these dolomitic extensions may actually represent a mixture of two phases.

Calcisiltite

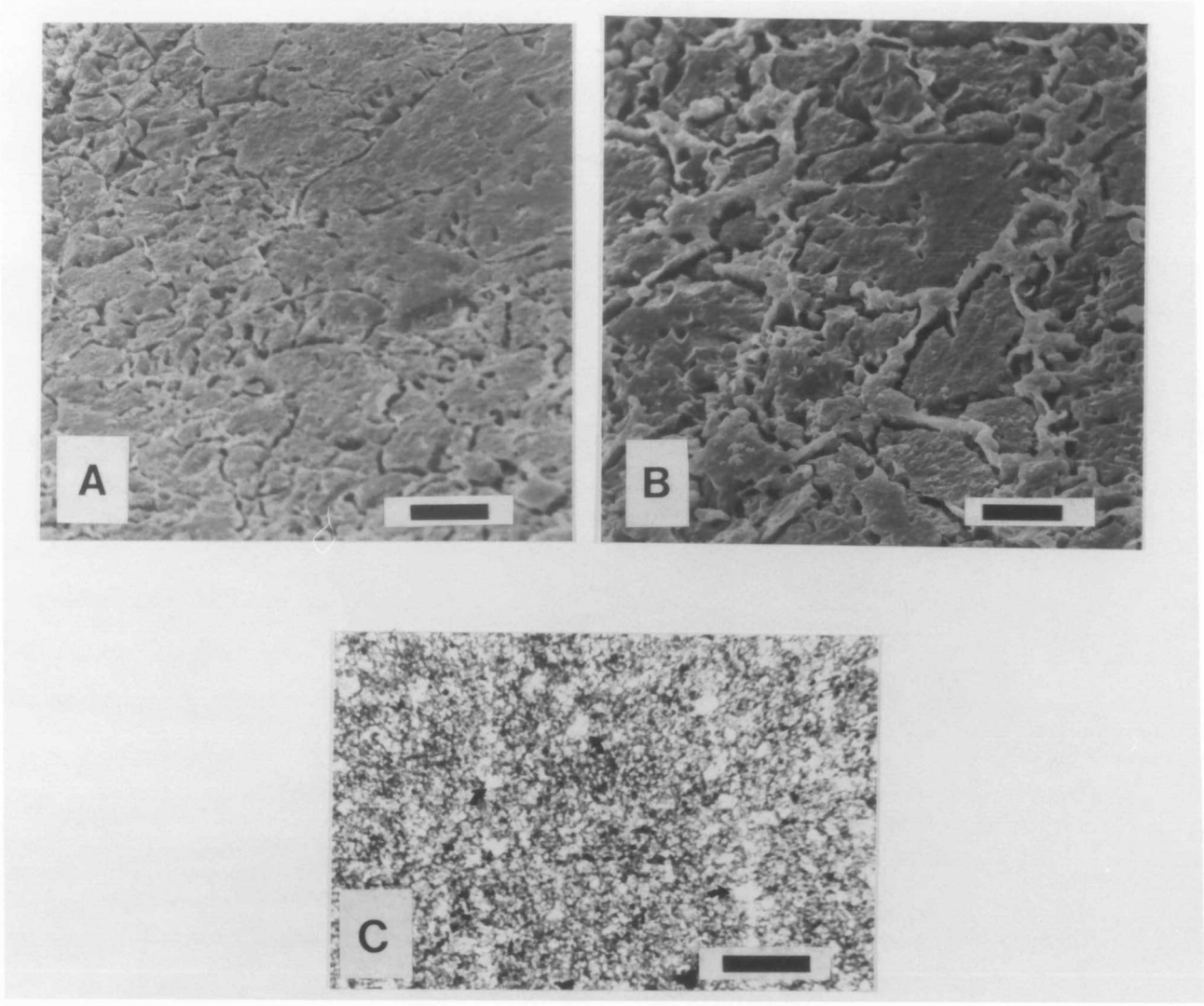
Limestone beds in the Whitesburg Formation consist of a poorly sorted mosaic of interlocking calcite grains (Fig, 2.5A and B) which are predominately of silt size (Fig. 2.6). The dominant size mode (15-20 micrometers) is within the arbitrary size range proposed by Folk (1965) for microspar (5-30 micrometers). The initial interpretation a carbonate petrographer might draw is that this mosaic is non-depositional, since as stated emphatically by Folk (1965, p. 40): "microspar is not simply a coarser mechanically-deposited silt but is definitely a product of neomorphism". However, several characteristics other than grain size fail to support a diagenetic origin; in fact, all directly refute criteria cited by Folk (1965) to support a neomorphic origin (see also Lindholm, 1969). Carbonate silt typically constitutes greater than 75% by volume of individual beds. Sedimentary bedding is preserved, and both quartz and feldspar silt grains, hydrodynamically equivalent

Figure 2.5. Thin section and SEM photomicrographs of slope calcisiltites.

A. SEM photomicrograph of typical deep-water calcisiltite. Note the poor sorting and absence of intercrytsalline material. Sample SC30. Scale bar = 20 micrometers.

B. SEM photomicrograph of calcisiltite with abundant intercrystalline aggregations which are more resistant to acid etching than calcite. Grains resemble shelf micrites, possessing no solid inclusions and only minor pits. Sample SC19. Scale bar = 10 micrometers.

C. Thin section photomicrograph of calcisiltite with admixed quartz silt grains (arrows). Sample SC20. Scale bar = 0.1 mm.


A
B
C

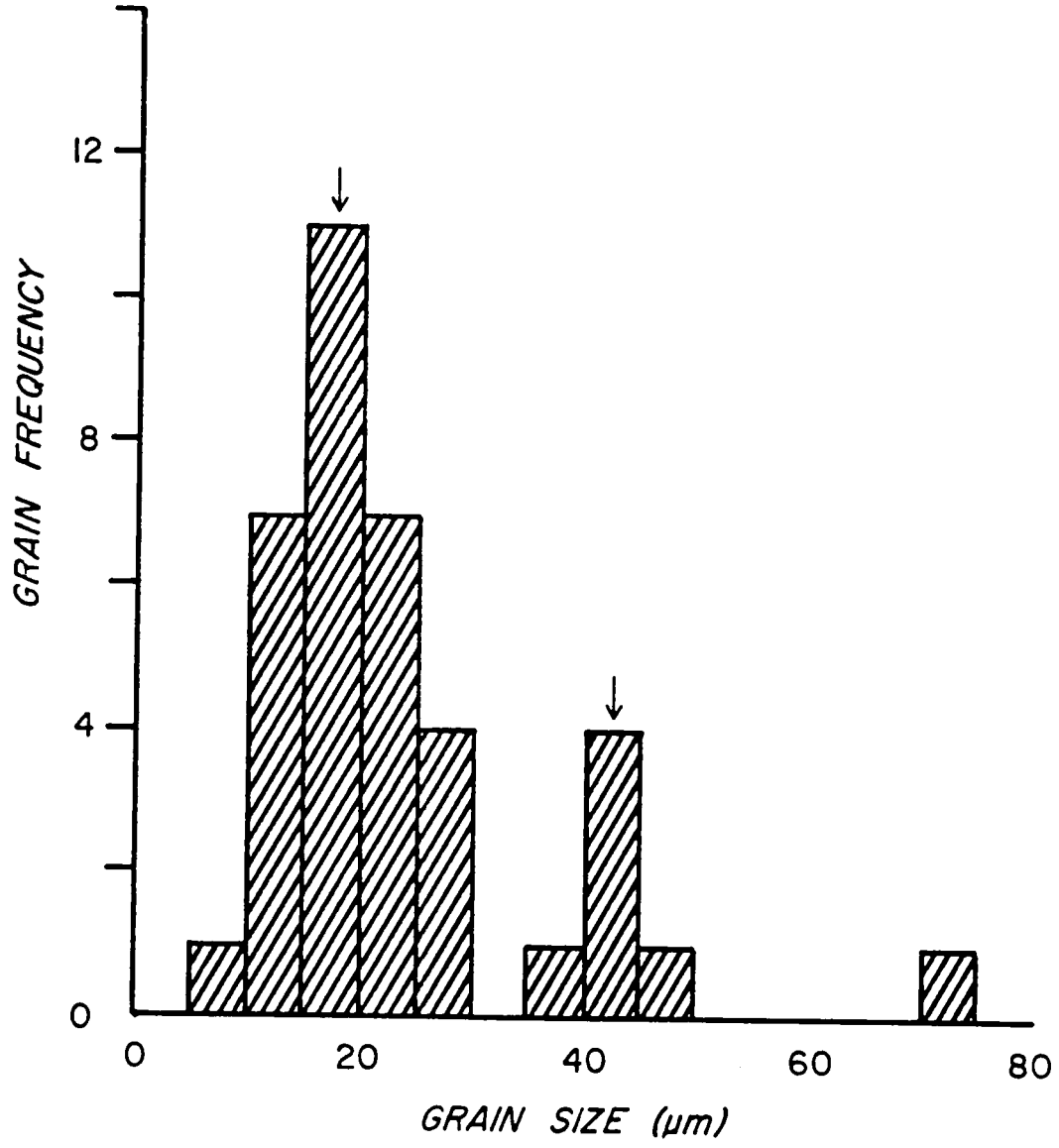


Figure 2.6. Grain size histogram of calcisiltite from the Whitesburg Formation. Sizes represent the long dimensions of individual grains measured directly from SEM photomicrographs. The distribution of sizes appears to be bimodal (arrows), with the lower size mode dominant. However, the limited number of grain measurements(N = 38) may be the cause for the observed size distribution.

in size to carbonate silt, are present (Fig. 2.5C). Using Stoke's Law, quartz grains of medium silt size would be the hydrodynamic equivalents of carbonate silt forming the dominant size mode in these Middle Ordovician limestones. Micritic peloids which form laminae within the silt matrix possess distinct grain boundaries, none of which are cross-cut by individual calcite grains. The likelihood that aggrading neomorphism may proceed to completion and still preserve details of the depositional texture and fabric seems very small. The occurrence of silt-size terrigenous clastics suggests hydrodynamic conditions were those necessary for deposition of this size fraction. Thus, the available evidence favors a depositional origin for the carbonate silt/microspar matrix in the Whitesburg Formation.

Under SEM, etched grain surfaces have a pitted appearance and contain scattered hollow inclusions (Fig. 2.5A). This type of grain texture is more abundant in the coarser particles (>40 micrometers). Grain boundaries do not truncate recognizable skeletal debris, providing further evidence in favor of a depositional origin for the matrix. Calcisiltites also possess intergranular aggregations with fabrics identical to their counterparts in shelf micrites (compare Fig. 2.5A with 2.3A). However, this material is not as ubiquitous as in the micritic matrix. Wiggins (1986) recognized "clay selvages" along crystal boundaries in

neomorphic microspars in Upper Paleozoic platform limestones. The intergranular aggregations in the Whitesburg calcisiltites do exhibit some gross similarities to this argillaceous material, but do not possess diagnostic criteria to suggest an equivalent origin.

Textural Comparison With Cenozoic Micrites

Mineralogic stabilization together with cementation in micropores appear to be the most important processes during the early stages of aragonite mud lithification (Lasemi and Sandberg, 1984; Moshier and McManus, 1986). Neomorphic calcite crystals produced have sizes that range from micrite to microspar (15 micrometers); in laboratory experiments (Moshier and McManus, 1986) a bimodal distribution of crystal sizes - 2 to 5 micrometers, 10 to 15 micrometers - was obtained following 100% transformation of an aragonite-dominated mud precursor. Diagenetic calcites often incorporate aragonite needles during growth, producing a mosaic with solid (crystal) relics and pitted appearance on polished, etched surfaces (Fig. 2.7A). Aragonite relic retention is variable and probably a function of the relative abundance of aragonite and calcite in the original mud, and diagenetic conditions - e.g., rate of mineralogic conversion, saturation with respect to aragonite,

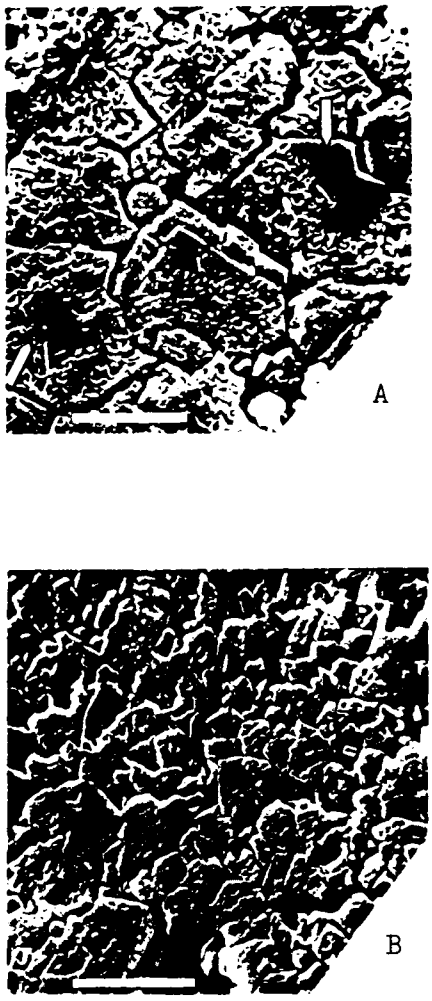


Figure 2.7. SEM photomicrographs of lightly etched Plio-Pleistocene aragonite-dominated (A) and calcite-dominated (B) micrite precursors. Note textural and fabric differences between the two samples. From Lasemi and Sandberg (1984).

presence/absence of organic coatings (Lasemi and Sandberg, 1984). Cements occluding secondary microporosity occur as unpitted, relic-poor crystals which fill pore spaces down to only a few micrometers in diameter, and may be continuous with neomorphic crystals.

Middle Ordovician shelf micrites possess features that differ significantly from these stabilized aragonitic-precursor muds. In terms of grain size, Middle Ordovician samples are dominated by "micrite" and contain neither an abundance of microspar-size crystals or a bimodal distribution (Fig. 2.2B). Calcite crystals do not contain identifiable solid (aragonite) inclusions, but instead have an unpitted appearance on both lightly and deeply etched surfaces. Based on these observations, Middle Ordovician samples more closely resemble micrites interpreted by Lasemi and Sandberg (1984) as having been predominately magnesian calcite. These micrite precursors generally lack microspar-sized crystals and pits, and possess no needle-shaped relics (Fig. 2.7B). Thus, when compared to Quaternary standards, Middle Ordovician micrites have textures and fabrics which favor a calcite-dominated precursor mineralogy.

The dominant grain size of less than 30 micrometers in Whitesburg calcisiltites might initially suggest an aragonite-dominated precursor. The previous discussion

concerning the probable sediment size together with the general lack of pitted crystal surfaces in polished, etched surfaces does not support this inference. Excluding size, a comparison of Middle Ordovician calcisiltites with stabilized Quaternary micrites would also suggest a calcite precursor. However, since no studies examining the textures of modern original carbonate silt exist with which to compare these Middle Ordovician samples, scanning electron microscopy provides no definite clues as to the primary mineralogy of these sediments.

Elemental Geochemistry of Shelf Micrites

Probable Origin of Micrite Precursor

Lime muds which accumulated on broad, shallow-water epicontinental shelves may have formed by physicochemical precipitation from restricted oceanic waters and/or breakdown of organismal calcium carbonate via numerous processes. Where inorganic precipitation has been suggested as an origin for modern lime muds, it appears to be associated with areas of elevated salinity resulting from evaporation as waters travel across the platform (Cloud, 1962; Broecker and Takahashi, 1966). Sedimentary structures

along with biotic and geochemical gradients should reflect the former presence of shelf-wide changes from open marine to hypersaline conditions. Inner shelf Ordovician facies do not contain evaporite minerals or pseudomorphs after evaporites. Faunal gradients characterized by the loss of stenohaline elements and their "replacement" by communities dominated by eurytopic taxa in an on-shelf direction have not been detected in this portion of the Chickamauga Group (Sickafoose, 1979; Weiss, 1981). Sodium concentrations from inner shelf facies average less than 150 ppm, significantly below values indicative of hypersalinity in Phanerozoic limestones (Veizer et al., 1977). These data, together with the fact that physicochemical precipitation is not widespread in modern humid carbonate environments suggests that the majority of the lime mud in this Ordovician sequence is of biotic origin.

Processes causing the breakdown of calcareous hard parts have been mentioned in a previous section, and are discussed more fully by Matthews (1966). Both mechanical and biological processes were probably active to varying degrees on the Middle Ordovician shelf; however, direct observations can only substantiate two of these processes. Near-shelf margin skeletal sands contain abraded and worn bryozoan, echinoderm, arthropod and articulate brachiopod fragments, indicating mechanical breakdown and trituration

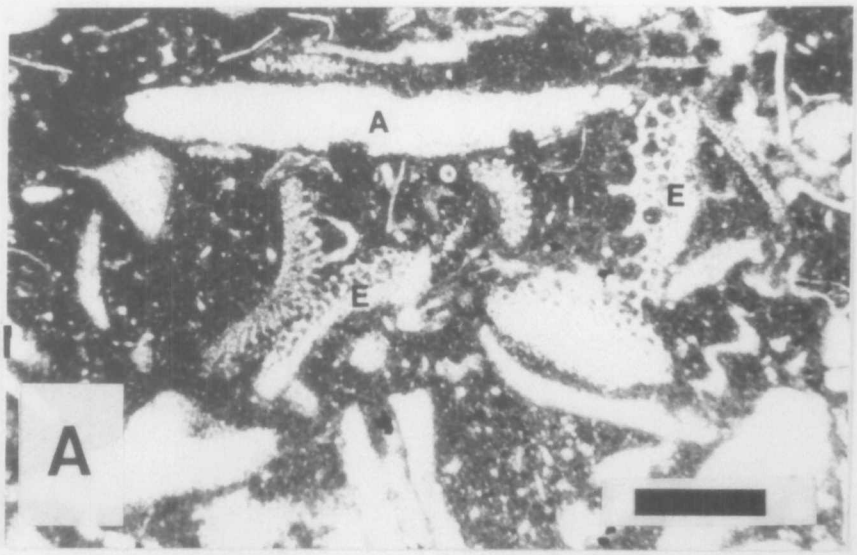
under turbulent conditions. Mud particles formed in this environment were probably dispersed across the shelf by tidal and storm currents similar to shelf-margin areas off Belize (Matthews, 1966). Bioerosion of allochems by the activities of endolithic organisms, evidenced by micrite- and spar-filled borings 50 to 500 micrometers in diameter, appears to have been another mud-generating process in most shelf facies. The excavated cavities exhibit a variety of morphologies from simple closed-end tubes (Fig. 2.8A) to branching tubules (Fig. 2.8B) some of which resemble probable sponge borings from other Ordovician strata (Lindstrom, 1974; Podhalanska, 1984). Particles exposed on the bottom for appreciable time periods contain an abundance of borings which may create elaborate galleries. These features are not restricted to particular substrates, although relative abundances appear to be highest in echinoderm ossicles. A recent study by Tudhope and Risk (1985) of modern lagoonal carbonate sediments indicates that approximately 25% of newly deposited grains experience boring, the intensity of which is largely dependent upon rates of sediment accumulation.

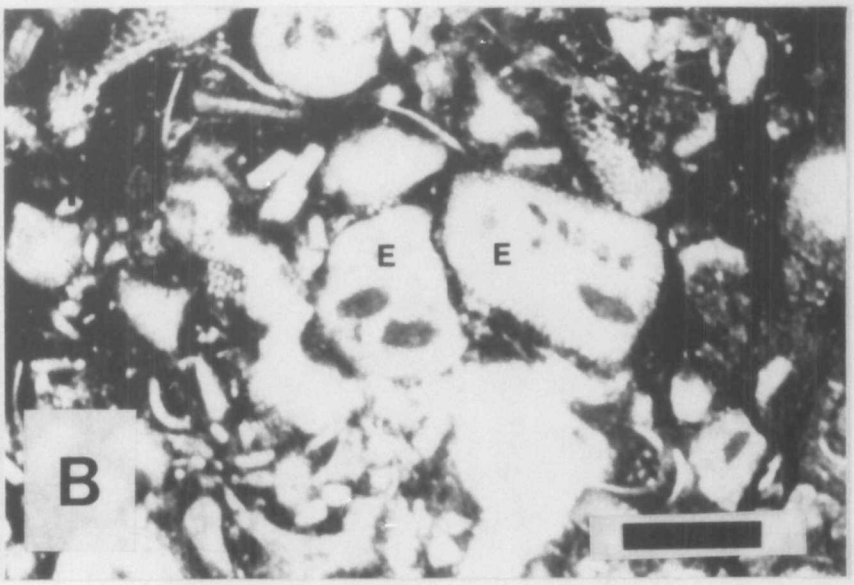
Finally, calcareous algae may not have been important mud contributors to Middle Ordovician shelf facies. Thalli of algal genera (excluding encrusting forms) constitute less than 10% by volume of shelf and ramp facies based on point

Figure 2.8. Thin section photomicrographs of bored skeletal grains from shallow-water limestones.

A. Intensely bored echinoderm (E) and arthropod (A) grains, with voids infilled by micritic sediment/cement. Sample MM3. Scale bar = 0.25mm.

B. Tubular, micrite-filled macroborings in disarticulated echinoderm plates (E). Sample SC17. Scale bar = 0.25mm.


A
E
E
A


E
E
B

count analysis. The highest abundances are found in shallow ramp facies of the Lenoir Formation where the flora is dominated by the problematic taxon Nuia. Chlorophytes and rhodophytes with originally magnesian calcite or aragonite thalli (see Chapter 3) are rare in samples from the onlap facies. Thus, calcareous algae may not have been important mud contributors to Middle Ordovician shelf facies.

Equilibration Trends for Aragonite- and Calcite-Dominated Micrite Precursors

Even though both strontium and magnesium are depleted in the solid phase during meteoric diagenesis, they are still the most applicable trace constituents for ascertaining original mineralogy. Using published partition coefficient values, the equilibrium concentrations of both elements in shallow marine aragonite and calcite are (Veizer, 1983):

ARAGONITE:	Sr,	7000-9400 ppm
	Mg,	750-6300 ppm
CALCITE:	Sr,	1000 ppm
	Mg,	16,300-75,400 ppm

The range in magnesium concentrations reflects variation in the magnitude of K_{cal} for calcites and aragonites precipitated directly from supersaturated solutions. The

differences in concentrations given for the inorganic precipitates above are comparable to those of calcareous skeletons secreted by marine organisms.

With these primary compositional differences in mind, idealized equilibration "trends" were derived for aragonite- and magnesian calcite-dominated micrite precursors (Fig. 2.9). These "trends" represent a simplified compositional path for carbonate muds undergoing equilibrium stabilization to diagenetic low-Mg calcite in meteoric waters. The qualifier "equilibrium" is important since the final element concentrations, and thus the slope of the trend in Sr-Mg compositional space, is based on the homogeneous distribution law. The method used to determine the Sr and Mg concentrations of carbonate muds and micrites is given in Appendix C. However, there are several caveats that should be kept in mind. Based on arguments in the previous section, it has been assumed the lime mud was completely biogenic in origin. The initial trace element concentrations are derived from representative concentrations in extant marine species of each taxanomic group which may have contributed to the mud fraction, except for the trilobites which are given values identical to cirripeds (ostracodes). Since the homogeneous distribution law was used to determine the final (diagenetic) compositions, it has been assumed that the majority of

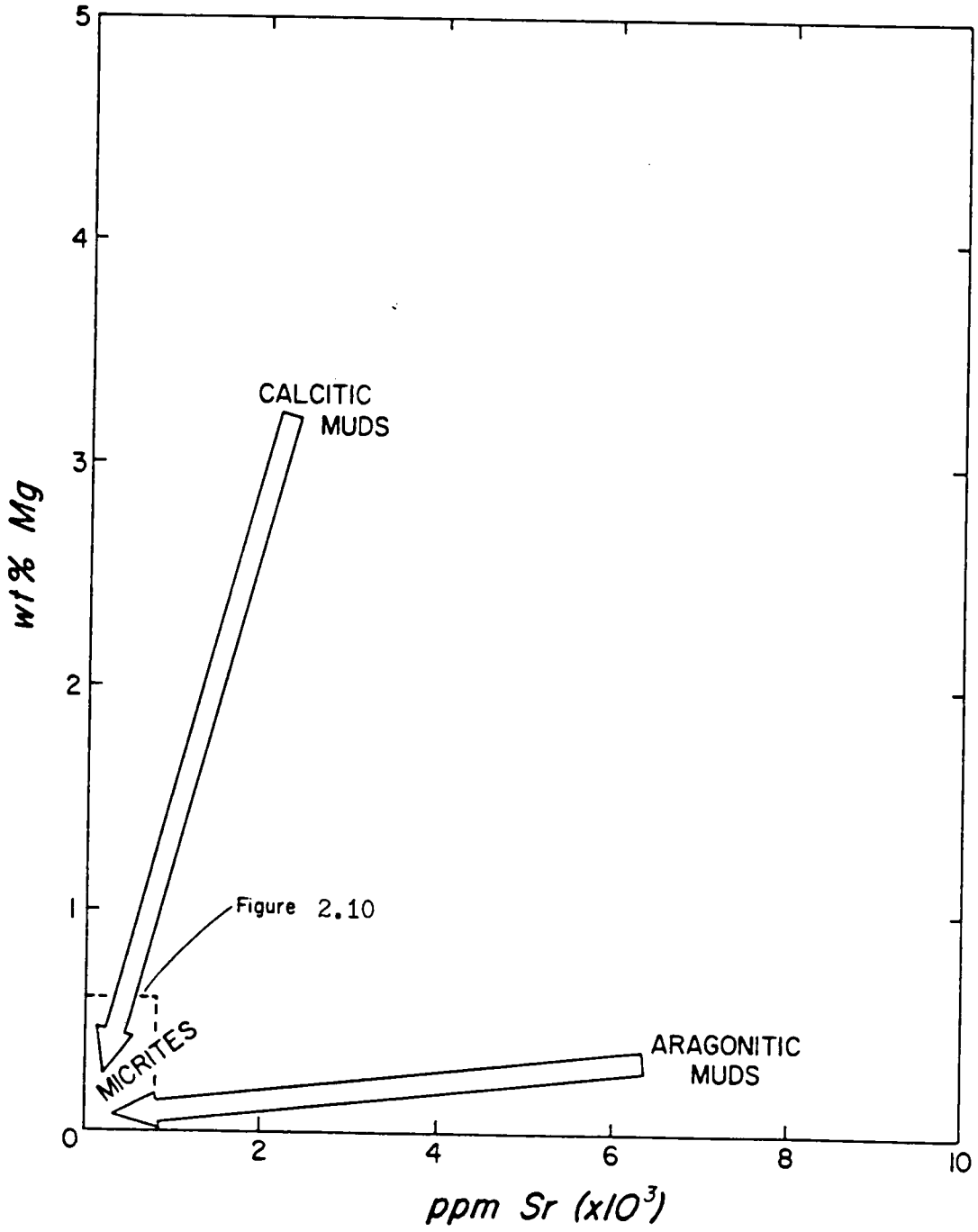


Figure 2.9. Trace element stabilization 'trends' for hypothetical calcite- and aragonite-dominated lime muds.

strontium and magnesium substituted for Ca ions in the growing crystal lattice. Other methods of incorporation such as interstitially between lattice planes, or occupying defect positions in the crystal structure are believed to be of only minor importance. For divalent cations such as strontium and magnesium the assumption of lattice substitution is warranted. Lastly, the meteoric-phreatic stabilization of lime muds (and allochems) is usually accomplished in a system characterizied by a low solute index (SI), where the SI is a measure of the relative proportion of the trace element signature derived from the external fluid vs. that derived from the carbonate precursor (Veizer, 1983). Under low SI conditions, the trace component has been repartitioned between the precipitating diagenetic calcite and external fluid according to the distribution coefficient.

In Figure 2.9, the equilibration of aragonite and magnesian calcite muds to micrite are depicted as arrows which are oriented differently in Mg-Sr compositional space. However, because of the incipient compositional differences between the lime-mud end members the "slope" for the magnesian calcite precursor is much greater than the "slope" for the aragonite precursor. The magnesian calcite-dominated precursor loses more than two weight percent (20,000 ppm) Mg, but an order of magnitude less Sr;

the relative depletion magnitudes are reversed for the aragonite-dominated precursor. This fundamental difference in compositional variation is the key to the interpretive power of such a diagram in mineralogical studies.

Strontium and Magnesium Composition of Micrites

Micrite separates from lower Middle Ordovician shelf facies and younger Chickamauga Group strata were analyzed for strontium, magnesium and manganese using atomic absorption spectroscopy (Table 2.1). Sample preparation and analytical conditions are discussed in more detail in Appendix B. Micrites of the younger Middle Chickamauga Group were from samples collected by Wedekind (1986).

Strontium and magnesium concentrations of micrites define a linear trend which closely resembles the magnesian calcite equilibration trend (Fig.2.10). Even micrites with relatively high strontium concentrations (>500 ppm) are located closer to this trend than the corresponding aragonite trend. The high degree of association of Middle Ordovician micrites with the idealized equilibration trend for magnesian calcite strongly favors an originally magnesian calcite precursor mineralogy for lime muds accumulating on the shelf. However, the probability is low that the original mud was totally calcitic. Since the

TABLE 2.1

TRACE ELEMENT COMPOSITION OF MIDDLE ORDOVICIAN SHELF MICRITES

	Formation	ppm Mg	ppm Sr	ppm Mn
Inner Shelf Facies	Lincolnshire	3340	435	137
	"	3000	483	127
	Benbolt	3530	302	153
	"	3490	294	146
Outer Shelf Facies	Lincolnshire	2810	230	118
	"	1550	175	98
	Rockdell	3680	457	164
	"	2660	208	232
	"	3550	268	269
	Holston	2110	135	186
	"	2600	176	508
	"	2210	179	470
	Rockdell	2180	134	149
	"	2450	170	149
	"	2590	193	157
	"	3060	277	226
	"	2390	164	159
	"	2040	166	168
	"	3440	266	272
	"	1710	153	191
	Holston	2770	217	245
	"	2370	177	277
	"	2510	188	255
	"	2410	209	356
	"	2400	134	323
	"	2730	148	203
Middle Chickamauga Group	Benbolt	5950	580	169
	"	5360	543	159
	Wardell	3030	339	86
	"	3830	336	49

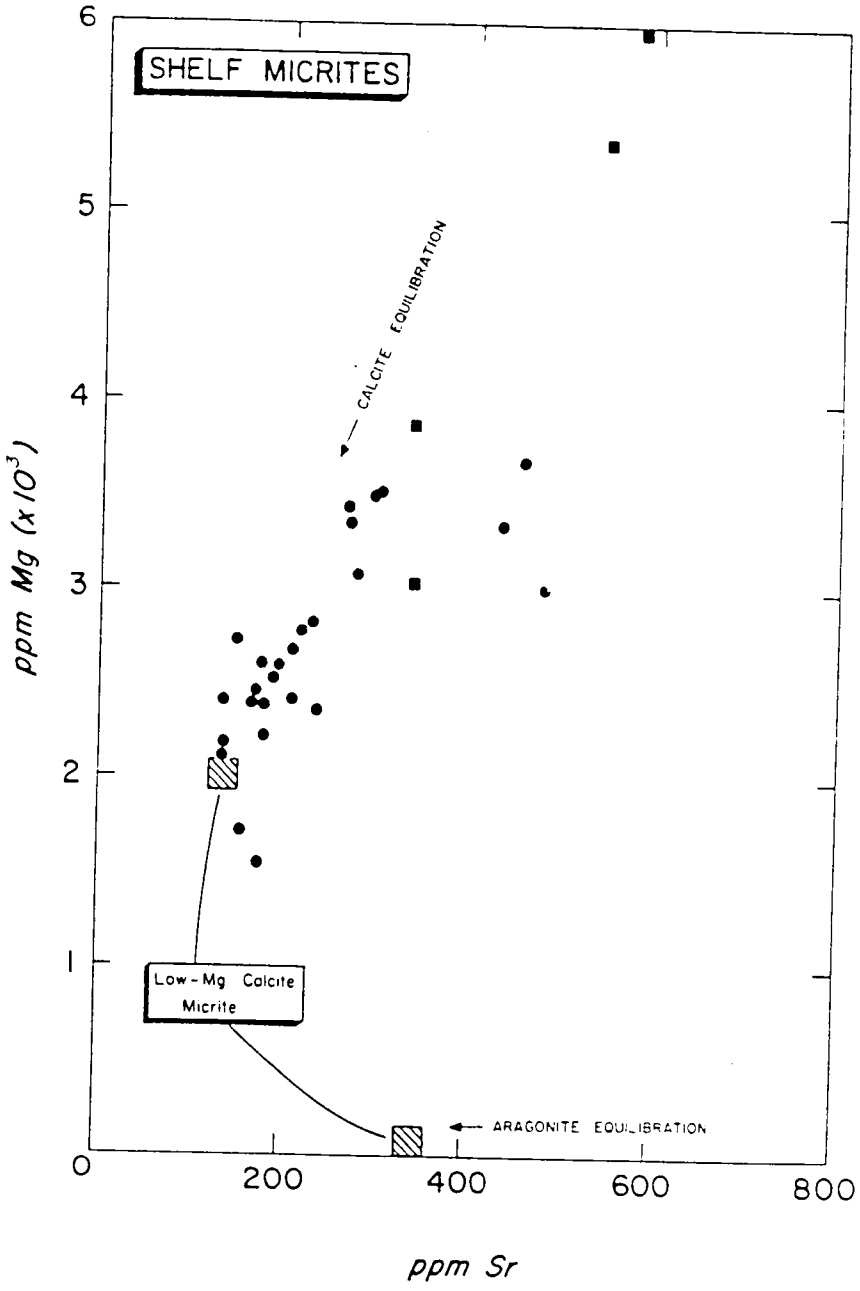
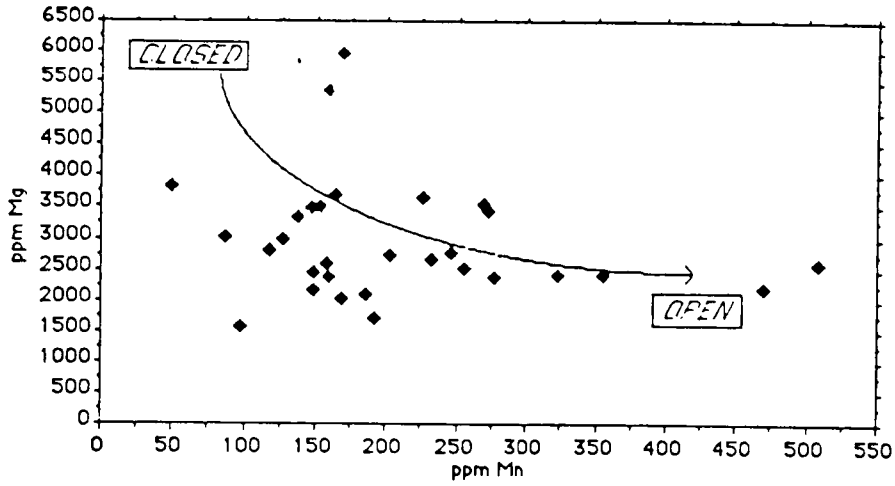


Figure 2.10. Strontium and magnesium concentration of Ordovician shelf micrites plotted with respect to calculated compositional end members for originally aragonitic and calcitic muds. Samples: ● = lower Chickamauga Group (this study); ■ = middle Chickamauga Group (Wedekind, 1986).

dominant carbonate phase will largely control the resultant element composition, especially in systems where the SI is low, the correspondence between the idealized trend and the actual data indicates that the most abundant polymorph in the original lime muds was magnesian calcite.

Comparison of inner and outer shelf micrites from the Lower Chickamauga along with Middle Chickamauga samples indicates that the dominant precursor mineralogy was invariant throughout the majority of Chickamauga deposition. Inner shelf micrites have compositions comparable with contemporaneous outer shelf micrites, suggesting a high degree of mineralogic uniformity over the entire shelf. Trace element variations which might reflect areal changes in the relative abundance of magnesian calcite and aragonite are not shown by the geochemical data. Micrites from overlying Middle Chickamauga shallow subtidal facies also fall in close proximity to the calcite equilibration trend. These data indicate no apparent change in lime mud mineralogy during the majority of Middle Ordovician sedimentation. Some micrites, particularly samples from the inner shelf and Middle Chickamauga, have experienced a lesser amount of depletion than outer shelf micrites. This enrichment may be due to magnesian calcite $\longrightarrow$ calcite transformation (and cementation) of inner shelf micrites with pore fluids more marine in composition. Another

possibility is that micrites may have undergone lithification at different rates. Kinetic effects have been shown to affect the partition coefficient for strontium in calcite (Lorens,1981); however, it is unknown if there are similar effects on the partitioning of magnesium. A third explanation may be that the diagenetic system in inner shelf micrites was less chemically open during mineralogic stabilization. One way to test this hypothesis would be to compare manganese concentrations between enriched and depleted micrites. Ideally, if the carbonate system was more open during lithification manganese concentration should be relatively higher and vice versa. Plots of (Mg,Sr) vs. Mn (Fig. 2.11) show an apparent negative correlation which suggests system openness was a contributing factor in the resultant trace element signature by removing strontium and magnesium from reaction sites and depositing manganous ions from the external solution. Element variations for both strontium and magnesium closely resemble the equilibration trends derived by Brand and Veizer (1980) for originally magnesian calcite phases. The association of high manganese micrites with shelf-margin buildups suggests the interaction of carbonate matrix with metal-rich reducing waters which probably originated in the adjacent shale basin (see Chapter 5).



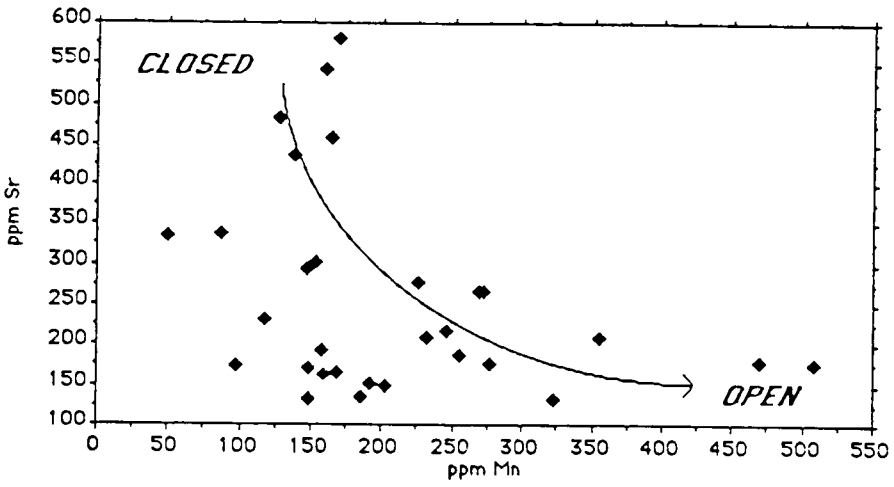


Figure 2.11. Trace element equilibration diagrams for shelf micrites (after Brand and Veizer, 1980). Since manganese is enriched and strontium/magnesium depleted in diagenetic calcites, as indicated by their respective k_{cal} values, the arrow indicates the change from low solute index (i.e., closed) to high solute index (i.e., open) systems. These changes in the diagenetic environment assume manganese is transported into sediments by pore waters.

Comparison with Other Phanerozoic Micrites

The most desirable approach to test the utility of Sr vs. Mg plots as mineralogic discriminators of lime muds would be to compare the composition of Quaternary micrites because the mineralogy of these samples can be well constrained. Geochemical investigations of modern micrites are, based on a literature search, non-existant at the present time. [A forthcoming paper in the Journal of Sedimentary Petrology will examine the petrography and geochemistry of Phanerozoic micrites (P. Sandberg, pers. comm.).] Lasemi and Sandberg (1984) give strontium and magnesium concentrations for three samples representing both aragonite- and magnesian calcite-dominated precursors (Fig. 2.12). Element concentrations for each inferred mud precursor are associated with their respective equilibration trend. Originally aragonitic muds contain relic needle inclusions, the presence of which probably accounts for the relatively high strontium concentrations in these samples. Aragonite precursors are enriched 2-3x in magnesium with respect to the idealized equilibration trend. This enrichment may be result of one or more of the following:

(1) abundant cement-filled microporosity;

(2) higher solute index with respect to magnesium (but not strontium);

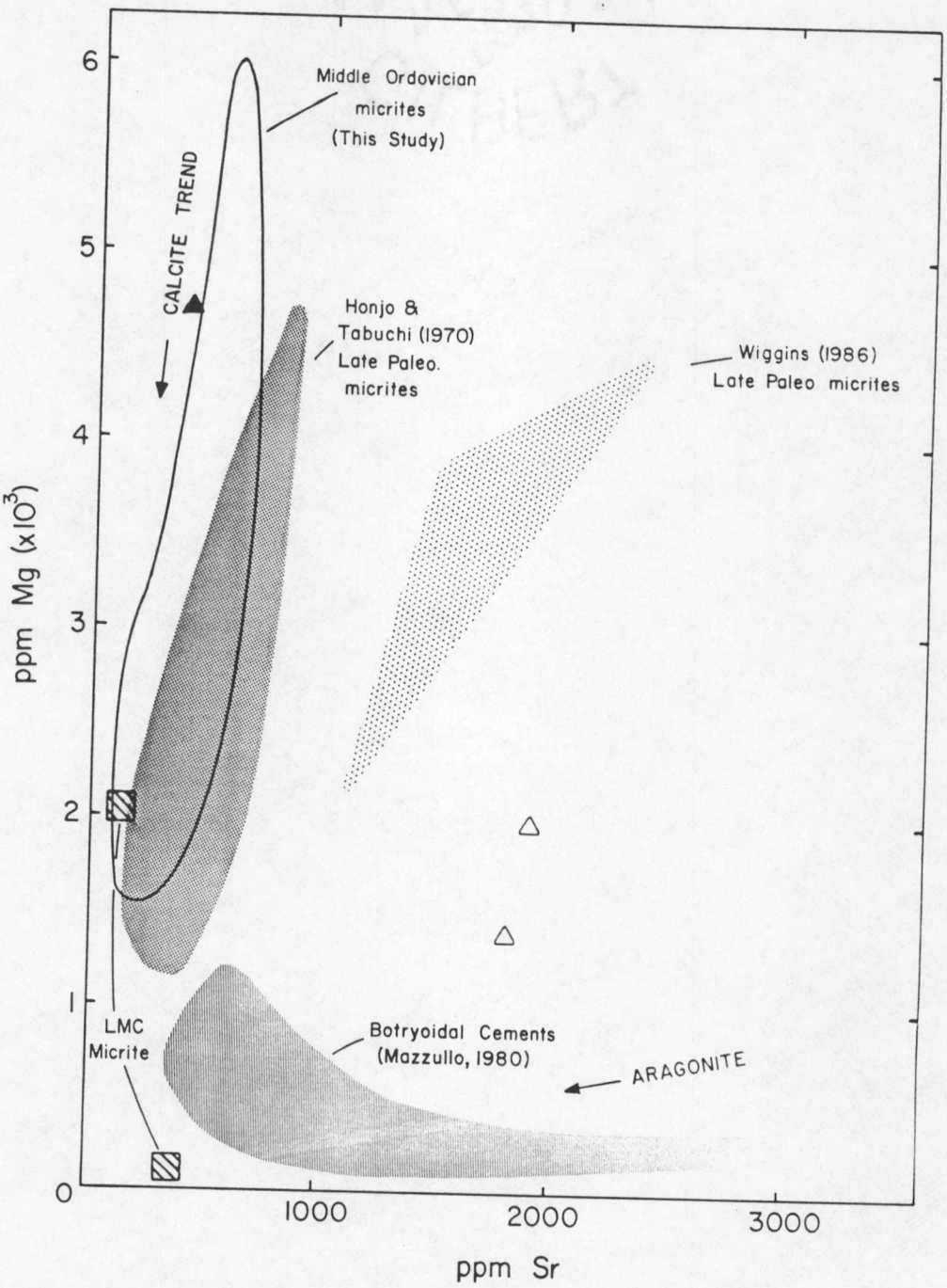


Figure 2.12. Elemental geochemistry of Ordovician micrites compared with other Phanerozoic micrites, and botryoidal cements which are interpreted as originally aragonite. The composition of stabilized calcite and aragonite micrite precursors are shown for reference purposes. Open and filled triangles are compositions of aragonite- and calcite-dominated micrite precursors, respectively, given in Lasemi and Sandberg (1984).

(3) significant magnesian calcite component in the original sediment.

The last factor should not be discounted as trivial in Quaternary micrites. Hussieni and Matthews (1972) showed that platform micrites from the Bahamas, long considered to be an area of primarily aragonite mud deposition, may also contain a significant amount (max. 60% by weight) of magnesian calcite in the mud fraction. Thus, even in environments where muds are presumed to be aragonite-dominated, magnesian calcite contributed by the breakdown of skeletal parts may also be important.

Upper Paleozoic micrites analyzed by other workers (Honjo and Tabuchi, 1970; Wiggins, 1986) occur as fields located between the two equilibration trends (Fig. 2.12). The samples from Honjo and Tabuchi (1970) define a linear trend which appears to have pivoted about the calcite trend to slightly lower magnesium concentrations. Micrite analyses by Wiggins (1986) of Pennsylvanian limestones are situated at even lower magnesium, and correspondingly higher strontium, concentrations. Assuming that the stabilization "trends" define the compositional limits of the original mud precursors and similar diagenetic conditions during lithification, the fields depicted represent micrites which possess different proportions of aragonite and magnesian calcite in the original sediment. The high-Sr micrites of

Wiggins (1986) are from interior-platform phylloid algal mudmounds. These enigmatic calcareous algae probably secreted high-Sr aragonite thalli which morphologically resembled the skeletons of modern codiaceans (see Chapter 3). Since the diagenesis of the matrix appears to have been characterized by a very low SI, the compositional field accurately reflects the stabilization of lime muds with a significant aragonite component. No additional diagenetic data is available on micrites analyzed by Honjo and Tabuchi (1970).

Botryoidal-cement fans believed to have been originally aragonitic provide comparative data for the aragonite-dominated precursor micrites. Element concentrations define a field that is almost completely below 0.1 weight percent (1000 ppm) magnesium and extends asymptotically along the strontium axis (Fig. 2.12). Cements which contain relict primary (aragonite?) fibers have strontium concentrations similar to inclusion-bearing neomorphic microspars analyzed by Lasemi and Sandberg (1984). Magnesium increases slightly in cements with few (if any) recognizable relict fibers. These relict-poor cements offer some idea of the probable compositions of aragonite-precursor micrites, albeit the stabilization process is not perfectly analogous between the two components. Additional geochemical data are necessary to

more fully access the utility of element diagrams such as these in predicting the relative abundances of original aragonite and magnesian calcite in lime muds.

Geochemistry of Slope Calcisiltites

Probable Origin of Carbonate Silt

Shelf-derived calcisiltites are interpreted as the fine trituration product of magnesian calcite echinoderm debris, for the following reasons:

1) Shelf-margin facies which may have provided a source of fine grained sediments consisted of poorly to well-washed skeletal sands dominated by echinoderms with subordinate bryozoans, arthropods and other marine taxa. Since these sediments were predominately magnesian calcite in mineralogy, it is highly probable sediments transported basinward had a comparable composition (see Boardman and Neumann, 1984).

2) The mechanical trituration of magnesian calcite echinoderm ossicles is known to yield silt-size particles with unit extinction (Matthews, 1966). Laboratory experiments by Chave (1964) showed echinoderm plates to be

among the least durable marine skeletons. The microstructure of ossicles may allow for comminution to finer particles under turbulent conditions

3) Echinoderm silt would provide suitable host substrates for the nucleation of optically-continuous rim cement during lithification. Diagenetic processess would destroy features such as concave edges characteristic of comminuted echinoderm debris, and produce a homogeneous grain texture.

Strontium and Magnesium Composition of Calcisiltites

If these calcisiltites are the trituration product of magnesian calcite bioclasts, their trace element compositions might record this precursor mineralogy as was apparently the case in shelf micrites. Strontium and magnesium concentrations were compared with a magnesian calcite stabilization "trend" similar to the one derived for micrites. The method used to determine the composition of original sediment and diagenetic calcite is given in Appendix B.

The calcisiltites analyzed exhibit considerably more variation in both strontium and magnesium values compared to contemporaneous shelf micrites (Fig. 2.13). There has been a noticeable shift of the calcisiltites to higher strontium

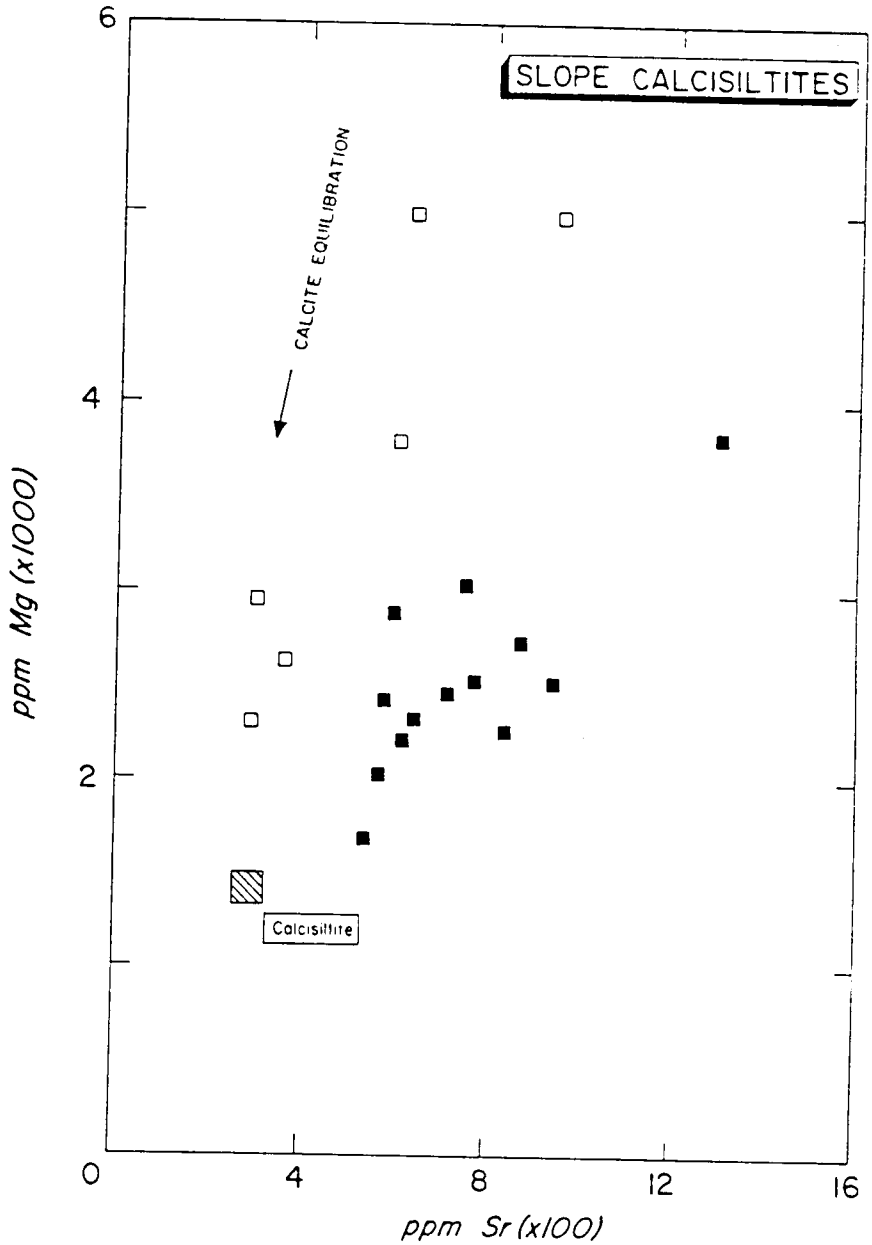


Figure 2.13. Strontium and magnesium concentration of Ordovician slope calcisiltites from the Whitesburg Formation, plotted with respect to the calculated compositional end member for originally calcitic sediment. Localities: ■ = Silver City; □ = Martin Mill Pike.

concentrations relative to those assuming meteoric diagenesis of a magnesian calcite precursor in a system with a low solute index. The criteria discussed by Lasemi and Sandberg (1984) would appear to indicate an originally aragonitic mineralogy due to the high absolute strontium values (generally >600 ppm). If precursor sediments were originally calcite, then these data question the use of absolute element concentrations when interpreting the mineralogical precursor, particularly in sequences were the diagenetic histories are either unknown or not well understood.

Diagenetic waters which filled interstitial pores during lithification were either connate or modified connate in nature. Using the homogeneous distribution law, the strontium concentration of low-Mg calcite precipitated from seawater is 350 ppm. (The molar ratio of Sr to Ca in marine water is from Veizer, 1983, Fig. 3.7.) Magnesium contents of bank-derived magnesian calcite grains which were stabilized in the deep marine realm range from 6300 to 7300 ppm (Gomberg and Bonatti, 1970). Assuming equivalent seawater compositions during the Ordovician, slope calcisiltites have bulk Mg/Sr ratios below those of calcites precipitated from marine waters (Fig. 2.14). Compactional features, presence of pseudospar, and bed-normal calcite veinlets indicate complete lithification was not attained

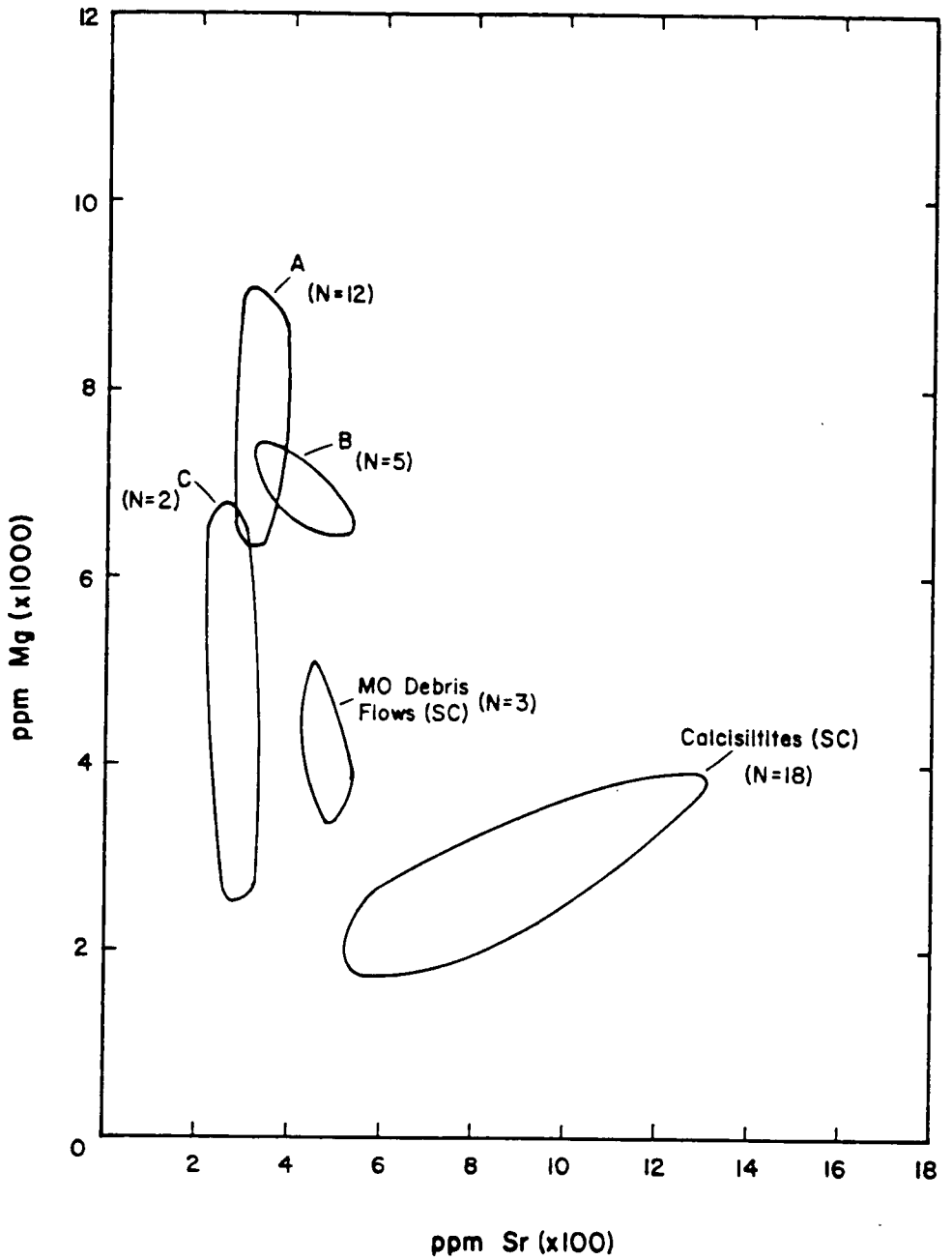


Figure 2.14. Elemental geochemistry of Ordovician calcisiltites from this study compared with modern and ancient diagenetic calcites precipitated from deep marine waters. Sources of data: A - radiaxial calcite cement (Saller, 1986); B - stabilized Mg-calcite skeletal grains (Gomberg and Bonatti, 1970); C - Devonian limestones (Tucker, 1973); Ordovician sediment gravity flows (this study).

until after burial.

Geochemical data indicate the depletion of Mg at the expense of Sr during burial diagenesis. The deviation from the idealized stabilization "trend" eliminates the possibility of this signature resulting from recrystallization and precipitation of carbonate minerals. Clay minerals in shales which enclose individual carbonate beds are active adsorbers and desorbers of ions during diagenesis. Experiments conducted by Bath (1977) showed the early release of strontium into Mg-K-Na-Cl solutions. The exchangeable amounts of strontium are on the order of 10's to 100's of micrograms per gram of clay. In addition to this early diagenetic desorption, strontium may also be released with other ions during clay mineral transformation reactions. Whereas Sr ions are poorly fixed by clays, diagenetic conditions may allow for the sorption of Mg ions by these same sediments. Drever (1971) suggested the amount of magnesium incorporated into non-exchangeable sites during early diagenesis by smectites is related to redox conditions, with more oxic sediments having lower amounts of magnesium. Clays possessing chlorite interlayers and discrete chlorites may form during later diagenesis in Mg-rich fluids (Dunoyer de Segonzac, 1970). Mineralogical analyses of shales indicate the presence of abundant mixed-layer illite-smectite, irregular and regular

mixed-layer chlorite-smectite and chlorite (see Chapter 5). Assuming the detrital clay fraction was dominated by smectite, the presence of chloritic clays indicates the net addition of magnesium during diagenesis.

The diagenetic history of slope carbonates favors a system more open with respect to both magnesium than strontium. The desorption of Sr from clays increased its concentration in interstitial fluids, while stabilization of Mg-calcite released both Mg and Sr into adjacent carbonates. Assuming low fluid flow rates (mm/yr), the difference in dissolved magnesium and relatively high porosities (<50%) would have permitted diffusion of this element into shales. The restricted flow conditions would have been incapable of transporting strontium from reaction zones, thus producing the enrichment of this element in diagenetic calcites. Comparison of Sr concentrations with other geochemical data shows only minor compositional change between early and late diagenetic calcites, indicating relatively high pore water Sr^{2+} levels throughout the diagenetic history.

Summary of Micrite and Calcisiltite Petrogenesis

Trace element analyses indicate the lithification of fine grained carbonates may or may not be related to the original mineral precursor. Shelf micrites lithified during shallow meteoric diagenesis form a Sr-Mg compositional trend which reflects the removal of both elements from sites of low-Mg calcite precipitation (Fig. 2.15). Deep-water calcisiltites with an original mineralogy identical to micrites experienced strontium retention relative to micrites, which reflects the sorption properties of clay minerals in bounding shales.

Discussion

Trace Element Equilibration Trends for Ancient Micrites

In their paper on the chemical diagenesis of limestones, Brand and Veizer (1980) defined equilibration trends for aragonite, calcite and magnesian calcite components in terms of strontium and manganese (see their Fig. 9). Skeletal allochems for which there exists a general consensus with respect to original mineralogy were

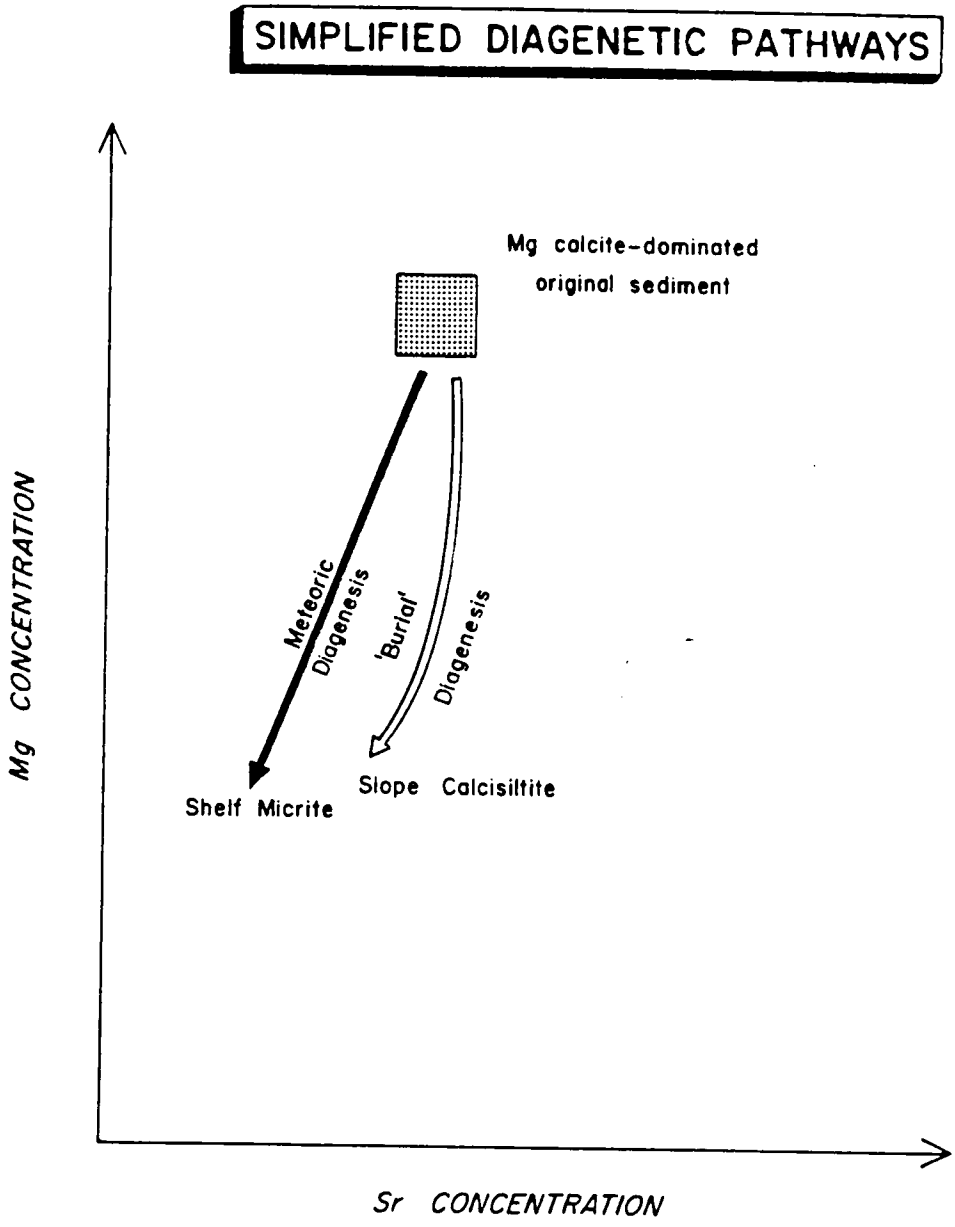


Figure 2.15. The effects of separate diagenetic histories on Sr and Mg composition of fine grained carbonate sediments.

chosen as standards for calcite and magnesian calcite phases. If necessary, petrography could be used to substantiate these interpretations. For their aragonite standard the authors selected micrites because (p. 1226) "by analogy with their Holocene counterparts they are believed to be stabilized aragonitic muds". However, based on other studies of Phanerozoic micrites (this study; Lasemi and Sandberg, in prep.) the assumption of an aragonite mud precursor should not be based entirely on uniformitarian principles, but be made only after careful distillation of empirical data.

Upon examination of the compositional trends of Brand and Veizer (1980), it is apparent a significant degree of overlap exists with respect to these two elements. Although this similarity may reflect equivalent compositional trends for these polymorphs during meteoric diagenesis, it is also possible that both may represent stabilization of a single polymorph (magnesian calcite) under different conditions. This "uncertainty" is made more evident by plotting the compositions of Middle Ordovician micrites with respect to these trends (Fig. 2.16).

Not withstanding the work of Brand and Veizer (1980), in light of recent work on micrites it is necessary to find a different component to use as the aragonite-mineral standard. The variability which appears to have existed in

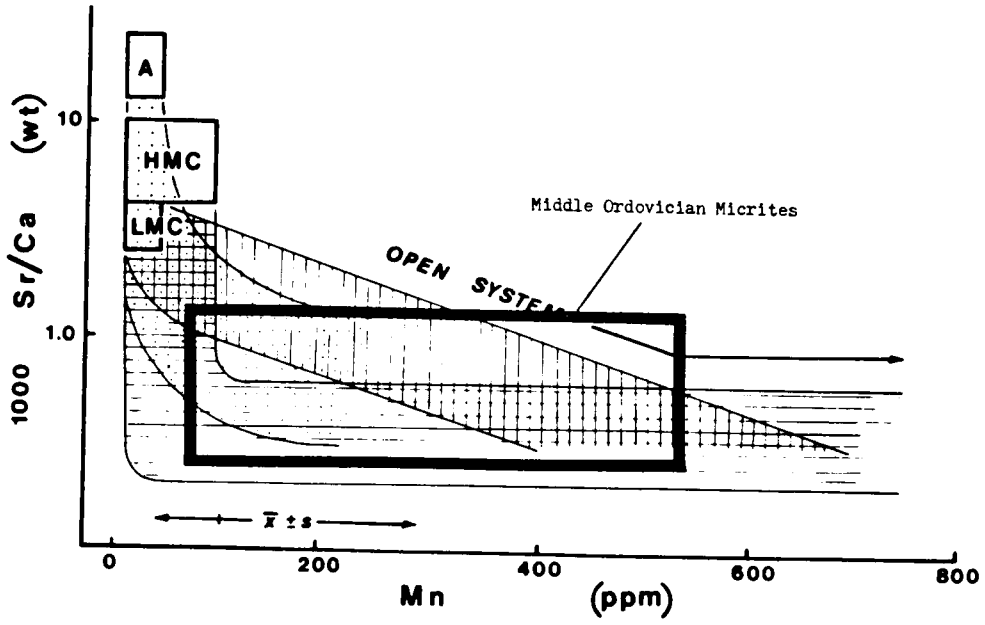


Figure 2.16. Composition of Ordovician micrites superposed on the diagenetic trends for aragonite (A), calcite (LMC) and magnesian calcite (HMC) constructed by Brand and Veizer (1980). Calcium concentration in Ordovician micrites assumed to equal 39.0 wt. % in calculating 1000Sr/Ca values.

ancient lime muds severely limits the usefulness of the published Mn-Sr trends. Neomorphosed molluscs may provide a more reliable measure of the diagenesis of aragonites.

Finely Crystalline (Penecontemporaneous?) Dolomites in Humid Tidal Flats

Finely to very finely crystalline dolomites typically occur as disseminated, matrix-replacive rhombohedra in peritidal mudstones, wackestones and packstones which form the basal deposits of the early Middle Ordovician onlap sequence. The restricted occurrence of these secondary dolomites in peritidal facies, and their absence in overlying/laterally equivalent subtidal facies indicates formation early in the diagenetic history. Five existing models have been used to explain early/penecontemporaneous dolomitization in intertidal-supratidal environments: Seepage Refluxion, Sabkha, Dorag, Coorong, and Tidal Pumping. The first two may be removed from consideration because both call upon the precipitation of evaporite minerals to generate sufficient Mg/Ca and CO_3/Ca ratios for dolomitization. Neither polished slabs nor thin sections of Middle Ordovician samples studied here contained evidence of either primary evaporites, or textures and fabrics indicative of the former presence of evaporite minerals

(e.g., pseudomorphs). Erosional and/or depositional topography may have allowed for the creation of semi-isolated pond environments analogous to areas of the Coorong Lagoon. However, sedimentary structures found in Coorong dolomites (mud-crack polygons and prisms, teepee-structures, breccias, various stromatolite morphotypes) are absent from Middle Ordovician peritidal deposits. Strontium concentrations in dolomitized micrites are identical (within analytical error) to concentrations in contemporaneous shelf micrites (Fig. 2.17, data in Table 2.2); sodium concentrations in dolomitized and undolomitized samples are also comparable. The depletion of these elements has been cited by other workers as evidence favoring the Dorag Model (Badiozimani, 1973). Uncertainties involving trace elememt distribution coefficients and recrystallization of originally non-stoichiometric, disordered dolomites makes tenuous any interpretations of the nature, composition and sources of dolomitizing fluids based on geochemical data (Morrow, 1982; Land, 1985; Hardie, 1987). Even though Middle Ordovician tidal flat dolomites may have precipitated from mixed meteoric-marine or tidally-cycled marine waters, the available data are inconclusive.

The interpreted original lime-mud mineralogy may have facilitated dolomitization. As an initial test for this

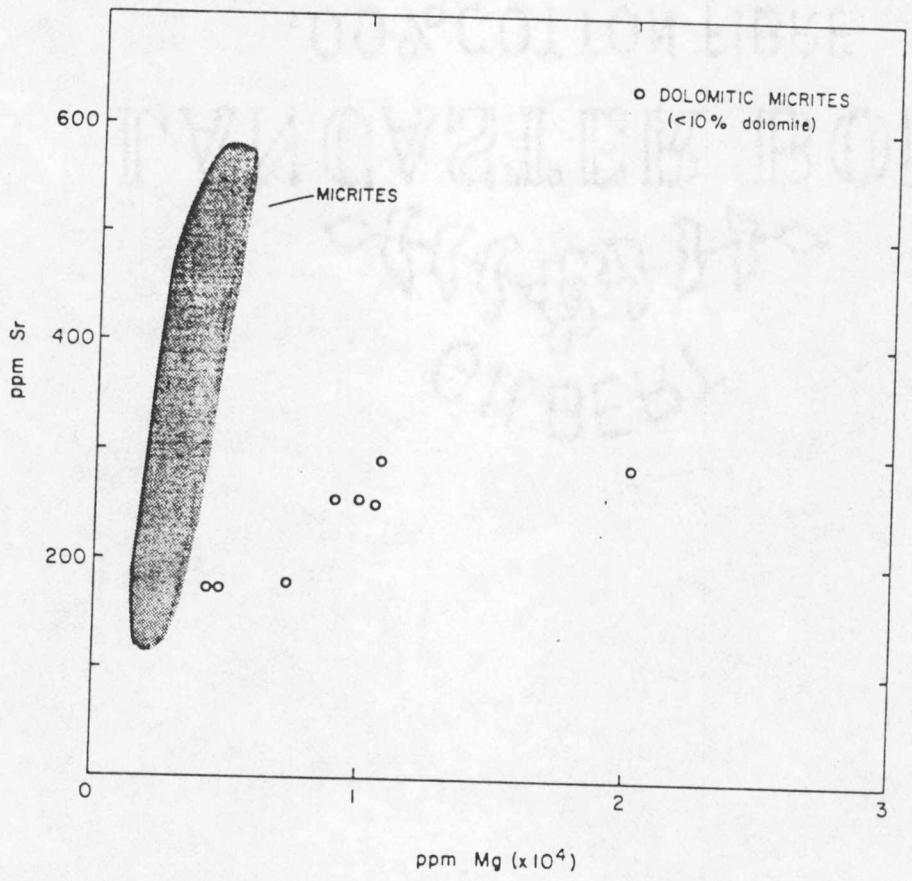


Figure 2.17. Strontium and magnesium concentration of Ordovician tidal flat dolomicrites compared to undolomitized Ordovician shelf micrites.

TABLE 2.2

ELEMENTAL GEOCHEMISTRY OF TIDAL FLAT DOLOMICRITES

	ppm Mg	ppm Sr	ppm Mn	ppm Fe
Five Oaks Fm.	5280	176	25	208
	5570	176	21	175
	7230	179	32	284
Mosheim Mbr.	9870	257	34	626
	10500	254	34	586
	20100	287	27	673
	10700	292	24	454

hypothesis of an autochthonous Mg2+ source, a mass balance calculation was performed on the following generalized dolomite-forming reaction:

Magnesian calcite = Calcite + Dolomite

The magnesium concentration of the original lime mud (10 mole % $MgCO_3$) is approximately equal to the composition shown in Figure 2.9. Diagenetic calcite composition selected represents the mean of micrites analyzed in this study. No geochemical data were obtained on the compositions of the finely crystalline dolomites; however, analyses by Sperber et al. (1984) indicate dolomites that are fine grained and associated with non-evaporitic settings are typically non-stoichiometric due to the presence of excess calcium (max. of 7 mole % $CaCO_3$) in the lattice. Using these initial assumptions, the balanced equation for the alteration of magnesian calcite to calcite and dolomite is as follows:

$$Ca_{.9}\,Mg_{.1}\,CO_3 = 0.795Ca_{.99}\,Mg_{.01}\,CO_3 + 0.205Ca_{.55}\,Mg_{.45}\,CO_3$$

Based on the molar volume of ideal dolomite, isochemical diagenesis of the original Mg-calcite sediment would produce a rock with approximately 30% dolomite and 70% calcite.

Since calcian dolomites would probably possess larger molar volumes as a result of disorder-related expansion of the structure (Land, 1985), the amount of early dolomite precipitated would be slightly higher than the value calculated above. Point count analyses of stained thin sections indicate less than 15 volume percent dolomite in all tidal flat limestones. Based on the above analysis and lack of evidence supporting other dolomitization models, peritidal dolomites from the Middle Ordovician could have precipitated from fluids which derived some of their Mg from stabilizing lime muds. This autochthonous magnesium, together with sufficient pore water alkalinity, may have facilitated dolomite precipitation in the absence of mixed waters and hydrologic pumping mechanisms.

The co-variation in iron and magnesium (Fig. 2.18) suggest dolomite abundance, which is directly proportional to magnesium concentration, may be tied to the openness of the diagenetic system during stabilization of carbonate matrix. Sediments which experienced thorough leaching in the vadose zone have relatively low magnesium concentrations reflecting extensive flushing of exsolved Mg ions from the system. Sediments that underwent a greater degree of their diagenesis below the surface in stagnated meteoric or mixed waters have magnesium concentrations that are higher suggesting either retention of Mg ions, and/or an influx of

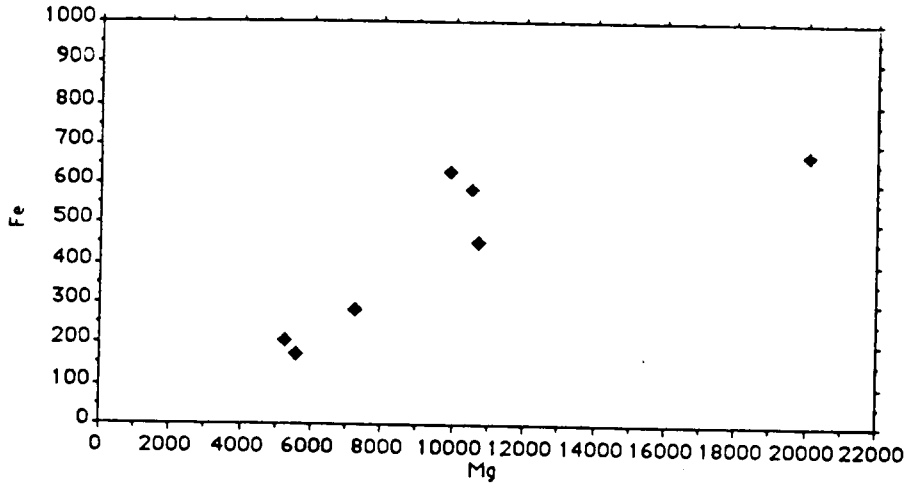


Figure 2.18. Iron and magnesium concentration of Ordovician tidal flat dolomicrites.

Mg into the system. In addition, dolomitized micrites with relatively high Fe contents also have pyrite disseminated within the micrite and/or along the margins of fenestrae. Although experimental work suggests sulfate inhibits dolomitization, it is possible that sulfate reduction promotes the formation of dolomite not by removing this anion but instead by increasing the IAP of the fluid via bicarbonate production (Hardie, 1987). The apparent correspondence between high Fe-Mg concentrations and presence of pyrite suggests dolomitization may have been enhanced by sulfate reduction at depth within the sediment.

Based on these observations, a model is proposed for the early dolomitization of calcite-dominated, humid tidal flats which form the base of transgressive sequences (Fig. 2.19). The model uses the total iron concentration as evidence for anoxic pore waters during dolomitization of tidal flat sediments. In light of the previous discussion concerning dolomite chemistry, the observed enrichment may reflect redox conditions during recrystallization of the metastable calcian dolomite during subsequent burial diagenesis. Using this scenario, the positive correlation between Fe and Mg is a product of the preferential substitution of ferrous iron into dolomite crystals; the more penecontemporaneous calcian dolomite precipitated, the greater the potential for incorporation of Fe(II) during

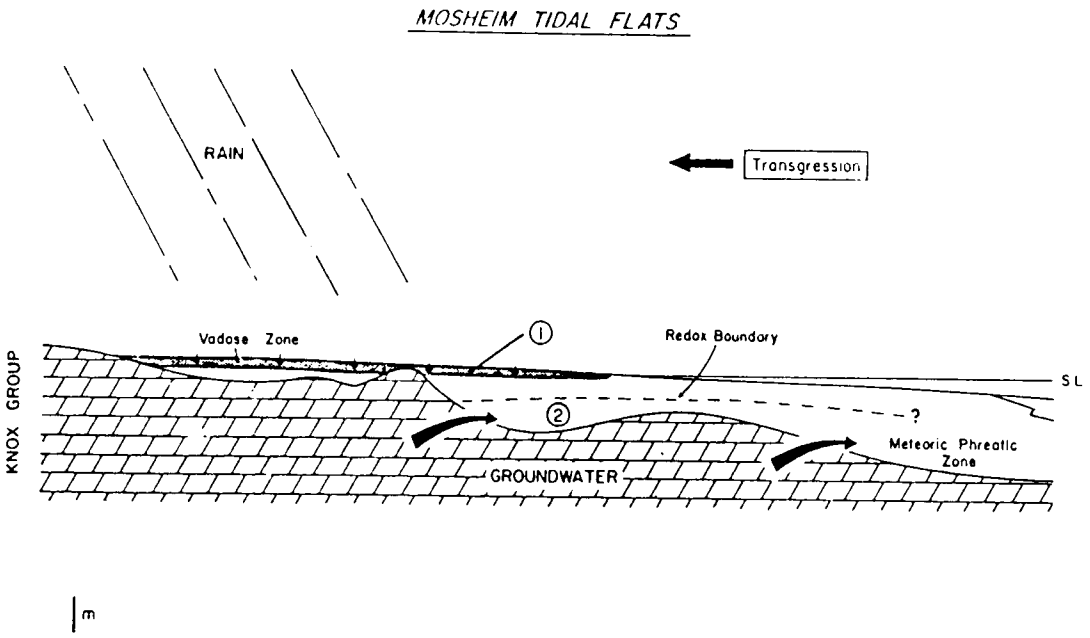


Figure 2.19. Preliminary hypothetical model for the early dolomitization of tidal mudflats at the base of an onlap sequence. Magnesian calcite stabilization in oxidizing pore waters would restrict the precipitation of dolomite in the vadose zone (1), and immediately below it. In the phreatic zone (2), alteration of magnesian calcite accompanied by organic matter oxidation in the presence of dissolved sulfate increased pore water Mg^{2+}/Ca^{2+} and CO_3/Ca^{2+} levels to enable dolomite precipitation. Seawater pumped through sediments during tidal cycling may have provided an additional source of magnesium ions to pore waters.

later ordering. Additional work is needed to resolve what this chemical tracer is telling us about the dolomitization history.

CHAPTER 3

ORIGINAL MINERALOGY OF SEDIMENTARY FACIES ALONG AN EARLY PALEOZOIC CARBONATE SHELF (MIDDLE ORDOVICIAN), EAST TENNESSEE

Introduction

In recent decades, numerous studies of Holocene carbonate environments have provided an understanding of sediment mineralogy and its variability with respect to latitude (Sellwood, 1975) and bathymetry (Pilkey and Blackwelder, 1968; Boardman and Neumann, 1984). Mineralogical variations with latitude reflect the presence/absence of such sediment-contributing calcareous biota as calcareous algae and hermatypic corals, and non-skeletal aragonite grains (ooids) which are restricted to warmer marine waters. The high calcite component in deep-water sediments results from the settling through the water column of foraminiferal and coccolith tests, and the location of the aragonite lysocline above the calcite lysocline. Even though the mineralogy of Holocene sediments

has been extensively studied, depositional and marine diagenetic constituents in limestones have escaped intense scrutiny. This lack of study is related to the type of information gathered during lithofacies analysis of carbonates.

Carbonate sedimentology has attained a sufficient level of understanding about petrogenesis to permit identification of original sediment mineralogy. However, no study examining the proportions of aragonite, magnesian calcite and calcite in a Phanerozoic platform/shelf sequence exists to date. If aragonite, calcite and Mg-calcite were present in the sediment, what were their relative abundances and how do these compare with Holocene warm-water carbonate sediments? These are questions this chapter will address.

Skeletal Allochems

Calcareous Algae

Chlorophytes. Thalli of extant green algae are composed of either magnesian calcite or aragonite. In the aragonitic codiacean Halimeda, the thallus consists of individual and

bundled crystals less than 1 micrometer in size (Flajs, 1977). Since most of the $CaCO_3$ precipitated is inter-filamental, skeletogenesis is passive and related to photosynthetic activity of individual cells which extract carbon dioxide from the interfilament fluid (Wray, 1977). Chlorophytes in Middle Ordovician shelf/ramp facies exhibit two modes of preservation. The first is represented by the codiacean Hedstroemia in which the tubule walls are composed of dark microcrystalline calcite with some organic matter (Fig. 3.1A). The dasyclads Vermiporella and Kazakhstanella, which represent the other mode, are preserved as molds filled with clear equant spar (see Moore, 1977, 1978). Halimeda grains in the Pleistocene Key Largo Limestone of Florida typically form moldic pores which are subsequently filled by drusy calcite cement (Stanley, 1966, Figure 10). Tubules within the plates are retained after dissolution by prior deposition of a thin cement fringe along their inner margins. The infilling of tubules in Kazakhstanella and Vermiporella by micritic sediment/cement provides the necessary solubility contrast to allow for gross preservation of the thallus during later diagenesis. The preservation of both these genera as spar-filled molds suggests an original aragonite mineralogy.

The microcrystalline thalli of Hedstroemia indicate either stablization of aragonite by process(es) different

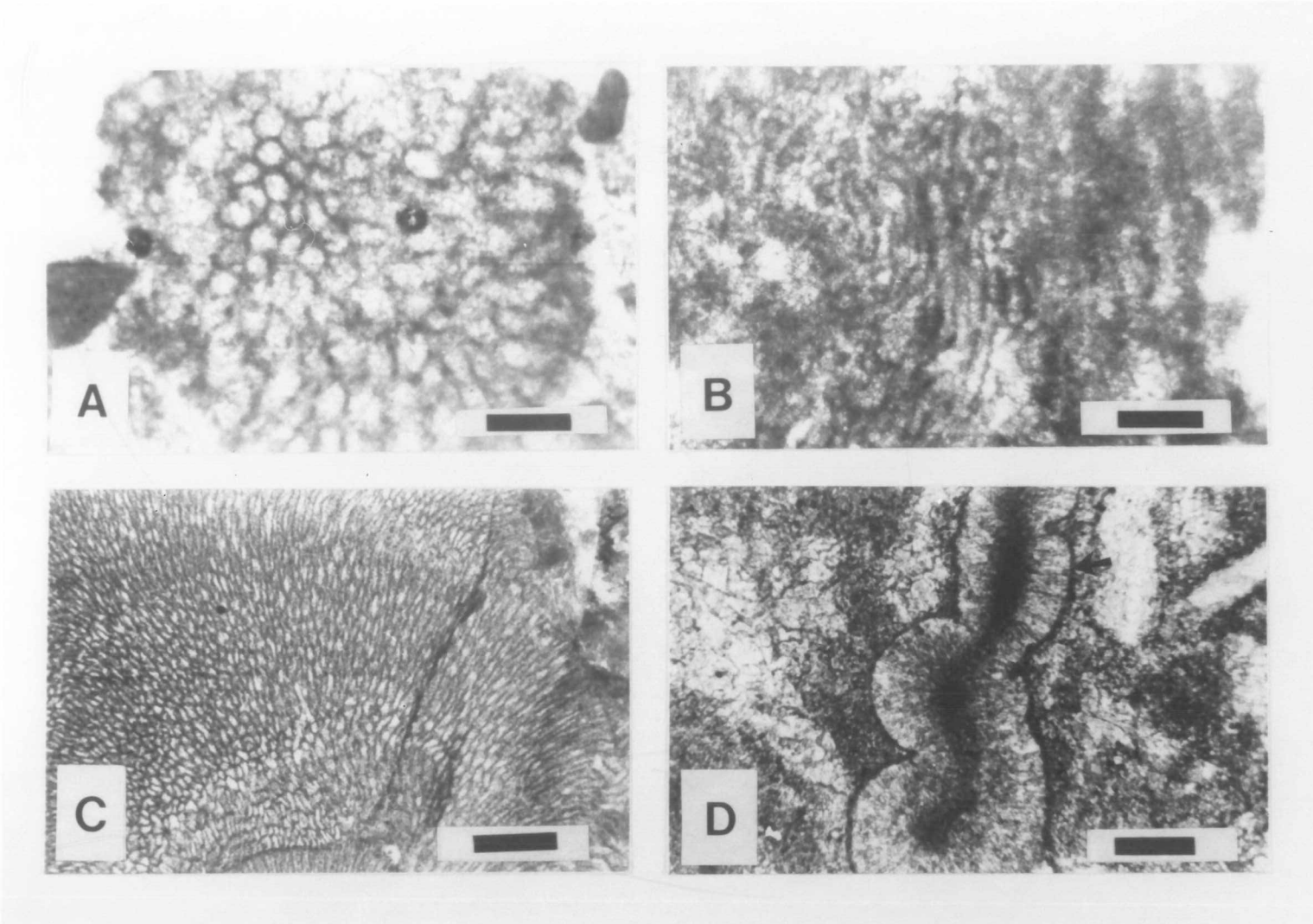
Figure 3.1. Thin section photomicrographs of calcareous algae.

A. Chlorophyte genus Hedstroemia with thallus consisting of dense, microcrystalline calcite. Sample CS9. Scale bar = 0.1 mm.

B. Filamentous tubules of the schizophyte genus Girvanella which form layered encrustations around skeletal grains producing algal oncoids. Sample CS3. Scale bar = 0.1 mm.

C. Well-preserved ultrastructure of the rhodophyte genus Solenopora. Thalli walls consist of dense, microcrystalline calcite; clear calcite microspar cement fills intrafilament chambers. Sample CS12. Scale bar = 0.25 mm.

D. Transported fragment of the problematic alga Nuia, which exhibits an inner core of dark microcrystalline calcite and surrounding radial prismatic calcite characteristic of this genus. Note extremely thin zone of micritization (arrow) along the outer margin. Sample MM2. Scale bar = 0.1 mm.


A
B
C
D

from Vermiporella and Kazakhstanella, or a different mineralogy. The transformation of aragonite to microcrystalline diagenetic low-Mg calcite is found in lithified Holocene sediments but is an extremely rare phenomenon (see Scherer, 1975). Moore (1978) found Hedstroemia in lithologies representing a range of paleoenvironments, and thus potential diagenetic histories. It is highly unlikely conditions prerequisite for this type of alteration could have been attained in such a wide spectrum of settings. Thus, unlike Halimeda, Hedstroemia thalli were originally calcite and not aragonite. Assuming calcification was extracellular as in Halimeda, the chemistry of ambient waters should be reflected in the precipitated carbonate. High magnesium concentrations characteristic of seawater would hinder the passive crystallization of low-Mg calcite in low-latitude zones and favor magnesian calcite precipitation. In addition, magnesian calcites undergo only minor textural and fabric changes during stablization to low-Mg calcite. Based on these arguments, Hedstroemia thalli were probably originally magnesian calcite rather than calcite.

Schizophytes. Skeletal carbonate of schizophyte algae is limited to micrometer-thick sheaths of microcrystalline

calcite or magnesian calcite about individual cell filaments (Wray, 1977). The dominant alga with schizophyte affinities is Girvanella, which commonly forms nodular encrustations around bioclastic debris (Fig. 3.1B). Less abundant filamentous tubules of the genus Sphaerocodium also occur in shelf limestones. A thin, microcrystalline calcite wall preserves the original morphology of the host filament as in the modern genus Plectonema (Riding, 1977). As in modern codiaceans, precipitation of this calcareous sheath was facilitated by the metabolic activities of the organism. Irregular-shaped patches of clear to cloudy neomorphic(?) spar and disseminated pyrite framboids occur within some oncolitic coatings containing Girvanella. Pyrite is a product of the oxidation of organic material in oxygen-poor microchemical environments of the coatings. The origin of neomorphic spar is uncertain, although it may also be linked to organic matter diagenesis because of its common association with pyrite. Middle Ordovician oncoid coatings sometimes exhibit a clotted to homogenous micritic texture lacking distinctive algal filaments. The latter fabric probably resulted from the precipitation of $CaCO_3$ in zones immediately adjacent to individual cell filaments, and/or trapping and binding of carbonate mud.

Oncoids from tidal-channel facies were analyzed for Mg, Sr and Mn (Table B.3). Brand and Veizer (1983) state the

chemistry of marine oncoids should approximate that of lime muds because of the particles high sediment/organic matter ratio. Magnesium and strontium concentrations show that oncoids lie along the same trend defined by micrites (Fig. 3.2), indicating a fair degree of chemical similarity (based on the limited analyses). The mean Mg concentration (2100 ppm) is similar to the mean Mg value in Holocene freshwater oncoids formed by schizophytes (2800 ppm; Muller and Friedman, 1968). However, Ordovician oncoids have significantly less Mg than microcrystalline sheaths of Plectonema (Riding, 1977).

In an earlier study, Biddle (1983) concluded that the calcified tubules of Girvanella were originally calcite based upon their morphological similarity to extant schizophytes, and the excellent preservation of the sheath's "crystal structure". Knowledge of calcification in modern algae and diagenesis previously discussed do not fully support this interpretation. Preservation of the microcrystalline sheath suggests an original 'calcite' mineralogy for Girvanella. Using arguments identical to those presented in the mineralogic discussion of Hedstroemia, it is probable that Girvanella sheath calcites were magnesian in composition. This inference is supported by oncoids lying along the same Sr-Mg trend as magnesian calcite-dominated precursor micrites, and oncoids having Mg

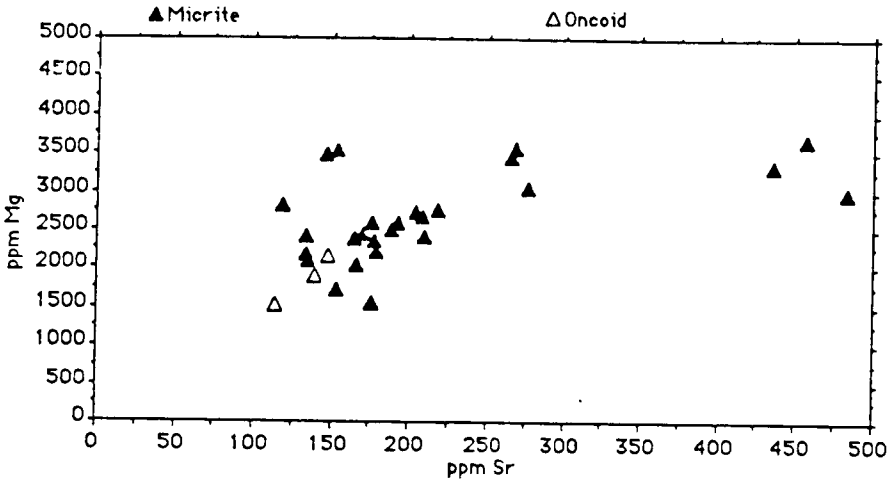


Figure 3.2. Strontium and magnesium concentration of Ordovician Girvanella-bearing oncoids and contemporaneous micrites. Note the compositional similarity between these two sedimentary components.

concentrations close to those for diagenetic calcites in equilibrium with meteoric waters (ca. 2000 ppm).

Rhodophytes. Modern species of this prolific group precipitate both aragonite and calcite with MgCO contents in the latter reaching 30 mole percent (Wray, 1977). Micrometer-sized crystallites are typically associated with the cell walls, although extracellular carbonate precipitation occurs in some taxa (Flajs, 1977). Solenopora is the dominant red alga in the Middle Ordovician shelf limestones. [The moniliporellacean Contexta is also present (Moore, 1978) but more limited in occurrence.] In thin section, Solenopora masses possess straight, nodose or crenulate walls of microcrystalline calcite with the remainder of the thallus filled by fine to very fine crystalline spar (Fig. 3.1C). The preserved walls resemble primary and secondary layers of extant calcitic rhodophytes.

Solenopora fragments analyzed by AAS have Mg/Sr ratios that fall within the range of Recent coralline genera (Lithothamium, Lithophyllum, and Goniolithon) (Fig. 3.3). Manganese concentrations exhibit an extremely broad range, with Mn/Sr ratios varying from <1 to approximately 6. Since living rhodophytes have manganese contents below 100 ppm (Milliman, 1974) the high values in some of the Middle

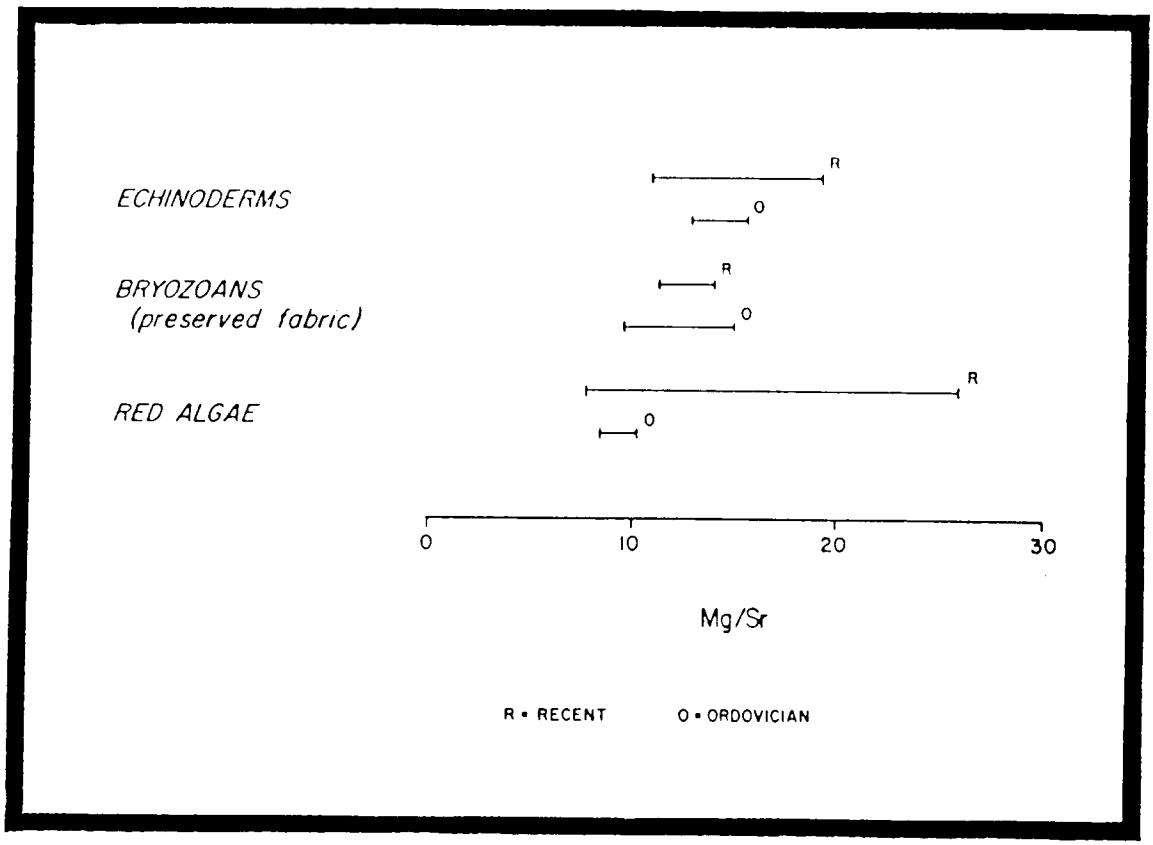


Figure 3.3. Range of Mg/Sr ratios in fossil and Recent calcareous marine organisms. Trace element concentrations for Ordovician taxa are given in Table 3.1. Data for Recent organisms are from Milliman (1974).

Ordovician fragments reflect enrichment during diagenesis.

The presence of ultrastructure similar to coralline algae, and comparable Mg/Sr ratios suggest a magnesian calcite precursor mineralogy for Solenopora. An unstable precursor is also supported by the diagenetic enrichment of manganese in some grains. Preservation of Contexta is comparable in many respects to Solenopora; however, this genus also exhibits preservational differences such as the loss of structure in both the hypo- and perithallus regions (see Moore, 1978, Plate IV, Figures 1 and 2). Although Contexta was not examined, the large degree of similarity with Solenopora also suggests an originally magnesian calcite mineralogy.

Problematical Algae. One of the more abundant organisms of supposed algal affinity in these Middle Ordovician limestones is Nuia. Originally classified as a chlorophyte and schizophyte, recent workers have recognized microstructural discrepancies between Nuia and these other algal groups (Toomey and Klement, 1966), and assigned this organism to a problematical taxonomic group (Moore, 1978; Wray, 1977). The 'thallus' is composed of articulated segments having two microstructural parts - a central canal of dark microcrystalline calcite and surrounding wall(s) of

radially-disposed calcite prisms (Fig. 3.1D). Microcrystalline calcite may also occur as irregularly-shaped areas in the prismatic walls, and as micron-thick boundaries separating successive prismatic layers. Staining reveals that calcites may be ferroan in composition.

Differences in preservation of Nuia and interpreted aragonitic algae favor a 'calcite' precursor. Based on the work of Richter and Fuchtbauer (1978), the occurrence of ferroan calcite indicates the original skeleton contained a significant amount of magnesium. Scherer (1975) found originally aragonitic corals which had undergone polymorphic transformation to Fe-rich spar, but the texture and fabric of these calcites differ from those in Nuia.

The gross microstructure of Nuia resembles to some degree that of the Mesozoic and Cenozoic problematical alga Microcodium. Microcodium "aggregates" occur as rosettes consisting of slightly elongate calcite prisms radiating from a central nucleus (Klappa, 1978). Grains also have transverse walls of porous microcrystalline calcite. Carbon isotopes reveal the calcite is an indirect biochemical precipitate apparently resulting from changes in pCO_2 during plant photosynthesis (Klappa, 1978). The similarities between Niua and Microcodium could reflect the evolution of analogous skeletogenetic pathways. Using this working

hypothesis, cell filament(s) would have resided in what is preserved as the central canal. The metabolic activity of the organism would have created a carbon dioxide-poor extracellular microenvironment, thus enabling indirect precipitation of a microcrystalline sheath. This coating may have served as a nucleation site for calcite crystals which form the prismatic wall.

Bryozoans

Both aragonite and magnesian calcite are precipitated during skeletogenesis in extant bryozoans (Chave, 1954; Lowenstam, 1954; Ryland, 1970). Exoskeletons consist of either a single polymorph, or a combination of both with each present as a well-defined, microstructurally distinct layer. Sandberg (1975) noted two microstructural types in modern cheilostomates, lamellar and spherulitic. The latter is divided into transverse and planar sub-types based on the c-axis orientation of crystallites with respect to the wall margins. Aragonite occurs as acicular crystals arranged in both planar and transverse spherulitic arrays; magnesian calcite occurs in a variety of crystal morphologies that form both microstructural types (Sandberg, 1975).

Middle Ordovician bryozoans exhibit two very distinct modes of preservation. The majority (including

cryptostomes, trepostomes, and fenestrates) possess a fibrous/lamellar microstructure which resembles the lamellar type mentioned above (Fig. 3.4A). Taxa may have a thin inner layer of microcrystalline calcite. The form genus Nicholsonella exhibits the second mode of preservation, characterized by the absence of recognizable skeletal microstructure. In specimens with micrite-filled zooecia, the original skeleton consists of cloudy, ferroan to nonferroan, anhedral calcite (Fig. 3.4B). If little or no micritic sediment/cement is present, zoaria are preserved as a mosaic of finely to very coarsely crystalline spar (Fig. 3.4C). Inclusion-rich zones of varying thickness within the mosaic provide the only evidence of the structure and dimensions of the colony. Crystals typically cross-cut the inclusion-rich bands, resulting in fabrics which closely resemble calcitization mosaics in originally aragonitic corals (Pingitore, 1976). (These calcite mosaics will be referred to as replacement-cement mosaics in the text.)

Geochemical analyses of entire zoaria (skeleton sensu stricto + intrazooecial cement) with lamellar microstructure and replacement-cement mosaics are given in Table B.3. Bryozoans with preserved microstructure have Mg/Sr ratios similar to extant cheilostomates with magnesian calcite exoskeletons (Fig. 3.3). As with solenoporacean algae, the range in Mn concentrations indicates diagenetic enrichment

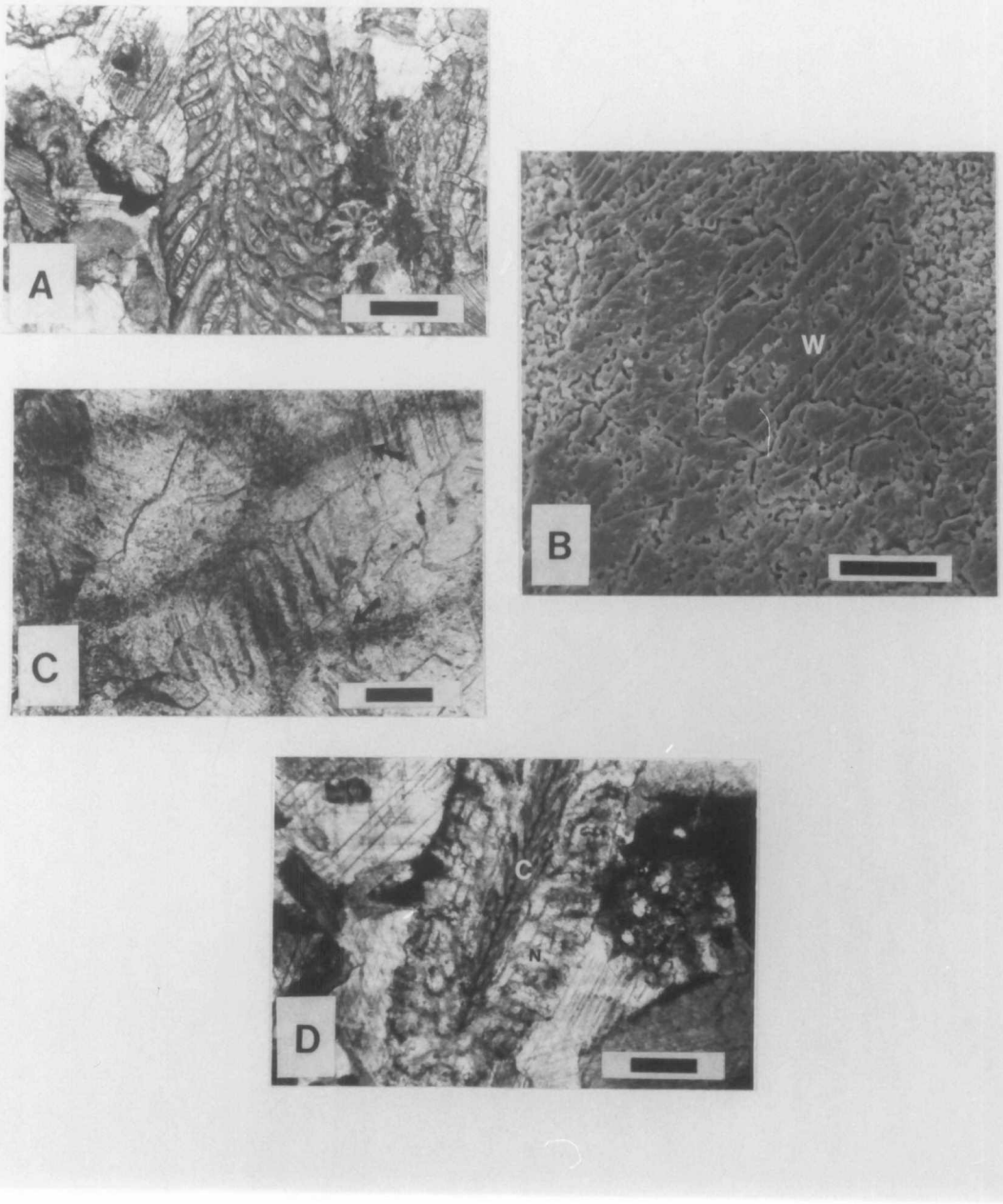
Figure 3.4. Thin section and SEM photomicrographs of bryozoans.

A. Foliate bryozoan with well-preserved lamellar microstructure comprising zoaria. Sample RHB31. Scale bar = 0.25 mm.

B. SEM photomicrograph of zooecial wall (W) from a nicholsonellid bryozoan in skeletal wackestone. Original skeleton preserved as anhedral calcite spar with irregular intercrystalline boundaries and abundant pits. Acicular aragonite and microdolomite inclusions are absent. Texture and fabric of diagenetic calcites closely resemble neomorphic spar replacing originally aragonitic corals. Sample CS51. Scale bar = 40 micrometers.

C. Oblique section of nicholsonellid replacement-cement mosaic in skeletal grainstone. Relict zooecial walls are preserved as inclusion-rich areas which cut across crystal boundaries (arrows). Sample CS30. Scale bar = 0.1 mm.

D. Juxtaposition of bryozoans with different modes of preservation. Foliate cryptostome (C; note median septum) was later encrusted by nicholsonellid(?) preserved as replacement-cement mosaic (N). Sample RHB34. Scale bar = 0.25 mm.


A
W
B
C
C
N
D

of this element in certain shelf facies.

The disparity in microstructural preservation indicates bryzoans constructed either calcite or aragonite exoskeletons. Although preservational differences observed might be attributed to recrystallization of a single polymorph via alternate diagenetic pathways, this is unlikely even if the bryozoa possessed dissimilar skeletal microstructures. The co-occurrence of zoaria with preserved microstructure and replacement-cement mosaics supports the idea of differing original mineralogies (Fig. 3.4D).

Sandberg (1975) discussed variations in diagenetic textures and fabrics in the bi-mineralic species Schizoporella floridana. Lamellar magnesian calcite of the original zoaria showed (p. 589) "...little change in fine structure with the magnifications and resolution possible in light microscope study of thin sections". Spherulitic layers of acicular aragonite in the original zoaria are replaced by a mosaic of coarsely crystalline calcite, indicating no transfer of microstructural information during aragonite stabilization. These differences provide a basis for the interpretation of the original mineralogy of Middle Ordovician bryozoans. Taxa possessing well-preserved lamellar microstructure secreted calcitic exoskeletons; Nicholsonella (and petrographically similar taxa) secreted aragonite. Bryozoans identified from lower Middle

Ordovician strata are classified in terms of their interpreted original mineralogy (Table 3.1) using these petrographic criteria. Genera and lineages with former calcitic exoskeletons far outnumber their aragonite-secreting counterparts. Even though calcitic taxa appear to be dominant, former aragonite bryozoa (particularly Nicholsonella) were important members of bryozoan faunas in certain facies (see Ruppel and Walker, 1982; Cristil, 1985).

Articulate Brachiopods

The calcareous valves of living articulates are composed exclusively of calcite with small amounts of magnesium in solid solution (Chave, 1954; Rudwick, 1970). The structure of shells consists of two layers, primary and secondary, both of which are secreted by the mantle (Rudwick, 1970). [A third (prismatic) layer is found among spiriferids Rudwick (1970).] The primary layer forms a thin sheath composed of microcrystalline calcite confined solely to the valve exterior. The majority of the shell is taken up by the underlying secondary layer which consists of stacked calcite fibers at shallow angles to the valve surface that are enclosed by protienaceous material. Petrographic and SEM examination of articulate brachiopods

TABLE 3.1

INTERPRETED ORIGINAL MINERALOGY OF BRYOZOA FROM THE MIDDLE ORDOVICIAN LOWER CHICKAMAUGA GROUP

REPLACEMENT-CEMENT MOSAIC IN ORIGINALLY ARAGONITIC FORMS	PRESERVED MICROSTRUCTURE IN ORIGINALLY CALCITIC FORMS	
Anolotichia	Helopora	Calipora
Nicholsonellids	Diploclema	Stictopora
Ceramoporoids	Ottoseetaxis	Stictoporella
Diplotrypa(?)	Astreptodictya	Pachydicta
	Anthrophragma	Hemiphragma
	Constellaria	Pavohallopora
	Batostoma	Prasopora
	Diplotrypa(?)	Mesotrypa
	Eridotrypa	
	Phylloporinids	
	Rhabdomisines	

Sources: Middle Ordovician bryozoan faunas - Ruppel(1979), Cristil(1985)
Additional microfabric data - Ross(1964), McKinney(1971), Karlins(1985)

revealed excellent preservation of the fibrous secondary layer (Fig. 3.5 A). The microcrystalline primary layer could not be identified with certainty in any valves examined. Absence of this external microstructural layer is the result of its thinness and taphonomic processes following death of the organism. Even though composed of stable calcite, its fine texture and lack of intercrystalline organic matter would enhance the possibility of dissolution (Moore, 1965). An extremely thin (10 micrometer), continuous layer of prismatic calcite texturally similar to prismatic layers in other Paleozoic articulates (Popp et al., 1986, Figure 2A, B) was observed in one valve (Fig. 3.5B). The fibrous calcite of the secondary layer is dull to non-luminescent and nonferroan based upon staining with potassium ferricyanide. Some valves possess thin zones parallel to the fibrous microstructure which consist of brightly luminescent spar (Fig. 3.5C). No evidence of dissolution (cement-filled moldic pores) or neomorphism was found.

Based on the high degree of microstructural preservation and non-luminescence, the secondary layer is interpreted as originally composed of calcite. The "recrystallized" microstructure observed by Al-Aasm and Veizer (1982), represented in this sequence by luminescent calcite, probably resulted from neomorphism/cementation

Figure 3.5. Thin section and SEM photomicrographs of articulate brachiopods and molluscs.

A. SEM photomicrograph of articulate brachiopod valve with well-preserved fibrous microstructure characteristic of the secondary layer. The merging of individual crystallites indicates further calcite precipitation during diagenesis. Minor areas of silica replacement (Q). Sample MM15. Scale bar = 30 micrometers.

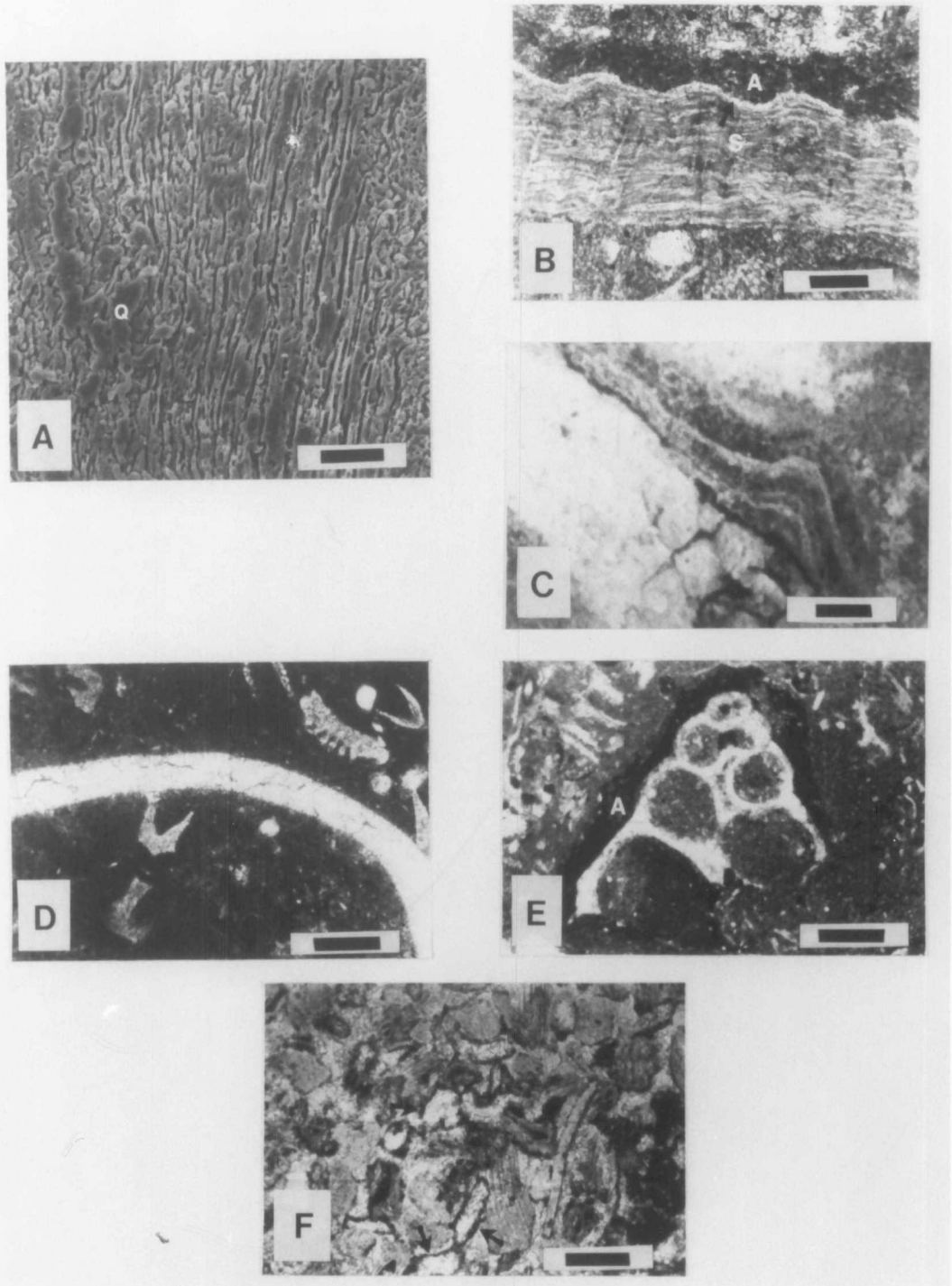
B. Disarticulated, pseudopunctate brachiopod valve which was encrusted by algae (A). Note the occurrence of an extremely thin prismatic layer (arrow) between the algal coating and fibrous secondary layer (S). SB18. Scale bar = 0.1 mm.

C. Cathodoluminescent photomicrograph of articulate brachiopod valve composed of interlayered luminescent and non-luminescent calcite. Sample DL3. Scale bar = 0.1 mm.

D. Mold of bivalve mollusc occluded by clear, nonferroan calcite spar. Sample SB11. Scale bar = 0.25 mm.

E. Low-spired gastropod which was coated by encrusting algae (A) in the marine environment. During postsedimentary diagenesis, dissolution of the original skeletal carbonate produced moldic porosity, which was subsequently filled by clear, nonferroan calcite. Sample SB17. Scale bar = 0.25 mm.

F. Finely comminuted molluscan debris which have been preserved as spar-filled moldic pores outlined by thin micrite envelopes (arrows). Sample CS13. Scale bar = 0.25 mm.


A
Q
B
A
C
C
D
E
A
F

associated with alteration of the embedded organic matrix followed by calcite precipitation during burial. The primary layer probably had an identical mineralogy based on the following evidence: 1)calcite mineralogy in living taxa, 2)absence of fossil or extant species with bi-mineralic skeletons, 3)existence of ways to remove this layer which do not require a metastable precursor.

Molluscs

Among marine invertebrates, the molluscs possess a diverse array of microstructures that in most cases may be composed of aragonite and (magnesian) calcite. Carter and Clark 1985 list major structural types and their respective mineralogies. One characteristic molluscs share with bryozoans is the co-occurrence of separate aragonite and calcite layers in some exoskeletons. Pteriomorph and mytilid bivalves contain mixtures of aragonite and calcite even in representatives dating as far back as the Early Paleozoic (see Carter, 1980, Figure 1). Each polymorph tends to occur as a distinct mono-mineralic layer with distinct boundaries; rarely do both minerals occur in the same layer (Carter, 1980). The vast majority of molluscs from Middle Ordovician limestones are preserved as clear equant spar mosaics with no relic microstructure (Fig. 3.5D

and E) indicating a dissolution-reprecipitation diagenetic sequence. Calcite that occluded the moldic pores is ferroan to nonferroan. In some lithologies the former shells are defined by micrite envelopes produced by the boring activity of endolithic organisms while shells were exposed on the seafloor (Fig. 3.5F). Nautiloid cephalopods and bivalves from drowned ramp sediments are the only groups whose shells underwent neomorphism rather than dissolution-reprecipitation. None of the structural types described in Table 3 were observed in thin section.

The diagenetic fabrics observed correspond to those of originally aragonitic skeletons discussed by Sorby (1879) and Bathurst (1958). This similarity and total absence of preserved microstructures indicate shells were originally aragonite with no interlayered calcite. (An outer calcitic layer may have existed in some early Paleozoic nautiloids. However, careful examination of thin sections failed to detect this layer.) In fossil assemblages where microstructural preservation indicates the retention of original mineralogy, molluscs consist of either interlayered aragonite and calcite, or aragonite (Stehli, 1956; Hallam and O'Hara, 1962; Brand, 1982).

Trilobites

The class Trilobita is the only important sediment-contributing group in this Middle Ordovician sequence without any direct descendant. Trilobite carapaces appear to consist of ordered calcite prisms whose c-axes are normal to the outer surface. Petrographic examination of numerous fragments revealed evidence of neither dissolution nor coarsely crystalline neomorphic fabrics (Fig. 3.6A). Similar microstructures have been noted by other workers (Sorby, 1879; James and Klappa, 1983). Under SEM, crystals are poorly defined, but occasionally exhibit an equant morphology and crude layering parallel to the skeletal surface. Calcite typically stains light blue with potassium ferricyanide and has moderately bright to dull luminescence.

The well-preserved nature of the carapaces and lack of either pervasive neomorphism or cement-filled moldic pores indicate a calcitic primary mineralogy. The question of whether trilobite skeletal calcite was magnesian in composition is problematic based on the available data and absence of direct descendants. Three pieces of evidence stongly support a magnesian calcite composition. First, ostracodes, the one arthropod group whose exoskeleton resembles those of trilobites (Tiegler and Towe, 1975), have magnesium contents ranging from 1 to 10 mole percent (Chave, 1954; Cadot et al.,1972). Since magnesium concentrations

Figure 3.6. Thin section photomicrographs of arthropods and echinoderms.

A. Abundant trilobite carapaces with fibrous skeletal microstructure in allochthonous debris/mud flow deposit. Sample SC32. Scale bar = 0.25 mm.

B. Articulated ostracode exhibiting well preserved microcrystalline fabric. Note epitaxial prismatic calcite cement occluding relict intraskeletal void. Sample CS12. Crossed polars. Scale bar = 0.25 mm.

C. Disarticulated ostracode valves which possess a two-layer microstructure (arrow). Sediments underwent compaction and attendant pressure solution, as evidenced by microstylolites (M) truncating grains. Sample SB 23. Scale bar = 0.25 mm.

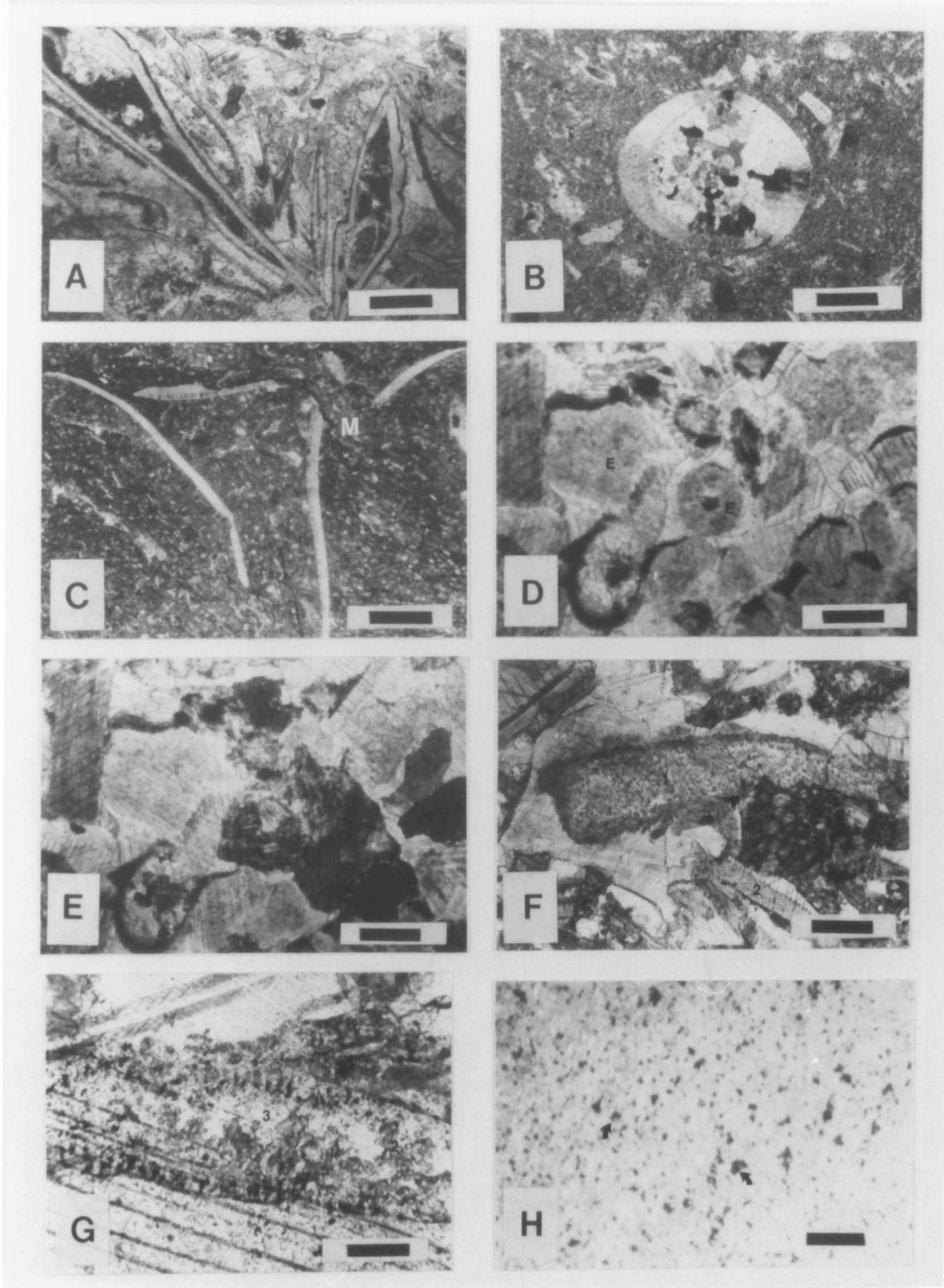
D. Echinoderm ossicles (E) preserved as dusty, inclusion-rich calcite surrounded by syntaxial calcite cement. Sample CS13. Scale bar = 0.25 mm.

E. Same as D under crossed polars; note that both the grain and associated cement go extinct in unison. Sample CS13. Scale bar = 0.25 mm.

F. Echinoderm grains preserved as a mosaic of finely crystalline, nonferroan equant calcite (1), and a single, inclusion-rich calcite crystal (2). Sample CS22. Scale bar = 0.25 mm.

G. Close-up of echinoderm ossicle which consists of (1) inclusion-rich calcite, (2) finely crystalline equant calcite cement, and (3) clear, coarsely crystalline calcite cement. Note how crystallographic twins for inclusion-rich calcite and associated cement are also present in the coarse calcite, suggesting an equivalent origin. Sample CS22. Scale bar = 0.1 mm.

H. Cathodoluminescent photomicrograph of an echinoderm grain with non-luminescent, euhedral to subhedral microdolomite inclusions (arrows) disseminated within brightly luminescent calcite. Sample DL17. Scale bar = 0.1 mm.


A
B
M
C
E
D
E
F
3
G
H

tend to be related to ambient water temperatures, it is conceivable that cuticular calcite secreted by trilobites possessed appreciable magnesium. Second, in some facies carapaces are composed of ferroan calcite and are luminescent. Chemical analyses of modern decapod crustaceans show low (<100 ppm) concentrations of Fe and Mn (Milliman, 1974), thus requiring incorporation of these elements during diagenesis. It is unlikely sufficient diagenetic calcite could have replaced the original organic matrix to produce the geochemical signatures found. Lastly, carapaces of Late Paleozoic trilobites have appreciable magnesium contents. The microstructural uniformity of trilobites throughout the Paleozoic suggests the original mineralogy remained unchanged.

Ostracodes

The mineralized carapace of Recent marine ostracodes consists of calcite with variable magnesium contents (Majewske, 1969). Crystals precipitated after molting are prismatic, with c axes normal to the shell surface as in trilobites. In some groups (Leperditiidae and Kirkbyidae) two distinct microstructural layers are recognizable - an outer microcrystalline layer, and an inner prismatic layer (Majewske, 1969). Microstructure of fossil ostracodes from

the Middle Ordovician is similar to that of living representatives. In thin section, carapaces possess both uniform microcrystalline (Fig. 3.6B) and two-layer (Fig. 3.6C) microstructures. The latter is only distinguishable in polarized light. The thickness ratio (prismatic/ microcrystalline) of the two layers in a valve ranges from approximately 1 to 4. Evidence of dissolution and neomorphism is lacking in this group.

In the absence of microprobe data, cathodoluminescence and staining provided semi-quantitative data on carapace geochemistry. Calcites are typically nonferroan and non-luminescent. A small number are composed of ferroan calcite.

The well-preserved carapace microstructure indicates a calcitic skeletal mineralogy. Cathodoluminescence and staining suggest carapaces were mono-mineralic and did not possess zones of different magnesium composition. Richter and Fuchtbauer (1978) concluded that fossilized carapaces are composed of either calcite or magnesian calcite.

Echinoderms

The polygonal plates (and columnals in stalked groups) which form the endoskeletons of modern echinoderms are in most instances composed of magnesian calcite (Chave, 1954;

Bathurst, 1975). The magnesium content in genera ranges from 4.4 to 15.7 mole % (Milliman, 1974). Each element possesses a "spongy or fenestrate structure" consisting of a framework of optically continuous calcite and an interconnected network of micropores. Probably the most diagnostic feature of echinoderm ossicles is their behavior as a single crystal in polarized light. Articulated and disarticulated ossicles from the Middle Ordovician behave optically as single crystals of calcite with uniform extinction (Fig. 3.6D andE). Adjacent elements in articulated skeletons have divergent c axis orientations as observed by Raup (1966). Even though all elements are similar optically, subtle differences in preservation exist among echinoderm grains. The majority of ossicles have a "dusty appearance" (Bathurst, 1975) which reflects the primary fenestrate microstructure. Some ossicles contain irregular-shaped areas lacking relict microstructure, but are instead composed of 1)one or a few crystals of clear spar, 2)finely crystalline equant calcite or microspar, 3)micrite, or 4)a combination of these (Fig. 3.6F and G). The sharp boundaries which separate dusty and clear calcite/micrite appear to be of diagenetic origin, and not the product of organismal boring.

Petrography and cathodoluminescence reveal the presence of disseminated euhedral to subhedral microdolomite

rhombohedra within the dusty calcite (Fig. 3.6H). Rhombs are generally less than 30 micrometers with maximum sizes reaching 50 micrometers. The inclusion density varies in grains probably due to differences in diagenesis (e.g. system openness) rather than original calcite compositions. Dusty calcites may be ferroan in composition and exhibit a range of luminescent intensities (bright to non-luminescent). Atomic absorption analyses of the calcite fraction of ossicles (Table B.3) indicate Mg contents significantly below those in living echinoderms. However, Mg/Sr ratios in Middle Ordovician echinoderm grains (Fig. 3.3) are within the range of Mg/Sr for modern, warm-water echinoids (Milliman, 1974).

The petrographic and geochemical data suggest an originally magnesian calcite mineralogy as in modern echinoderms. The variable luminescence and ferroan composition indicate a metastable precursor, which is also supported by the presence of microdolomite inclusions in these and other Paleozoic echinoderms (James and Klappa, 1983; Lohmann and Meyers, 1977). The restriction of rhombs to ossicles favors an autochthonous origin for Mg ions necessary for dolomite authigenesis. Magnesian calcite exsolution, expressed by the simplified reaction (Land, 1967)

Mg-calcite $\longrightarrow$ calcite + dolomite

would be a likely stabilization process for echinoderms because of their relatively high Mg contents. Initial reaction would first produce very finely crystalline (<10 micrometers) disordered protodolomite crystals which would then serve as "nucleation sites" for continued dolomite growth (Macqueen et al., 1974), the end result being numerous rhombs within diagenetic (low-Mg) calcite.

The occurrence of apparent secondary porosity is unexpected in light of accepted stabilization processes for biogenic magnesian calcites (see Land, 1967). Schroder (1979) found that skeletal alteration in some cases may not be controlled by either allochem type or mineralogy, and that one allochem may be affected by more than one process. Petrography suggests that clear spar and micritic sediment were deposited within voids produced by dissolution and/or collapse of the delicate fenestrate microstructure. The loss of relict microstructure has been observed in other echinoderms, however this fabric has gained little attention because of the abundance of grains composed of dusty calcite. The restriction of this type of preservation to shelf-margin grainstones and packstones indicates a possible link to diagenetic conditions in this portion of the stratigraphic sequence during burial. However, the

implications of these observations cannot be fully evaluated at this time.

Discussion of Interpreted Skeletal Mineralogies

Aragonite versus 'Calcite'

The dominant sediment-contributing biota in the Middle Ordovician basin either actively or passively produced skeletons of aragonite, calcite or magnesian calcite. Distinction between organisms precipitating 'calcite' or aragonite can be made by the style of particle preservation (Fig 3.7). The alteration of aragonite to diagenetic low-Mg calcite can occur via dissolution-reprecipitation, with an intervening void stage, and calcitization involving the migration of micrometer-thick diagenetic fronts across a given particle. Former aragonite skeletons in Middle Ordovician limestones are preserved as either moldic pores filled with clear, ferroan to nonferroan calcite spar (type I) or finely to coarsely crystalline, inclusion-rich, ferroan to nonferroan neomorphic spar (type II).

The stabilization of magnesian calcite to diagenetic low-Mg calcite is less destructive to the skeletal microstructure, although textural alteration is visible

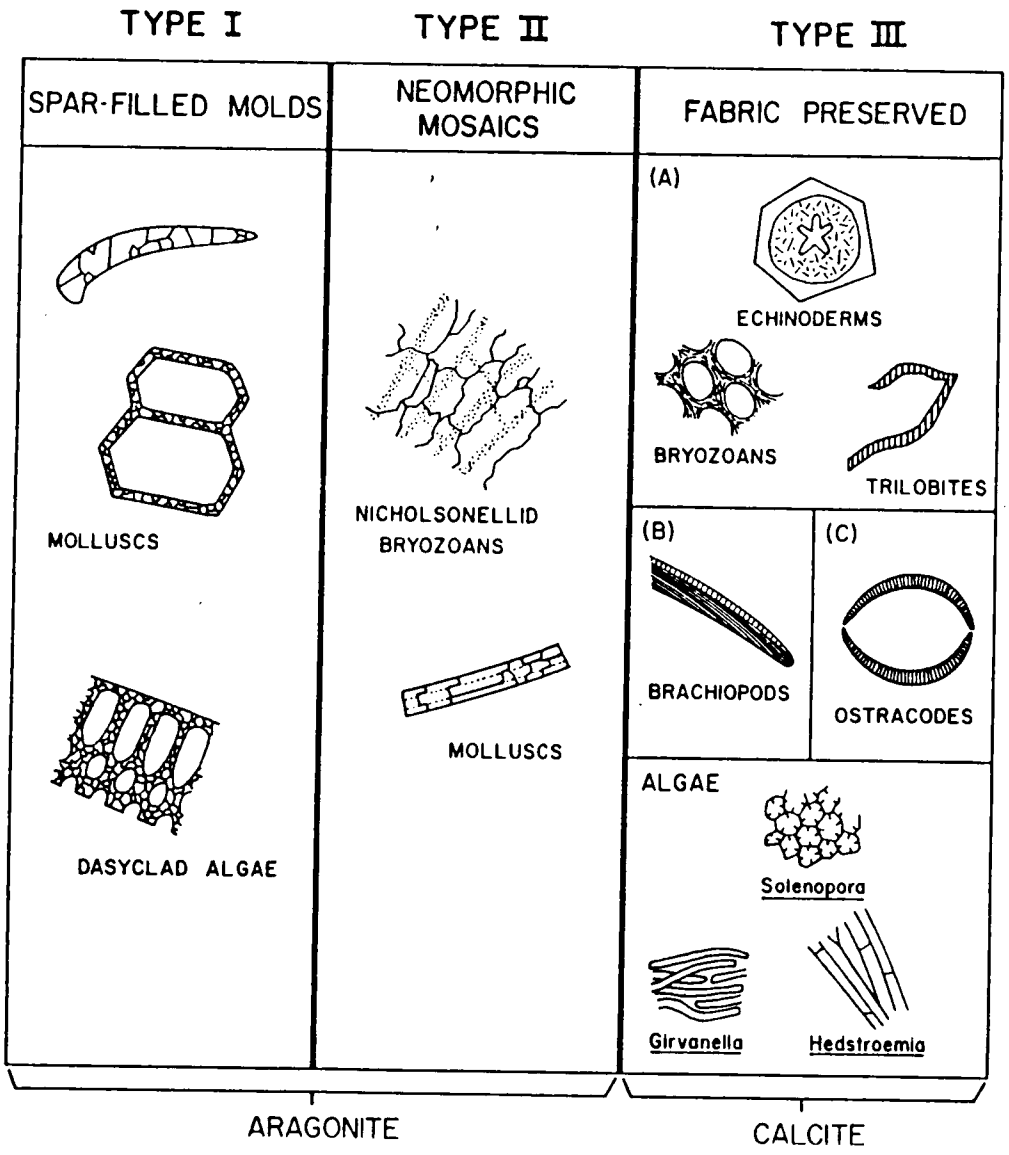


Figure 3.7. Summary sketch showing the recognized types of skeletal preservation in Middle Ordovician in eastern Tennessee.

under SEM. Original 'calcite' skeletons generally occur as particles in which the original microstructure is retained (type III). Unfortunately, microstructures alone do not allow for the recognition of biota with originally calcite or magnesian calcite hard parts in this third group. Comparison of Middle Ordovician taxa with modern relatives provides a first approximation, but this jump can be misleading because of the large time span involved and the fact that several important groups (trilobites, anthozoans, stromatoporoids and some calcareous algae) do not have direct tracable descendants. Skeletons within this group can be divided into three sub-groups (A,B and C of Fig. 3.7) based on the presence of one or all of the following.

1) Microdolomite inclusions produced by exsolution of Mg ions during stabilization.

2) Replacement of allochem by ferroan calcite.

3) Allochems having bright luminescence rather than a dull to non-luminescence.

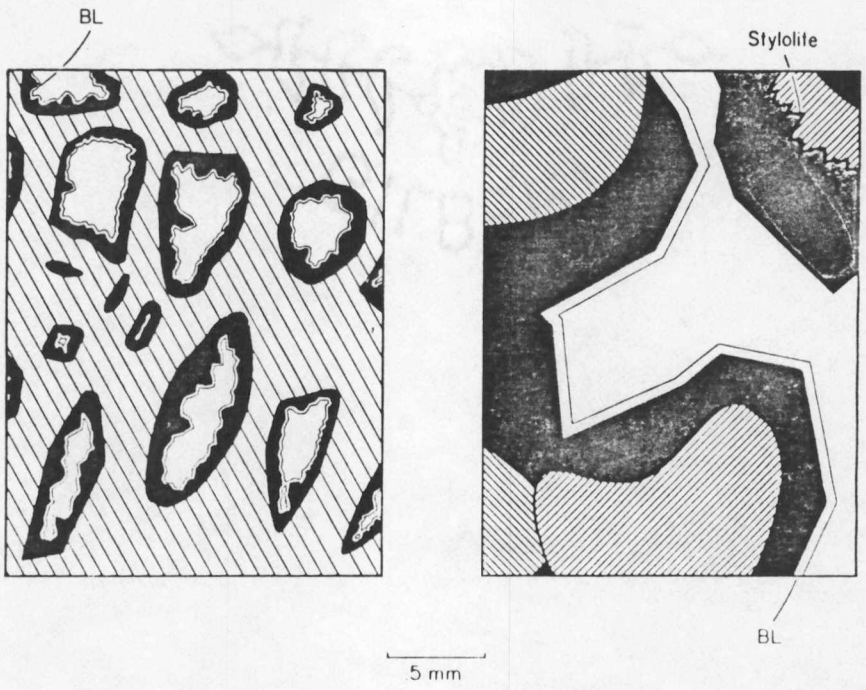
4) Trace element compositions similar to modern representatives which secrete magnesian calcite, or interpreted magnesian calcite components.

Echinoderms, bryozoans, and trilobites in sub-group A, and calcareous algae (including Nuia) are characterized by more than one of these criteria, while articulate brachiopods (sub-group B) exhibit none of them; ostracodes (sub-group C)

may or may not exhibit some of these features (Fig. 3.7).

Phreatic Diagenesis of Nicholsonellid Bryozoans

The cross-cutting spar mosaics associated with Nicholsonella reflect a sequence of diagenetic events that are not characteristic of other formerly aragonitic skeletons. Several lines of evidence, both petrographic and geochemical, indicate that stablization of metastable aragonite and intrazooecial calcite cementation occurred under phreatic conditions. Longitudinal and transverse sections show the calcite mosaics to be non-fabric selective, with intercrystalline boundaries cutting across the relict zoarium. Inclusion-poor calcites which occupy intrazooecial pores are interpreted as void-filling calcite cement, and are neither neomorphosed skeletal aragonite or marine cement. This interpretation is supported by the following fabric data: 1)luminescent zonations identical to inter- and intraparticle meteoric/burial phreatic cements (Fig. 3.8); 2)presence of crystallographic luminescent zone boundaries; 3)change from irregular to planar intercrystalline boundaries when moving from inclusion-rich to -poor areas of a single crystal (Fig. 3.9A); 4)abundance of enfacial junctions. Replacement-cement mosaics and interparticle equant cements interpreted as meteoric/burial



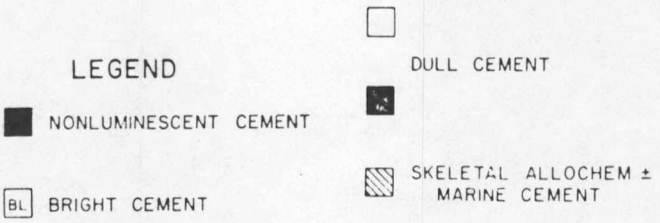


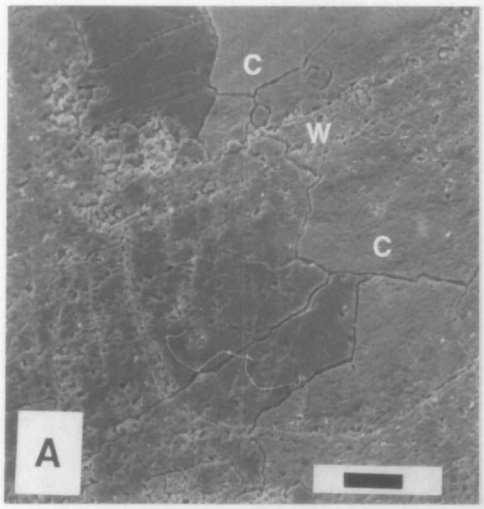
Figure 3.8. Schematic illustration comparing meteoric and burial calcite cement and clear, intrazooecial spar in nicholsonellid replacement-cement mosaic. Note the existance of identical cathodoluminescent zonation in both types of spar.

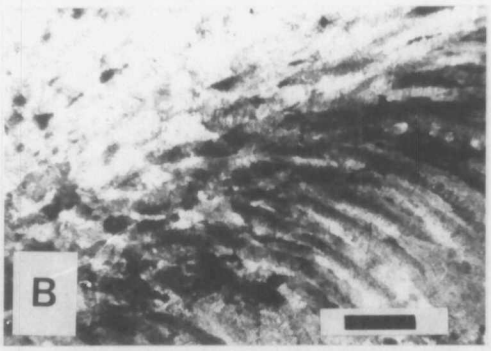
Figure 3.9. Diagenetic textures and fabrics associated with nicholsonellid replacement-cement mosaics.

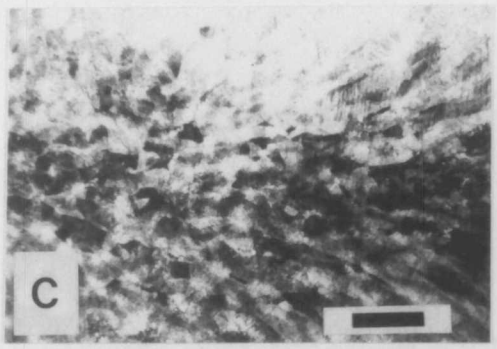
A. SEM photomicrograph of non-fabric selective calcite mosaic. Note the general difference in the nature of the intercrystalline boundaries between relict walls (W) and pore-filling cement (C). Sample CS41. Scale bar = 40 micrometers.

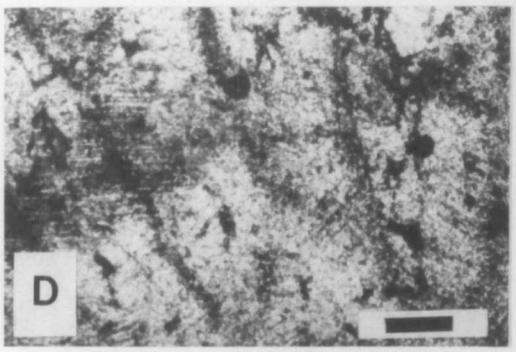
B, C. Portion of a replacement-cement mosiac after successive 20^0 rotations of the polarizer-analyzer orientation relative to the specimen. Note how the extinction zone sweeps through the spar mosaic. Sample CS26. Crossed polars. Scale bar = 0.25 mm.

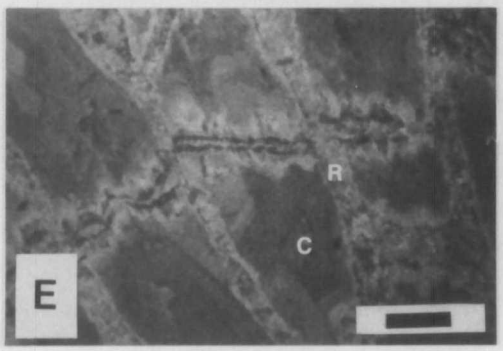
D, E. Plane light - cathodoluminescent photomicrograph pair of replacement-cement mosaic showing the presence of abundant brightly luminescent calcite (B) in inclusion-rich relict walls, indicating Mn alloenrichment during skeletal neomorphism. Calcite cement (C) occluding intrazooecial pores is dull luminescent. Sample CS16. Scale bar = 0.1 mm.


C
W
C
A


B


C


D


R
C
E

in origin have similar Sr and Mg concentrations (Fig. 3.10). Petrographic and cathodoluminescent features indicative of vadose diagenesis were not observed in these bryozoans.

Diagenetic calcites are typically equant in transverse sections, but in longitudinal sections have a sub-equant to bladed morphology with elongation directions parallel to relict walls (Fig. 3.4C). SEM clearly shows the cross-cutting fabric of anhedral calcites with respect to relict walls. Adjacent crystals in foliate growth forms have approximately the same optic axis orientations, giving the overall mosaic sweeping extinction upon rotation of the stage (Fig. 3.9B and C). Inclusion-rich portions of some of the coarsely crystalline calcites have slightly undulose extinction.

In specimens with interzooecial sediment, the relict walls consist of coarse, anhedral spar with abundant sub-micrometer inclusions/pits (Fig. 3.4B). Crystals tend to be coarse although microcrystalline grains (<10 micrometers) are associated with the coarser spar. No recognizable solid inclusions (microdolomite, aragonite) were found within these calcites.

Inclusion-rich calcites representing the relict walls have luminescent intensities varying from bright (Fig. 3.9 E) to dull and non-luminescent. Assuming Mn is the activator of luminescence and all biogenic calcites are

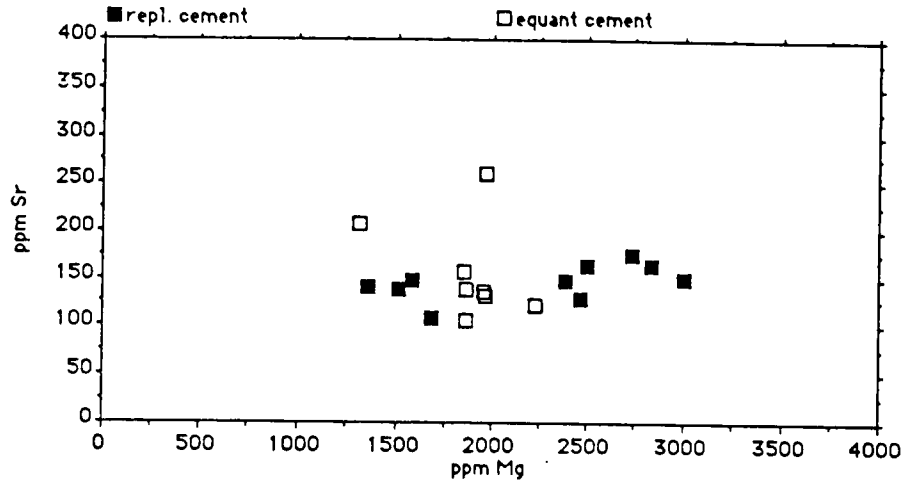


Figure 3.10. Strontium and magnesium concentration of nicholsonellid replacement-cement mosaics and coarsely crystalline, burial calcite cement. The overall lack of differentiation between these calcites is a result of the large volume of intrazooecial pore space in colonies. Replacement-cement mosaics with magnesium concentrations >2200 ppm may be due to the presence of minor intraskeletal, synsedimentary Mg-calcite cement.

non-luminescent (Czerniakowski et al., 1984), the presence of brightly luminescent calcite indicates mineralogical stablization in a chemically open system in which external fluids could affect the composition of diagenetic calcites. Modern taxa with microstructures probably resembling those in nicholsonellids have a micrometer-thick zone of secondary porosity separating aragonite and diagenetic (low-Mg) calcite that is open to dissolved ions (see Martin et al., 1986).

The available data allows for the development of a diagenetic model for Nicholsonella, the major stages of which are illustrated diagrammatically in Figure 3.11. Assuming an originally porous, spherulitic microstructure, neomorphism via micrometer-scale dissolution-reprecipitation to inclusion-rich calcite initiated within zooecial walls, possibly in areas of abundant organic matter. Neomorphism may have occurred at either discrete "inversion centers" which acted as loci for continued growth of crystals, or scattered areas within a single wall which eventually coalesced (the former is shown in Fig. 3.11). If the latter was operative, "sub-crystals" must have possessed equivalent optic axis orientations, indicating a high degree of microstructural control during the replacement process. The migration of recrystallization fronts through walls eventually produced a mosaic of interlocking, inclusion-rich

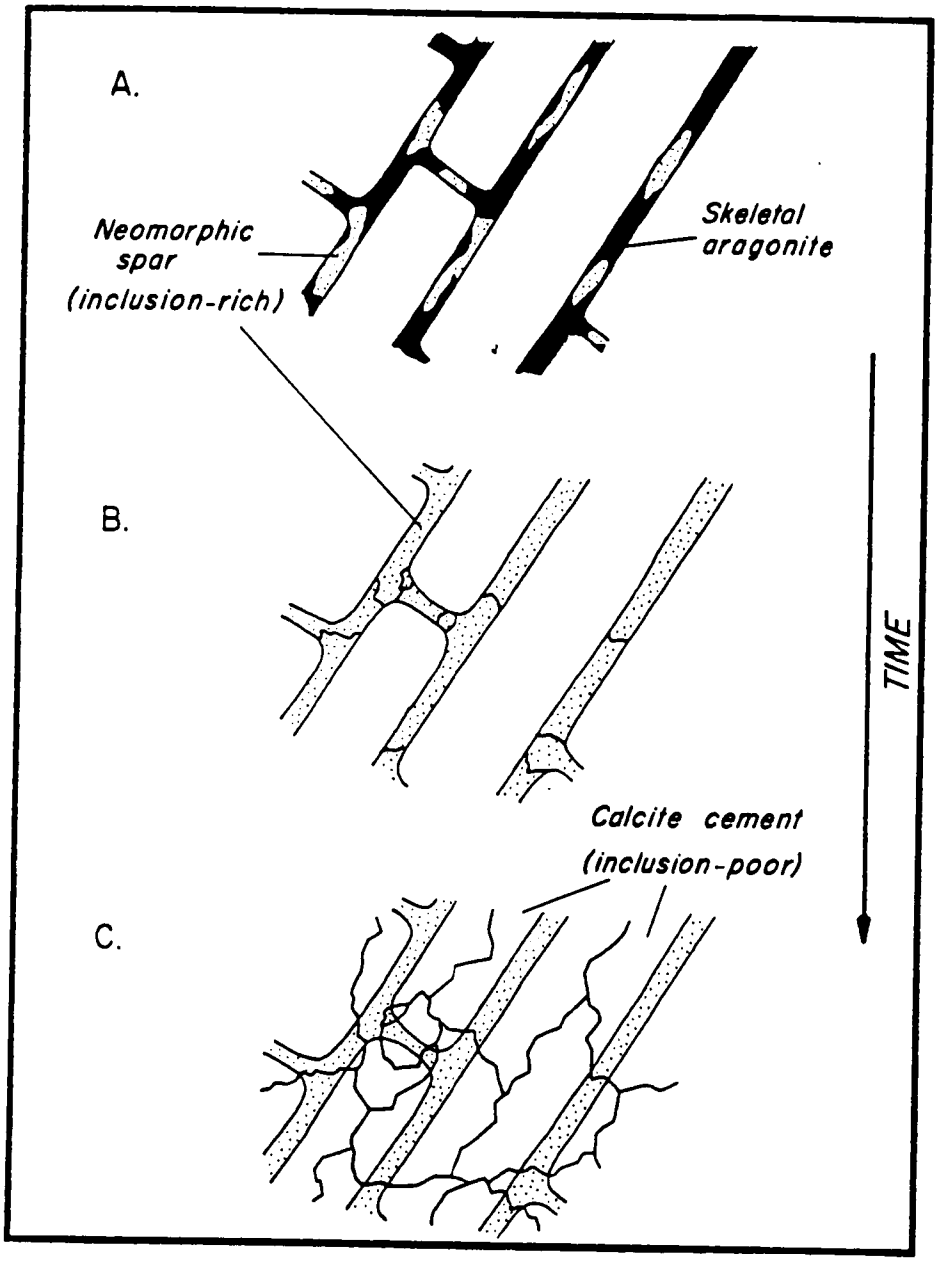


Figure 3.11. Model for shallow meteoric- to burial-phreatic diagenesis of originally aragonitic nicholsonellid bryozoans. Spar mosaics consist of an early "recrystallization phase" (A and B) represented by inclusion-rich calcite of variable luminescence, and a later "cementation phase" (C) represented by inclusion-poor calcite with luminescence and elemental geochemistry similar to other phreatic cements.

spar. After neomorphism the newly formed diagenetic calcites provided substrates for the heterogeneous nucleation of calcite cements which filled the remaining pore space. The sweeping extinction commonly observed is the result of cement crystals inheriting the same crystallographic orientation as neomorphic hosts.

Paleobiomineralization of Paleozoic Marine Organisms

In Table 3.2, the interpreted mineralogy of calcareous marine organisms and ooids from the Middle Ordovician is given along with representatives from older and younger Paleozoic limestones. Variations in ooid mineralogy have been addressed by other workers and will not be discussed here. Based on this limited data set, most groups that were important sediment producers maintained a uniform skeletal mineralogy for approximately 240 million years, at least in terms of the major $CaCO_3$ polymorphs. The chlorophyte algae represent the only taxon to have undergone any polymorphic change through the Paleozoic, and this appears restricted to the codiaceans represented by *Hedstroemia* in the Middle Ordovician and phylloid algae in the Pennsylvanian.

As mentioned during the discussion of chlorophytes, *Halimeda* forms its thallus passively from slightly modified seawater (intercellular space calcification mode of Bohm et

TABLE 3.2

SUMMARY OF INTERPRETED MINERALOGY OF BIOTIC COMPONENTS AND OOIDS FROM SELECTED PALEOZOIC AGES

Component	Early Cambrian	Middle Ordovician	Pennsylvanian Lower	Pennsylvanian Upper
	---	A(dasy) MG(cod)	---	A(cod)
Red algae	---	MG	---	---
Blue-green algae		MG	---	---
Bryozoans	---	A,MG	---	"C"
Brachiopods	---	C	C	"C"
Molluscs	A	A	A	A
Trilobites	MG	MG	---	---
Ostracodes	---	C/MG	---	---
Echinoderms	MG	MG	MG	"C"
Ooids	MG	MG	---	A,"C"

Explanation: A = aragonite
C = calcite
MG = magnesian calcite
"C" = calcite/magnesian calcite

al., 1978). The morphological similarity between this genus and Hedstroemia suggests comparable calcification mechanisms. Phylloid algae such as Eugonophyllum possessed structures resembling codiaceans (a medullary hypothallus with interwoven and branching filaments), and probably also precipitated CaCO via the intercellular space mode. Since the calcification process was isolated from organic layers, the resultant carbonate may be considered a type of non-skeletal deposit. Assuming this type of calcification, the apparent variation among codiaceans may be related to the same factor(s) influencing ooid and cement mineralogies - i.e., atmospheric carbon dioxide, Mg/Ca in marine waters. It is interesting to note that, based on the available data, the interpreted mineralogies of ooids and codiacean algae in these two periods correspond to one another.

Non-skeletal Allochems

Peloids

This group includes all particles which satisfy the definition of peloids proposed by McKee and Gutschick (1969) - i.e., variably-shaped silt- and sand-size grains composed

of microcrystalline carbonate. (The reason for using a definition without any genetic meaning was simply to facilitate petrographic analysis.) Illing (1954) proposed five(5) modes of origin for marine peloids: 1) marine cementation of finely comminuted skeletal material; 2) reworking of carbonate mud by organisms (i.e., pelletization); 3) diagenetic alteration of skeletal grains (i.e., micritization); 4) detrital fragments (i.e., small intraclasts); and 5) composite grains (i.e., grapestone grains, etc.). Most of these mechanisms contribute peloidal sediments to shallow-water carbonate environments; however, studies of Recent sediments indicate that pelletization and micritization predominate over the others. Peloids found in deep-water carbonates are the result of either resedimentation of shallow-water particles, or pelletization of shelf-derived muds in the upper (mixed) ocean layers. The mineralogy of Holocene peloids is remarkably uniform, thus supporting the dominance of one or two mechanisms for their formation. Grains are typically composed of randomly-oriented aragonite crystals less than 5 micrometers in size (Illing, 1954; Purdy, 1963; Logan, 1969; Bathurst, 1975). The original mineralogy of peloids produced by micritization appears to be controlled in most cases by the mineralogy of the skeletal substrate.

Peloids are most abundant in peritidal and shallow subtidal facies of the lower Chickamauga Group, with rare (<1%) occurrences in deeper water facies. A brief summary of the petrography of this allochem group is given in Table 3.3. In all samples, grains are of either depositional or early diagenetic origin, and not the result of neomorphism altering the original sediment texture. Several lines of evidence point towards a predominately fecal origin for peloidal grains in tidal flat and quiet subtidal, inner shelf facies. These particles have shapes identical to modern fecal grains, and in some instances are blackened due to the presence of disseminated pyrite framboids, which are an indirect product of the sulphate reduction of mucilaginous organic matter which bound constituent mud particles (see Illing, 1954). Peliods exhibit compactional fabrics such as the interpenetration of detrital quartz into grain margins and the structure grumeleuse of Cayeux (1935). The latter fabric represents (Beales, 1965) "...closely packed [peloidal] grains [which] appear to have merged on recrystallization". Grain size distribution is relatively uniform within a single inferred paleoenvironment. For example, peloids in tidal flat facies have a relatively narrow range of diameters (90 - 150 micrometers). Lastly, facies with evidence of intense bioturbation possess

TABLE 3.3

PETROGRAPHY OF PELOIDS FROM THE LOWER CHICKAMAUGA GROUP AND EQUIVALENTS

Environment	Shape	Mean Dimensions	Boundaries w/ matrix
Tidal	Ellipsoidal, tubular, spherical	0.1-0.2 mm	Sharp
Shallow subtidal	Ellipsoidal tubular, irregular	<1 mm	Sharp to slightly diffuse

abundant peloids which partially fill burrows. Since these grains represent the biogenic reworking of muddy substrates for their high organic content, the original mineralogy was identical to the lime mud precursor (see Chapter 2).

Subtidal packstones and grainstones often contain irregularly-shaped grains of microcrystalline calcite. Some of these particles have gross shapes resembling skeletal allochems (Fig. 3.12A). Although these peloids could have resulted from comminution of coarser micritic intraclasts, the presence of bioclasts exhibiting varying degrees of micritization and absence of intraclasts favors an early diagenetic origin. Skeletal allochems showing evidence of micritization are mostly arthropod and echinoderm fragments. Since both these substrates were originally magnesian calcite, the resultant peloids had an identical mineralogy.

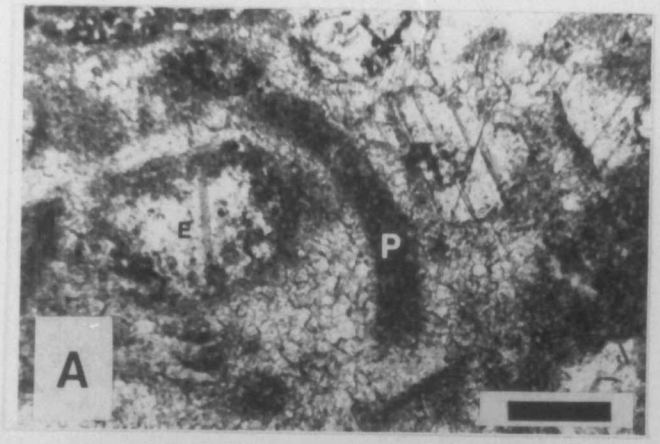
Peloids are a very minor constituent in fine-grained allochthonous carbonates deposited in the slope environment. These grains are no different petrographically from their shelf counterparts (see Table 3.3). Peloids are concentrated along thin laminae within individual beds, and are not part of any internal size grading. These peloids were either originally formed in shallow water and transported off-shelf with other carbonate sediments, or resulted from pelletization of shelf-derived muds in the

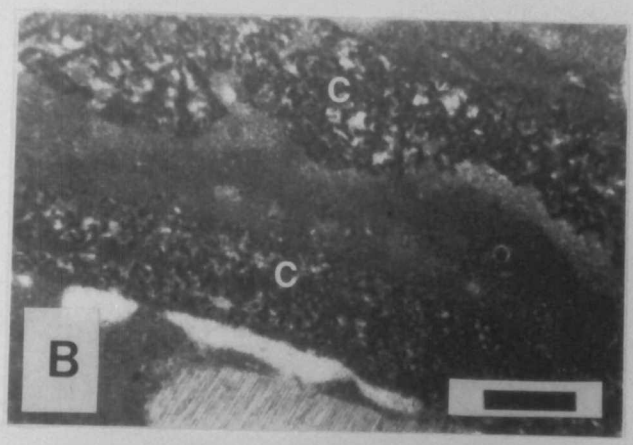
Figure 3.12. Thin section photomicrographs of non-skeletal allochems.

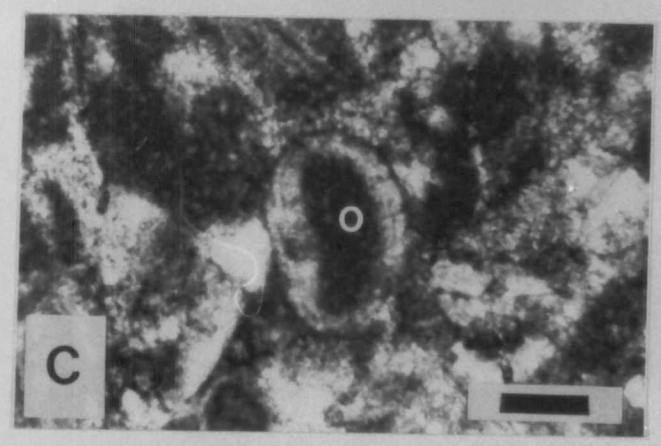
A. Elongate peloid (P) which probably formed via the complete micritization of a skeletal grain (arthropod, molluscs?) by boring algae and/or fungi. Partially micritized echinoderm grain (E) is present to the left. Sample SC11. Sacle bar = 0.1 mm.

B. Elongated algal intraclasts (C) in skeletal wackestone of outer shelf lithofacies. Sample RHB36. Scale bar = 0.25 mm.

C. Superficial ooid (O) with peloid nucleus and cortex of radial-prismatic calcite. Sample CS7. Scale bar = 0.1 mm.


E
P
A


C
C
B


O
C

mixed ocean layer followed by gravitational settling. Since both hypotheses indicate the unpelletized lime mud originated from the shelf, the deep-water peloids had an original mineralogy identical to precursor shelf muds (see Chapter 2).

Intraclasts

This allochem group is similar to peloids in that particles are typically polygenetic in origin. Particles which have been grouped as intraclasts include 1)aggregate grains (grapestone of Illing, 1954), 2)large micritized skeletal grains, 3)reworked submarine hardgrounds, beachrock and supratidal/intertidal sediments, and 4)older, lithified carbonate particles. In transgressive sequences, aggregate grains are rarely preserved due to post-depositional compaction destroying grain integrity; older lithoclasts are abundant only above unconformities and exposure surfaces. The majority of intraclasts in carbonate basins represent either micritized grains or reworked synsedimentary resediments.

Intraclasts are important only in peritidal and shelf-margin facies of the lower Chickamauga Group - i.e., environments favorable for hardening and synsedimentary

lithification of carbonate sediments. Clasts deposited in peritidal environments consist exclusively of lime mudstone, and represent the redeposition during storms of hardened and indurated muddy supratidal sediments (Shinn, 1983). The presence of diagnostic sedimentary features in clasts (e.g. fenestral vugs) attest to this supratidal origin. Intraclasts in shelf-margin Holston Formation are highly elongate and composed of either lime mudstone or peloidal lime mudstone (Fig. 3.12B), the latter having a faintly laminated appearance. Peloidal intraclasts have luminescence unlike associated depositional micrites. The fabric of these particles - especially the peloidal type - resemble Girvanella-bearing intraclasts with structure grumelesce microfabrics of the Cow Head Group (Coniglio and James, 1985). The similarity between the Middle Ordovician clasts and interpreted algal intraclasts would appear to suggest a compatible origin. If this is true, algally-constructed mounds or buildups should be present in this portion of the shelf. Algal buildups have not been identified in the Holston Formation. However, encrusting algae did aid in trapping and stabilizing fine sediments in mounds of the more shelfward Rockdell Formation (see Ruppel and Walker, 1982). Based on the above evidence, these clasts are interpreted to represent algal-bearing pieces of

the Rockdell lime mud mounds that were eroded and transported basinward, probably by storm currents impinging along the shelf. Neumann et al. (1970) found that when currents sufficient to erode subtidal algal mats are present, pieces 2 to 3 centimeters in diameter may be transported short distances. The observed microfabrics reflect synsedimentary processes (overcalcification) of the filamentous algae comprising these laminae (Coniglio and James, 1985).

Based on the above origins, some general mineralogical interpretations can be made for both peritidal and shelf-margin clasts. Peritidal intraclasts had a primary mineralogy similar to carbonate muds deposited on supratidal flats by storm flood currents. The mineralogy of algal intraclasts is more enigmatic. The microcrystalline calcite constituting the majority of each clast is probably dominated by algally-percipitated magnesian calcite as are algal oncoids, although trapped depositional lime mud may also be present. For simplicity, these particles will be assumed to have both a diagenetic component (magnesian calcite) and sedimentary component (lime mud) in a 1:1 ratio.

Ooids

Holocene ooids forming in well-agitated, shallow marine environments are composed of either aragonite, magnesian calcite, or both polymorphs that occur as mineralogically distinct layers. Aragonitic cortices possess either a concentric fabric in which laminae consist of equant, sub-micrometer crystals with optic axes oriented normal to the grain surface, or a microcrystalline fabric (Bathurst, 1975; Land et al., 1979). Cortices consisting of anhedral, radially-fibrous crystallites consist exclusively of magnesian calcite (Land et al., 1979). Studies of modern ooids (Illing, 1954; Bathurst, 1975; Land et al., 1979) indicate a predominance of concentric aragonite cortices.

The Chickamauga Group and its equivalents have suprisingly few oolitic facies. Those documented are restricted primarily to the mixed carbonate-siliciclastic lithologies of the Ottosee and Chapman Ridge formations (Cantrell and Walker, 1985, Asreen, 1984). Ooid-bearing units in the onlap sequence were only found in peritidal deposits of the Five Oaks Formation (Fig. 3.12C) and resemble superficial ooids described by other workers (Sickafosse, 1979). Cortices of peritidal ooids from the Middle Ordovician are poorly developed and have a radial-prismatic microstructure with the long axes of

crystallites oriented normal to the ooid surface. Neomorphic fabrics and cement-filled oomoldic porosity are absent.

The presence of radial-fibrous microstructure indicates a calcitic mineralogy for the cortices. Sorby (1879) first proposed an originally calcitic mineralogy for radial ooids because (p. 75) "...crystals are of such a uniform size...and so definitely oriented, that I can scarcely attribute them to the recrystallization of aragonite". The observed microstructure closely resembles the cortices of primary calcite ooids (Wilkinson and Landing, 1978), and do not exhibit diagenetic fabrics characteristic of interpreted aragonite ooids. Ooid shoal deposits in the Ottosee Formation also possess well-preserved cortical fabrics, suggesting a comparable original mineralogy. In addition, mollusc nuclei consist of clear, coarsely crystalline equant spar, while the cortex consists of radial-fibrous calcite. Petrography of Ottosee ooids viewed in light of recent work suggests the radial-fibrous microstructure is a primary feature indicative of an originally calcitic cortex, and not the product of post-depositional calcitization of aragonite. The mineralogical interpretation for ooids in this sequence agrees with petrographic studies of other oolitic deposits of Ordovician age (Sandberg, 1983).

Synsedimentary Cements

Modern

Calcium carbonate cements percipitated from seawater exhibit a wide variety of textures and fabrics (see James and Choquette, 1984 for a review). Aragonite cements in shallow-water facies consist of acicular crystallites that form 1)epitaxial, isopachous fringes, 2)botyroidal fans, and 3)spherulitic meshworks (James and Ginsburg, 1979; Dravis, 1979). Magnesian calcite represents the other major marine cementing agent on carbonate banks, typically occurring as massive to peloidal micritic crystallites, and bladed isopachous fringes (Land and Goreau, 1970; Ginsburg et al., 1971; James et al., 1976). Deep-water carbonate cements possess mineralogies and fabrics similar to their shallow-water counterparts (Milliman, 1966; Gervitz and Friedman, 1966; Mullins et al., 1980) along with rarer equant mosaics and bladed fringes composed of low-Mg calcite. Magnesian calcite appears to be the dominant cement mineralogy in modern oceans (James and Choquette, 1984). The precipitation of aragonite cements appears to be

controlled by both kinetic and/or compostional factors (Givens and Wilkinson, 1985; Burton and Walter, 1987).

Criteria for Recognition of Synsedimentary Cements in Limestones

Carbonate petrographers often take a uniformitarian approach in diagenetic studies and interpret any carbonate cement possessing either a fibrous or bladed morphology as being marine in origin. Although supportive evidence may be presented to substaniate this interpretation, certain textures, fabrics and geochemical signatures are better than others. The combined petrographic-geochemical evidence may be ranked in a four-tiered heirarchy of groups of criteria of decreasing reliability (Fig. 3.13). These criteria can be applied to any cement morphology and/or fabric (see Wilkinson et al., 1982; Walker et al., 1985).

In addition, cements which lack Holocene marine analogues have been interpreted as synsedimentary. Wilkinson et al. (1982) found drusy equant calcite mosaics to be an important marine cement in Middle Ordovician hardgrounds. Numerous workers have recognized features that suggest a marine origin for some monocrystalline syntaxial overgrowths on echinoderm grains (Purser, 1969; Cantrell and

Level of Assurance	Major Criteria
High	GROUP I: association with marine sediments and organisms - cement overlain or interlayered with geopedal internal sediment - cement cross-cut by marcoborings - micritized, oxide stained cement margins - cement truncated along ommission surfaces representing hardgrounds - cement margins encrusted by marine coelobites
	GROUP II: evidence of originally metastable mineralogy - disseminated microdolomite or aragonite inclusions in diagenetic calcite - botryoidal fabric consisting of equant calcite - square-ended crystal terminations - enriched strontium concentrations
	GROUP III: 13C/12C ratios comparable to marine carbonates from the same sequence (assuming minor vital effect).
Low	GROUP IV: petrographic features indicative of early phreatic cementation - initial fibrous to bladed morphology occluding pore space - isopachous fabric - euhedral crystal terminations at contacts with other cements

Figure 3.13. Criteria for recognizing synsedimentary cements in ancient limestones.

Walker, 1985; Walker et al., 1985). The realization that equant and echinoderm syntaxial overgrowth cements could have been precipitated from Paleozoic seawater complicates matters, because these textures and fabrics in shallow-water facies are often very similar to common meteoric cements. The precipitation of marine equant and echinoderm overgrowth cements during the Phanerozoic may have been governed by temporal variations in sea water chemistry (PCO_2, Mg/Ca). Because of a lack of detailed cement geochemical data in this study, the following line of reasoning was adopted in ascertaining the origin of echinoderm overgrowth and equant cements: since both are typically precipitated from meteoric and burial fluids (Longman, 1980), it is assumed nonferroan overgrowths are non-marine in origin unless they either 1) possess criteria listed under levels I or II in Figure 3.13, 2) show evidence of competitive growth fabrics with interpreted marine cements or 3) exhibit a high inclusion density.

The relative abundance of "inclusions" in echinoderm overgrowth cement may offer additional evidence to petrographically distinguish their origin (marine vs meteoric). Early overgrowth calcites which exhibit fabrics indicative of synsedimentary precipitation are exclusively inclusion-rich in this sequence, whereas interpreted

meteoric calcite cements are almost completely free of inclusions. However, inclusion-rich cements have noticeable variations in terms of inclusion density across the shelf. If this feature is to be successfully used as a criterion for identifying marine cements, the above textural variation must be explained in addition to characterizing the nature and composition of these inclusions. Marine overgrowths may also consist of clear, inclusion-poor calcite (see Wilkinson et al., 1982). The existence of conditions whereby both textural varieties could have precipitated may cause the actual abundance to be underestimated. Although this feature may aid initial assessment of the proportion of marine and meteoric cement, care should be exercised, particularly in shelf/platform sequences where both paleoenvironmental and petrographic data is cursory.

Ordovician

The following sections present a brief description of calcite spar interpreted as marine-phreatic in origin. For a more indepth discussion of synsedimentary cements from these limestones, the reader is referred to Jernigan (1987).

Fibrous and Bladed Cements. These cements in shallow-water facies occur as isopachous to nonisopachous fringes of inclusion-rich(IR) to inclusion-poor(IP), nonferroan spar that typically occlude primary voids (Fig. 3. 14A and B). Some cement rims have textures resembling radiaxial fibrous calcite-fascicular optic calcite (RFC-FOC; Kendall and Tucker, 1973). In pores filled by more than a single cement generation, fibrous/bladed cement is always the initial precipitate on polycrystalline substrates. Cements may be overlain by internal sediments and contain zones of metal-oxide staining. These cements are also found in bioclastic sediment gravity flows where they form the initial cement generation on arthropod debris.

Echinoderm Overgrowths. This cement occurs as IR to IP single calcite crystals in optical continuity with echinoderm grains (Fig. 3.6D and E). The inclusion-rich portion of the overgrowth is always directly adjacent to the ossicle, and may exhibit competitive growth fabrics with fibrous spar (Fig. 3.14C). The interference between these cements results in a planar to gently curved compromise

Figure 3.14. Thin section and SEM photomicrographs of interpreted synsedimentary cements.

A. Interparticle radiaxial fibrous calcite-fascicular optic calcite (F) which nucleated on calcitic skeletal particles. Sample RHB45. Scale bar = 0.25 mm.

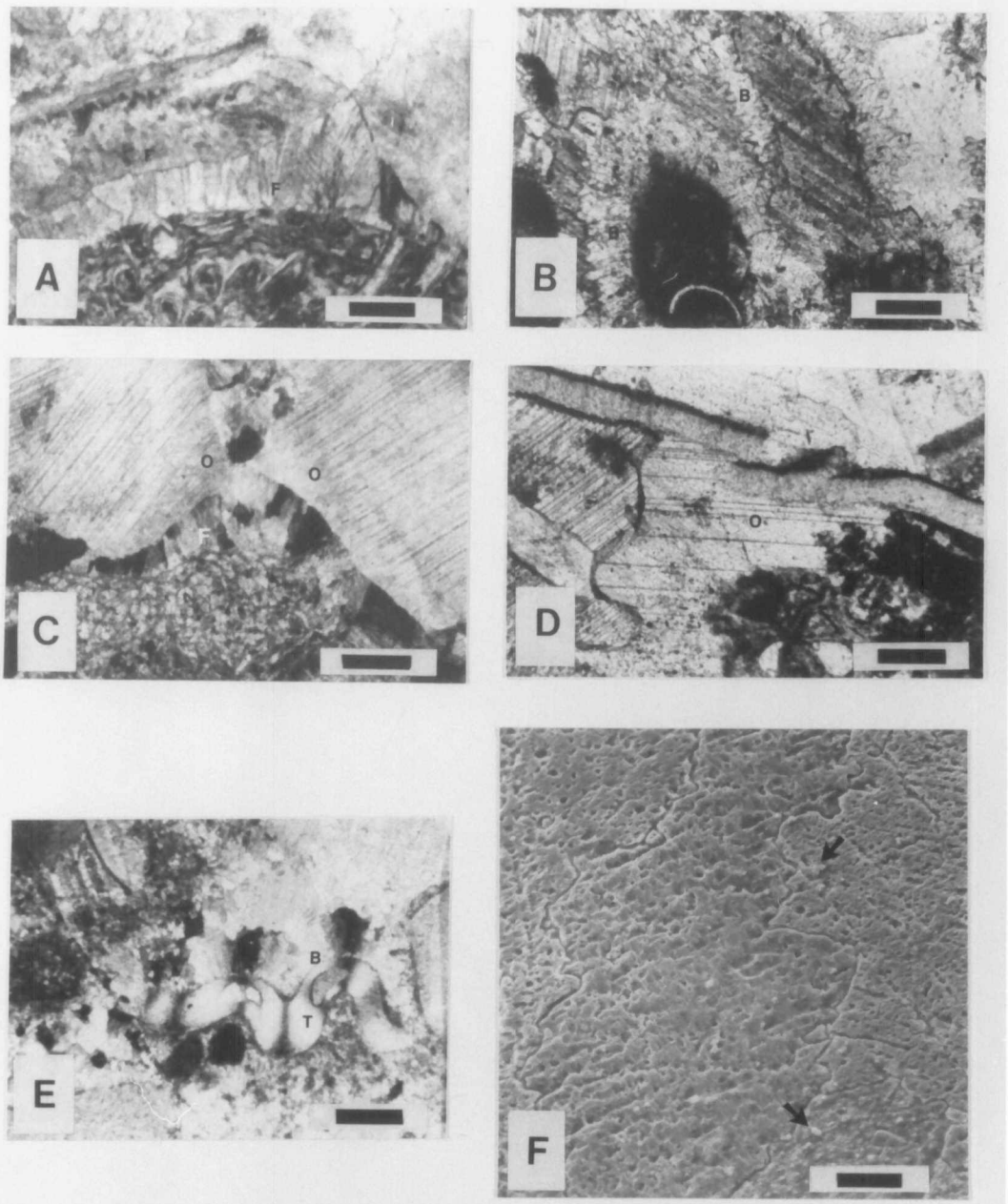
B. Isopachous rims of bladed calcite (B) which nucleated on skeletal and non-skeletal grains. The remaining relict pore space is occluded by both echinoderm syntaxial overgrowth calcite and equant calcite cements. Note well-developed scalenohedral crystal terminations on bladed crystals. Sample CS45. Scale bar = 0.1 mm.

C. Compromise growth boundaries between inclusion-rich radiaxial fibrous calcite-fascicular optic calcite (F) and microdolomite-bearing echinoderm syntaxial overgrowth calcite (O) cements. Contact between echinoderm grains and associated cements are indicated by dashed lines. Note the fibrous cement increases in thickness away from the echinoderm grains. Sample RHB45. Scale bar = 0.25 mm.

D. Clear echinoderm overgrowth calcite cement (O) present along the fractured surfaces of an arthropod grain. Sample CS27. Scale bar = 0.1 mm.

E. Bored trilobite carapace (T) with a bladed fringe of epitaxial calcite cement (B). Extinction extends from the trilobite into the adjoining calcite cement. Micritic and peloidal material underlies the trilobite fragment. Sample DL4. Scale bar = 0.25 mm.

F. SEM photomicrograph of radiaxial fibrous-fascicular optic calcite cement with rare microdolomite inclusions (arrows). Sample RHB45. Scale bar = 30 micrometers.


A
F
B
B
C
O
O
F
D
O
E
B
T
F

boundary which resembles the polygonal cement boundaries of Shinn (1975). Such fabrics provide strong evidence for contemporaneous precipitation and thus a marine origin for IR overgrowths, assuming the fibrous spar has been correctly interpreted.

Echinoderm overgrowth cements complicate diagenetic studies in that a change in pore-water chemistry (marine to meteoric) is not reflected by any change in texture other than usually a decrease in inclusion density. Instead of nucleating a new crystal morphology, synsedimentary and postsedimentary overgrowths form a single, optically continuous crystal. Because of this crystallographic uniformity, distinction between marine, meteoric and burial zones may be initially ambiguous. However, detailed petrographic analysis supplimented by cathodoluminescence provides two pieces of evidence, which together with the absence of synsedimentary fabrics and/or chemical tracers (see Fig. 3.13) indicate a non-marine origin for IP overgrowth cements. First, clear calcites have moderate to dull luminescence similar to late-stage, Fe^{2+}-rich equant cements. Since dissolved iron concentrations in oxygenated marine waters are extremely low (Morse et al. 1985), these luminescent zones were probably precipitated after sufficient burial to isolate pore waters from near-surface

conditions. Secondly, clear overgrowths are commonly found along the fractured surfaces of skeletal grains, and in extreme cases may completely enclose broken allochem fragments (Fig. 3.14D). Even though grain compaction may commence after only 10 meters of burial (Meyers, 1980), marine cementation is restricted to depths of only a few centimeters (James and Choquette, 1984). Thus, cements in direct contact with the fractured surfaces of allochems could not have been precipitated in the marine-phreatic realm.

Microcrystalline Calcite. Micritic magnesian calcite is one of the most abundant cements in modern shallow- and deep-water carbonates (Milliman, 1966; Ginsburg et al., 1971; James et al. 1976; Macintyre, 1977). However, this cement is rarely distinguished in ancient limestones because of its close similarity to depositional micrite. Thus, the importance of this cement type has in all likelihood been grossly underestimated in diagenetic studies of Phanerozoic carbonate sequences.

Allochems in both outer shelf facies and drowned ramp facies have thin (<0.2 mm) isopachous coatings and intrabiotic fillings of dense microcrystalline calcite of

probable cement origin. In addition to displaying fabrics similar to modern micritic cements, these Middle Ordovician calcites possess other features indicative of a precipitational origin: 1)sharp contacts with skeletal substrates, 2)no evidence of encrusting algae and, 3)absence of fine grained bioclastic debris. Nucleation of fibrous spar on microcrystalline cement offers positive evidence of a marine origin.

Original Mineralogy of Synsedimentary Cements

Fibrous and Bladed Calcite. The following petrographic and geochemical data suggest a primary magnesian calcite mineralogy for these cements. (Even though much of the data is from cements occurring in shelf facies, fibrous/bladed cements in deep-water carbonates have similar properties, and in the absence of geochemical data are assumed to have possessed equivalent original mineralogies.)

(1) In pores that are only partially occluded, crystals have sclenohedral/pyramidal terminations (Fig. 3.14B and E); no evidence of square-ended rays typical of aragonitic cements were observed (Loucks and Folk,

1976).

(2) Crystals possess elongation directions normal to the host substrate and relatively uniform optic axis orientations. Diagenetic stablization of aragonitic botyriodal cements produces a mosaic of equant to subequant spar that lacks optical continuity (Mazzullo, 1980; Sandberg, 1983, 1985).

(3) Radiaxial fibrous calcite-fascicular optic calcite mosaics sometimes contain very finely crystalline microdolomite inclusions (Fig. 3.14F).

(4) Cement fringes exhibit a syntaxial relationship with skeletal substrates interpreted as originally calcite (Fig. 3.14E). Boundaries marking the original pore margin in some instances are undiscernable. Syntaxy between cement and its host substrate indicates similar mineralogies at the time of growth and/or neomorphism (James and Klappa, 1983).

(5) Chemical analyses give mole % $MgCO_3$ contents comparable to interpreted magnesian calcite cements and above those of botryoidal aragonite cements. In addition, the range of Sr concentrations is below the typical Sr values of botyroidal cements (see Jernigan, 1987).

Echinoderm Overgrowths. Monocrystalline overgrowths represent another form of syntaxial crystal growth. The original cement mineralogy of inclusion-rich overgrowths could be either calcite, or possibly aragonite that possessed optic axes orientations identical to the echinoderm substrate. Aragonitic marine cements only exhibit growth syntaxy on aragonite substrates such as molluscs and scleractinian corals. The inferred magnesian calcite mineralogy of echinoderms eliminates the likelihood of a primary aragonite mineralogy for this cement. Wilkinson et al. (1982) proposed a calcite precursor mineralogy for echinoderm "rim cement" in submarine hardgrounds based on their similarity to meteoric overgrowths, and repeated formation within the sediment. The syntaxial relationship between substrate and cement favors a magnesian calcite cement mineralogy since the echinoderm grains probably did not stablize to calcite in the marine environment (see Berner, 1966). Very finely crystalline microdolomite rhombohedra within the IR overgrowth cements support this interpretation. The inclusion-poor overgrowths were probably composed of calcite. This is implied by their meteoric origin, and the general consensus among carbonate petrographers that magnesian calcite does not precipitate from meteoric waters

with low Mg/Ca ratios.

Microcrystalline Calcite. Holocene submarine micritic cements are almost exclusively magnesian calcite in composition regardless of water depth. [The only exception is the microcrystalline aragonite cement in portions of the Persian Gulf (Shinn, 1969).] The fabric similarities between these modern cements and Middle Ordovician counterparts should probably reflect some degree of mineralogical equivalence, and thus a magnesian calcite composition is proposed for this cement. Isotope and trace element data would greatly aid in the interpretation of this cement's original mineralogy.

Original Mineralogy of Sedimentary Facies

In order to assess any regional geochemical variations in this sequence, the original mineralogy was determined for shelf facies using the interpreted mineralogies of particle types and synsedimentary cements, and constituent analyses of 120 thin sections from representative lithofacies.

Constituent particle percentages are based on a minimum of 400 points per sample; the maximum range (95% confidence level) for a particular constituent particle is + 5% (see Van der Plas and Tobi, 1965). If the microscope cross-hairs landed on identifiable intrabiotic pore space, the respective point was counted as matrix and not allochem.

Grain percentages obtained using this method only approximate the proportions of calcareous organisms inhabiting a particular environment. Grain compositions in contiguous environments are significantly influenced by 1)the rate of skeletal growth, 2)organism's life span, 3)organism's susceptibility to post-mortem disintegration, and 4)resistance of a skeleton to mechanical and biological breakdown (Bathurst, 1975). Some carbonate-secreting organisms are probably excluded from the allochem fraction during sedimentation, and diagenetic processes (grain compaction and neomorphism) may further modify the allochemical composition. Discussions of mineralogical differences between carbonate facies must take into consideration the above factors.

Original mineralogies of the sediment coomponent from the Middle Ordovician are plotted as fields on the ternary diagram in Figure 3.15. (See Appendix F for additional explanation concerning the procedure and data.) The

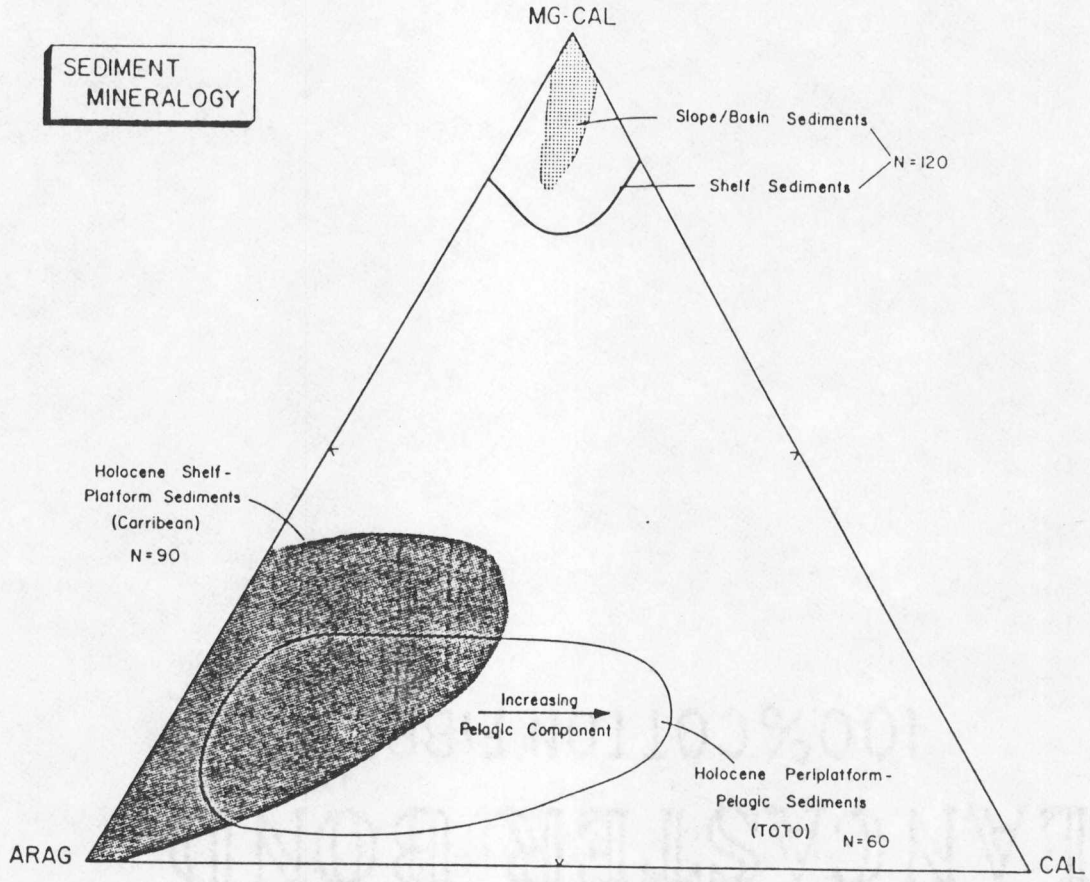


Figure 3.15. Original mineralogy of Middle Ordovician sedimentary facies (N=120) and Holocene platform, periplatform and pelagic sediments (N=155). Data for modern analogues derived from Till (1968), Stehli and Hower (1961), Pilkey and Rucker (1966).

mineralogy of Recent, low-latitude platform and deep-water carbonate sediments similar to the chlorozoan/oolith-pellet grain association of Lees (1975) are shown for comparison. The Middle Ordovician facies as a group are characterizied by appreciably more magnesian calcite than modern carbonates, even taking into consideration the confidence limits of the constituent particle analyses and diagenetic alteration. The calcite + magnesian calcite fraction is typically less than 50% on Pleistocene-Holocene banks, while during the Middle Ordovician both polymorphs constituted greater than 85% of the sediment. A more representative Recent analogue for the Middle Ordovician sediments appears to be the formol/pellet grain association of Lees (1975) which characterizes temperate water areas. In both settings, the high calcite percentages reflect the scarcity of indigenous aragonite-secreting biota. Paleogeographic reconstructions of plates after Scotese et al. (1979) shows the Laurentian land mass, which included the North American craton, was positioned in the Southern Hemisphere Equatorial zone during the Middle Ordovician, excluding ambient temperature as a reason for the calcite-dominated sediment composition. Salinity variations were also unimportant, as facies suites and reconstructed shelf paleocommunities indicate relatively uniform normal marine salinities over

the entire shelf. The lack of abundant aragonite in this shelf setting reflects a fundamental differences in the abundance of the major sediment-producing marine organisms. Assuming an aragonitic primary mineralogy for ancient epicontinental limestones based only on comparison with modern shallow-water carbonates is a conclusion which should be made only after careful petrographic analysis.

Shallow-water facies suites exhibit subtle differences in their original sediment mineralogy as shown by considerable overlap of the respective fields (Fig. 3.16). The differences present reflect variations in the proportion of aragonite and calcite; magnesian calcite has approximately equal ranges in each facies suite. This mineralogical uniformity indicates the dominance of calcite-secreting organisms in both inner and outer shelf facies suites. Shelf-wide compositional gradients resulting from facies dominated by aragonitic and calcitic biota were nonexistant. Environmental gradients (e.g., water turbulence, depth) may have had some minor affect on the bulk sediment mineralogy, but such variations probably would be undetected in bulk chemical analyses of component facies. The homogenous mineralogy of shelf sediments is another characteristic which differentiates this Paleozoic setting from modern carbonate banks such the Belize shelf (see

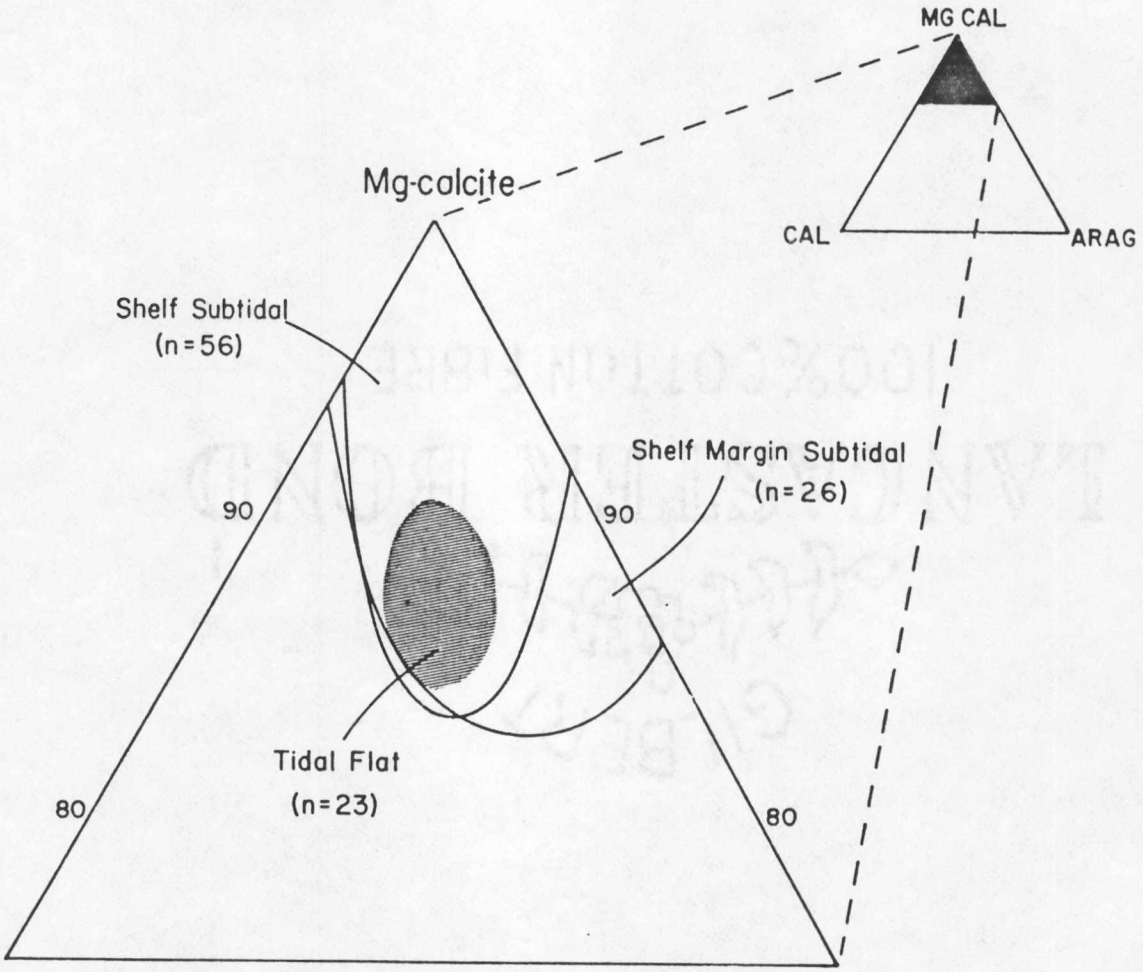


Figure 3.16. Interpreted original mineralogy of major sedimentary facies suites on the Ordovician ramp and shelf. N = 120.

Seigel, 1961; Matthews, 1966; Bosence et al., 1985).

Mean volumes of fibrous/bladed + micritic cements from inner and outer shelf facies (Fig. 3.17) show a decrease in the intensity of marine cementation toward the northwest, away from the shelf margin. Although IR echinoderm overgrowths are excluded, their addition would simply intensify the trend shown. The wide range in volumes, particularly the fibrous/bladed cement, in outer shelf facies (RHB and CS localities) suggest sedimentation rates may have fluctuated considerably during deposition. Stratigraphic intervals with well-developed marine cements in the lower Holston Formation are also characterizied by metal-oxide coatings on allochems and replacement phosphate minerals (see Chapter 5). The presence of these non-carbonate phases in some abundance reflects the prolonged interaction of oceanic waters with the carbonate sediments. The absence of these minerals at other intervals probably resulted from decreased exposure to flushing marine waters.

Most of the mineralogic fields defined by the sediments experience no pronounced shifts if synsedimentary cement volumes are included. The only change would be a minor shifting of the shelf-margin facies suite toward the magnesian calcite apex due to the relative abundance of

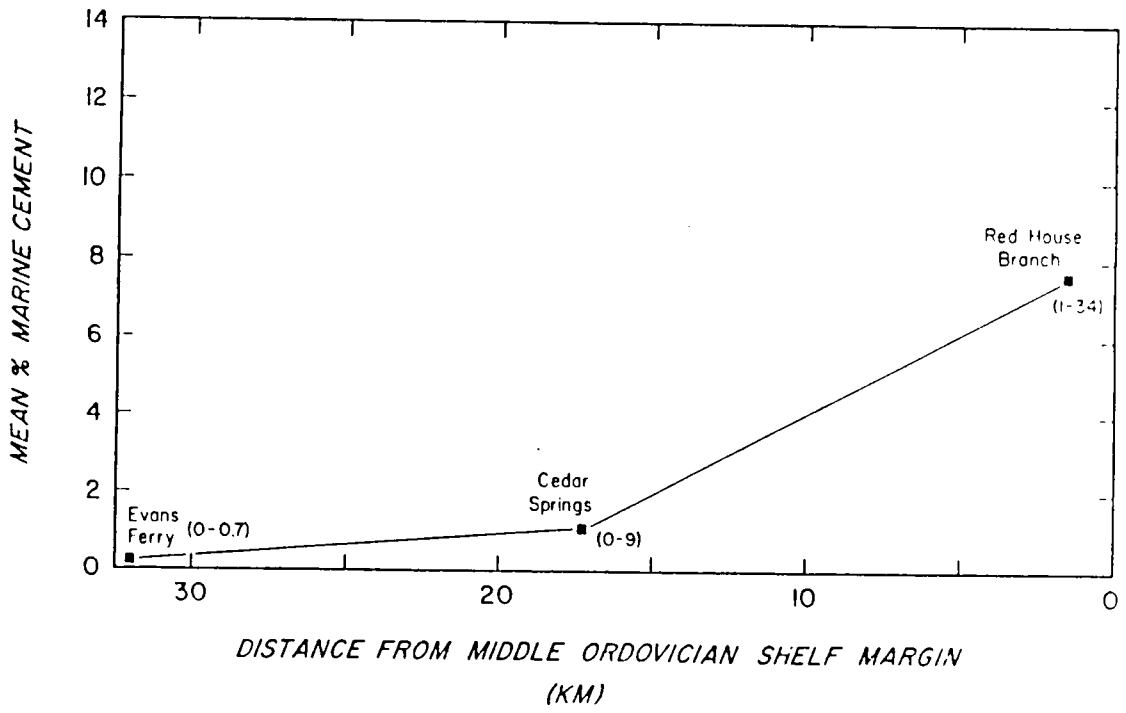


Figure 3.17. Cross-shelf variation in marine lithification as reflected by the abundance of interpreted synsedimentary cements. Data shown above are for fibrous and microcrystalline calcite in grain-supported lithologies from the lower Chickamauga Group and Holston Formations. Square dots represent mean cement volume; values in parentheses indicate the range in cement volumes for a given locality. Evans Ferry data from Jernigan (1987).

synsedimentary Mg-calcite cement. Thus, the areas delimited in Figure 3.16 accurately reflect the proportions of aragonite, calcite and Mg-calcite in Middle Ordovician sedimentary facies prior to stabilization by non-marine waters.

Implications of these interpretations bring to light other fundamental differences between Paleozoic and younger (Cenozoic) carbonate deposits. The original mineralogy of the Middle Ordovician deep-water carbonate facies lies totally within the shallow-water field, while Holocene carbonate oozes only partially lie inside the field for coeval shallow-water facies (Fig. 3.15). The inter-relationship between the two fields reflects a fundamental difference in sediment contribution to periplatform and abyssal settings during the Paleozoic and Cenozoic. Modern carbonate oozes contain a mixture of banktop aragonite and magnesian calcite admixed with calcite tests of pelagic organisms, with the latter increasing in volume with distance from the platform. The relative contribution of the shoal-derived sediment source also has a temporal component that appears to be related to sea level changes (Boardman et al., 1986). Paleontologic evidence indicates the bulk volume of skeletonized pelagic biota was relatively low in Paleozoic oceans. Deep-water limestones

such as the Whitesburg Formation are periplatform carbonates sensu Cook et al. (1983), consisting of predominately shoal-water, shelf-derived sediments with allochems of indigenous calcareous biota (trilobites, tintinnines, cephalopods) comprising a very minor portion of the total sediment. Because of the lack of an important pelagic component, we would expect the original mineralogies of Early Paleozoic shallow- and deep-water fields to be similar.

A calcite-dominated precursor mineralogy also has diagenetic implications with respect to sources of carbonate cement and porosity development. The dissolution of aragonite grains supplies an important source of autochthonous calcium carbonate for cementation (see Bathurst, 1975). Loss of this potential source means others must become relatively more important during lithification of a given sediment thickness. The abundance of pressure solutional features (stylolites, compactional fabrics) indicates this mechanism was a major supplier of carbonate in this Ordovician transgressive sequence. The scarcity of aragonitic components also limited the development of secondary (moldic) porosity during meteoric/burial phreatic diagenesis. The majority of pre-burial porosity in carbonate sequences dominated by calcitic allochems is

intergranular in nature. Such knowledge concerning the potential for porosity enhancement should aid in the recognition of zones that could provide conduits for the migration of burial fluids and associated hydrocarbons.

CHAPTER 4

CARBONATE GEOCHEMICAL FACIES IN A RAMP-TO-SHELF TRANSITION, MIDDLE ORDOVICIAN, EAST TENNESSEE

Introduction

Geochemical data on Phanerozoic limestones and dolostones collected over the last few decades suggests that individual facies or facies suites may possess distinctive minor/trace element compositions. Some of these data have been restricted to a specific carbonate sequence to aid in deciphering local stratigraphic problems (e.g. Chester, 1965; Davies, 1972). Other elements, particularly strontium, manganese and sodium, have been studied in different shelf/platform facies in attempts to identify factors that influence their concentrations (Veizer and Demovic, 1974; Bencini and Turi, 1974; Veizer et al., 1977; Shanmugam and Benedict, 1983). The original sediment mineralogy is often mentioned as a likely factor controlling the distribution of carbonate-bound manganese and strontium in limestones. Middle Ordovician ramp and shelf carbonates

possessed a relatively uniform bulk mineralogy at the time of deposition (see Chapter 3). This sequence affords an opportunity to access more closely the significance of original mineralogy and other depositionally-controlled factors on shelf-wide trace element distributions. Although the primary mineralogy contributed to the geochemistry of shelf limestones, variations between component facies are the product of other depositional and diagenetic factors.

Multivariate cluster analysis was used to group shelf lithotypes with similar trace element signatures. The nature and stratigraphic distribution of these statistical groups were analyzed to understand the factors (depositional and/or diagenetic) which controlled geochemical variations across the shelf.

Methods

Carbonate lithic samples were collected from exposures which span the ramp and early shelf-basin phases of deposition during the Middle Ordovician (see locality map in Chapter 1). Uncovered and stained thin sections of 190 samples were examined using conventional petrography. Sixty selected samples were examined under cathodoluminescence

using a Nuclide ELM-2A Luminoscope. These samples and 16 lithic samples collected from the St. Clair locality by Walker and Misra (1982) were analyzed to determine whole-rock concentrations of Mg, Sr, Mn, Fe, Na, and Zn of the acid-soluble fraction using a Varian AA475 atomic absorption spectrophotometer. (Sample preparation and operating conditions during analysis are discussed in Appendix B). Insoluble residues after carbonate removal include clay/mica, quartz, plagioclase feldspar, pyrite, Fe-Mn oxides and phosphatic minerals. Multivariate cluster analysis (SAS) was performed on trace element and constituent data from 140 samples to define groups with similar lithologic and geochemical characteristics. Duplicate samples excluded from statistical analysis were then placed in their respective groups. The distribution of geochemical facies is based on the clustering of all 206 carbonate samples.

The geologic and stratigraphic setting of the Middle Ordovician sequence has been summarized previously in Chapter 1.

Carbonate Geochemical Facies

The identification of lithofacies with similar geochemical signatures in previous studies (e.g., Adams and Weaver, 1958; Chester, 1965; Shanmugam and Benedict, 1983) has generally disregarded all but the most basic lithologic and paleoenvironmental data, and used a very limited number of geochemical variables. Since carbonate sediments may undergo early lithification in the environment of deposition and certain environments are more susceptible to specific diagenetic processes than others, it is prudent that discernment of geochemical facies in carbonate sequences should include both detailed lithologic data and a more complete characterization of the geochemistry. Variables used in the clustering procedure are listed in Table 4.1. Trace element compositions represent whole-rock analyses and are given in Appendix B. Petrographic data includes the volume abundances of grain types, depositional matrix and diagenetic features (cement, dolomite) derived from point count analyses of thin sections representative of lithofacies for which geochemical data was available.

A Q-mode cluster analysis on the unstandardized data set (SAS CLUSTER; Fig. 4.1) indicates different degrees of similarity between the six sample groupings identified. The

Figure 4.1. Simplified Q-mode cluster dendogram constructed from S.A.S. "tree diagram". Clusters which are outlined and identified by Roman numerals represent groups of samples with maximum association, and form the geochemical facies as defined in this study.

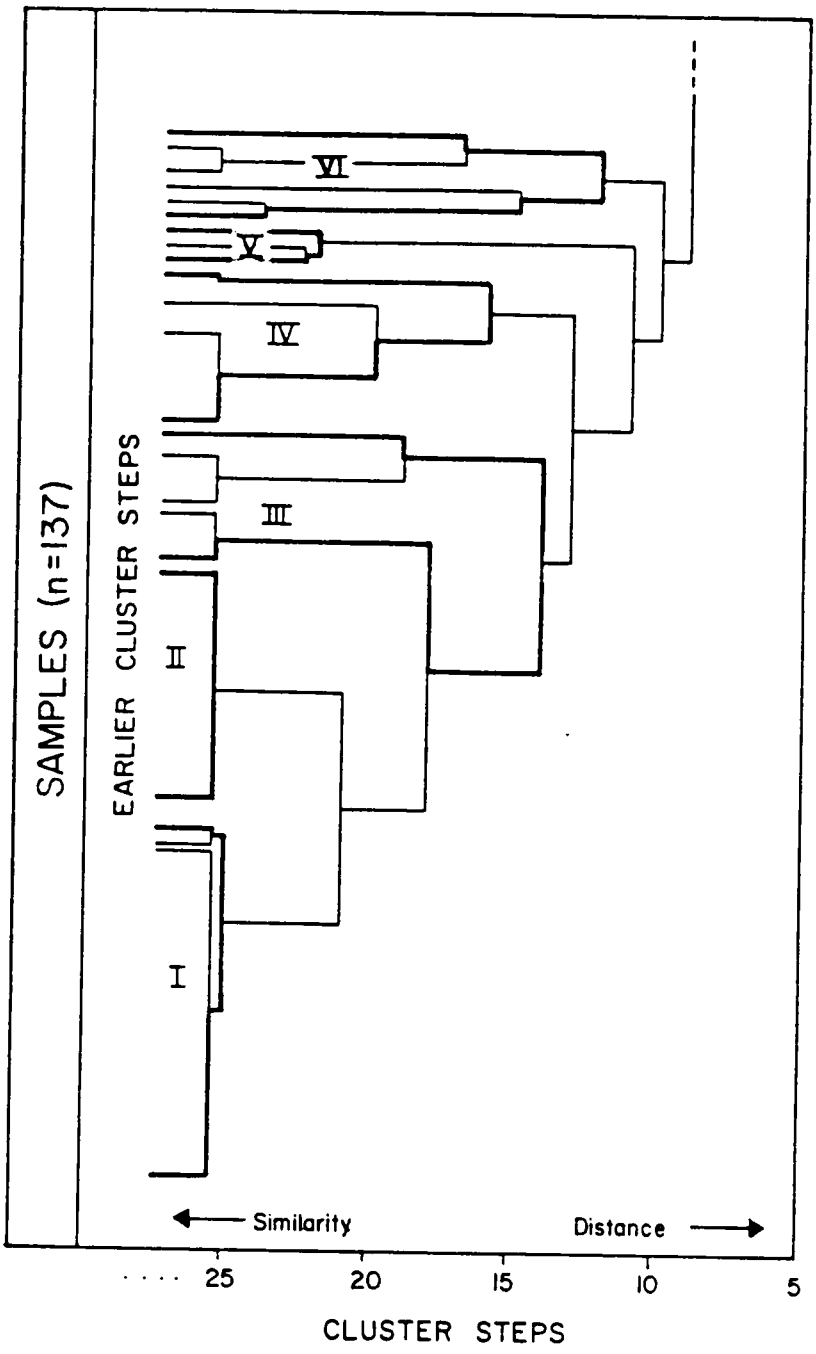

SAMPLES (n=137)
EARLIER CLUSTER STEPS
VI
V
IV
III
II
I
Similarity
Distance
25
20
15
10
5
CLUSTER STEPS

TABLE 4.1

GEOCHEMICAL AND LITHOLOGIC VARIABLES USED TO CHARACTERIZE SAMPLES FOR Q-MODE CLUSTER ANALYSIS

GEOCHEMICAL	LITHOLOGIC
SR = Strontium	MIC = Micrite/Microspar
MN = Manganese	SILT = Carbonate Silt
FE = Iron	PELO = Peloids
NA = Sodium	ARTHRO = Arthropods (trilobites and ostracodes)
ZN = Znic	MOLL = Molluscs
MG = Magnesium	ECHINO = Echinoderms
	BRACH = Calcareous Brachiopods
	BRYO = Bryozoans
	CALALG = Calcareous red and green algae + problematic forms (Nuia)
	BGALG = Blue-green algae (mostly Girvanella)
	EQCMT = Equant Cement
	MARCMT = Interpreted Marine Cement
	OVG = Echinoderm Overgrowth Cement
	BRQDOLO = Saddle (Baroque) Dolomite
	FNDOLO = Fine Grained Dolomite
	PYRI = Diagenetic Pyrite
	STYLO = Stylolite
	PCTIR = Percent Insoluble Residue

end of the routine shows the clustering of individual samples or sample pairs at very low levels of similarity with respect to the remainder of the sample set. These samples could be interpreted as a seventh cluster characterizied by a high degree of lithologic and/or trace element dissimilarity. Most of the samples occur in close stratigraphic association with samples comprising the other groups. Since this procedure was adopted to help discern patterns of geochemical variation in this sequence, these "unique" samples were excluded from further analysis.

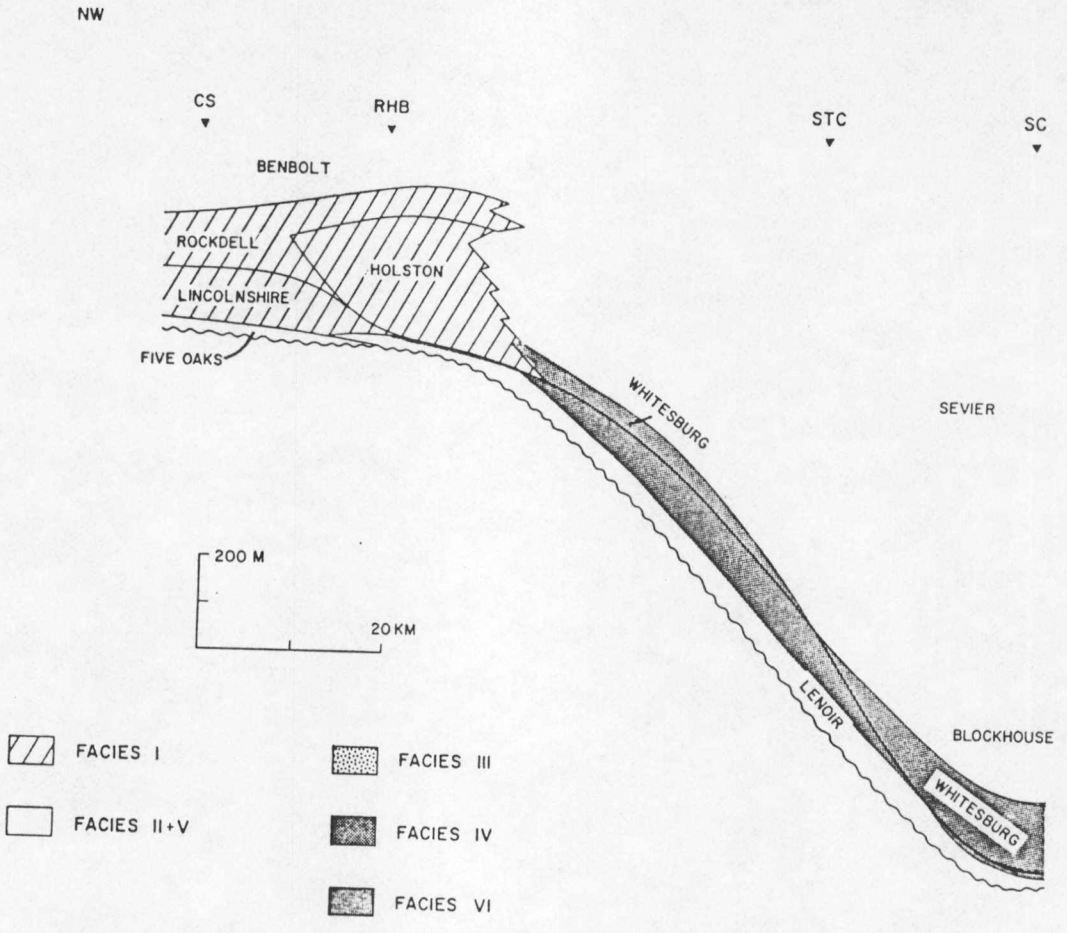
Lithologic, diagenetic and geochemical characteristics of each geochemical facies is summarized in Table 4.2. The stratigraphic distribution of geochemical facies (Fig. 4.2) indicates each is restricted to certain parts of the ramp-shelf sequence, the only exception being samples of Facies II+V which occurs as a regionally continuous unit immediately over the post-Knox unconformity. Shelf and peritidal ramp lithofacies (Facies I,II and V) have low whole-rock strontium, manganese and iron concentrations (Fig. 4.3), although protected lagoonal and some tidal flat deposits on the inner shelf (Facies III) may have strontium and manganese abundances approaching those of deeper-water lithofacies (Facies IV) which are enriched in whole-rock strontium, manganese and iron. Bathymetrically-displaced ramp deposits have a relatively complex association of

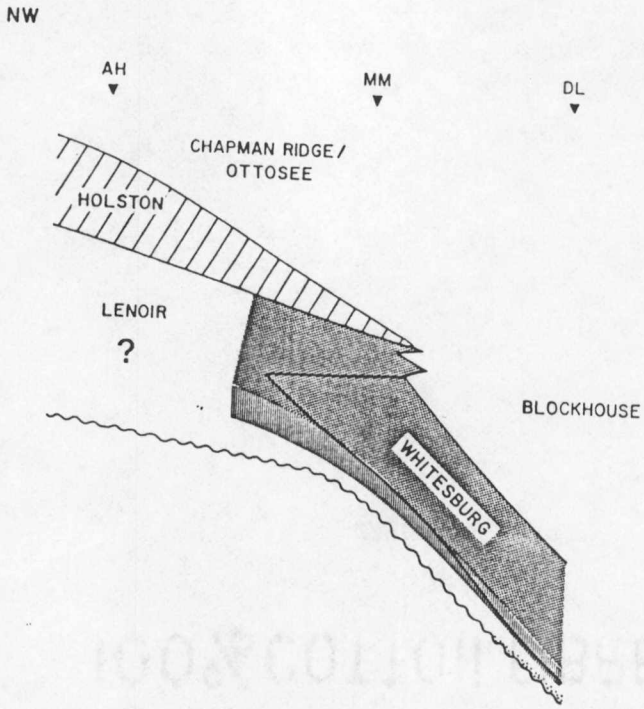
TABLE 4.2

SUMMARY OF GEOCHEMICAL FACIES

GEOCHEMICAL FACIES	UNITS	LITHOFACIES	ENVIRONMENTS	DIAGENESIS	ELEMENTAL COMPOSITIONS (mean)
I	Lincolnshire, Rockdell, Holston	Skeletal wkst., pkst. and gnst., occasional to rarely abundant boundstone masses	Open marine shelf interior sand blanket and shelf-edge sand banks and organic buildups	Compaction, rare to abundant synsedimentary cements, stromatactis, Fe-Mn oxide crusts and internal sediments in buildups, luminescent postsedimentary cements, complex CL zonation, ferroan saddle dolomite	Sr: 179 ppm Mn: 235 ppm Fe: 637 ppm Mg: 3170 ppm
II	Blackford, rare samples from the Lincolnshire, Rockdell and Holston, Mosheim, Lenoir	Thick bdd. lime mdst. fenestral lime mdst., skeletal-peloidal wkst.	Tidal mudflat, open marine shallow ramp to shelf, shelf-edge mudmounds	Tidal: fenestrae (+py), dolomite, xl silt, CL zoned to NL equant calcite cement with pendant and pore-rimming fabrics. Subtidal: luminescent postsedimentary cements, neomorphic spar, minor synsedimentary cements and compactional fabrics	Sr: 378 ppm Mn: 130 ppm Fe: 583 ppm Mg: 6040 ppm
III	Blackford, parts of Lincolnshire, Benbolt and Lenoir	Redbeds, thin bdd. skeletal pkst., argillaceous lime mdst. and skeletal wkst.	Supratidal, peritidal sand banks, quiet water subtidal	Supratidal: fenestrae, compactional fabrics, dedolomite Peritidal: compaction, abundant neomorphic spar, CL zoned postsedimentary calcite cements, rare synsedimentary cements Subtidal: neomorphic spar, compaction, prismatic rim and pore central equant calcite cement, compaction, diagenetic quartz	Sr: 411 ppm Mn: 410 ppm Fe: 818 ppm Mg: 3720 ppm
IV	Whitesburg, Lenoir	Dark gray to black, thin even beds of calcisiltite and calcareous shale nodular bdd., argillaceous skeletal wkst.	Slope, open marine deep subtidal	Abundant compactional features, neomorphic spar, calcite veins, rare cements, dolomite, diagenetic quartz	Sr: 780 ppm Mn: 351 ppm Fe: 1890 ppm Mg: 3760 ppm
V	Five Oaks, parts of Benbolt	Peloidal pkst.-gnst.	Peritidal	Dolomite, fenestrae, keystone vugs, xl silt, NL prismatic and CL zoned pore central equant calcite cements, rare vadose cement, minor compactional fabrics	Sr: 286 ppm Mn: 174 ppm Fe: 1180 ppm Mg: 5280 ppm
VI	Whitesburg, Lenoir	Thin to nodular bdd., dark gray to black, argillaceous skeletal wkst. and pkst.	Foreslope, drowned ramp and shelf	Compaction, py, non-ferroan synsedimentary cement, ferroan and brightly luminescent postsedimentary calcite cements, rare phosphate and chamosite	Sr: 450 ppm Mn: 882 ppm Fe: 5780 ppm Mg: 5280 ppm

Figure 4.2. Cross-sections (see Chapter 1 for comparison) showing the regional distribution of geochemical facies. Facies II and V were combined due to their close stratigraphic association in onlap peritidal facies. Lack of lithologic and geochemical data from the Lenoir Formation at Alcoa Highway locality (AH) limits the identification of geochemical facies in the southern cross-section. Scale applies to both cross-sections.


NW
SE
CS
RHB
STC
SC
BENBOLT
ROCKDELL
HOLSTON
LINCOLNSHIRE
FIVE OAKS
WHITESBURG
SEVIER
200 M
20 KM
LENOIR
BLOCKHOUSE
WHITESBURG
FACIES I
FACIES II+V
FACIES III
FACIES IV
FACIES VI


NW
SE
AH
MM
DL
CHAPMAN RIDGE/
OTTOSEE
HOLSTON
LENOIR
?
BLOCKHOUSE
WHITESBURG

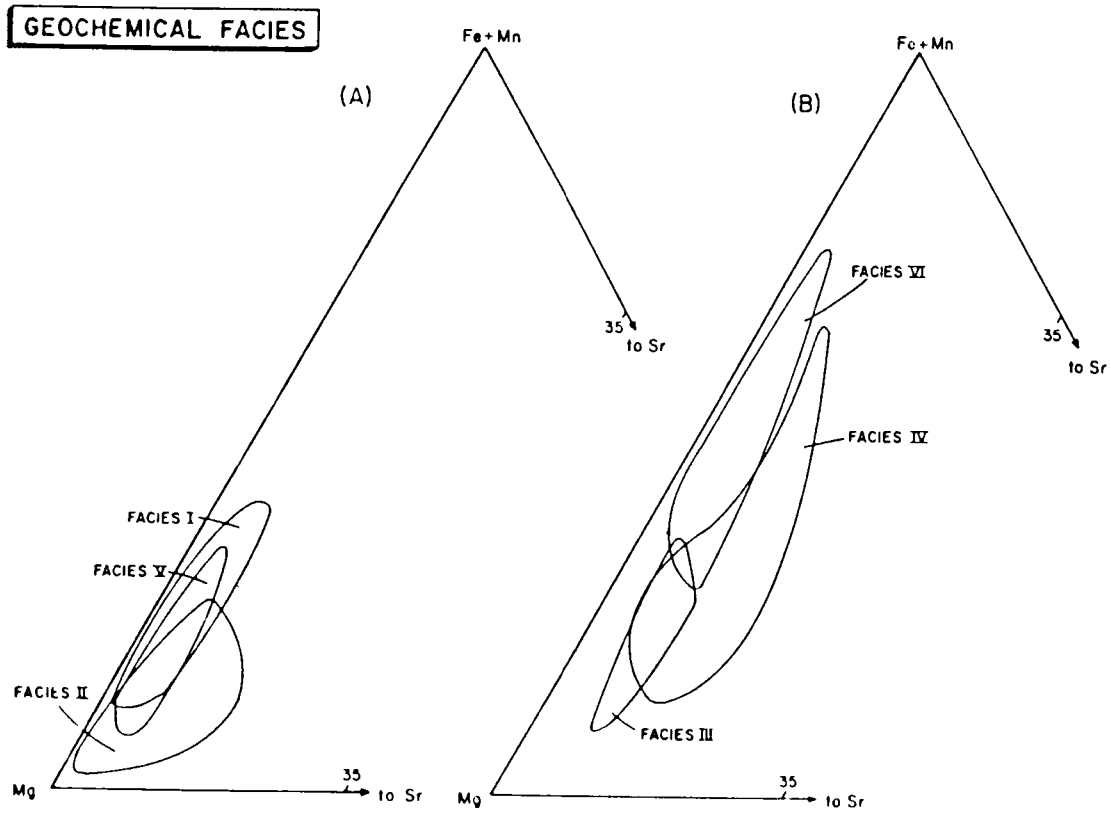


Figure 4.3. Compositional fields for geochemical facies based on the elements strontium, manganese, iron and magnesium. Location of fields represents the relative contribution of redox-sensitive (Fe, Mn) and nonredox-sensitive (Sr, Mg) elements such that the total (Sr + Mn + Fe + Mg) equals 100 percent. All facies are situated along the Mg-(Fe+Mn) join, indicating minimal aragonite in the original sediments.

geochemical facies. For example, the Lenoir Formation at the DL locality exhibits a Facies III-II-VI transition over a stratigraphic thickness of less than 25 meters.

Trace element geochemistry of this carbonate sequence shows both similarities with and differences from other Phanerozoic limestones. The relative increase in strontium from shallow to deep-water deposits noted by Veizer (1974) is present in the Middle Ordovician carbonates, although displaced limestones may be enriched in this element. Depth-related changes in manganese identical to those noted by Bencini and Turi (1974) and Shanmugam and Benedict (1983) are also present, but are not as distinctive as variations in these previous investigations. Instead, the highest manganese concentrations in the Middle Ordovician sequence are associated with drowned ramp and foreslope deposits overlain by deep-water facies (Fig. 4.2).

Interpretation of Geochemical Facies Distribution

Combined petrographic and geochemical data offer insights into factors which influence, either directly or indirectly, the trace element composition of shelf

limestones. The following discussion concerns those elements which tend to exhibit a high degree of specificity with respect to the basin stratigraphy. The data suggest the geochemical signatures reflect depositional and diagenetic inputs.

Manganese: Paleobathymetric Autoenrichment Versus Diagenetic Alloenrichment

Acid-soluble manganese concentrations in shelf limestones are arranged with respect to interpreted paleobathymetry in Figure 4.4. Overall, limestones appear to exhibit an general increase in manganese with paleobathymetry, lithologies from shallow facies may have bulk concentrations above deeper-water facies. Lime mudstones and wackestones of Facies II show the only uniform manganese enrichment in this sequence. Samples from other geochemical facies exhibit a decrease with water depth (Facies III), or no consistent variation with respect to this parameter.

Previous studies of shallow and deep-water carbonates by Bencini and Turi (1974) and Shanmugam and Benedict (1983) showed depth-related variations in manganese concentrations. Variations in the relative proportion of aragonite and calcite in sediments have been suggested as totally or partially responsible for the manganese variations. Since

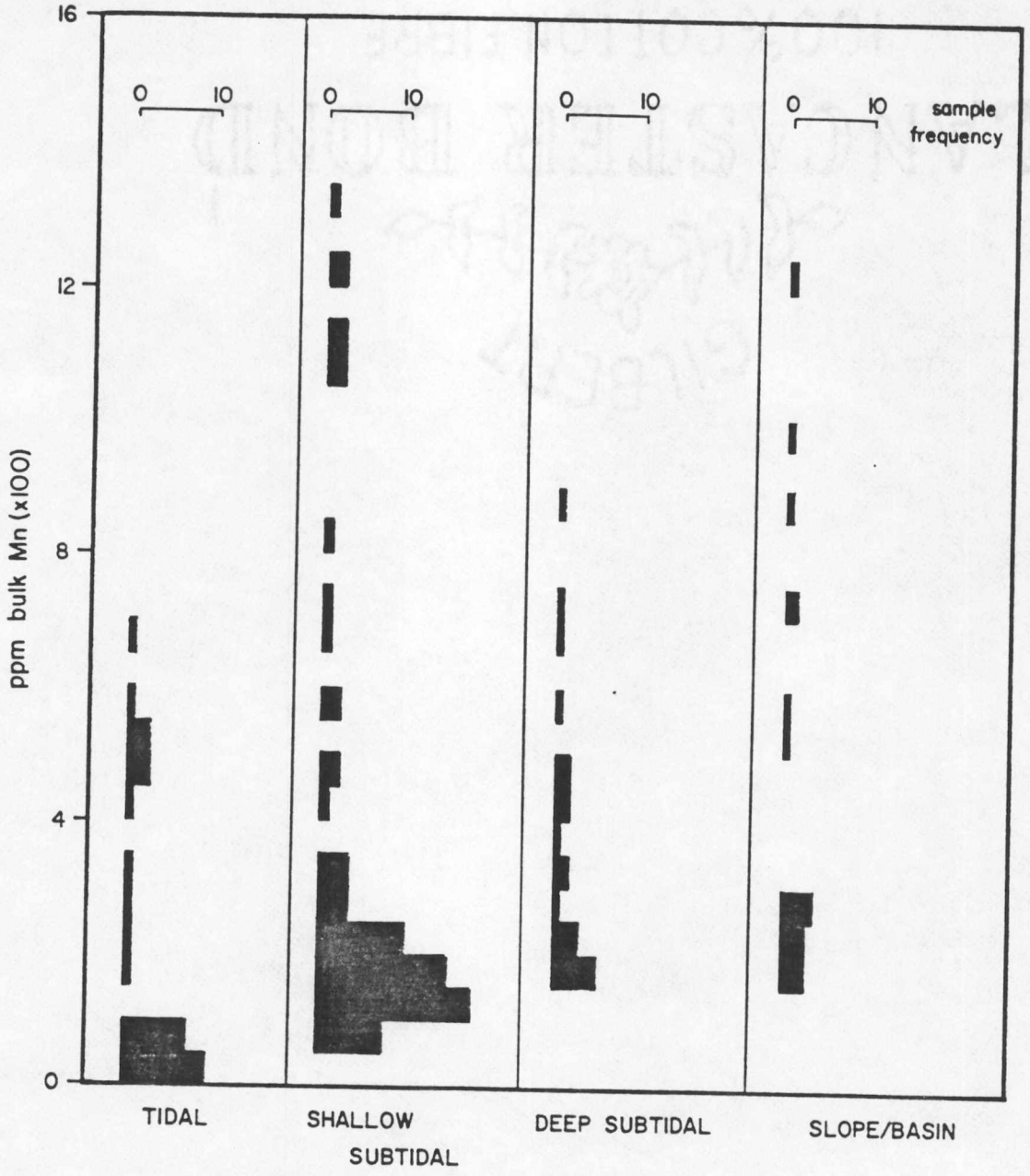


Figure 4.4. Histograms of bulk manganese concentrations for samples separated with respect to inferred paleobathymetry. Relative depths for samples are based on combined stratigraphic, sedimentologic and biotic data collected during slab and petrographic analysis. N = 140.

Middle Ordovician sediments had the same original mineralogy, this factor had no influence on the observed manganese gradients. More importantly, the lower than expected correlation between paleobathymetry and bulk manganese in this sequence suggests other factor(s) influenced the availability of this element's incorporation in diagenetic calcites.

Lagoonal and back-reef sediments on the Belize shelf show a positive correlation between leachable Mn and percentage of admixed argillaceous sediment (Billings and Ragland, 1968). Since this covariance is not a result of selective removal from clay particles during sample preparation, this element appears to have been derived from carbonate sediments, and possibly Mn-oxide phases coating detrital grains. The latter would provide a major source of Mn(II) ions to pore waters under reducing conditions. In environments with low terrigenous input, trace metals such as manganese may be complexed with organic matter (Morse et al., 1985), then released into pore waters after oxidation of organic carbon by microbes.

Since manganese may have initially been associated with the non-carbonate fraction, its eventual incorporation into precipitating carbonates was controlled by the chemical environment. Oxidizing waters would possess minor amounts of dissolved Mn(II) due to this element's low solubility in

most natural waters (Hem, 1972). Depletion of oxygen would increase manganese solubility, making this ion more available for substitution into calcite. Changes in the ionic strength and/or composition of the fluid may also influence dissolved Mn(II) levels, and possibly offset changes in redox potential. Finally, the kinetics of redox processes involving manganese differ from other redox-sensitive elements such as iron. Experiments show the oxidation of Mn(II) to be an autocatalytic process which consists of several reaction steps (Stumm and Morgan, 1981). The nature of the oxidation process allows for low oxygenation rates in most waters, and the sorption of significant quantities of Mn(II) onto Mn-oxides in suspension.

In some instances acid-soluble manganese (and iron) concentrations in Middle Ordovician limestones exhibit varying degrees of correlation with the insoluble residue. For example, argillaceous to non-argillaceous limestones of the Lenoir Formation possess a strong covariance ($r=0.88$) between Mn and insoluble residue (Fig. 4.5; data from Benedict and Walker, 1978). Assuming a cause-effect relationship exists, over 75% of the manganese in the carbonate fraction is controlled by the insoluble residue at this section (I40 at Midway Rd. east of Knoxville). Such a high degree of correlation is rare for shelf and ramp

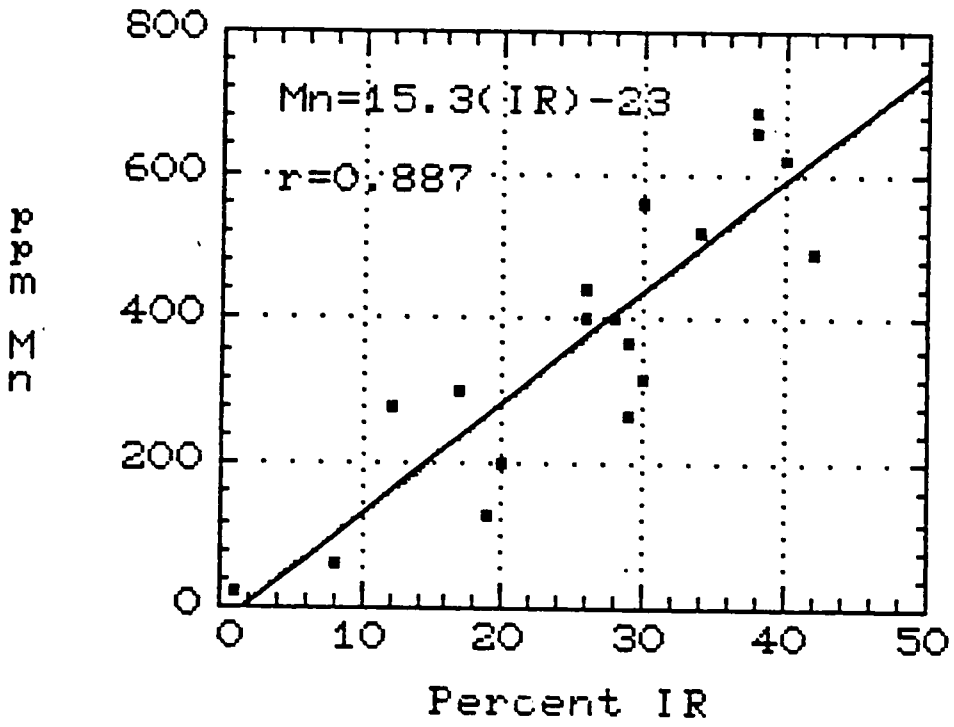


Figure 4.5. Plot of bulk manganese versus acid-insoluble residue (IR) for the Lenoir Formation. Data from Benedict and Walker (1978).

facies. At first glance, graphical comparison of manganese with the noncarbonate fractions of shallow and deep-water lithofacies along the shelf indicates no relationship. However, since manganese is not highly concentrated in most diagenetic waters (see Veizer, 1984), samples which exhibit significant enrichment indicate an atypical diagenetic system. Upon selectively discarding samples from Facies I, IV and VI, the remaining samples do exhibit a slight positive correlation with insoluble residue (Fig. 4.6).

Two scenarios might offer an explanation for the observed manganese distribution. First, the covariance between manganese and insoluble residue is fortuitous, and Mn content is controlled largely by other factors. The second possibility is that terrigenous detritus produced by continental weathering supplied a potential source of manganese in the form of Mn(IV) oxide-oyxhydroxide coatings (Bencini and Turi, 1974), and diagenetic processes redistributed this depositional input. A correlation coefficient of ca. 0.9 strongly suggests some cause-effect relationship between manganese and argillaceous sediment. If this is true, then evidence should exist which indicates a general correspondence between manganese in the carbonate fraction and terrigenous material, and/or diagenetic transport of manganese through parts of the shelf-basin interface. Facies III and IV, which have relatively high

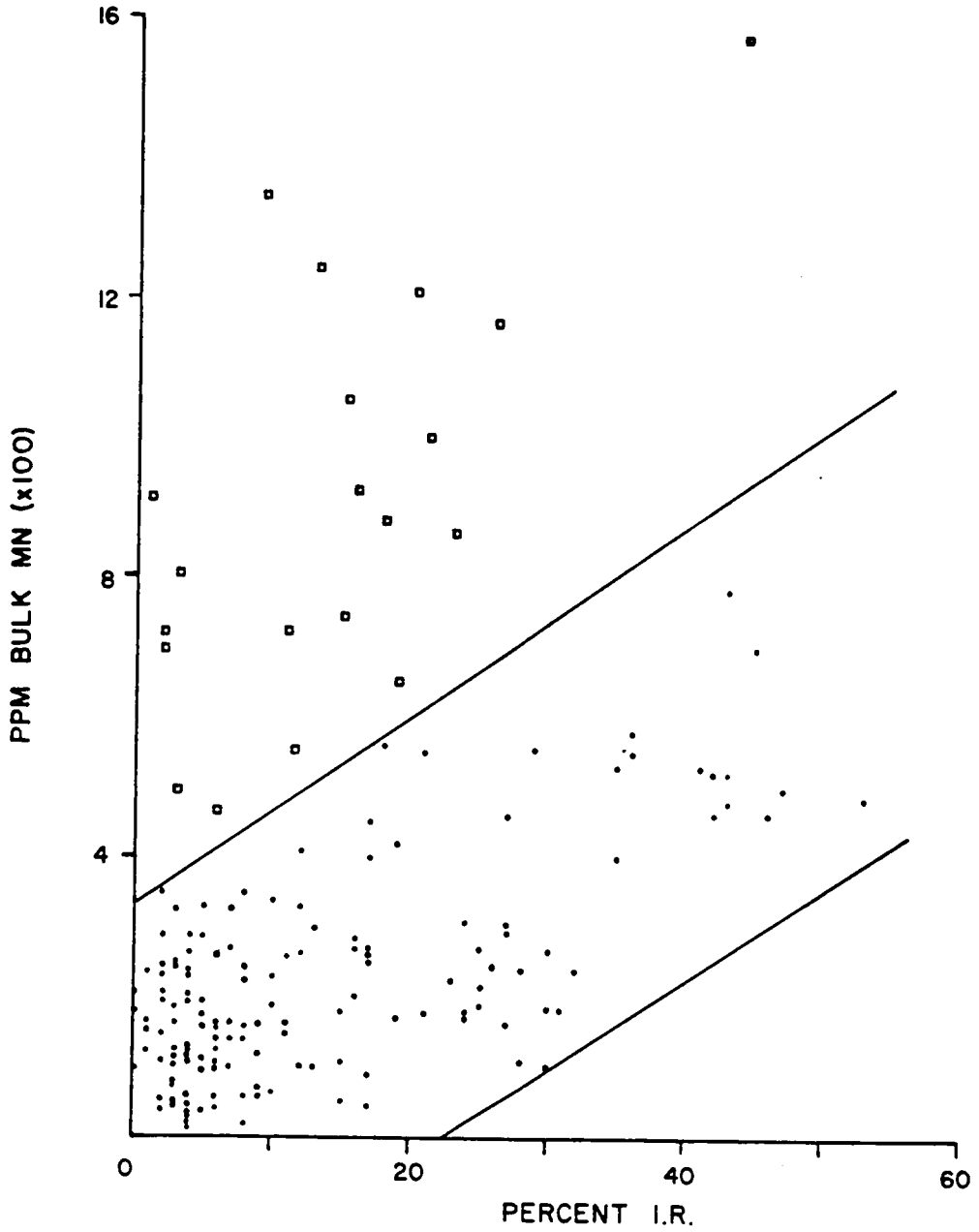
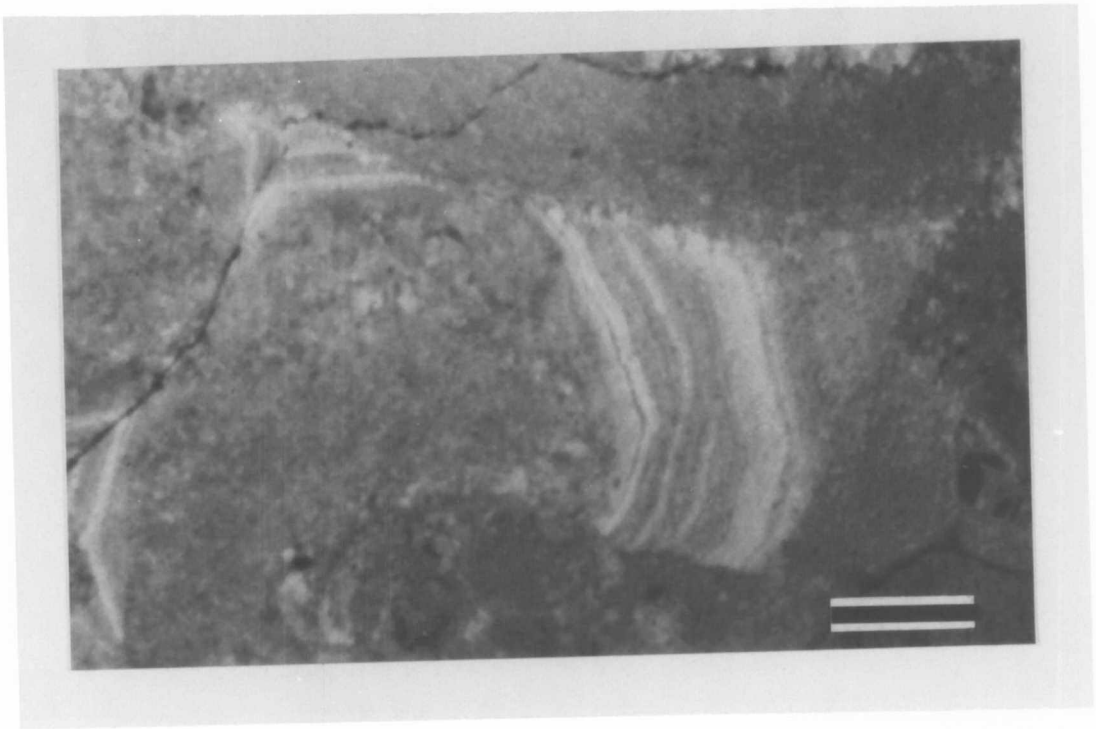


Figure 4.6. Plot of bulk manganese versus acid-insoluble residue (IR) for selected samples from each geochemical facies. Open squares represent either Facies VI samples, or samples from Facies I-V which are enriched in manganese. The majority of samples belonging to Facies I-V show manganese to be directly related to the amount of insoluble residue.

mean manganese concentrations (Fig. 4.3) have high insoluble residues after acid leaching, or are interbedded with shaly lithologies. The high Mn variance in Facies I and significant enrichment in Facies VI indicate the movement of burial fluids from the shale basin through certain parts of the carbonate sequence. Manganese-rich skeletal packstone and grainstone from the lower Lincolnshire Formation at CS have minor amounts of synsedimentary cements, and abundant compactional features (stylolites, grain breakage, solutional grain/cement contacts) and postsedimentary echinoderm overgrowth and equant cements which have brightly luminescent zones (Fig. 4.7). These diagenetic features indicate a significant amount of pore space remained open after early diagenesis, allowing for the precipitation of Mn-rich cements from basin-derived fluids. Skeletal packstones and grainstones from the Lenoir at DL represent a similar diagenetic history. The relatively high mobility of manganese (Parker et al., 1985) would allow for large-scale transport by fluids to different parts of a sedimentary basin.

Manganese-enriched zones of Facies VI typically occur where stratigraphic analysis indicates rapid changes in water depth associated with ramp drowning. Petrography shows a paucity of diagenetic features characteristic of early marine lithification. Thus, this portion of the

Figure 4.7. Numerous brightly luminescent cement zones in echinoderm syntaxial overgrowth calcite from skeletal packstone, lower Lincolnshire Formation. Sample CS17. Scale bar = 0.1 mm.



bathymetrically-displaced sediments could have also received basin-derived waters with high Mn(II) concentrations during later diagenesis. A more detailed examination of this zone is presented in Chapter 5.

Thus, the manganese distribution reflects both the interaction of a depositional input of this element, and later diagenetic redistribution. Manganese associated with clays (and possibly organic matter) provided the majority of the original manganese source to shelf lithofacies (alloenrichment of Pingitore, 1978). Since fine grained argillaceous sediments are generally restricted to quiet-water, sub-wave base parts of ramps and shelves, the original manganese "reservoirs" would have been more abundant in: (1)distal portions of carbonate ramps, (2)protected, peritidal to subtidal environments on the inner parts of rimmed shelves, and (3)slope/basin environments. The early reduction of Mn(IV) would produce Mn(II)-rich interstitial waters after a limited amount of burial (Forelich et al., 1979). The manganese content of a given facies would be largely dependent on the "openness" of the system and paleohydrology of Mn(II) enriched burial fluids. Only in areas where clay-rich sediments were less open to gain/loss of manganese does a relationship exist between this element's concentration in the carbonate fraction and argillaceous content.

Strontium and Magnesium Depletion in Matrix- and Grain-Supported Lithologies

Since the majority of grains and depositional matrix was originally magnesian calcite, both magnesium and strontium will be depleted during meteoric and burial diagenesis. Comparison of geochemical data indicates shelf packstone-grainstone lithofacies which dominate Facies I are more depleted in these two elements than ramp/shelf lime mudstone-wackestone lithofacies of Facies II (Figure 4.3). Even in a specific unit, micrite-rich lithologies contain higher Sr (and Mg) concentrations (Fig. 4.8). The possibility exists that variations in the relative abundances of allochems and/or depositional matrix may have influenced the measured concentrations of strontium and magnesium. To test this hypothesis, a linear correlation matrix was generated to test the correlation of Sr content with the dominant skeletal allochems and micrite (Fig. 4.9). (The remaining constituents were not used because of the large number of sampling zeros after constituent particle analysis.) None of the allochems exhibit any significant correlation to bulk strontium concentrations. Arthropod debris appears to weakly correlate with this element ($r=0.63$); however, a plot of these two variables (Fig. 4.10) shows a true correlation does not exist. The data indicate grain composition exerted no control on strontium

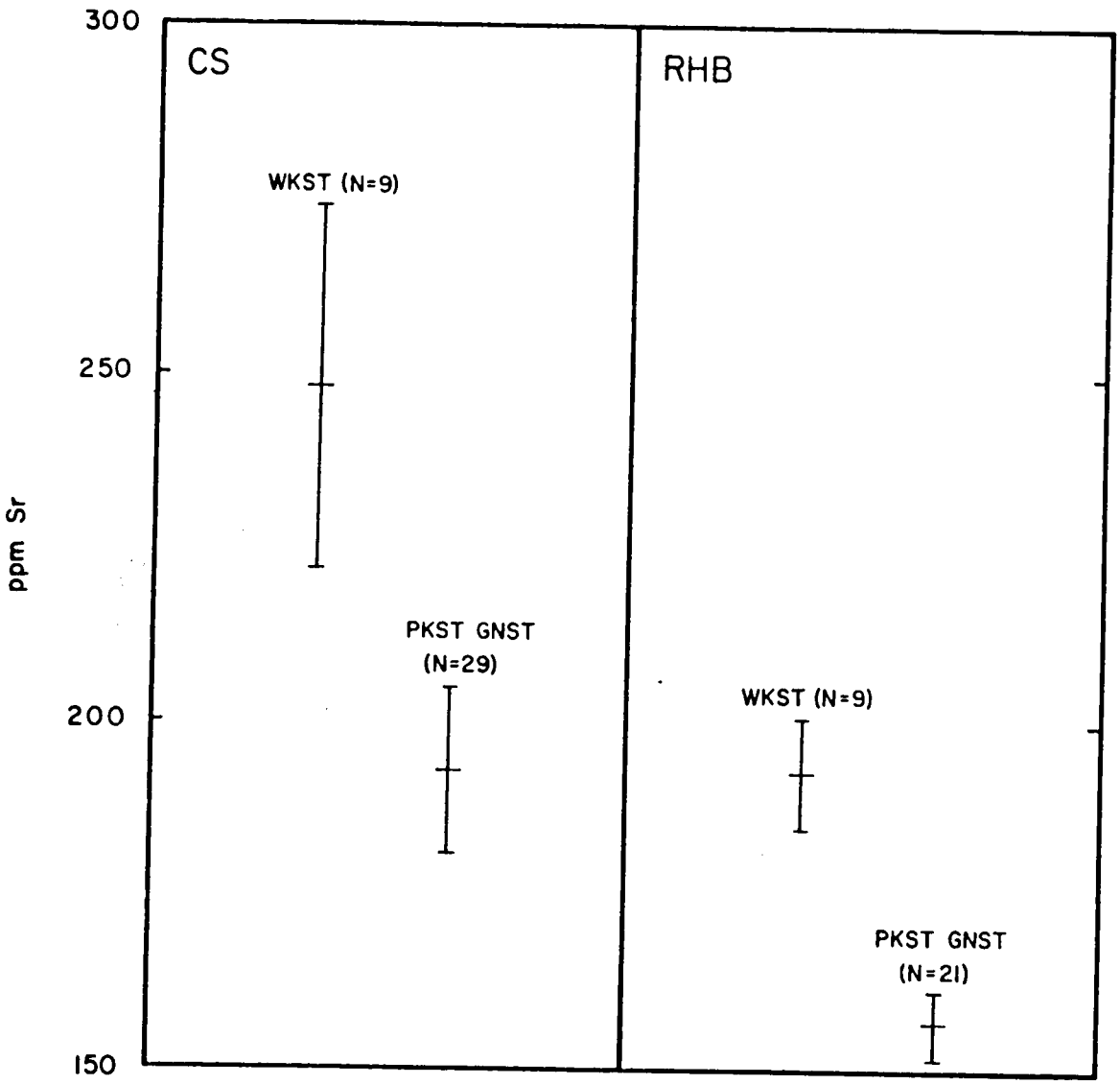


Figure 4.8. Mean and standard deviation of bulk strontium concentrations in grain- and mud-supported lithologies from the lower Chickamauga Group at the Cedar Springs and Red House Branch localities. Number of samples indicated in parentheses.

	Sr	ECHINO	BRYO	ARTHRO	BRACH	MICMSP
Sr	1.0000					
ECHINO	-0.4823	1.0000				
BRYO	-0.3822	0.0068	1.0000			
ARTHRO	0.6297	-0.3364	-0.3437	1.0000		
BRACH	0.2097	-0.0942	0.0569	0.2415	1.0000	
MICMSP	0.5020	-0.3813	-0.1669	0.0869	0.2451	1.0000

Explanation:

ECHINO = echinoderms
BRYO = bryozoans
ARTHRO = arthropods
BRACH = brachiopods
MICMSP = micrite + microspar

Figure 4.9. Correlation matrix of dominant skeletal allochems, micrite and bulk strontium in shelf limestones.

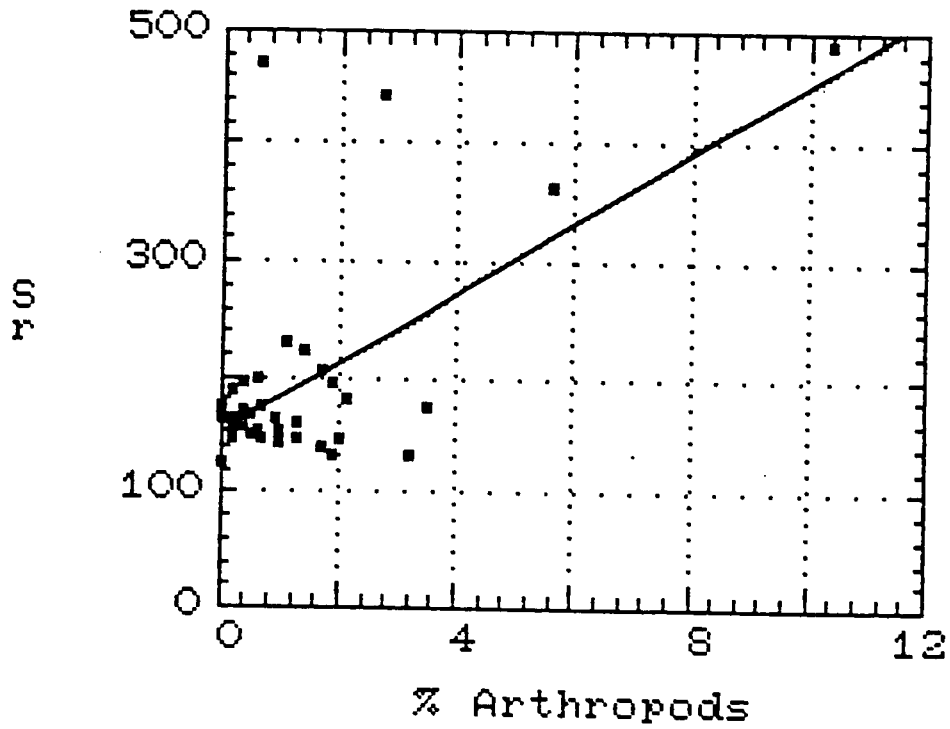


Figure 4.10. Plot of bulk strontium versus volume percent of arthropods in shelf limestones. Percentages are based on constituent particle analyses of thin sections (minimum of 400 points per sample).

distribution.

Magnesium and strontium enrichment in matrix-supported lithologies may reflect a more physically-closed system in which the fine grained matrix restricted efficient removal of Sr and Mg ions from reaction sites. A second hypothesis is that slower water exchange failed to completely eliminate diffusion gradients for these two elements. The continual flushing of pore fluids with low Mg/Ca compositions through grain-supported lithologies caused more thorough equilibration of unstable mineralogies, in addition to the precipitation of larger volumes of calcite cement. Under certain conditions, a more closed system could have facilitated the precipitation of matrix-replacive dolomite (see Chapter 2).

Strontium Enrichment in Slope and Deep Subtidal Lithofacies

Samples from the lower Chickamauga Group and equivalents may be separated into high and low strontium groups which exhibit some degree of facies specificity. The 'high' strontium group consists of deep water calcisiltites and subtidal, argillaceous lime wackestones of Facies IV (Fig. 4.3; Table 4.2). The remaining facies have mean concentrations less than 500 ppm, and comprise the 'low' strontium group (Fig. 4.3; Table 4.2). Veizer and Demovic

(1974) suggested an underlying mineralogical control to the facies distribution of the high and low strontium groups in carbonate platform limestones similar to that in the Middle Ordovician. However, the uniform mineralogy of sedimentary facies in the Middle Ordovician precludes this as a factor in the Sr variations in this sequence.

The concentration of nonredox-sensitive elements is generally thought to be controlled by the nature of pore fluids (excluding possible kinetic effects). The importance of this factor is magnified by the ratio of metastable to stable components, or diagenetic potential, of the original sediment as suggested by Veizer and Demovic (1974). Assuming diffusion and fluid flow are sufficient to limit any concentration gradients, recrystallization and cementation in a particular diagenetic zone produces compositional uniformity with respect to the pore waters (Benson, 1974). Platform carbonates typically have diagenetic histories that differ from periplatform carbonates as a result of compositional differences in their respective pore waters. Lithification of shallow-water carbonate sediments typically occurs in contact with meteoric-derived fluids. Periplatform sediments have much less chance of encountering such waters during their diagenesis. Instead, these sediments undergo lithification in contact with unaltered to altered marine waters which are either trapped in grain

interstices and driven by compaction through the sequence, or actively pumped through sediments by some other mechanism such as Kohout convection (Mullins et al., 1985).

Strontium concentrations of diagenetic calcites in equilibrium with deep marine waters range from 200 to 400 ppm (see discussion in Chapter 2). Lithologies which comprise Facies IV have whole-rock Sr contents as much as 4x greater than the equilibrium concentrations. Petrography indicates samples were not lithified until after burial. This suggests diagenetic fluids must have become enriched in dissolved Sr after the sediments were no longer in contact with marine waters.

Thus, argillaceous sediments associated with Facies IV samples influenced strontium contents in diagenetic calcites precipitated during burial diagenesis. Strontium on exchange sites may be replaced by other cations (K,Mg,Na) in sea water (Bath, 1977), with the exchangable amounts on the order of 10's of micrograms per gram of clay. Calcites would have relatively high strontium contents as a result of precipitation from Sr-enriched connate waters.

Occurrence of Facies II in Onlap Tidal Flat Deposits

Trace element signatures of tidal mudflat and shallow subtidal lithofacies of the Lenoir Formation drowned as a

result of tectonic downwarping offer insight into the rate of early diagenesis. Bathymetrically-displaced lime mudstone and fenestral lime mudstone of the Mosheim Member belong to the same facies as tidal deposits which did not experience drowning (see Fig. 4.2). A comparison of mean whole-rock concentrations between these two groups (Table 4.3) indicates a high degree of similarity, even for redox-sensitive constituents such as manganese and iron.

Petrography reveals numerous diagenetic features common to lithologies in both the Mosheim and Five Oaks, indicating analogous diagenetic histories (Fig. 4.11; Table 4.4). Deep burial-related phases are either absent or rare in bathymetrically-displaced tidal flat sequences. Such uniformity in the context of active tectonism suggests complete (or near complete) lithification of sediments prior to subsidence. Advanced stages of diagenetic alteration in peritidal deposits now residing in modern deeper-water settings have been recognized by Enos and Freeman (1979) and Freeman-Lynde et al. (1986).

Middle Ordovician tidal deposits passed through the meteoric vadose and shallow meteoric-phreatic zones during their diagenetic history. A humid climate (indicated by the lack of evaporite/evaporite-pseudomorphs and low sodium concentrations) together with the aerial extent of these exposed mudflats over the karstified Knox carbonates allowed

TABLE 4.3

MEAN TRACE ELEMENT COMPOSITION OF DROWNED (MOSHEIM) AND SHELF (FIVE OAKS) CARBONATE TIDAL FLAT LITHOFACIES

Element	Mosheim Mbr. (n=10)	Five Oaks Fm. (n=11)
Fe	650 ppm	458 ppm
Mn	52 ppm	44 ppm
Sr	250 ppm	233 ppm
Na	109 ppm	90 ppm
Zn	6 ppm	7 ppm

Figure 4.11. Diagenetic features in onlap tidal flat deposits of the Mosheim Member of the Lenoir Formation and Five Oaks Formation.

A, B. Plane light - cathodoluminescence photomicrograph pair showing growth fabric of equant calcite cement filling irregular fenestra. Non-luminescent and brightly luminescent zones exhibit a pendant cement fabric, in which calcite grew downwards from the roof of the fenestra. This early cement offered sites for precipitation of dull luminescent to non-luminescent calcite which occludes the remainder of the relict pore space. Sample MMd. Scale bar = 0.5 mm.

C. Pendant, finely crystalline calcite cement (arrow) along the roof of a laminoid fenestra. The remainder of the relict pore space is filled by a later generation of coarsely crystalline equant calcite cement (E). Sample CS2. Scale bar = 0.1 mm.

D. Single generation of geopedal crystal silt (S) which partially and completely fill fenestrae/keystone vugs. Sample CS7. Scale bar = 0.25 mm.

E. Single generation of crystal silt (S) which fills a significant amount of relict fenestral porosity. Note silt abutting earlier calcite cement crystals (arrow). Sample MMd. Scale bar = 0.25 mm.

F. Irregular fenestrae in lime mudstone. Sample CS1. Scale bar = 0.25 mm.

G. Thin section photonegative of fenestal lime mudstone which possesses both irregular and laminoid fenestrae. Relict porosity occluded by equant calcite cement (dark areas) and geopedal crystal silt (arrow). Sample MMc. Scale bar = 1 cm. Stratigraphic up to the left.

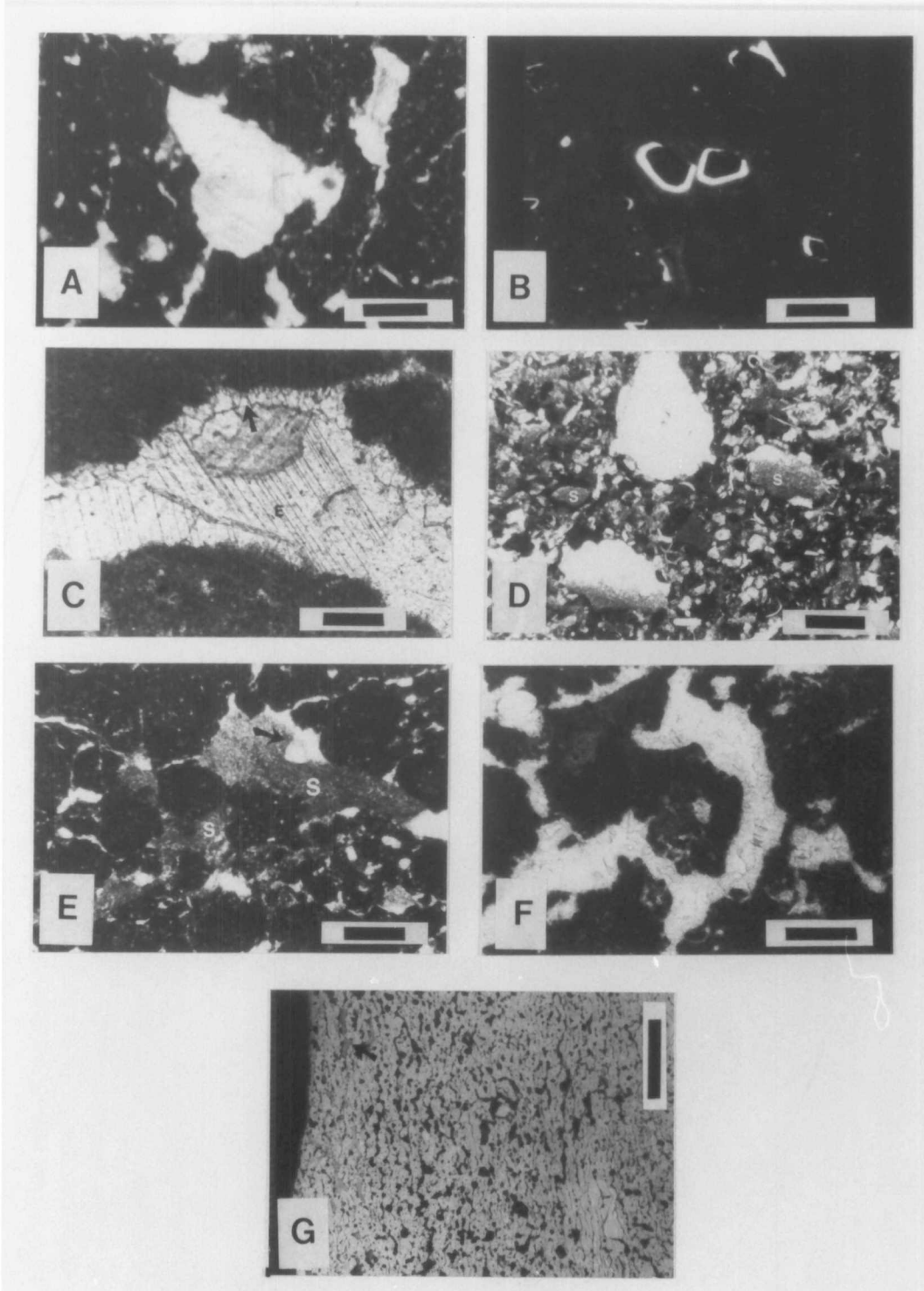

A
B
C
D
E
F
G
S
S
S
S

TABLE 4.4

DIAGENETIC FEATURES OF BASAL ONLAP TIDAL FACIES

	Mosheim Mbr.	Five Oaks Fm.
Features		
Irregular fenestrae	X	X
Laminoid fenestrae	X	X
Crystal silt	X	X
Pyrite	X	X
Micritization of skeletal grains		X
Keystone vugs		X
Solution-enlarged vugs	X	X
Finely crystalline dolomite	X	X
Cements		
Nonferroan equant calcite:		
-pendant fabric	X	X
-pore rimming	X	X
Nonferroan echinoderm overgrowth calcite		X
Fibrous/bladed calcite:		
-isopachous	X	X
-pendant		X
Meniscus micritic cement		X
CL zonation in cements*		
NL - BL - DL zonation	X	X
Uniform BL		X
Uniform NL		X

* NL=nonluminescent; BL=brightly luminescent; DL=dull luminescent.

for large volumes of meteoric waters to recharge in areas to the west, and circulate eastward through a shallow meteoric lens. This lens may have been separated from marine waters further to the east by a meteoric-marine mixing, or transition, zone. Grover and Read (1983) favor the early lithification of contemporaneous Middle Ordovician peritidal facies (New Market Limestone) in vadose and shallow phreatic zones, although they propose a westward flow of influxing waters originating from highlands further to the east. Given the relatively fast rates of cementation and recrystallization characteristic of the active meteoric-phreatic environment, it is possible diagenesis of Mosheim tidal flats could have occurred in a more confined hydrologic system. This basal tidal flat sequence represents a thin, diachronous, but physically continuous "unit" whose petrogenesis was dependent on diagenetic processes in the environment of deposition, and was largely independent of regional geodynamic events.

CHAPTER 5

SHELF LIMESTONE-SHALE BASIN INTERACTION DURING EARLY AND LATE DIAGENESIS: AN EXAMPLE FROM THE MIDDLE ORDOVICIAN OF EAST TENNESSEE

Introduction

Middle Ordovician carbonate-shelf to siliciclastic-basin facies in eastern Tennessee offer a well studied stratigraphic package in which to access the interaction of carbonate and fine grained siliciclastic sediments through their entire diagenetic history. Petrography and geochemistry indicate that processes occurring in a foredeep shale basin are recorded by both nearby shallow-water facies, and drowned sediments which were partially lithified in the marine realm. The purpose of this chapter is to identify petrographic and geochemical criteria in limestones which reflect their interaction with argillaceous lithologies during synsedimentary and burial diagenesis. After discussing the mineralogy and diagenesis of shales in the Sevier Basin, the next two sections

examines the petrography and geochemistry of limestones buried by siliciclastic deposits of the Sevier Formation. The final section looks at diagenetic features related to the movement of shale-derived fluids into shelf carbonates (Holston Fm. and Chickamauga Gp.), along with syndepositional iron and manganese oxide deposits.

Clay Mineralogy of Shales from the Sevier Basin

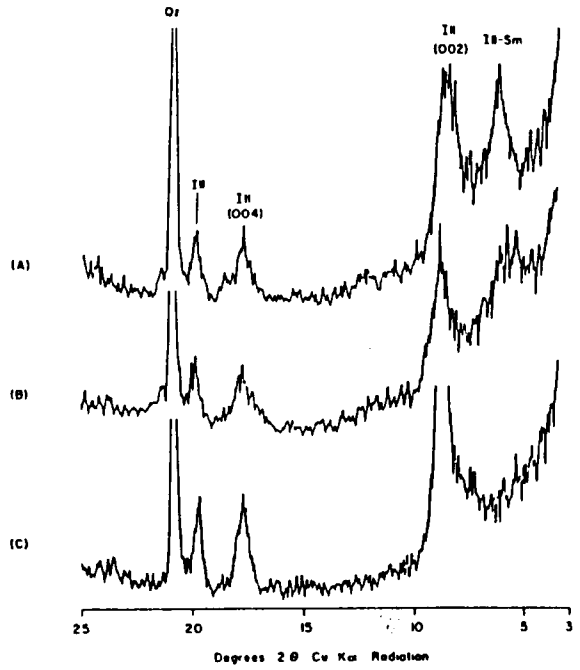
In order to understand possible affects of shale diagenesis on carbonate sediments, it was necessary to determine the clay mineralogy of shale lithologies. These data were used to infer the probable original clay assemblage. The mineralogy of the clay fraction was ascertained by XRD analysis using various sample treatments. However, the mineralogy of shales may not accurately represent the mineralogy of clayey oozes at the time of deposition or early diagenesis. Numerous studies have documented the diagenetic alteration and formation of clays in sedimentary sequences (see Dunoyer de Segonzac, 1970 for a review). Minerals comprising the original clay fraction may be either degraded or regraded during loss of expandable layers. In addition to these transformations, entirely new

clays not present at deposition may form, in some instances at the expense of detrital clays. Various factors control the diagenetic clay assemblage: (1)ionic strength, composition and compaction of fluid, (2)permeability, (3)presence of organic matter, (4)burial history. The composition of the original clays imparts significant control on degradational and regradational pathways during burial diagenesis. Using clay mineralogies of basinal shales together with knowledge of basin history should enable an approximation of the original clay assemblage.

X-ray patterns for slope shales are shown in Figure 5.1. Mineralogical analyses from this study allow for the recognition of two clay suites which exhibit variation within the basin (Table 5.1). The first is proximal to the carbonate shelf and consists of smectite-illite along with minor kaolinite (sample MM-S2, Fig. 5.1). The second contains no mixed-layer illite-smectite, but instead has either mixed-layer chlorite-smectite or discrete chlorite (samples DL-S1 and DL-S3, Fig. 5.1). This suite characterizes lithologies deposited in the basin, although one sample also from the upper Whitesburg Formation at the MM locality has this clay suite. Illite with <20% expandable interlayers is the dominant species in all shales analyzed. Chlorites in most samples are poorly crystallized except at the DL locality. Samples from the Sevier Shale

Figure 5.1. Representative x-ray diffraction patterns from calcareous shales of the Whitesburg Formation. Size fraction in all samples <5 micrometers. A - untreated; B - glycolated; C - heated to 550 °C for one hour. Mineral explanation: Ill=illite; Ill-Sm=mixed-layer illite-smectite; Chl-Sm= mixed-layer chlorite-smectite; Chl=chlorite; Kaol=kaolinite; Qz=quartz; Cc=calcite.

MM-S2


Or
Ilt
(002)
Ilt-Sm
Ilt
(004)
(A)
(B)
(C)
25
20
15
10
5
3
Degrees 2θ Cu Kα Radiation

DL-S3

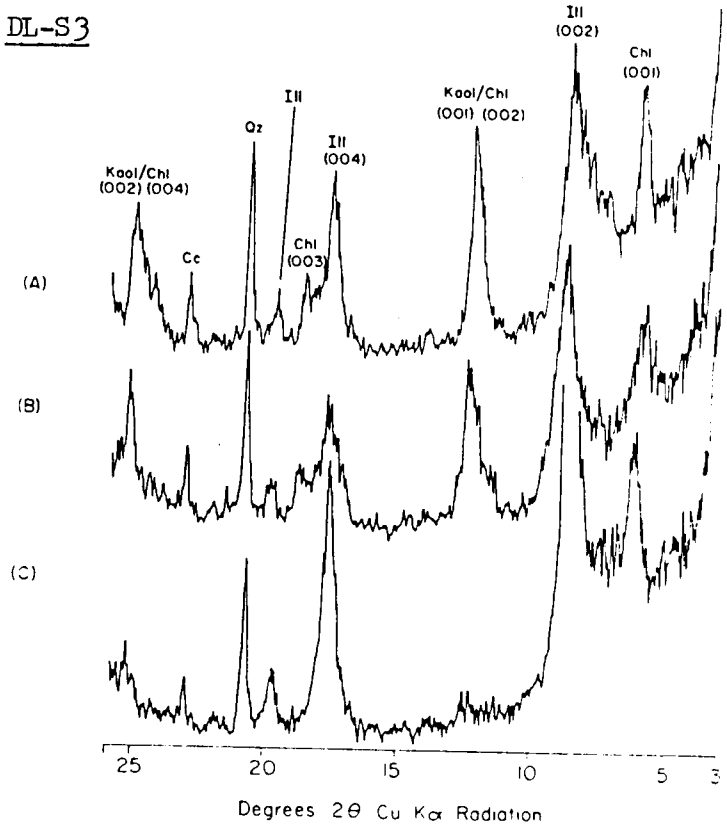

Ill
(002)
Chl
(001)
Kaol/Chl
(001) (002)
Ill
Qz
Ill
(004)
Kaol/Chl
(002) (004)
Cc
Chl
(003)
(A)
(B)
(C)
25
20
15
10
5
3
Degrees 2θ Cu Kα Radiation

TABLE 5.1

MINERAL COMPOSITION OF MIDDLE ORDOVICIAN SHALES AND TECTONOSTRATIGRAPHIC ANALOGUES

Age		Qtz	Chl/Chl-Sm	Ill/Ill-Sm	Sm	Kaol
Middle Ordovician						
Whitesburg Fm.	I	++	--	++	--	+
	II	++	++	++	--	+
Sevier Fm.		++	++	++	--	+
Quaternary						
Sunda Arc		++	+	++	++	++
Middle America		++	--	++	++	++

Explanation: ++, abundant; +, rare; --, absent.

analyzed by Metcalfe (1974) contain abundant illite with minor amounts of chlorite and kaolinite (Table 5.1), and thus resemble the second suite in terms of their clay mineralogy.

There are different ways this data may be used to constrain the probable original clay mineralogy. The method adopted in this study was to first compare Middle Ordovician samples with Recent deep-water clay oozes from convergent margins with similar source terrains. Source area characterization was made using Q-F-L compositions of associated sandstones. After comparison of respective mineralogies, differences (if any) were evaluated in light of clay mineral diagenesis and burial history to determine if the Middle Ordovician suites could have resulted from degradation, regradation or precipitation during late diagenesis. The following discussion assumes clay fractionation was minimal once clays entered the basin, as in Recent marine environments (Taggart and Kaiser, 1960). Thus, the suites identified are presumed to reflect variations in either diagenetic alteration or sediment provenance.

Sandstone compositional modes for Blountian clastics indicate a predominately sedimentary source (Table 5.2), with secondary contributions from metamorphic and igneous rocks (Mack, 1985). This provenance interpretation is

TABLE 5.2

MEAN DETRITAL MODES (%) OF SANDSTONES FROM THE BLOUNT CLASTIC WEDGE AND CENOZOIC CONVERGENT MARGIN ANALOGUES

Area	Quartz	Feldspar	Lithics
Blount wedge, southern Appalachians	76	12	12
Middle America Trench	41	22	37
Sunda Arc	68	15	17

(Data from Moore, 1979; Enkeboll, 1981; Mack, 1985.)

supported by clast lithologies in conglomeratic facies of the coeval Tellico Formation. Portions of the Middle America Trench and Sunda Arc have facies sequences and detrital compositions resembling the Middle Ordovician foredeep basin. Siliciclastic detritus supplied to the deep marine realm in both these convergent margins contains abundant quartz and feldspar grains derived from mixed sedimentary-metamorphic source terrains (Table 5.2). The majority of sediments channelled through submarine canyons and into the Middle America Trench are eroded from Paleozoic and younger metamorphic, igneous and sedimentary rocks on the mainland (Enkeboll, 1981), while in the Sunda Arc weathering is concentrated in the early Tertiary sedimentary and Pre-Tertiary metamorphic and igneous rocks exposed in the frontal arc (Moore, 1979). Arc volcanics are not a major sediment source in either continental margin, as was also the case during infilling of the Sevier Basin. However, the presence of altered tuffs and bentonites in the Middle Ordovician sequence attest to the existence of volcanism during sedimentation (see discussion of Mack, 1985 by Shanmugam et al., 1985). The apparently anomalous sandstone compositions in Blountian clastics may have resulted from the paleotopography of the tectonic highlands which caused the preferential transport of coarser (sand-size) volcanic detritus eastward away from the Sevier

Basin.

The mineralogy of clay oozes from the Sunda Arc is dominated by smectite with subordinate illite/mica and kaolinite (Cook et al., 1974, Tables 1 and 9). Chlorite is rare in the fine silt and clay fractions in cored sediments. No published data is available on the clay mineralogy of oozes from the Middle America Trench. Muds associated with carbonate nodules from this Trench possess abundant illite/mica, kaolinite and smectite (Wada et al., 1981). The clay assemblage of both convergent margins is typical of Recent sediments derived from continental areas influenced by a tropical-subtropical climate (see Grim, 1968).

Comparison of Middle Ordovician shales and modern sediments show significant mineralogic similarity (Table 1). Other than variations in the relative abundance of each clay, the only noticeable discrepancy is the presence of chloritic clays in Middle Ordovician shales (suite #2). Assuming the sandstone compositions are reliable provenance indicators, the original clay sediments have undergone appreciable diagenetic modification with respect to their modern analogues. This should be expected for several reasons:

(1) High potential for transformation of the dominant detrital clay minerals.

(2) Significant amount of sediment overburden.

(3) Structural deformation which may increase temperature and pressure above levels resulting from normal burial.

Shales in the Sevier Basin were buried under from 2.5 to 3 kilometers of younger sediments. (This figure does not consider tectonic loading resulting from Late Paleozoic deformation.) The sediment overburden would have been sufficient to initiate smectite to illite conversion in basinal shales (Fig. 5.2). Further burial due to stacking of thrust sheets may have caused continued smectite conversion and increased illite crystallinity in parts of the hinterland. Thus, mixed-layer illite-smectite and some percentage of the 1.0 nm illite peak is attributed to the illitization of detrital smectite. The formation of chloritic clays in Middle Ordovician shales may have been contemporaneous with smectite conversion during burial. Magnesium-bearing pore fluids could provide the necessary chemical environment to form mixed-layer chlorite-smectite (Fig. 5.2), which in some parts of the basinal sequence may have altered to non-expandable 1.4 nm chlorite. Further discussion of these diagenetic clay transformations is presented in the section on deep burial diagenesis.

Based on mineralogic data and basin history, it is likely that the deep-water shales of the Sevier Basin had an original mineralogy similar to modern tectono-stratigraphic

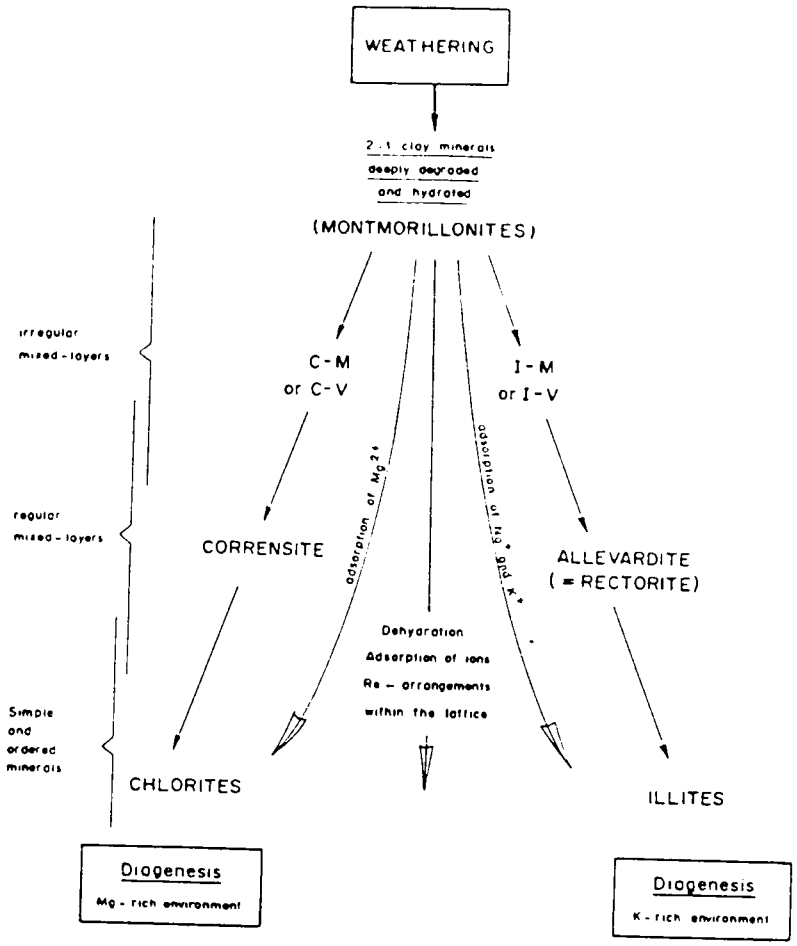


Figure 5.2. Transformation of detrital smectite clays during burial. From Dunoyer de Segonzac (1970).

analogues such as the Sunda Arc. Some illite and chlorite represent diagenetic products formed by regradational processes of a smectitic precursor during both sedimentary and tectonic loading. Therefore, the original mineralogy of detrital clays was dominated by smectite and illite, with minor chlorite and kaolinite components.

Geochemical Classification of Slope Lithofacies, Sevier Basin

Berner (1981) proposed a geochemical classification based on the concentration of dissolved oxygen and sulfide (Fig. 5.3). The geochemical environments distinguished by this scheme are characterized by the presence/absence of certain diagenetic minerals (oxides, sulfides, carbonates). In an attempt to make this classification more applicable to Phanerozoic rocks, Maynard (1982) used the degree of bioturbation and organic carbon content (which is related to color) as indirect measures of oxygenation in sediments. Dissolved sulfide was assessed directly via mineralogical analyses of lithologies for sulfide-bearing phases.

Argillaceous sediments are primarily affected by only one geochemical environment which is closely linked to

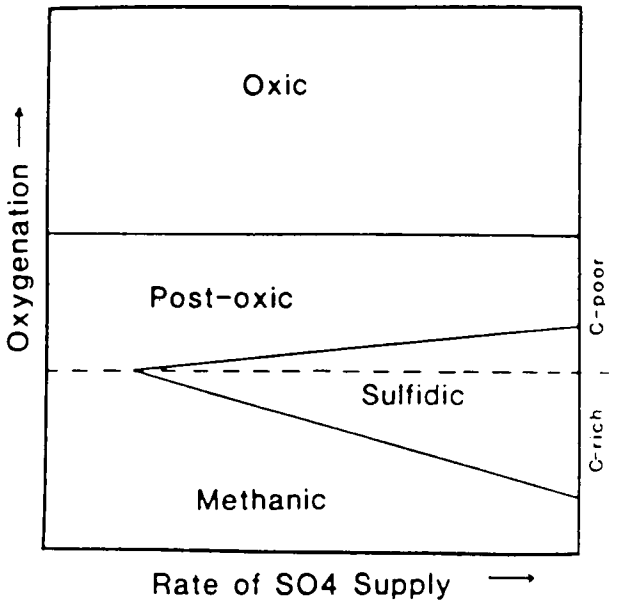


Figure 5.3. Classification of diagenetic environments after Berner (1981). From Maynard (1982).

bottom conditions at the time of deposition (Maynard, 1982). This is not necessarily the case for carbonates which may be undergo alteration in several geochemical environments during their diagenetic history. The control on which environment(s) a sediment may encounter is the concentration of available organic carbon (Berner, 1981). The organic content of marine sediments is governed by the combined interaction of biologic productivity, sedimentation rate and bottom-water circulation. Since these factors exhibit variation within a sedimentary basin, a given lithofacies may experience different diagenetic histories at different localities in the same basin.

Calcareous shale interbeds of the Whitesburg Formation are thinly laminated, gray to black in color and slightly pyritic. Fabrics suggesting biogenic sediment reworking are restricted to the lower portion of the formation (see Walker and Benedict, 1980). Interbedded limestones typically contain finely crystalline diagenetic (framboidal) pyrite. Clayey shales which comprise the Blockhouse Formation have similar bedding character, but generally have a darker color (dark gray to black) with respect to the Whitesburg shales. Bedding type, mineralogy and color of both these lithologies indicate geochemical conditions that correspond to the suboxic and anoxic zones. The darker color of deeper water Blockhouse shales reflects higher organic contents which

resulted from more stagnant bottom circulation at water depths greater than several hundred meters. Methane generation by anaerobic microbes may have succeeded sulfate reduction in these sediments if organic material remained unoxidized after sulfate depletion.

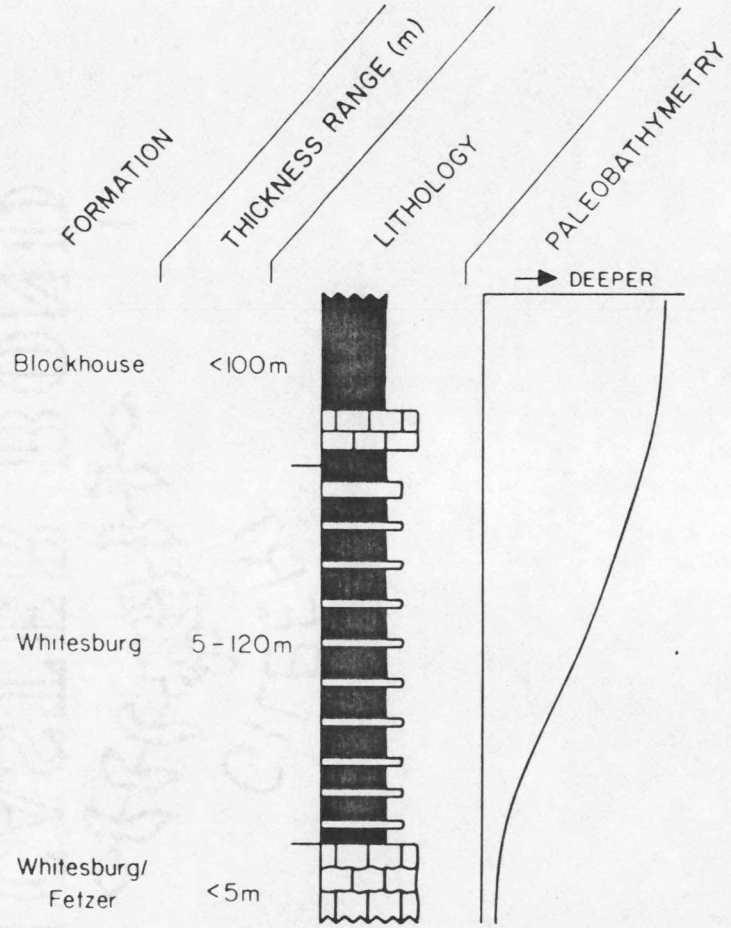
Slope Lithofacies

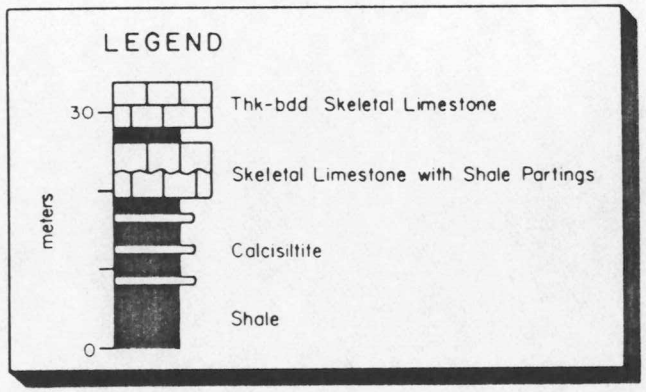
Lithotypes and Petrography

Sediments deposited along the western margin of the Sevier Basin represent the mixing of shelf-derived carbonates from the west and northwest with fine grained siliciclastics eroded from continental areas to the south and southeast. In general, the facies consists of dark calcisiltite (micrograinstone) and skeletal limestone occurring as thin to thick beds in gray to black, fissile shale (Fig. 5.4). Calcisiltite dominates most of the slope deposits during the early phases of basin formation, attaining thicknesses of >100 meters in some areas. Skeletal limestone (wackestone-packstone) is rare and overlies calcisiltites, thus representing deposition along the toe-of-slope environment.

Both carbonate lithologies are allochthonous in origin,

Figure 5.4. Composite stratigraphic section of shelf-to-basin transition from numerous localities in northeastern Tennessee.


FORMATION
THICKNESS RANGE (m)
LITHOLOGY
PALEOBATHYMETRY
DEEPER
Blockhouse
<100m
Whitesburg
5-120m
Whitesburg/
Fetzer
<5m


LEGEND
30
meters
0
Thk-bdd Skeletal Limestone
Skeletal Limestone with Shale Partings
Calcisiltite
Shale

and reflect the sporadic off-shelf transport of unconsolidated sediments by different mechanisms. Carbonate silt was reworked during storms, and redeposited downslope by either debris flows (Shanmugam and Benedict, 1978) or gravity settling from off-shelf directed plumes. The latter mechanism, analogous to modern hemipelagites, is supported by the very thin to thin bedding, dark color and undulose lower bedding contacts of these limestones (Fig. 5.5A). The massively bedded skeletal limestones possess sharp (erosional?) bases and can be traced laterally in outcrop for several 10's of meters. The sheet-like morphology, location in the slope sequence, and sediment texture indicate deposition as carbonate mud flows and debris flows. The wackestone lithology suggests some degree of matrix support, especially in the lower portion of the sediment flow. Packstone caps are analogous to sands found along the tops of modern debris flows (Cook and Mullins, 1983).

Compactional fabrics indicate lithification of calcisiltite beds did not occur until after burial by younger sediments. Thin arthropod carapaces exhibit minor breakage as evidenced by cracks normal to grain surfaces. The fragmented portions sometimes have experienced displacement along these surfaces. Compaction is also indicated by the interpenetration of quartz silt grains into the outer margins of calcareous arthropod skeletons (Fig.

Figure 5.5. Deep-water limestones from the Whitesburg and Blockhouse Formations.

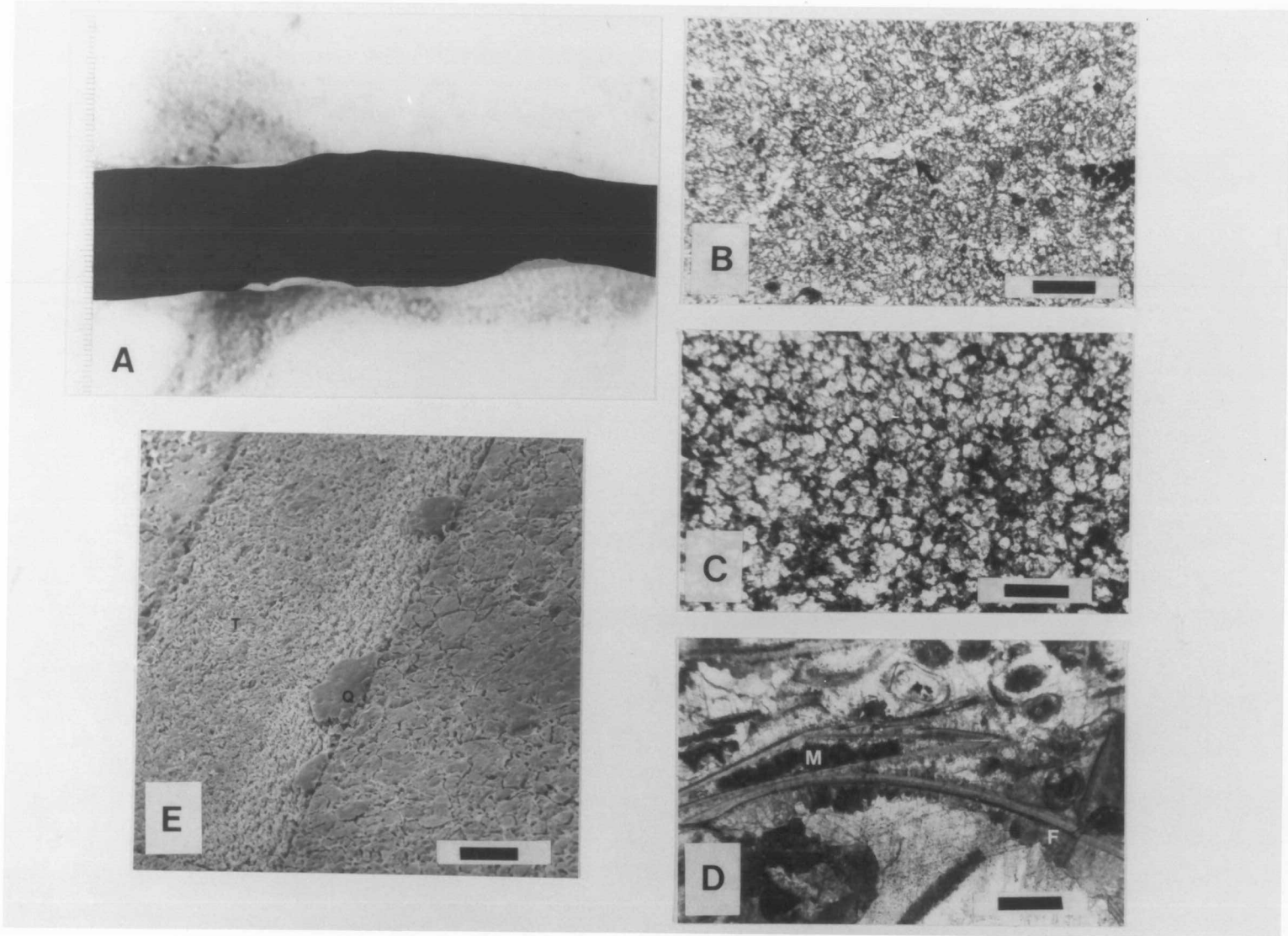
A. Photograph of calcisiltite bed from the Whitesburg Formation. Note the dark color and undulose lower bed contact. Sample SC23. Scale in mm.

B. Thin section photomicrograph of calcisiltite bed showing the interpenetration of detrital quartz grain into the outer margin of arthropod grain (arrow). Sample SC24. Scale bar = 0.1 mm.

C. Area of well-developed equant neomorphic calcspar along the margin of calcisiltite bed. Note abundant impurities present along intercrystalline boundaries. Sample SC22. Scale bar = 0.1 mm.

D. Synsedimentary radiaxial fibrous calcite (F) and microcrystalline calcite (M) cements precipitated in relict inter- and intraparticle pore space, respectively, of carbonate mud/debris flow. Sample SC32. Crossed polars. Scale bar = 0.25 mm.

E. SEM photomicrograph of etched sample illustrating silica replacement (Q) along the margin of trilobite carapace (T). Grains to the right represent calcisiltite matrix. Sample SC30. Scale bar = 50 micrometers.


A
B
C
T
Q
E
M
F
D

5.5B), and plastic deformation of trilobite spines. The latter is restricted to shaly areas along bed margins. Grain penetration fabrics are identical to those observed in experimentally-compacted muddy carbonates (wackestone) by Shinn and Robbin (1983). Another feature suggesting burial diagenesis is neomorphic calcspar (Fig. 5.5C) which possesses two fabrics - small, isolated patches within the silt matrix, and bed-parallel zones of variable thickness. The latter resemble zones of neomorphic microspar and pseudospar along the lower bed contacts of deep-water calciturbidites (Scholle, 1971). Calcspar areas have interstitial and intracrystal inclusions, loose packing and curved intercrystalline boundaries characteristic of this type of diagenetic calcite (Folk, 1965), and grade into un-neomorphosed carbonate silt. Bed-parallel zones in most instances are in direct contact with argillaceous sediments. Individual crystals do not truncate adjacent skeletal allochems. The overall similarity between slope neomorphic calcspars and calcites interpreted as the product of aggrading neomorphism of fine grained sediments suggests equivalent processes. However, because the Ordovician sediments consisted of lime silt, the resultant fabric does not indicate as intense a level of grain aggradation as it might if the original sediments had been clay-sized.

Identifiable cements are very rare in calcisiltites,

and when present are restricted to intraskeletal voids and secondary molds. These pores are filled by a single generation of ferroan to nonferroan equant calcite, similar to blocky calcites from deep-water turbidites described by Schlanger (1980). An entire pore is typically occluded by only a few crystals.

Lithification of calcisiltites at MM and SC localities was completed prior to significant burial. This is interpreted from the nature of parallel to sub-parallel calcite veinlets which cut through individual beds at a high angle. Veinlet thicknesses range from 10 to 300 micrometer, although the majority are <100 micrometer. Margins separating vein calcite from silt and/or neomorphic calcspar vary from sharp to diffuse. Veinlets rarely show disruption of truncated allochems, and in only one instance do allochems exhibit displacement on opposite sides of the veinlet. The above characteristics favor a micrometer-scale recrystallization origin rather than a process involving opening and subsequent fracture-filling by calcite. Submicroscopic cracks provided conduits through which pore fluids migrated under pressure and neomorphosed the surrounding carbonate silt matrix (Misik, 1971).

The petrography of sediment gravity flows offers a striking contrast to the calcisiltites which covered most of the shelf slope. The most noticeable differences are the

abundance of calcite cement, and lack of compactional fabrics. Cements filling primary porosity include: (1)inclusion-rich to inclusion-poor echinoderm overgrowths, (2) clear bladed calcite, (3)inclusion-rich radiaxial fibrous calcite-facsicular optic calcite(RFC-FOC), and (4)clear, fine to coarsely crystalline equant calcite (Fig. 5.5D). Bladed and RFC-FOC spars are particularly well-developed in packstone capping the thicker flow units, occurring as thin, nonisopachous, epitaxial fringes on calcitic bioclasts. Syntaxial overgrowths on echinoderms closely resemble shelf equivalents except for the presence of undulose extinction in cements from deep-water mud/debris flows. Nonferroan equant calcite fills molds resulting from dissolution of aragonitic skeletons and the remaining primary interparticle pore space. Equant to bladed neomorphic pseudospar is present in this lithofacies. Although these calcites texturally resemble depositional carbonate silt, neomorphic spar from sediment gravity flows oftentimes possesses a brownish color in plane light due to the incorporation of micrometer-size inclusions during the recrystallization process. Silica replacement of arthropod debris (Fig. 5.5E) and thin (<100 micrometers thick) calcite veinlets analogous to diagenetic features in calcisiltites also occur in these lithologies.

Summary. Petrography, and trace element data presented in Chapter 2, favor separate diagenetic histories for slope calcisiltites and skeletal limestones. Strontium-magnesium compositions and cement fabrics indicate Middle Ordovician sediment gravity flows experienced considerable grain alteration and lithification while in contact with cold marine bottom waters. The presence of grain compaction and neomorphic calcspar in calcisiltites favor lithification during subsequent burial, where the shales may have exerted some influence on lithification processes. Pervasive seafloor lithification of allochthonous sediments was limited to slope areas characterizied by relatively low sediment accumulation rates. Based on these interpretations, the following discussion is restricted to the calcisiltite lithology.

Elemental Geochemistry of Calcisiltites

Middle Ordovician basinal facies in some areas experienced rather intense structural deformation, in addition to faulting. This deformation is reflected at the Douglas Lake section by development of a weak penetrative cleavage in shales and limestones of the Whitesburg Formation. This fabric brings to mind the possibility of a

significant change in bulk chemical composition during deformation. Marshak and Engelder (1985) detected an increase in Sr/Ca ratio between cleaved and uncleaved limestones, although they were unable to propose a possible mechanism which preferentially incorporates strontium during cleavage formation. A comparison of calcium concentrations in their samples indicates the loss of calcite at the expense of siliciclastic minerals. Assuming neither precipitation of new carbonate phases nor interaction with large volumes of external fluids, the geochemical signature should experience little (if any) change from the pre-deformed state. Manganese and strontium concentrations from cleaved and uncleaved calcisiltites were compared in order to assess potential compositional changes during structural deformation (Fig. 5.6). These elements were selected because both are primarily associated with the carbonate fraction; thus, variations in Sr and/or Mn should indicate fundamental differences in geochemistry following deformation. Concentration ranges shown by the histograms indicate no detectable change in either element between the two sample sets. Cleaved limestones do exhibit less variation, as indicated by a lower standard deviation, but this alone does not necessarily prove alteration of the pre-deformation element composition. Large-scale chemical rearrangement associated with movement of chemically-active

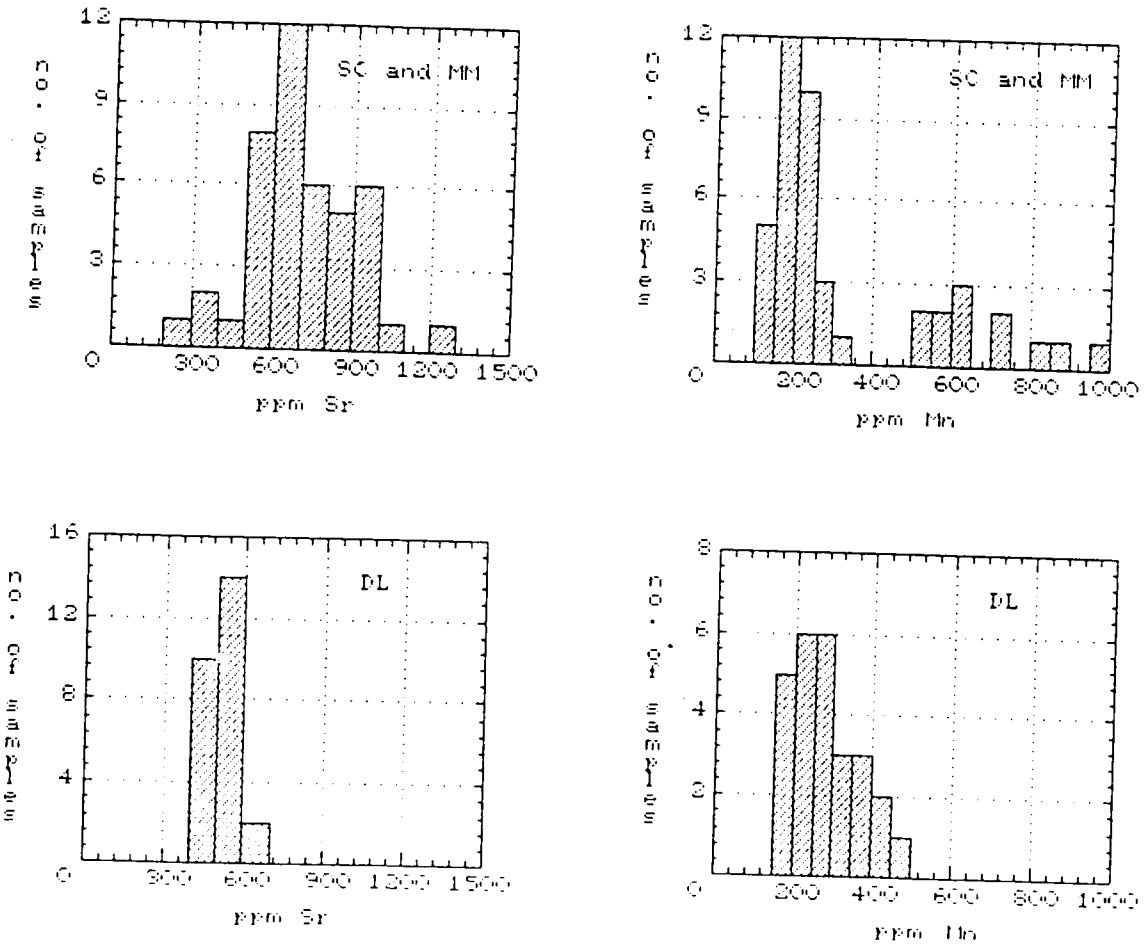


Figure 5.6. Frequency histograms which compare manganese and strontium concentrations in uncleaved (SC and MM) and cleaved (DL) limestones of the Whitesburg Formation.

fluids should be reflected by changes in grain texture and fabric more pronounced than observed in these samples. The possibility does exist that a particular bed or beds may have incorporated some ions during deformation. However, since this cleavage is primarily solutional in nature the amount of calcite precipitation accompanying deformation was probably minor.

Calcisiltite beds possess a high degree of compositional variability throughout the Sevier Basin. Magnesium concentrations separate limestones with respect to geographic position in the basin (Fig. 5.7). Based on the location of each section from the shelf, diagenetic calcites exhibit an apparent magnesium enrichment in an upslope direction. The magnesium enrichment shelfward is opposite to the regional trend from limestones of the Cambro-Ordovician Cow Head Group in the northern Appalachians (Suchecki and Hubert, 1984).

Iron exhibits a positive correlation with manganese in the carbonate fraction of slope limestones. However, samples define separate Fe-Mn trends with respect to locality. Calcisiltites from Silver City (SC) are enriched in manganese as shown by trend I in Figure 5.8, while Douglas Lake (DL) samples are enriched in iron as shown by trend II of the same figure. Most of the samples from Martin Mill Pike (MM) have whole-rock iron and manganese

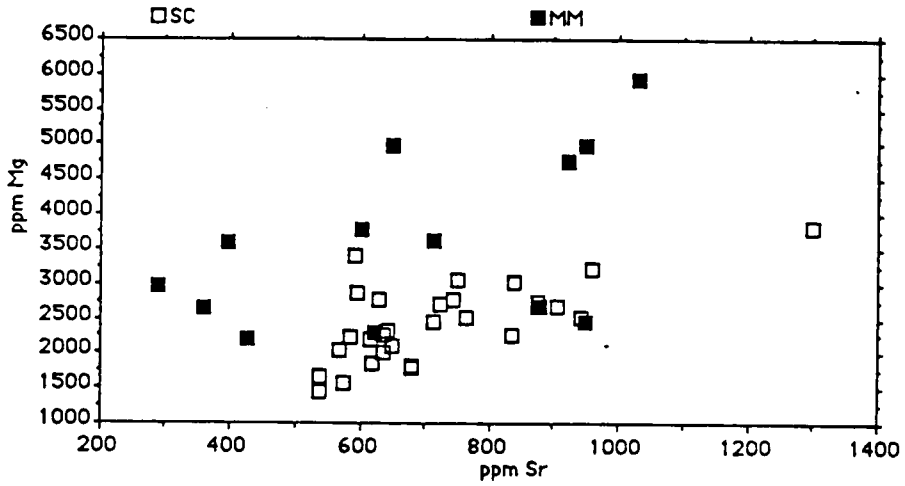


Figure 5.7. Plot of strontium versus magnesium concentration in calcisiltites from the Silver City (SC) and Martin Mill Pike (MM) localities. The majority of MM samples have Mg-Sr compositions different from SC samples. Limestones from the Douglas Lake locality have elemental concentrations similar to the SC population.

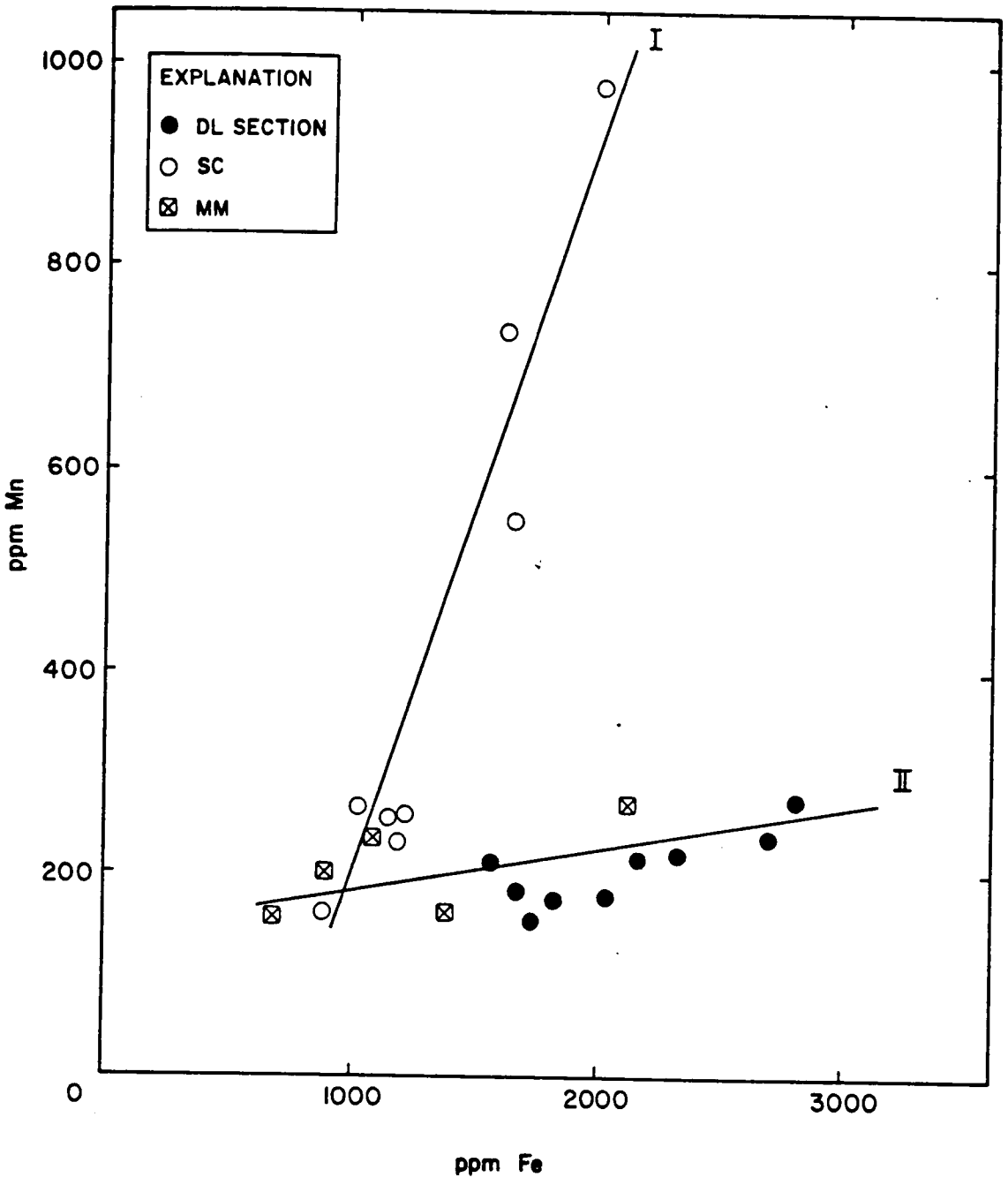


Figure 5.8. Plot of bulk iron versus bulk manganese in calcisiltite beds. Trend I defined by samples from the Silver City (SC) locality exhibits considerably more variation in manganese, while trend II defined by samples from the Douglas Lake (DL) locality exhibits more iron variation. Most of the samples from the Martin Mill (MM) locality occur where these two compositional trends merge.

concentrations where these two trends converge. The distinction shown by these trends is also reflected by the presence of ferroan calcite at Douglas Lake and its virtual absence at Silver City. Since Fe-rich calcites are precipitated are significant burial, the iron enrichment at the DL locality may reflect greater deep burial diagenesis than at the SC locality.

Calcisiltite and neomorphic calcspar from all three localities were sub-sampled to determine if intra-bed compositional variability was present. (See appendix B for further discussion of sampling procedure and preparation.) Element compositions and diagenetic features are given in Table 5.3.

Figure 5.9 shows the mean and standard deviation for manganese, strontium and magnesium from calcisiltite beds at the Martin Mill Pike and Silver City localities. Even though the calcisiltite has higher mean concentrations, a clear geochemical distinction between these components appears to exist only for magnesium and manganese. Bulk sample concentrations are similar to the carbonate silt, indicating the lack of pervasive neomorphism.

TABLE 5.3

TRACE ELEMENT ANALYSES OF SLOPE LIMESTONE BEDS (WHITESBURG FM.), MIDDLE ORDOVICIAN SEVIER BASIN

	Sample	Mn	Sr	Mg
SC18-u	neomorphic calcspar	148	538	1450
-m		116	536	1670
-l	neomorphic calcspar	184	573	1580
SC19-m		158	594	2870
-l	neomorphic calcspar	178	649	2100
SC20-m	neomorphic calcspar	205	679	1810
-l		189	764	2530
SC22-u	neomorphic calcspar	224	634	2270
-m		237	640	2330
-l	neomorphic calcspar	226	617	1850
SC23-u	neomorphic calcspar	236	636	2010
-m		213	572	2440
-l		312	873	2740
SC26-u		825	1300	3820
-m		541	614	2210
-l		615	940	2520
SC27-u		588	834	2260
-m		643	712	2460
-l		573	749	3040
SC29-m		641	566	2030
-l	neomorphic calcspar	724	679	1800
DL24-a	neomorphic calcspar	283	544	1860
-b	"	474	526	1680
-c	"	402	567	1690
-d	"	315	558	1430
-e	"	414	523	2160
-f	"	292	501	1830

TABLE 5.3 (Continued)

		Mn	Sr	Mg
DL25-a	neomorphic calcspar	250	437	1480
-b	"	253	419	1760
-c	"	267	427	1880
-d	"	252	422	1960
-e	"	246	427	1640
DL28-a	neomorphic calcspar	351	503	2010
-b	"	354	470	1750
-c	"	380	488	1770
-d	"	344	461	1770
-e	"	348	472	1920
MM4-a		-	282	2300
-b		132	289	2950
-c		132	359	2640
-d	neomorphic calcspar	184	425	2190
MM5-a		204	500	17600
-b		169	647	4990
-c		145	602	3790
-d	neomorphic calcspar	158	620	2290
MM6-u	neomorphic calcspar	169	875	2260
-m		163	950	4980
-l	neomorphic calcspar	239	970	2440

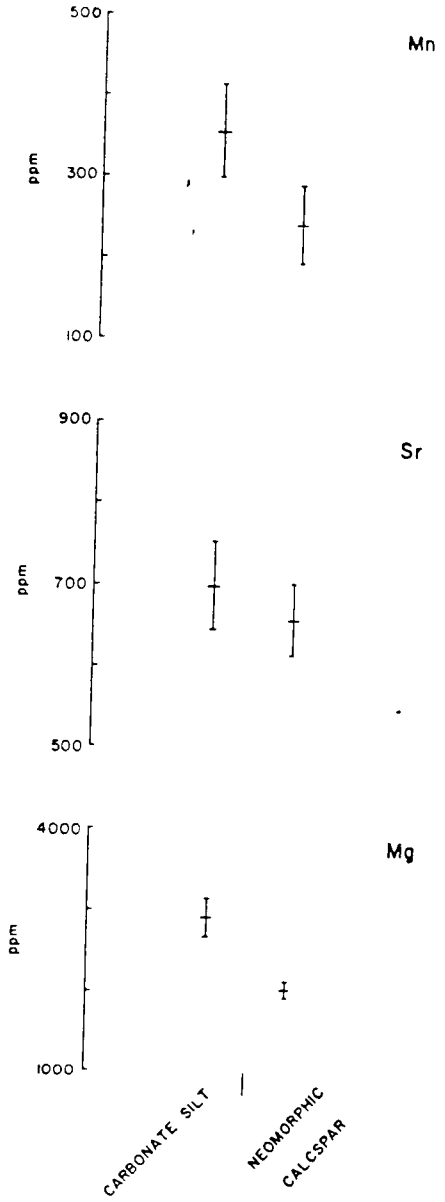


Figure 5.9. Mean and standard deviation of manganese, strontium and magnesium in carbonate silt and neomorphic calcspar fractions in calcisiltite beds.

Discussion of Calcisiltite Geochemistry

The compositional variations within individual limestone beds offer some insight into the affects of associated shales on the chemical evolution of pore waters during shallow burial diagenesis.

Trace element compositions suggest this interaction of clay and carbonate during diagenesis on a centimeter scale with bed contacts representing a transitional zone. Manganese enrichment in the carbonate silt resulted from the mobilization of this cation via reduction of labile Mn-oxide phases coating siliciclastic sediments in the suboxic and anoxic zones. The high magnesium concentrations in un-neomorphosed carbonate silt reflects early recrystallization/cementation in contact with waters more connate in character. The depletion of magnesium in neomorphic calcspar resulted from the preferential adsorption of this ion onto detrital clays in immediately adjacent shale. The lower manganese in neomorphic spar reflects the exhaustion of this early source of dissolved Mn(II) to pore waters. This scenario offers the simplest interpretation of the available data.

After deposition of sediment, manganese oxides and oxyhydroxides within the upper centimeters of the underlying shale will begin to undergo reduction, and Mn(II) ions diffuse upwards toward the new sediment-water interface. In

environments with low sedimentation rates, a portion of this dissolved Mn(II) is incorporated in the carbonate sediments (see Boyle, 1983), while the remainder is redeposited as solid Mn(IV) phases in the overlying shale. However, if subsequent deposition occurred before complete Mn redistribution, shales below each carbonate bed would be enriched in solid manganese by some fraction that is proportional to the sedimentation rate. After these earliest diagenetic changes, sediments then entered the anoxic zone which dominates the early diagenesis of deep-water sediments as indicated by the mineralogy and fabric of shale interbeds. Organic matter oxidation in the presence of dissolved sulfate and reduction of trapped solid manganese raised the pore water alkalinity, causing supersaturation with respect to carbonates (Hesse, 1986). Manganese ions diffused into carbonates, and were incorporated into precipitating diagenetic calcites. The paucity of ferroan calcite at SC and MM suggests lithification occurred primarily in the anoxic zone where sulfide and carbonate ions competed for the available dissolved Fe(II) ions.

The elemental data indicates early diagenetic histories were not uniform over the entire basin, as shown by differences in Mn/Fe ratios of limestones from SC and DL. Limestones from Douglas Lake consist entirely of neomorphic

calcspar, indicating more thorough interaction of carbonate sediments with enclosing shales. Ferroan composition of calcites suggests the diagenesis occurred in the presence of sulfide-poor interstitial waters not associated with the sulfate-reducing zone. The limited diagenesis in the anoxic zone may indicate higher sediment accumulation rates, which would have increased the amount of organic carbon causing a reduction of the depth of sulfate depletion, and/or introduction of more unoxidized organic matter into different geochemical environments. Lower manganese concentrations may have also resulted from local stagnation in this portion of the basin, allowing the release of manganese ions into overlying anoxic bottom waters. Diagenesis would have progressed into the carbonate reduction or methanic zone soon after burial.

The regional variations in magnesium can also be interpreted as a combination of depositional and diagenetic processes. The upslope magnesium enrichment may reflect depth-related changes in the oxygenation of bottom waters within the basin. Assuming similar clay mineralogies, argillaceous sediments deposited in a few hundred meters of water (Martin Mill Pike) would have adsorded less magnesium than sediment deposited further off-slope (Silver City, Douglas Lake). This relationship is a result of differences in the sedimentation rate and/or degree of anoxia in bottom

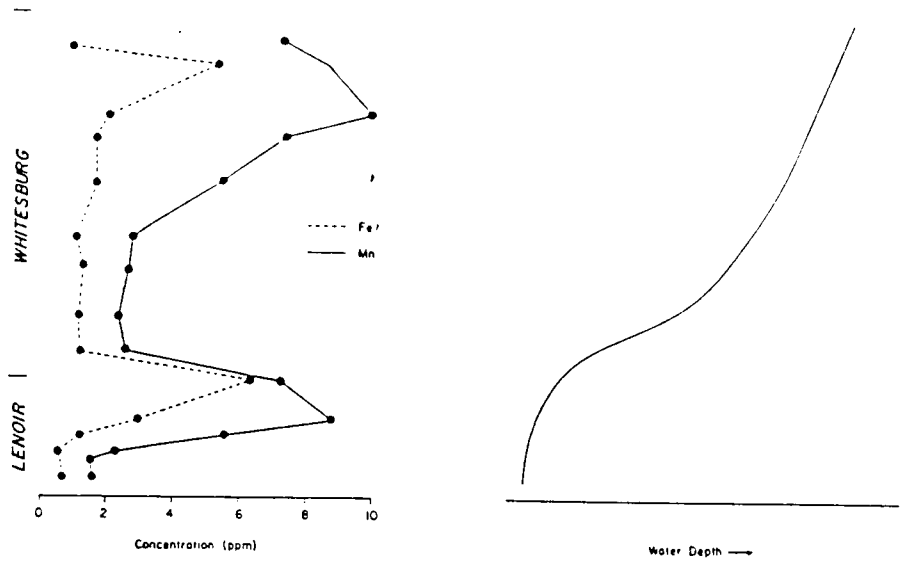
sediments, causing exchange of Mg for Fe(II) on clays by a process noted by Drever (1971).

Bathymetrically-Displaced Ramp/Shelf and Foreslope Deposits

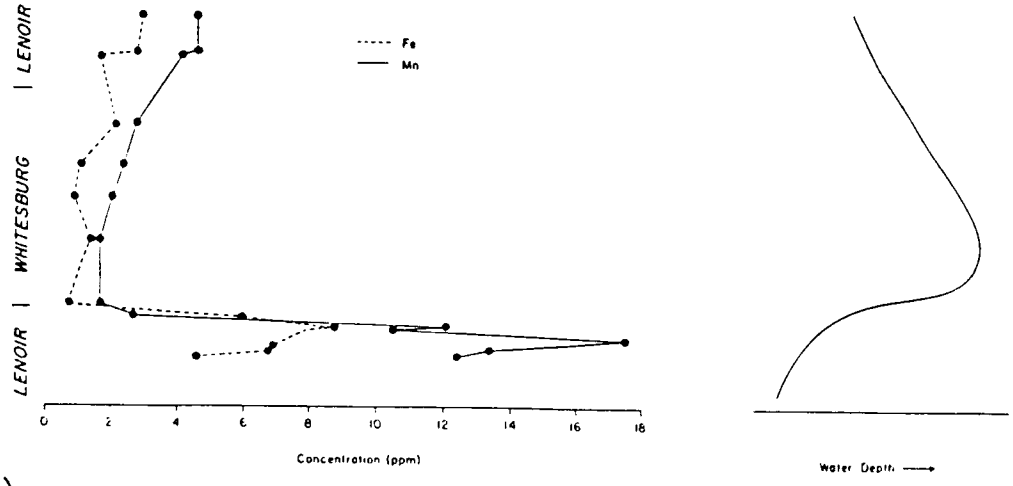
Compositional gradients involving redox-sensitive elements (Mn, Fe) may occur within the interval represented by slope deposition at a given locality. At both Martin Mill Pike and Silver City, manganese and iron show a uniform increase from the basal contact with drowned ramp facies (Lenoir Formation) to the top (Fig. 5.10). This up-section concentration change was not detected at the Douglas Lake section. Recent sediments off continental shelves typically exhibit an increase in manganese with depth, or distance from the shelf. The correspondence between inferred bathymetry and acid-soluble manganese at Silver City (Fig. 5.10A) suggests a possible environmental input to the observed variation. However, this mechanism cannot explain the trend at the Martin Mill Pike section since Whitesburg deposition occurred during a gradual shallowing in this part of the basin (5.10B).

At the Silver City locality, the manganese increase in

Figure 5.10. Stratigraphic variation in bulk, acid-soluble manganese and iron from sequences associated with drowning of shallow-water areas during downwarping. Depth profiles constructed from stratigraphic, sedimentologic and biotic data collected during slab and petrographic analysis.


WHITESBURG
LENOIR
Fe
Mn
0
2
4
6
8
10
Concentration (ppm)
Water Depth

(A)


LENOIR
WHITESBURG
LENOIR
Fe
Mn
0
2
4
6
8
10
12
14
16
18
Concentration (ppm)
Water Depth

(B)

the Whitesburg corresponds to a relative decrease in the abundance of neomorphic calcspar. The highly mobile nature of Mn means the early input of terrigenous-derived Mn2+ ions to interstitial waters was removed from the system prior to lithification. This hypothesis of an "open" diagenetic system with respect to manganese is supported by the presence of anomalously high manganese abundances in drowned shallow-water facies below and laterally adjacent to the interbedded shales and calcisiltites (Fig. 5.10). Atomic absorption analyses indicate concentrations >1000 ppm for manganese within an approximately 10 meter interval below the Lenoir-Whitesburg contact. Comparison of acid-soluble Mn from the Martin Mill and Silver City sections with samples from undrowned parts of the basin (Fig. 5.11) suggest a net influx of these elements during diagenesis. Stratigraphic trends for iron at SC and MM resemble manganese, offering further evidence for the likelihood of solute transport out of the slope-sediment system.

Lithologies through which these enriched basinal waters moved were argillaceous echinoderm-arthropod wackestones and packstones deposited within the shallow to deep ramp environments. This portion of the ramp experienced minor early lithification, as indicated by the very limited development of nonferroan marine cements, and presence of abundant compactional features such as microstylolite seams

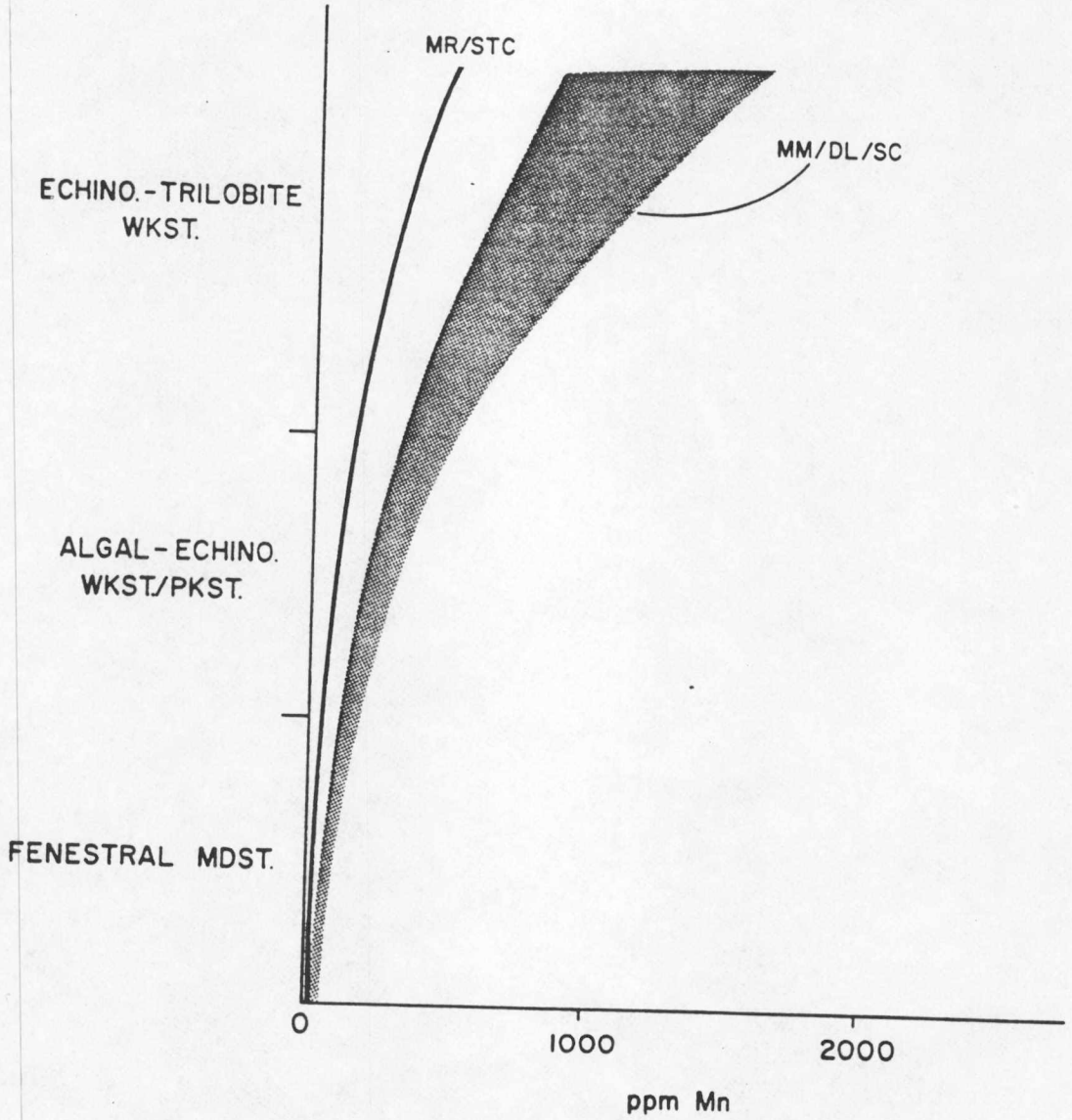


Figure 5.11. Diagrammatic representation of changes in bulk, acid-soluble manganese in the lower 50 meters of the Lenoir Formation at Midway Road (MR), St. Clair (STC), Martin Mill (MM), Silver City (SC) and Douglas Lake (DL) localities. Those shallow-water areas which experienced rapid subsidence and subsequent drowning have higher manganese concentrations than undrowned areas. Data for Midway Rd. section from Benedict and Walker (1978).

which truncate allochems (Fig. 5.12A) and fragmented grains (Fig. 5.12B). Ramp sediments remained relatively unlithified prior to drowning and subsequent burial by slope deposits, enabling fluids expelled from basinal deposits to migrate through with little resistance. Thus, Fe and Mn enrichment in these displaced sediments is believed to reflect the advective transport of mobile redox-sensitive ions from dewatering of shales. The reason limestone beds further above the contact have higher concentrations may be related to flow conditions together with earlier lithification.

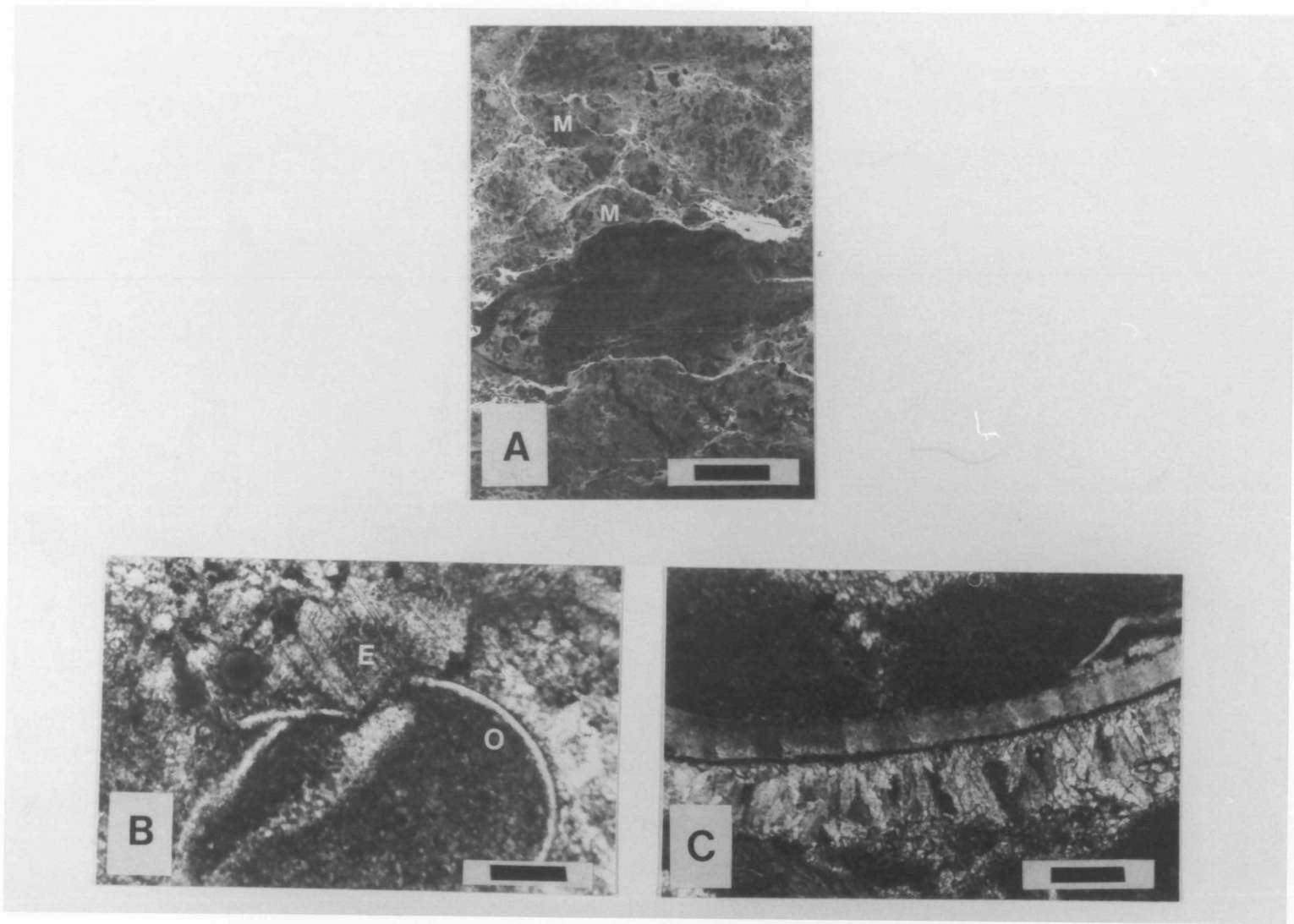
Early cements precipitated from these iron and manganese enriched fluids have a fibrous to bladed morphology, and fabrics which resemble marine-phreatic cements (Fig. 5.12C). Ferroan fibrous/bladed spar associated with argillaceous sediments have been reported from other sequences, particularly the Jurassic of England (Talbot, 1971). These cements have also been interpreted as non-marine in origin. Although fibrous/bladed spar is typically assumed to be precipitated by marine waters, Given and Wilkinson (1985) demonstrated that morphology is controlled by Mg/Ca ratios in pore waters and alkalinity (see their Fig. 11). Connate fluids expelled from argillaceous sediments rich in smectite would have low dissolved magnesium due to exchange with clays and

Figure 5.12. Diagenetic features in bathymetrically-displaced shallow-water deposits of the Lenoir Formation.

A. Thin section photonegative with well-developed microstylolite swarms (white stringers), which produce carbonate-rich micronodules (M) in some instances. Sample MM1. Scale bar = 2 cm.

B. Photomicrograph showing thin-walled ostracode (O) which has been fractured at contact with an echinoderm grain (E). Sample MM1. Scale bar = 0.1 mm.

C. Photomicrograph of clear, ferroan fibrous/bladed calcite cement which has nucleated on micritic coating/cement on trilobite carapace. Sample MM2. Scale bar = 0.1 mm.


M
M
A
E
O
B
C

relatively high dissolved carbonate due to organic matter oxidation. Thus, fibrous to bladed spar containing high manganese and/or iron may indicate the movement of early compaction-driven waters from associated shales.

Sedimentation lags associated with drowning of shallow water sediments commonly result in formation of condensation surfaces and submarine hardgrounds (Kendall and Schlanger, 1981). It is likely that drowned ramp packestones and wackestones may have experienced some lithification (particularly the lime mud matrix) while in contact with seawater. Whole-rock magnesium and strontium concentrations are similar to sediment gravity flow deposits believed to have undergone deep marine diagenesis. However, the following evidence indicates diagenesis continued into the subsurface.

(1) pore-filling cements have textures and fabrics different from other marine cements,

(2) precipitation of ferroan carbonates requires high Fe(II) with limited sulphate/sulfide, a situation unlikely in marine waters,

(3) hardgrounds associated with Middle Ordovician downslope buildups in Virginia (Read, 1980) have pyritic and phosphatic crusts.

Diagenetic pyrite and collaphane are present, but comprise less than 5 precent of samples and do not occur as extensive crusts along bedding planes. The limited degree of marine diagenesis following subsidence may indicate a relatively

brief lag time, which might be expected along a newly formed slope where associated shelf sediments are poorly consolidated.

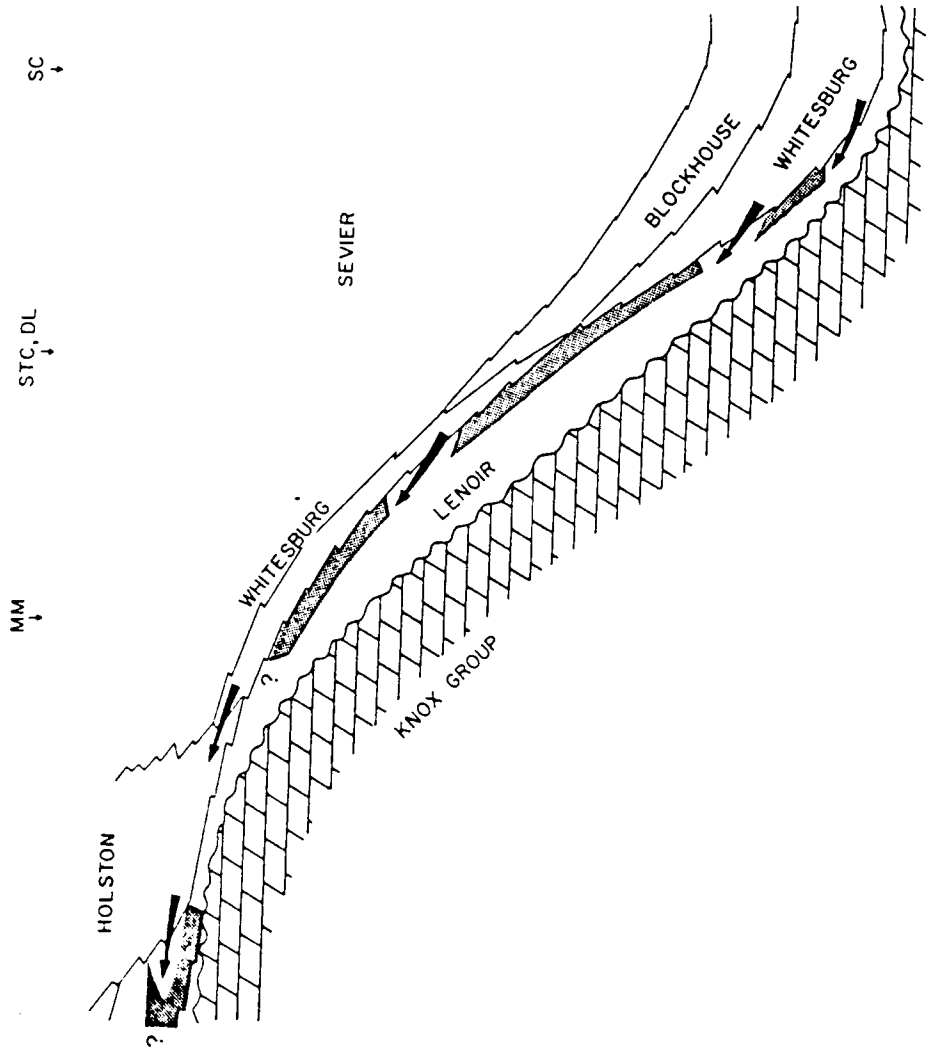
Distances over which shale-derived constituents may have been transported by fluids is uncertain. Relatively high Mn concentrations in certain outer shelf facies could reflect the introduction of these basin-derived waters (Fig. 5.13; see Chapter 4).

Carbonate Shelf Lithofacies

Synsedimentary Iron-Manganese Oxides

Syndepositional diagenesis of shelf-marginal facies includes the precipitation and deposition of metal oxides containing abundant Fe (and Mn), in addition to carbonate cementation. These oxides are so abundant in some parts of the outer shelf, they impart an easily recognizable coloration to certain units which is used as a guide in deciphering the stratigraphy (see Ruppel and Walker, 1982). The occurrence of Fe-Mn oxides in platform-margin buildups and sediments has been noted from several modern areas (James and Ginsburg, 1979; Land and Moore, 1980; Marshall, 1985). However, these minerals have garnered only cursory

Figure 5.13. Generalized cross-section of Ordovician shelf-to-basin transition which depicts probable fluid migration paths during burial of drowned carbonates, and stratigraphic zone of iron and manganese enrichment. Stratigraphic relations used in this diagram from Ruppel and Walker (1984).


SC
STC, DL
MM
SEVIER
BLOCKHOUSE
WHITESBURG
WHITESBURG
LENOIR
KNOX GROUP
HOLSTON
?
?

treatment, with no attempt to integrate their formation with either depositional or diagenetic processes.

The majority of iron in sedimentary rocks is derived from weathering of igneous and other rocks under humid climatic conditions. Iron and other metals are transported to marine basins by various mechanisms including adsorption and chelation on particulate organic matter, and oxide-oxyhydroxide coatings on detrital clays (Tucker, 1981). However, since iron and manganese are redox-sensitive elements, it is not uncommon for them to be recycled numerous times within the sediment column. This high degree of diagenetic mobility is best illustrated in deep-water (pelagic) environments, where diffusive and advective transport augmented by low rates of sedimentation combine to produce seafloor pavements rich in transition metals.

Hematite in Middle Ordovician shelf facies reflects the synsedimentary redistribution of continental-derived iron upslope from basin to shelf. Iron was transported to the Sevier foredeep by rivers draining the tectonic highlands to the east. A small but volumetrically insignificant contribution may have been supplied by exposed Knox Group carbonates. An eastern source is suggested by the decrease in hematite abundance from outer to inner shelf. Holston lithologies which represent shelf-marginal deposition (Red

House Branch or Alcoa Highway sections) contain hematite and Mn oxides throughout their entire thickness, while more on-shelf subtidal facies exhibit a lesser abundance of this material (Cedar Springs and Solway Bridge sections among others). Oxides in the latter occur at only scattered intervals in the Lower Chickamauga. The shelfward decrease does not appear to be in response to changing environmental conditions, because equivalent facies show the same trend as the sequence as a whole. Variations in hematite abundance along depositional strike also exist and may be considerable over relatively short distances.

Slab examination and petrography revealed Fe-Mn oxides occur in several forms: fine, disseminated particles in micrite; crusts and replacement rims (including impregnation of porous allochems such as echinoderm ossicles); peloidal internal sediments. A more detailed accounting of each is given in the following discussion. The following descriptions are primarily from build-up facies (reef core and flanking skeletal sands) of the Holston Formation, since these deposits exhibit the most striking occurrences of this material.

Reddish micrite. The red to maroon color which characterizes shelf-margin wackestones and packstones is due

primarily to the presence of Fe-Mn oxides within the micritic matrix. Insoluble residues remaining after acid digestion of the carbonate fraction are reddish in color. Oxides are present in both intra- and interparticle matrix. This material tends to be rather uniformly distributed with occasional dense, irregular patches and scattered silt-sized grains present in the reddish matrix.

Although Fe-Mn oxides in most samples exhibit a homogenous distribution, mottling indicates small-scale variations in their relative abundance. Some build-up samples contain areas outlined by reddish to maroon matrix which are filled by isopachous to geopedal, greenish, oxide-free microcrystalline calcite and later pore-filling calcite cement (Fig. 5.14A). In some cases, the relict pores are entirely filled with microcrystalline calcite. These areas of purer carbonate sometimes have preservational fabrics resembling the spicular networks of sponges. Larger cavities may have faint to distinct Fe-Mn oxide "laminations" less than 0.2 mm thick alternating with micrite (Fig. 5.14B). These laminae may exhibit anti-gravitational fabrics, and can merge into Fe-Mn coatings on skeletal grains. Where present this layering provides a precise record of the cavity filling process in the absence of other features.

Focke and Gebelein (1978) distinguished depositional

Figure 5.14. Photomicrographs of iron-manganese oxides from the Holston Formation.

A. Relict void in boundstone facies containing geopedal micritic sediment/cement (M) and inclusion-rich radiaxial fibrous calcite-fascicular optic calcite (F). Distinction between void-filling sediment/cement and depositional matrix is possible due to the reddish color of the latter caused by the presence of finely disseminated hematite. Scale bar = 0.25 mm.

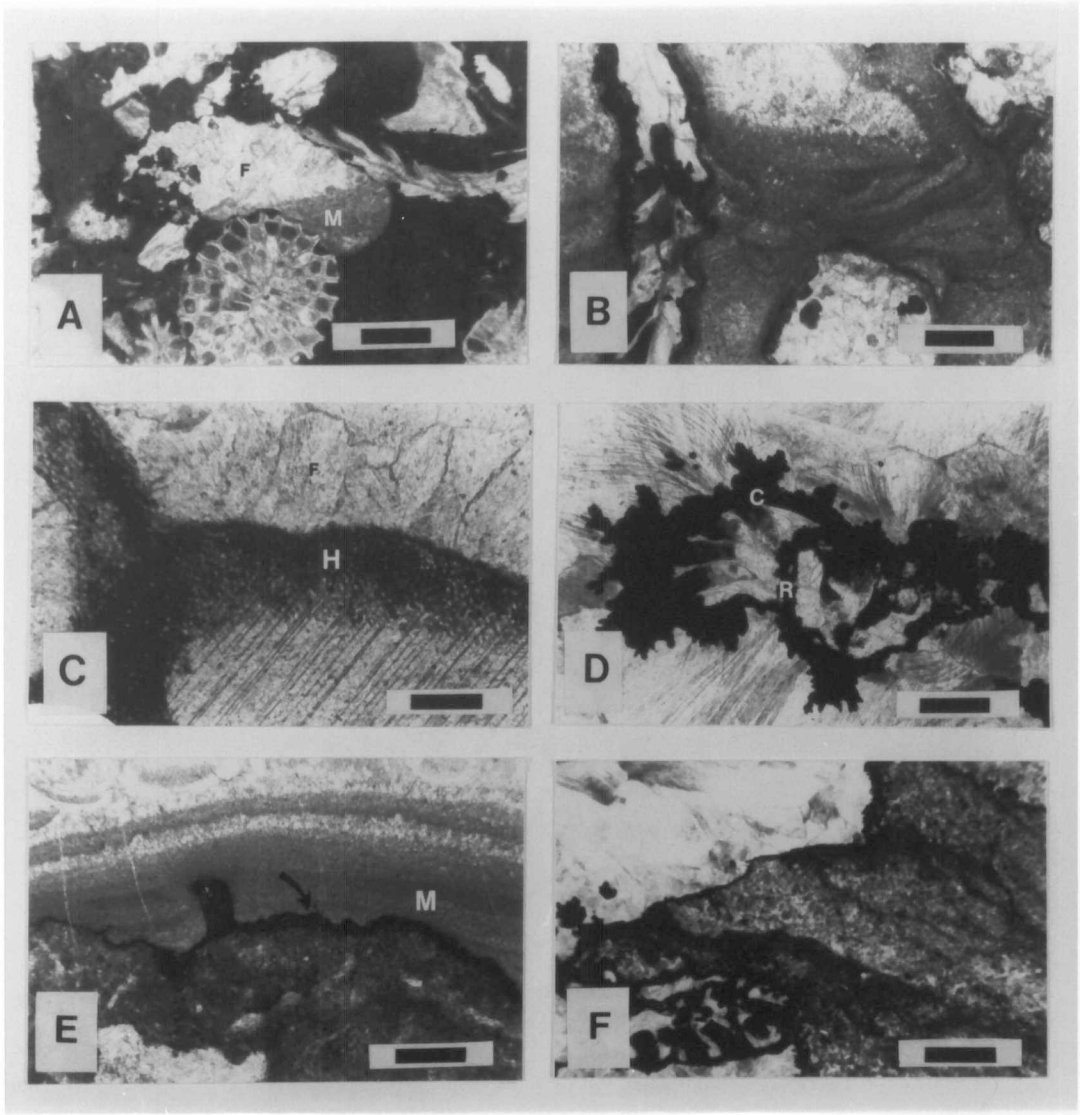
B. Alternating hematite-rich and hematite-poor microlaminations within depositional micrite which partially fills a cavity. Scale bar = 0.25 mm.

C. Hematite replacement and cementation (H) along the outer margin of articulated echinoderm ossicles. Relict intergranular pore space is filled with radiaxial fibrous calcite-fascicular optic calcite (F) which appears to have nucleated on the hematized grain. Scale bar = 0.1 mm.

D. Grain-metal oxide aggregation in bryozoan boundstone mass. Opaque oxide phase exhibits both cement (C) and replacement (R) fabrics with the associated bryozoan. Inclusion-rich radiaxial fibrous calcite-fascicular optic calcite fills the relict void. Scale bar = 0.25 mm.

E. Boundstone cavity whose wall is coated with iron-manganese oxides (arrow). The formation of this noncarbonate phase allows for the discrimination of the original cavity from micritic sediment/cement (M) which partially floors this early pore space. Scale bar = 0.25 mm.

F. Crudely laminated peloidal sediments which appear truncated by a cavity wall which has been impregnated by iron and manganese oxides. Grain-metal oxide aggregation is present in the lower left corner. Scale bar = 0.25 mm.


A
F
M
B
C
F
H
D
C
R
E
M
F

micrite from microcrystalline calcite cement in Bermudian fore-reef limestones by color, with micrites having a brown color and cements being clearer and more transparent. This distinction might also be used to explain the patches of oxide-free micrite in these buildups. The isopachous fabric and other petrographic evidence of physicochemical precipitation support a cement origin for the greenish micrite. The syndepositional incorporation of hematite and other oxides may serve as a useful fingerprint of depositional micrite, and thus should not be disregarded during petrographic analysis.

The interlaminated micrite and Fe-Mn oxides offers a fortuitous tool in understanding the history of cavity filling in these shelf-margin deposits. Reddish laminae are interpreted to represent the periodic "deposition" of hematite along the accretionary surfaces of newly deposited internal sediments/cement, and thus may be thought of as short-term "disconformities" in the cavity-filling process. Based on this interpretation, each micrite-hematite couplet indicates alternating "fast" and "slow" rates of net sedimentation (Fig. 5.15). Study of the abundance and frequency of this type of compositional layering in analogous subfacies of ancient bioherms may allow for a better understanding of reefoid limestones.

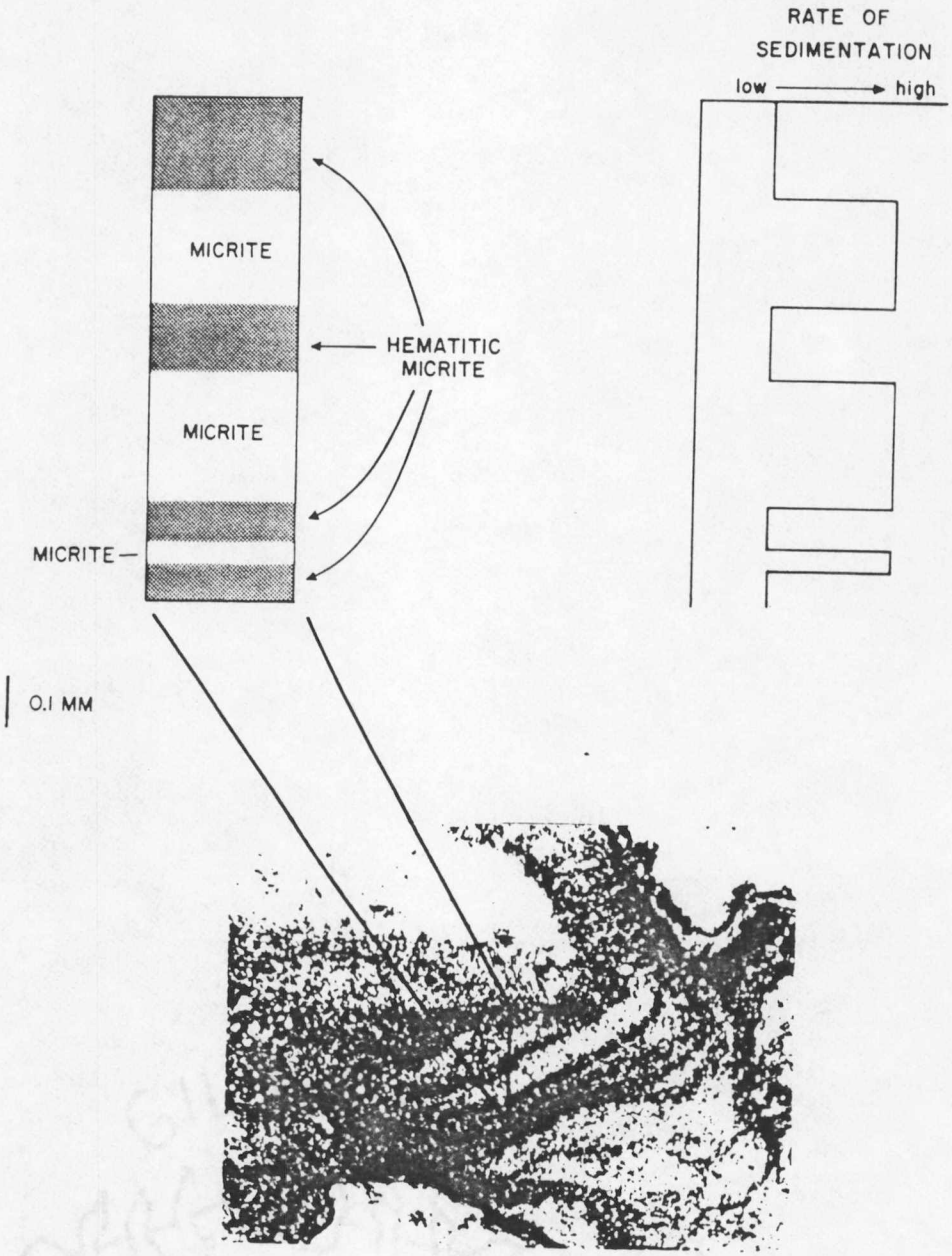


Figure 5.15. Close-up of hematite-rich and -poor microlaminations in internal sediments, and inferred fluctuations in respective sediment accumulation rates.

Crusts and replacement rims. Cavity walls often have thin (<0.5 mm) surficial crusts of opaque Fe-Mn oxides. These deposits possess fabrics that constitute a gradation between replacement and precipitation within pores. The latter is characterized by a sharp contact between oxide and host carbonate, and occasional spalling of crusts from grains with the resultant pore space filled by clear equant spar. Skeletal allochems have dense oxide rims which grade into more translucent reddish-orange replacement hematite in grain interiors (Fig. 5.14C). This mode of occurrence is common in grain-supported lithologies. Algal tubules recognized in modern Fe-oxide coatings by James and Ginsburg (1979) are absent from this Paleozoic occurrence.

Substrates associated with these oxide coatings/replacements include: (1)various skeletal allochems; (2)cavity walls; (3)syndepositional cements. The last type is poorly developed in these shelf-marginal deposits for one reason or another; thus, oxides typically separate depositional components from internal sediments and RFC-FOC cement. Fe-Mn oxide clumps and grain-oxide aggregations are found enclosed by inclusion-rich RFC-FOC cement (Fig. 5.14D). These fabrics offer positive petrographic evidence for a synsedimentary origin, with precipitation having occurred sporadically in the very early

diagenetic history of these organic build-ups.

The restriction of oxides to original pore walls is reflected by allochems having nonisopachous coatings along their outer margins. Contacts with allochems and walls may be irregular, occasionally with a serrate or peaked morphology resembling stylolites (Fig. 5.14E). Similar crust morphologies have been reported from Holocene fore-reef sediments (James and Ginsburg, 1979; Land and Moore, 1980). Crusts are observed truncating skeletal grains and sediment laminations in some of the Middle Ordovician build-ups (Fig. 5.14F).

The above fabrics suggest crust formation occurred during brief interval(s) of nondeposition which also correspond to periods of CaCO undersaturation. Fabrics in portions of build-ups reflect the complex nature of processes leading to cavity formation. In cavities where the texture of the host limestone and internal sediments are similar, the presence of these surficial oxide crusts provides the only clue to the dimensions of the original cavity. Fabrics indicating early dissolution are also present in correlative mudmound facies in the Rockdell Formation at Cedar Springs.

The complex history of organic build-ups is depicted schematically by the sequence of sketches in Figure 5.16. Initial cavities were probably small and constructional in

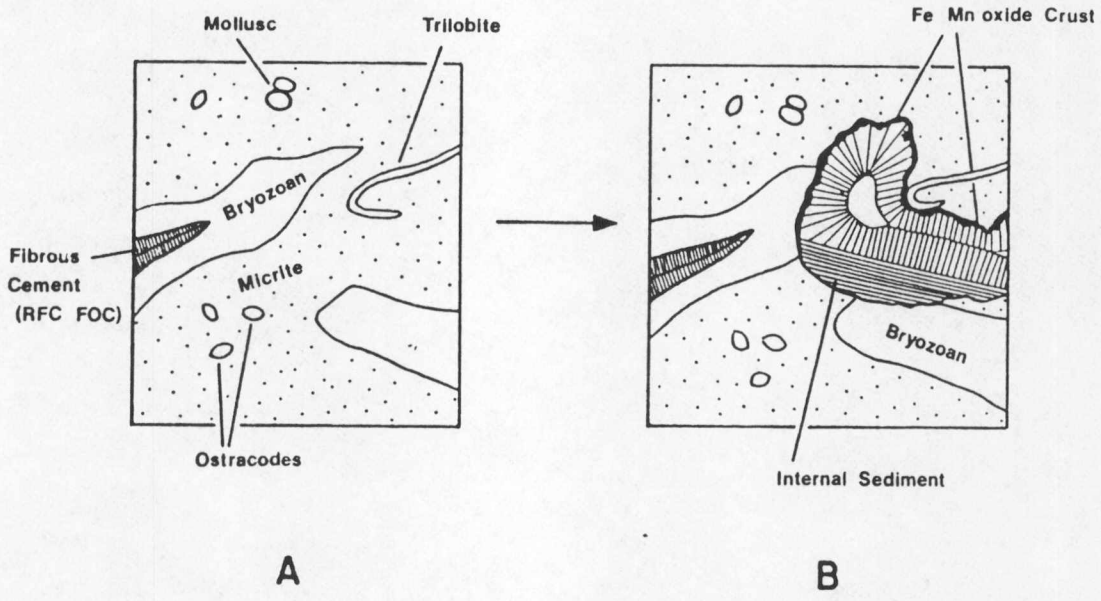


Figure 5.16. Diagrammatic sketch of bryozoan boundstone lithofacies showing diagenetic changes accompanying secondary cavity formation/enlargement and penecontemporaneous iron and manganese oxide precipitation. A = immediately after deposition; B = after exposure to marine waters.

nature, and filled by micritic internal sediment/cement and fibrous magnesian calcite spar (RFC-FOC precursor). Fe-Mn oxide coatings may mark the original dimensions of these first-generation cavities. At some point during lithification, pore waters within these limestones became undersaturated with respect to $CaCO_3$, and the ensuing dissolution produced second-generation cavities. The formation of Fe-Mn oxide crusts was penecontemporaneous with solution enlargement. This process may have recurred, causing another episode of dissolution/cavity enhancement and sedimentation. Local dissolution along cavity walls and skeletal grains may have been facilitated by the formation of iron oxyhydroxides in the presence of seawater bicarbonate:

$$2Fe^{2+} + 4HCO_3^- + 1/2O_2 \longrightarrow 2FeOOH + 4CO_2 + H_2O$$

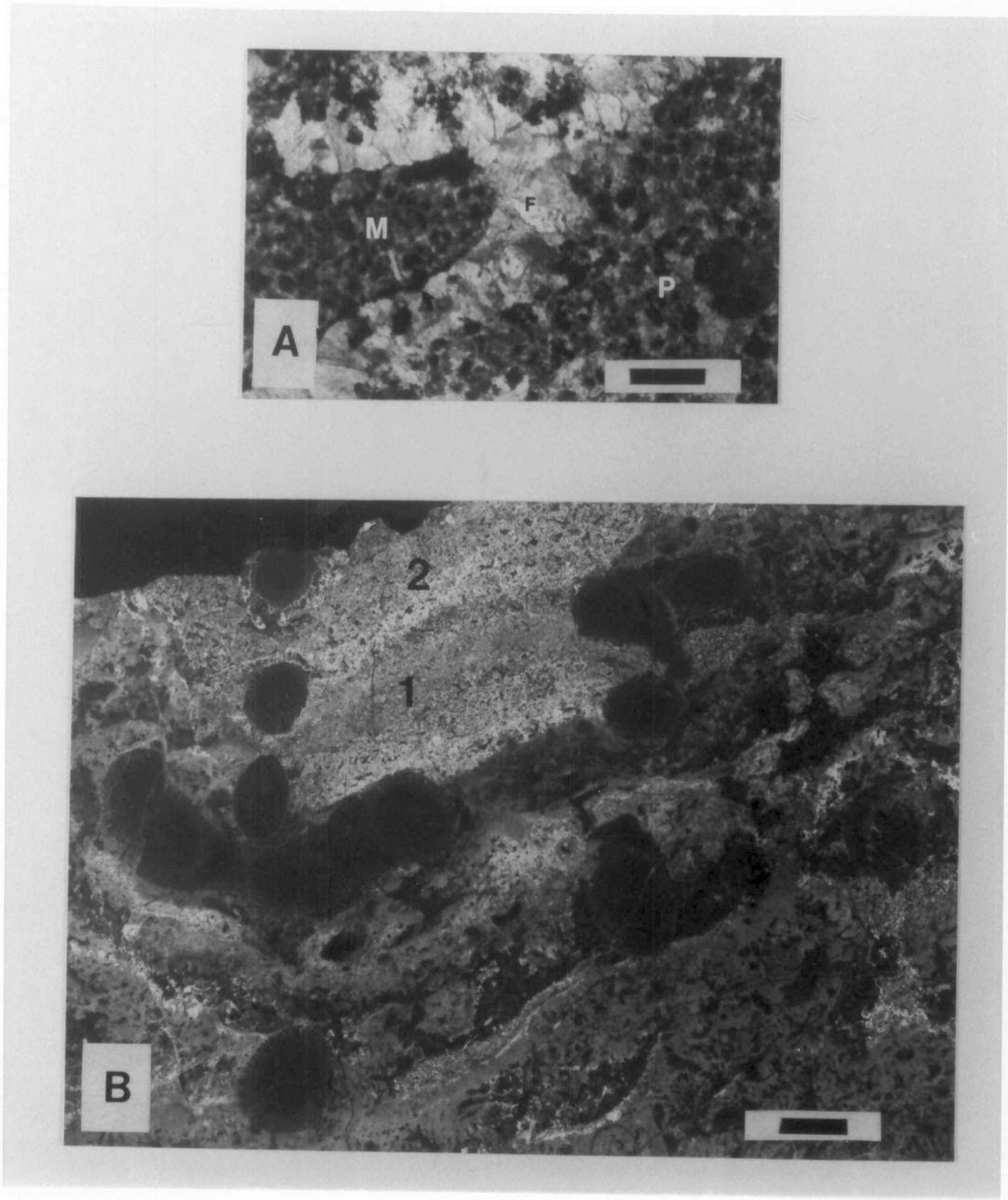
which decreases alkalinity in the surrounding microenvironment.

Peloidal internal sediments. The most unique occurrence of Fe-Mn oxides in Middle Ordovician shelf facies is as sand- to silt-size grains or peloids which constitute geopedal internal sediments in cavities (Fig. 5.17A). Modern reef/fore-reef environments do not contain this type of sediment filling large pores. Like surficial crusts,

Figure 5.17. Hematitic peloidal sediments in boundstone facies of the Holston Formation.

A. Photomicrograph of cavity which contains two generations of pore filling. The original (constructional) cavity was occluded by peloidal microcrystalline calcite cement (M). Later, this synsedimentary cement was partially removed, with the secondary cavity wall impregnated to varying degrees by iron-manganese oxides forming a discontinuous rind (arrow). This second generation cavity was filled by hematitic peloidal sediments (P) and radiaxial fibrous calcite-fascicular optic calcite (F). Scale bar = 0.25 mm.

B. Thin section photonegative of bryozoan boundstone with cavity filled by two generations of hematitic peloidal sediment (1,2). Scale bar = 2 cm.


M
F
P
A
2
1
B

grains vary in appearance from opaque to translucent reddish-orange similar to replacement hematite. Carbonate peloids, some with an Fe-oxide outer margin, are commonly admixed with Fe-Mn oxide peloids. The oxide rims suggest a replacement origin rather than either homogeneous nucleation or aggregation of finer material in suspension.

Although the genesis appears straightforward, uncertainty exists as to whether oxide replacement occurred in situ, or prior to deposition of mechanically deposited internal sediments. These sediments exhibit compositional grading in which dense, opaque particles pass upwards into less altered sediments on a scale of <1 cm (Fig. 5.17B). A single cavity may contain several of these graded subunits superposed one on another. This grading would have resulted from the differential settling rates of Fe and Mn-oxide particles (more dense) and carbonate particles (less dense). However, Fe-Mn peloids commonly have angular shapes, suggesting minimal reworking and abrasion. Some individual grains appear to actually be aggregates of finer grains. The low probability of these grains maintaining their integrity during current transport makes a sedimentary origin somewhat doubtful.

The exact process is uncertain, but I favor deposition within selected cavities by water currents channelled through the cavernous pore network. Replaced peloids formed

by erosion of crusts or reddish micrite, in addition to carbonate peloids, and other sediments were periodically swept through build-ups probably during storm events. If these layers were formed by reworking of particles, they must have been derived from local parts of the shelf-margin environment and transported for only short distances.

Origin of Fe and Mn-oxides in shelf margin limestones. The occurrence of Fe-Mn oxides in outer shelf facies requires the existence of certain conditions other than simply a source of iron and manganese, as suggested by their limited occurrence in other shelf/platform sequences. One prerequisite is periods of low sediment accumulation. Crusts on cavity walls and allochems represent intervals of neither sedimentation nor cementation in that part of the shelf margin. Bathymetry may also have controlled the formation of these oxide minerals, especially surficial crusts. Modern Fe-Mn crusts are restricted to water depths exceeding 50 meters (James and Ginsburg, 1979; Land and Moore, 1980). This relationship with bathymetry may be linked to the sporadic nature of sedimentation in fore-reef settings. The only true depth restriction is related to the position of the permanent thermocline, which separates oxygen-rich waters of the surficial mixed zone from

oxygen-poor deep waters.

The final aspect of origin involves a mechanism permitting the shelfward transport of iron and manganese from the basin. The absence of a lithofacies suite characteristic of strong coastal upwelling (organic-rich shales, phosphorites, bedded chert) suggest regionally significant coastal upwelling was not occurring within the Middle Ordovician basin (see Parrish et al., 1981). This is also supported by the paleogeographic location of the Laurentia land mass with respect to probable atmospheric circulation belts. Conditions necessary for other types of upwelling were not present, although an area of obstruction-related upwelling may have existed near the shelf re-entrant situated west of the DL section.

However, the organic-rich nature of some basinal shales and limited occurrence of phosphatic minerals appear to indicate some movement of deep waters upslope to shallower levels. The presence of syndepositional dissolution also necessitates the periodic introduction of $CaCO_3$ -undersaturated waters along the shelf margin. One logical source of undersaturated waters is at depth, below the permanent thermocline. Alternative upwelling mechanisms which could mix deep waters may have been operative in the absence of wind-driven upwelling. One possibility involves the generation of internal tides, producing tidally induced

upwelling similar to that described by Thompson and Goldring (1981). Temperature variations along a portion of the Great Barrier Reef may represent the presence of internal Kelvin and tidal waves which produce significant mixing about the thermocline (Wolanski and Pickard, 1983). Measurements indicate both wave types are coherent with cross-shelf currents, and thus may propagate westward from the shelf margin. Wolanski and Pickard (1983) suggest internal tidal waves should "...be expected at the shelf break in view of the large width of the continental shelf (ca. 120 km) and steep slope of the shelf" (p. 79). The approximate width of the Middle Ordovician shelf increased from 100 to 150 km during the early phases of sedimentation. Facies reconstruction and paleobathymetric analysis suggest slope inclination similar to modern continental slope areas (2 to 4 degrees; see Shanmugam and Walker, 1980). The occurrence of sediment gravity flows indicate inclinations may have varied during basin evolution. Shelf topography and probable oceanographic conditions support the viability of internal tides as an upwelling mechanism during the Middle Ordovician. This process also offers an explanation for variations in Fe-oxide abundances along depositional strike through the focusing of the tidal flow at certain areas along the shelf margin.

Deep Burial Diagenesis of Shelf Limestones

Petrography. Some shelf facies consisting of grain- and matrix-supported lithologies contain abundant evidence of physical and chemical compaction. Physical compaction involves the decrease in inter- and intraparticle pore space by breakage and plastic deformation of grains without noticeable dissolution of material. In the Middle Ordovician sequence, these fabrics are well developed in outer shelf packstones and grainstones, with minor synsedimentary cements (e.g., CS locality). Grain breakage is indicated by the fragmentation of polycrystalline skeletal debris (Fig. 5.18A and B), and collapse of micrite envelopes. Displacement of fragments is generally minor (<0.1 mm), although some pieces may exhibit rather appreciable offset (0.5 mm). The importance of early lithification in inhibiting breakage is shown by contrasting compactional fabrics associated with ostracodes. Where articulated valves are filled by synsedimentary RFC-FOC calcite, no fracturing occured; instead, the grain+cement behaved as a single unit and exhibits pressure solution contacts typical of echinoderms (Fig. 5.18C). Valves lacking early cements experienced fracturing at numerous points with attendant telescoping of pieces across the pore space in response to local stresses (Fig. 5.18D). Drag

Figure 5.18. Photomicrographs of compactional fabrics in shelf limestones.

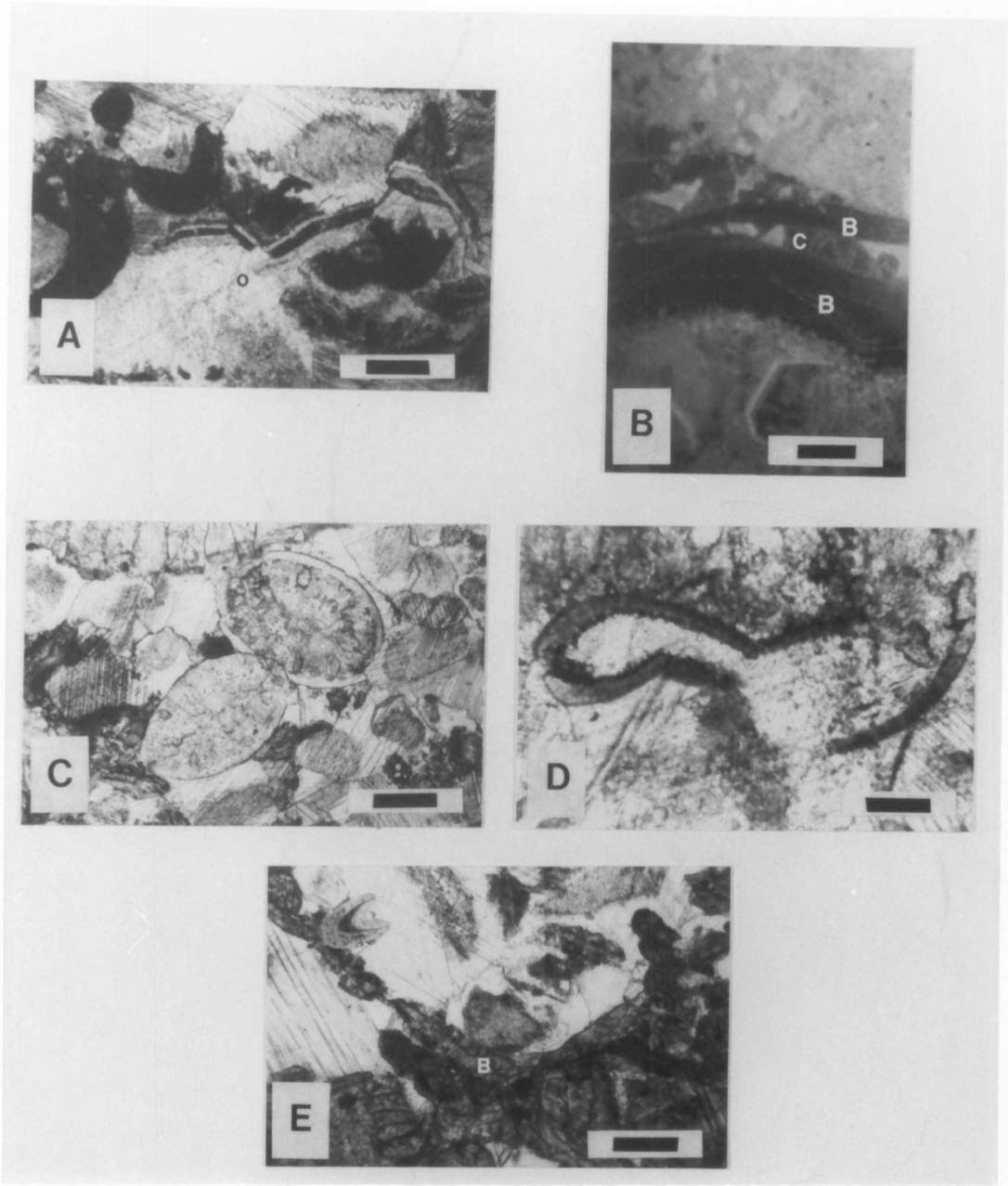
A. Arthropod fragment and prismatic cement fringe which has been fractured and displaced at several points. Echinoderm overgrowth calcite (O) partially encloses some of the fractured pieces. Sample CS43. Scale bar = 0.25 mm.

B. Non-luminescent articulate brachiopod (B) fractured along its fibrous secondary layer, with luminescent-zoned calcite cement (C) infilling the spalled areas. Sample CS25. Scale bar = 0.1 mm.

C. Concavo-convex grain contact between articulated ostracodes having radiaxial fibrous calcite-fascicular optic calcite occluding all relict intraskeletal pore space. Sample CS30. Scale bar = 0.25 mm.

D. Ostracode carapce which has been fractured across the skeletal microstructure, and pieces telescoped towards one another. Compacted grain is enclosed by echinoderm overgrowth calcite. Sample CS59. Scale bar = 0.1 mm.

E. Plastic deformation of bryozoan frond (B) around an echinoderm and its associated overgrowth cement. This fabric shows that mechanical compaction may have continued to significant burial depths, well after meteoric diagenesis. Sample CS22. Scale bar = 0.25 mm.


A
o
B
C
B
B
C
D
E
B

fabrics indicative of plastic deformation typically occur among brachiopods, trilobites and foliate bryozoans in contact with echinoderm grains (Fig. 5.18E). Similar compactional fabrics and cement-compaction relationships were observed by Moore and Druckman (1981) and Moore (1985) in oolitic facies of the Smackover Formation. However, compacted bryozoans similar to those noted by Meyers (1980) in Mississippian skeletal limestones are absent in these Middle Ordovician rocks.

Intergranular pressure solution can produce increased packing density by a decrease in the volume of components. Contacts in Middle Ordovician skeletal limestones range from simple point types which reflect minimal amounts of pressure solution to concavo-convex and sutured types indicating more intense grain interaction. One of the most common fabrics involves the interpenetration of echinoderm overgrowth cements into other grains, including echinoderms. Pressure solution not involving echinoderms results in tangential and sutured contacts with minor grain interpenetration.

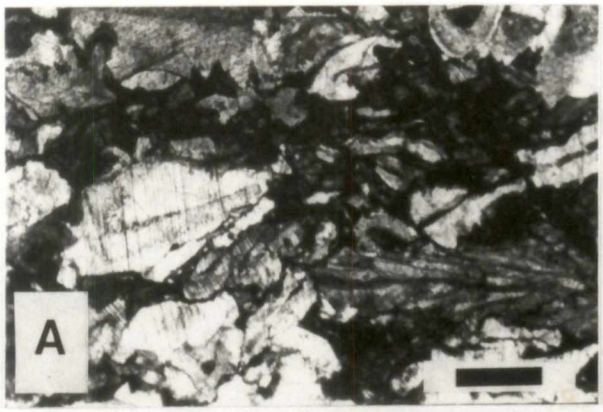
A combination of these compactional processes in grain-supported lithologies may result in highly overpacked zones which possess numerous sutured contacts that coalesce to form anastomosing stylolites (Fig. 5.19A). Echinoderm ossicles are relatively abundant and least deformed in these areas, while other skeletal allochems have experienced

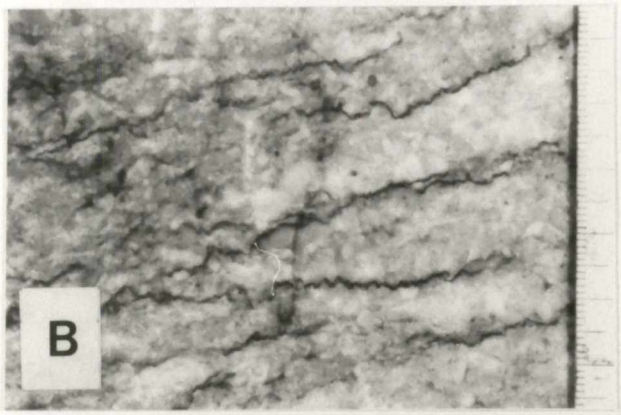
Figure 5.19. Compactional fabrics in shelf limestones.

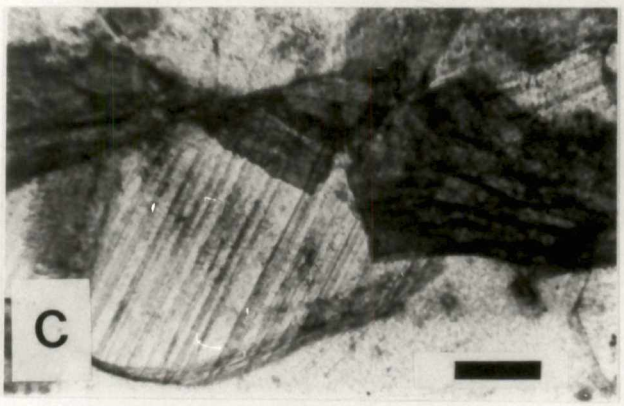
A. Thin section photomicrograph of bed-parallel zone in which grains and cements exhibit a fitted fabric as a result of considerable pressure solution. Contacts between grains represent microstylolites that collectively have an anastomosing network. Sample CS33. Scale bar = 0.25 mm.

B. Slab photograph of skeletal packstone with numerous closely spaced bed-parallel stylolites. Sample RHB35. Scale in mm.

C. Thin section photomicrograph of broken foliate bryozoan fragment with coarsely crystalline, clear equant calcite cement infilling the fractured area. Sample CS32. Scale = 0.1 mm.


A


B


C

appreciable compaction. Comparison of these bed-parallel zones with other areas offers striking evidence of how original allochem abundances may become diagenetically altered during burial.

Major through-going stylolites and microstylolite swarms are ubiquitous in shelf grain-supported and mud-supported lithologies, respectively. Ruppel (1979) found stylolites to be common solutional features in the Holston Formation and subtidal facies of the Lower Chickamauga Group. Stylolites in grain-supported lithologies are either parallel or slightly inclined to bedding (Fig. 5.19B), or form complex anastomosing networks. Mean amplitudes along a given stylolite are less than 1 cm. The bed-parallel orientation and lack of associated deformational fabrics suggest a mode of formation due to localized dissolution in response to overburden loading.

The relative timing of compaction and stylolitization can be determined from analysis of cement-compaction relationships [see Meyers (1980), Moore and Druckman (1981) and McGill (1982) for additional examples]. Physical compaction commenced early in the shallow burial zone as indicated by the nucleation of nonferroan prismatic cements with early luminescent zones on fractured surfaces (Fig. 5.18B), and continued well into the deep burial zone. During the later stages of diagenesis, clear echinoderm

overgrowth and coarse equant calcite cements were precipitated within these fractured areas (Fig 5.19C), in some instances enclosing most of the grain (Fig. 5.18B). The timing of chemical compaction and stylolitization is oftentimes ambiguous because of the removal of earlier cement generations by pressure solution. For example, a sutured contact between two grains may have formed either before or after precipitation of intergranular cement. Concavo-convex contacts between clear echinoderm overgrowths and skeletal allochems indicates chemical compaction did not begin until after shallow meteoric cementation. Stylolites occasionally truncate deep burial (ferroan) cements and calcite-filled fractures in outer shelf facies, indicating the prevalence of this process during the later stages of diagenesis.

Dull luminescent, ferroan to nonferroan calcite cement in outer shelf facies occurs as either medium to very coarsely crystalline equant calcite (size terms after Folk, 1965), or compositionally distinct zones within echinoderm overgrowths which post-date earlier nonferroan cement in outer shelf facies (Fig. 5.20A and B). Crystals are usually clear, although some may contain abundant fluid inclusions. Even though only some cements stain blue with potassium ferricyanide, this late cement generation is characterized by dull luminescence with occasional thin, brightly

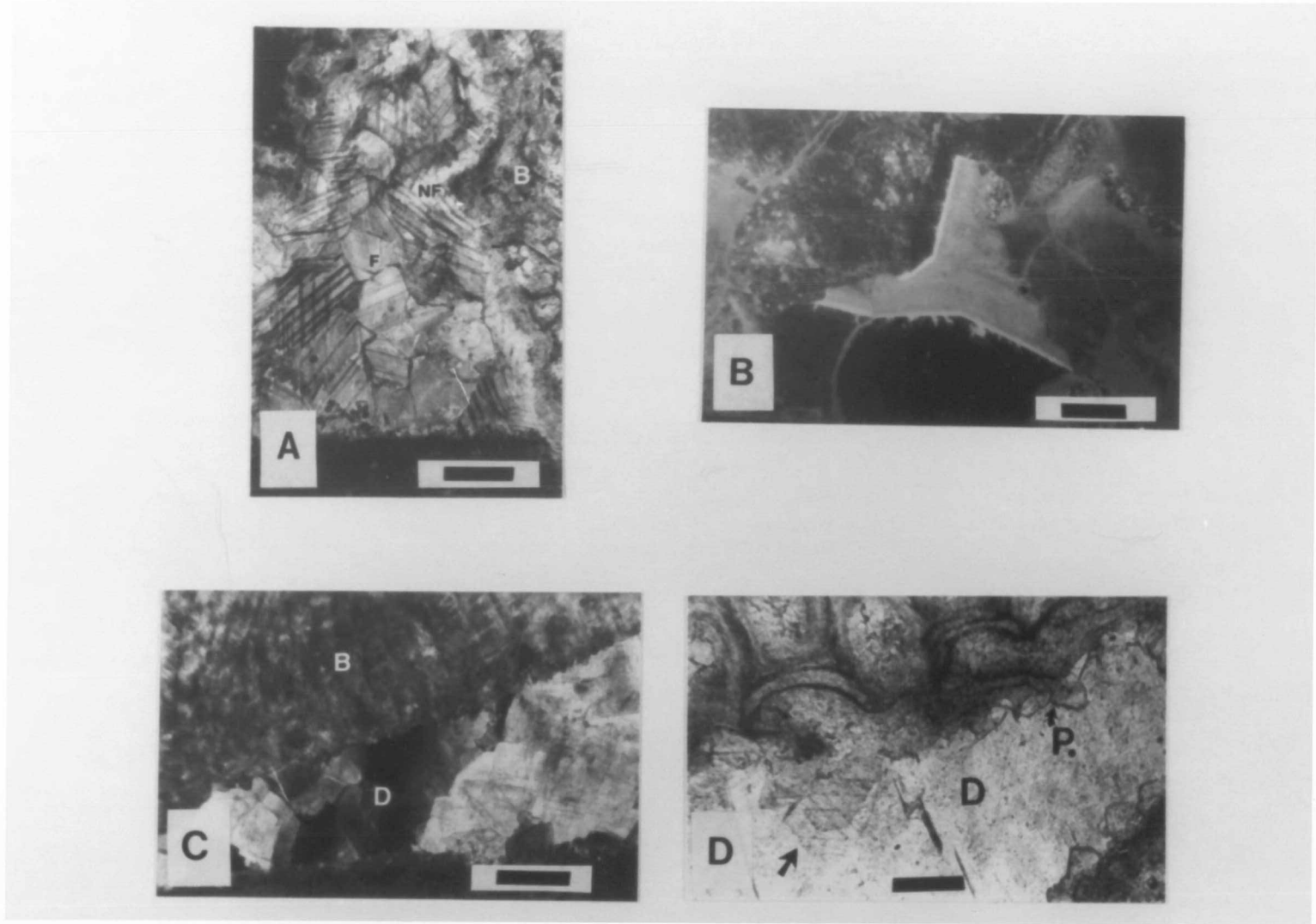
Figure 5.20. Photomicrographs of deep burial cements in shelf limestones.

A. Shelter void under an encrusting bryozoan (B) which has been occluded by first inclusion-rich to -poor, nonferroan (NF) calcite cement and then clear, ferroan (F) calcite cement. Both compositional types of calite may co-occur within a single crystal. RHB42. Stained thin section. Scale bar = 0.25 mm.

B. Luminescent calcite cements which possess the following sequence of zones: non-luminescent - bright luminescent - dull luminescent. The final luminescent zone corresponds to ferroan calcite based on staining of thin sections. Sample RHB41. Scale bar = 0.1 mm.

C. Baroque dolomite mosaic (D) which has occluded a significant portion of the primary porosity beneath a nicholsonellid bryozoan (B). Subhedral crystals have sweeping extinction characteristic of this dolomite type. Sample RHB36. Crossed polars. Scale bar = 0.25 mm.

D. Relict pore occluded by baroque dolomite (D) and prismatic calcite (P) cements. Calcite crystal indicated with the arrow has been incompletely replaced by dolomite along its margin. Crystal twins extending through both precursor calcite and replacive dolomite reveal the original dimensions and morphology of the earlier calcite cement generation. Sample RHB25. Stained thin section. Scale bar = 0.1 mm.


A
NF
B
F
B
C
B
D
D
P.
D

luminescent zones. Equant cements filling primary and secondary/fracture porosity have non-drusy growth fabrics and are well developed only in areas containing minor amounts of echinoderm debris. Trace element analyses of coarse equant cements (Table 5.4) indicate low magnesium and strontium, and slight manganese enrichment in crystals. Concentrations are similar to burial cements from other carbonate sequences (James and Klappa, 1983; Moore and Druckman, 1981; Stueber et al., 1984). The consistency in reported values suggests the smaller number of analyses reflects the general composition of this burial cement generation. This late-stage cement differs from isopachous prismatic cement rims which precipitated in the meteoric zone in this sequence.

Ferroan dolomite is the most distinctive precipitate in outer shelf facies at the CS and RHB localities. Crystals occur as medium to very coarsely crystalline, euhedral to subhedral mosaics which rarely occlude an entire pore (Fig. 5.20C). Coarser dolomites possess sweeping extinction and curved growth faces characteristic of the warped crystal lattice of saddle dolomite (Radke and Mathis, 1980). These saddle dolomites are often pleochroic from colorless to tan, and contain abundant micron to submicron inclusions, some of which are calcite as revealed by staining. Crystals have very dull luminescence although cores may possess slightly

TABLE 5.4

TRACE ELEMENT COMPOSITION OF COARSELY CRYSTALLINE EQUANT CALCITE CEMENTS FROM THE HOLSTON FORMATION

	ppm Mg	ppm Sr	ppm Mn
	1310	207	434
	1970	130	304
	1860	137	484
	1860	105	724
	1970	259	NA
	1950	136	NA
	2230	122	NA
	1850	157	NA
Mean	1890	157	486
Std. Dev.	260	51	175

(NA = not analyzed)

Data from Jernigan, 1987 and this study.

higher luminescent intensity than rims.

Petrographic analysis indicates dolomites are both void-filling and replacement in origin. Evidence for a cement origin includes occurrence in relict pores, incorporation of precursor cements (Fig 5.21A and B) and relatively coarse crystal size. Luminescent zones in earlier prismatic calcite cements follow intercrystalline boundaries with dolomites. Although these cements appear unaffected, calcites in some instances have been replaced by saddle dolomite (Fig. 5.20D). The former calcspar crystals occur as finely crystalline prismatic ghosts along the original pore margins. In cases of partial replacement, crystallographic twins may extend through calcite and into dolomite. Extinction may also vary between pore-filling and replacement dolomite. The selective dolomitization of earlier calcite cements probably took place along micrometer-thick solution fronts undersaturated with respect to calcite which progressed inwards from dolomite- precursor calcite contacts. Calcite pseudomorphs suggest replacement occurred at the molecular level via addition of Mg and removal of Ca from reaction sites. Such replacement fabrics should not be surprising since the crystal structure of dolomite closely resembles calcite, the only major difference being the substitution of magnesium for calcium in alternating cation layers (Reeder, 1983). Areas of

Figure 5.21. Photomicrographs which illustrate the fabric interrelationships between luminescent-zoned, precursor prismatic and equant calcite cement, and very dull to non-luminescent baroque dolospar cement (D). Note how dolomite crystals enclose calcite cements. Sample RHB25. Scale bars = 0.1 mm.


D
D
A
D
B

finely crystalline replacement dolomite may occur adjacent to pore-filling dolomite (Fig. 5.22A).

Fabric criteria presented below indicate that dolomite precipitation occurred during a brief period in the burial history. First, dolomites may exhibit evidence of minor dissolution or dedolomitization. Late burial dedolomitization has been noted in other platform sequences (Woronick and Land, 1985), indicating temporal variation in fluid composition and/or temperature. Second, veins filled with coarse ferroan calcite cross-cut dolomites in some samples. Dolomite fragments may appear to "float" in vein calcite, although this could be an artifact of sample preparation. Thirdly, dolomite crystals in the uppermost stratigraphic occurrences (upper Holston and Rockdell Formations) are not as coarse as those in lower stratigraphic occurrences (lower Holston), and form replacement mosaics along cavity floors (Fig. 5.22B).

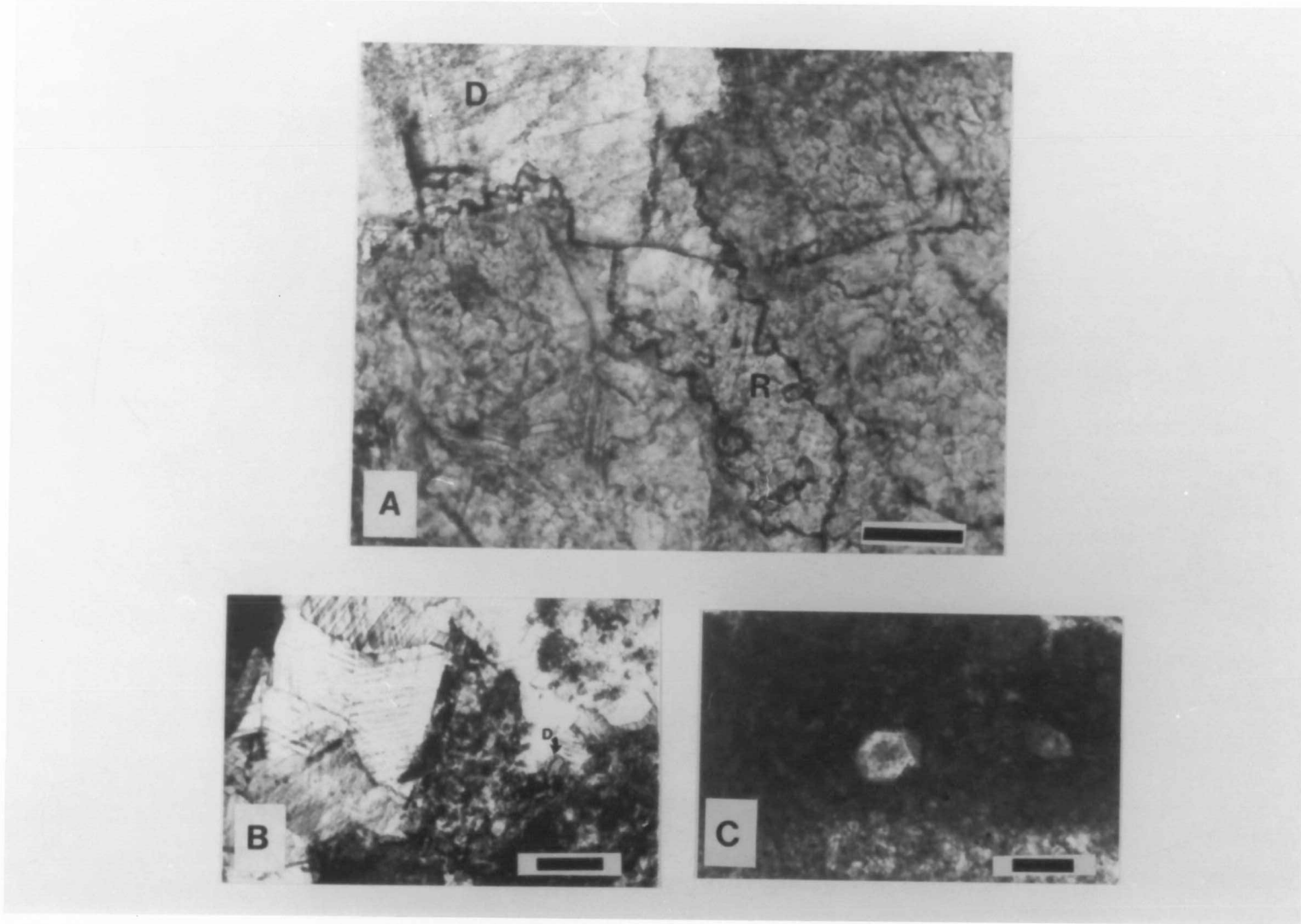
Identical ferroan dolomites are present in some shelf-marginal facies around the Knoxville area, suggesting analogous diagenetic histories. However, other parts of the sequence (e.g., Holston Formation) contain no dolomite (see McGill, 1982). The presence/absence of deep burial dolomite was sensitive to previous diagenetic histories along the shelf margin which governed available pore space at the time of introduction of dolomitizing fluids.

Figure 5.22. Photomicrographs of deep burial diagenetic features in shelf limestones.

A. Close association between coarsely crystalline baroque dolospar cement (D), and finely crystalline replacement dolomite mosaic (R). The former has replaced bryozoan + intrazooecial cement within a very limited area. Sample RHB35. Stained thin section. Scale bar = 0.1 mm.

B. Portion of vein which has minor ferroan dolomite cement (D) along its walls. The remainder of the vein is filled by coarsely crystalline ferroan calcite. Sample RHB43. Scale bar = 0.25 mm.

C. Euhedral authigenic quartz replacing micrite in skeletal packstone. Note the well-developed crystal faces and cloudy centered-clear rim appearence of euhedra. RHB37. Scale bar = 0.1 mm.

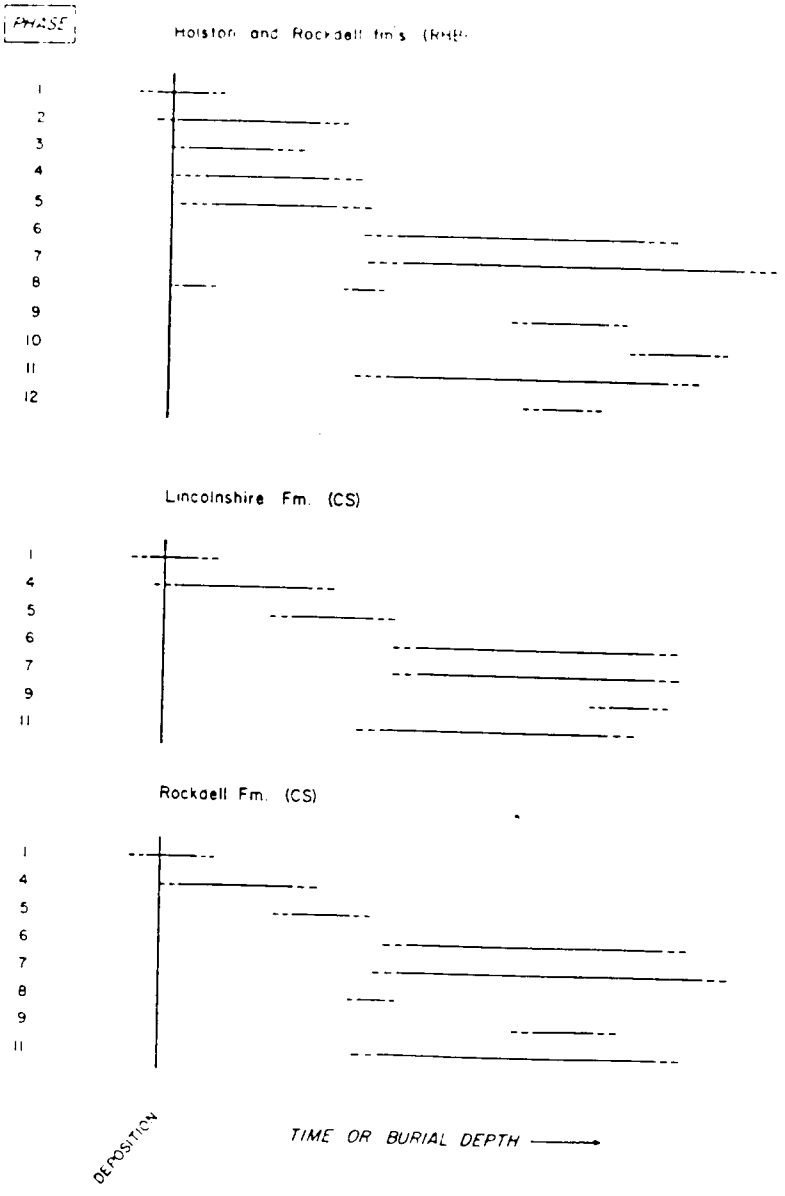

D
R
A
B
D
C

Quartz is a very minor replacement phase in outer shelf facies, occurring as matrix-supported, doubly-terminated euhedra with hexagonal outlines in cross-section (Fig. 5.22C). These elongate crystals have maximum lengths of 400 micrometers and widths of 100 micrometers. In cross-sections, euhedra often possess a cloudy center containing numerous calcite inclusions, and an extremely thin, clear outer rim.

The timing of forementioned diagenetic phases with respect to other processes is depicted in Figure 5.23.

Distribution of deep burial diagenetic features. Figure 5.24 shows the regional distribution and relative abundance of deep burial precipitates together with compactional features from inner to outer shelf carbonates based on this study and additional work by students at the University of Tennessee, Knoxville. The on-shelf increase in compaction reflects the combined effects of variations in hydrodynamic conditions, sediment composition, and the onlap nature of most of this part of the shelf sequence. Transgressive marine units commonly possess overpacked grain fabrics with attendant compaction, and poorly developed marine-phreatic cements (see Heckel, 1983). Shelf-wide variations in the degree of compaction have been recognized in other

Figure 5.23. Diagenetic histories of outer shelf limestones in the northern part of the study area. Temporal relationships shown are based on superposition of pore-filling materials, and cross-cutting relationships between pore-filling cements and other diagenetic features.

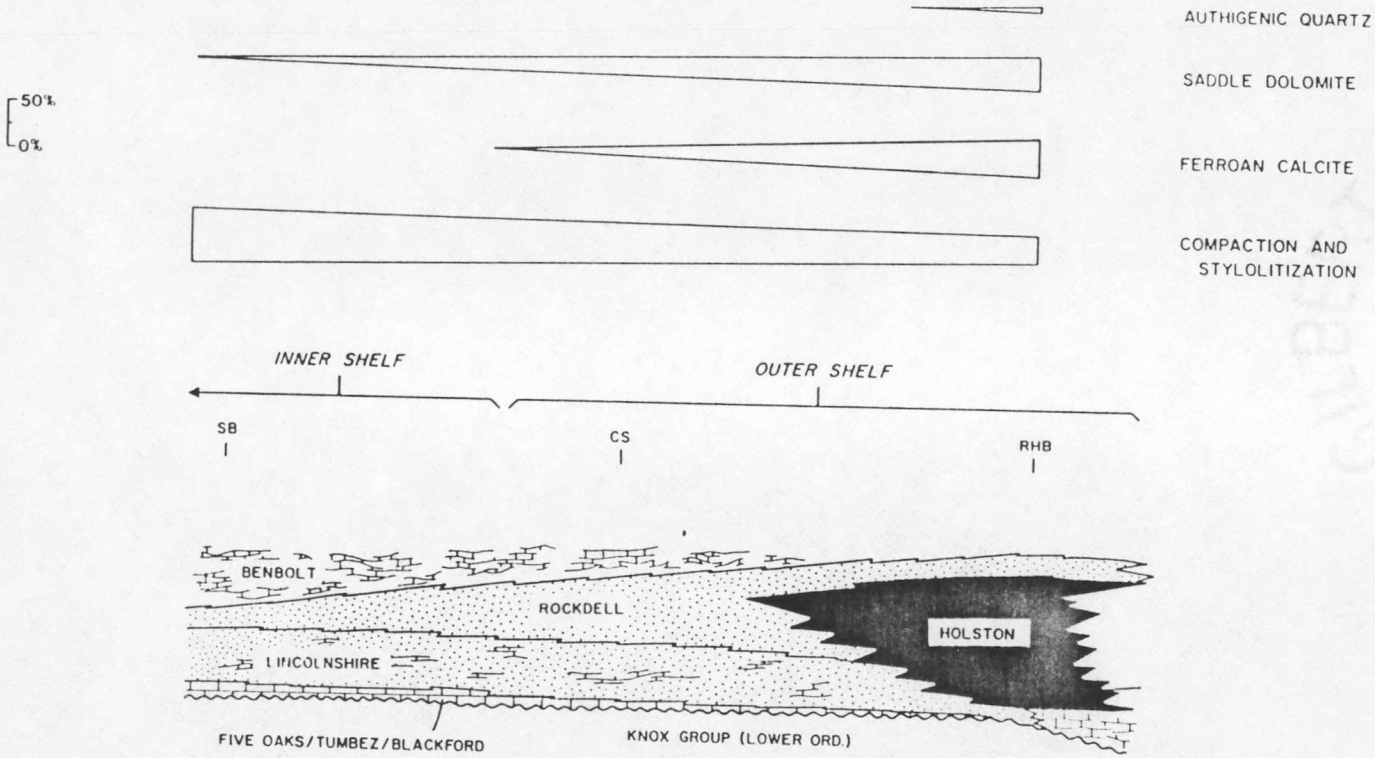


EXPLANATION

1 ..... Boring/Micritization
2 ..... Fe-Mn oxides
3 ..... Microcrystalline Cement
4 ..... Fibrous/Bladed Cement
5 ..... IR Echinoderm Overgrowth
6 ..... IP Echinoderm Overgrowth
7 ..... Equant Cement
8 ..... Dissloution
9 ..... Saddle Dolomite
10 ..... Fractures
11 ..... Compaction/Stylolitization
12 ..... Authigenic Quartz

Figure 5.24. Composite schematic diagram showing cross-shelf variations in the relative abundance of deep-burial phases in terms of the percentage of samples containing each phase. Stratigraphic relationships based on published cross-sections (see Walker et al., 1980; Ruppel and Walker, 1984).

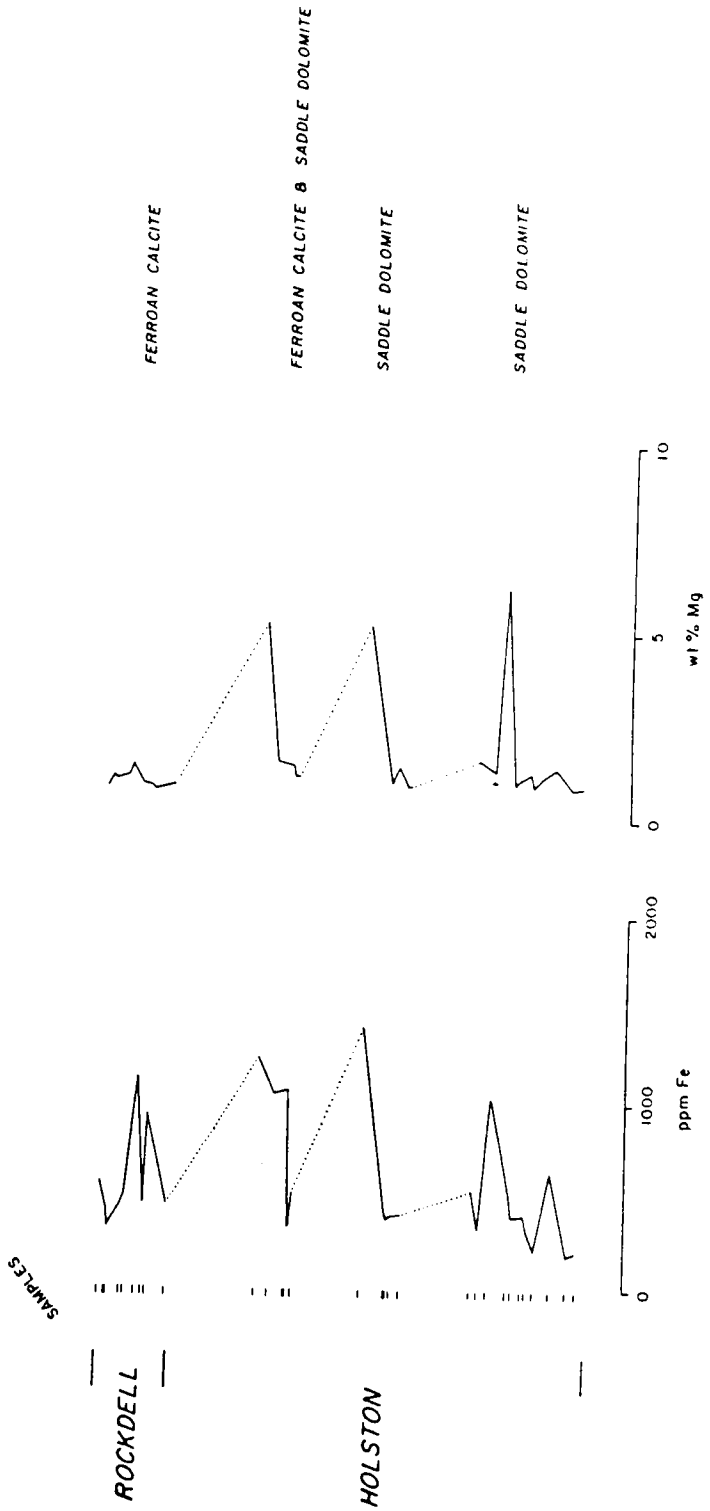
BURIAL DIAGENETIC FEATURES



shelf/platform settings (Kearns et al., 1986). The abundance of coarsely crystalline calcite, ferroan dolospar and euhedral replacement quartz exhibit an antithetic relationship with respect to physical and chemical compaction, with these precipitates decreasing shelfward at the expense of nonferroan calcite.

Variations in ferroan calcite and dolomite also possess a stratigraphic component. Both these deep burial precipitates are confined to relatively small stratigraphic intervals within outer shelf facies (Fig. 5.25). Dolomite-bearing strata may be recognized by elevated bulk magnesium and iron concentrations, while intervals containing abundant ferroan calcite are marked by only iron enrichment. The restriction of ferroan carbonates to limited parts of the shelf sequence reflect differences in the intensity of earlier synsedimentary and meteoric cementation, producing zones of enhanced porosity and permeability which served as conduits for burial waters, interlaminated with less porous zones. The limited development of secondary porosity indicates cementation and compaction exerted significant control over flow paths of burial waters which precipitated these cement generations. Bed-normal fractures may have provided additional migration routes for fluids at some points in the burial history.

Figure 5.25. Stratigraphic variation in bulk iron and magnesium concentrations in shelf-margin limestones at Red House Branch.


FERROAN CALCITE
FERROAN CALCITE & SADDLE DOLOMITE
SADDLE DOLOMITE
SADDLE DOLOMITE
wt % Mg
0
5
10
ppm Fe
0
1000
2000
SAMPLES
ROCKDELL
HOLSTON

Origin of deep burial fluids. The geographic distribution of ferroan carbonates and authigenic quartz offers positive evidence that burial fluids which precipitated these phases were derived from the shale basin to the east. These expelled waters entered the carbonate shelf at intervals containing minor marine and/or shallow meteoric cements, and thus relict porosity, and underwent dilution as they interacted with indigenous waters. Whether the fluids already filling pores were meteoric, modified connate or a mixture of these two end members cannot be determined from the available data. The close association of identified cement phases and argillaceous sediments has been noted in other Phanerozoic sequences (Kahle, 1965; Oldershaw and Scoffin, 1967; Mattes and Mountjoy, 1980; McHargue and Price, 1982). This relationship is based on the potential for clay minerals to influence fluid compositions during burial. Clay mineral-fluid interaction, in conjunction with increased temperature, created conditions for precipitation of the above cements.

Based on the lithofacies distribution and diagenetic histories, the potential direction of fluid movement and the magnitude of the lateral flow component may be evaluated. The movement of subsurface waters is governed in large part by regional variations in the fluid potential (Φ), which may

be expressed by the equation

$$\phi = gz + (p-p_o)/d$$

where

g = acceleration of gravity

z = elevation from standard datum

$(p-p_o)$ = difference in fluid pressure with respect to atmospheric pressure

d = fluid density.

The fluid potential within a stratigraphic package consists of two additive terms: the depth potential (gz) and pressure potential $[(p-p_o)/d]$. Waters are directed from regions of high potential to those of lower potential. Assuming hydrostatic pressure and using approximate thicknesses for younger Paleozoic units, the maximum calculated fluid potentials in the Blockhouse and lower Sevier shales at the end of the Devonian were double those in shelf facies. The existence of this difference in fluid potential during most of Paleozoic time means compaction-driven waters would move updip towards the carbonate shelf. Numerical modeling of compaction-driven flow by Bethke (1985) shows the tendency for fluids to migrate laterally to the margins of subsiding basins. Other potentials may influence groundwater migration within a basin, but in most instances these other potentials are so minor as to be dwarfed by the combined depth and pressure potentials.

Even though flow conditions favored the horizontal migration of expelled waters, the actual flow geometries and volumes depend largely on the regional stratigraphic package. Using relations derived by Margara (1976), the ratio of horizontal to vertical flow components (q_H/q_V) in response to depth and pressure potential may be expressed as

$$q_H/q_V = k_H/k_V[(1-h)/x]$$

where k_H and k_V are horizontal and vertical permeabilities, respectively, and $(1-h)/x$ the rate of thickness change of additional sediment with distance. The permeability ratio in thick shale sequences is only slightly greater than unity. In addition, the water volume throughput is lower in sequences where the permeability ratio is low than where this value is high. Thus, flow vectors in the Blockhouse and Sevier Formations were not as significant as they must have been in the Whitesburg, where the permeability contrast between shales and limestone beds would have permitted significant horizontal flow.

The abundance of shale may have also facilitated the development of overpressured zones during burial. Such intervals could have resulted from the combined effects of continuous sediment loading and incomplete sediment compaction in conjunction with dehydration of detrital smectites. The increased fluid pressures characterizing these zones would have enhanced local potential gradients in

the basin due to fluid pressures which deviated from hydroststic.

The foregoing discussion suggests that the volume of fluids expelled from the Sevier Basin and entering the carbonate shelf may have been limited. If the regional lithofacies did not favor movement of compaction-driven fluids, the question remains: how did waters which apparently precipitated the abundant burial calcspar and dolomite interact with shelf limestones? One scenario is that only fluids derived from immediately adjacent shales entered the shelf. Burial fluids generated further toward the basin axis could have been tapped by fractures which created new permeability conduits for migration of bicarbonate-rich shale waters. During updip movement in response to fluid potential, the decrease in pressure may have caused CO_2 outgassing which would have allowed for carbonate precipitation in fractures and the neighboring pore system (Choquette and James, 1987).

The above hypothesis provides a plausible first approximation of shelf-basin interaction during deep burial. Lack of appreciable fluid migration would explain the limited abundance of ferroan calcite and dolomite present in outer shelf facies compared to other sequences. Saddle dolomite was deposited prior to fracture development whereas calcite precipitation occurred both before and during

fracturing. Jernigan (1987) observed rare, clear echinoderm overgrowth cements which possessed a nonferroan - ferroan - nonferroan zonation. It is unlikely the observed Fe(II) variation only reflects changes in pore water oxidation-reduction potentials, unless the youngest nonferroan zone was precipitated after structural deformation. The observed zonation may represent depletion of a limited amount of Fe(II) exported to the shelf from the shale basin. The youngest nonferroan zone eventually occluded the last remaining pore space, perhaps as a result of pressure solution and local reprecipitation (autocementation of Choquette and James, 1987). Inasmuch as dissolution involves allochems, matrix, and previous cements, this reprecipitated calcite would be nonferroan (see Wong and Oldershaw, 1981). The transition from ferroan to nonferroan cement marks the termination of basinal influence on pore water chemistry.

Chemistry of shale-derived brines. Pore waters from deeply buried shales are saline brines, although overpressured zones associated with smectite to illite conversion may have lower amounts of total dissolved solids (see Schmidt, 1973). If saline fluids entered the shelf, a record of their movement should be preserved in the

limestones. Diagenetic mineralogy and trace element geochemistry suggest the late-stage fluids which precipitated deep burial cements were saline in composition.

Analyses of waters in equilibrium with saddle dolomite, fluid inclusion compositions and presence of saddle dolomite as a gangue mineral in Mississippi Valley-type deposits together indicate this variety of dolomite is associated with saline host fluids (Radke and Mathis, 1980). Euhedral quartz has also been linked to precipitation from hypersaline waters. The co-occurrence of both these minerals offers support for a saline fluid composition.

Element compositions of coarse equant calcite cement were used to obtain the probable concentration of the burial fluid. Crystal size suggests the deep burial cement generation precipitated from pore waters only slightly supersaturated with respect to calcite. Low degrees of supersaturation correspond to relatively slow crystallization rates. These assumptions were considered when selecting distribution coefficient values for strontium and manganese, since the partitioning of these elements between calcite and solution is influenced by crystallization kinetics (Lorens, 1981). The calculated element concentrations for deep burial waters in equilibrium with these calcites (Fig. 5.26) are compared to published concentrations of oil field waters reported by Veizer (1983)

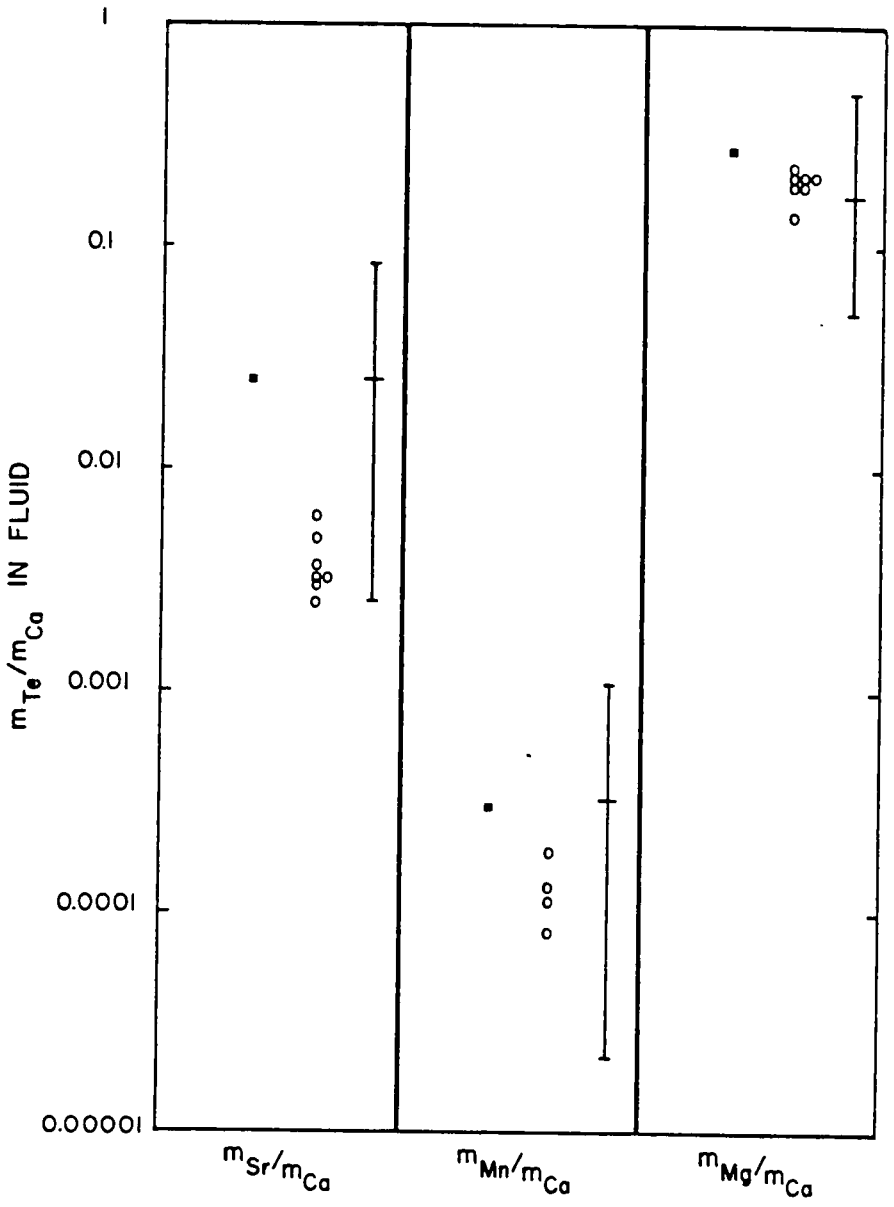


Figure 5.26. Plot comparing the calculated m_{Te}/m_{Ca} ratios of burial waters in equilibrium with deep burial calcite cement (open circles), and published element compositions of deep burial brines. ■ = mean for oil waters (Veizer, 1984); ⊢ represents the mean and range in Smackover brines (Moore, 1985).

and Smackover brines analyzed by Moore (1985). Assuming equilibrium, the overall similarity between the three data sets - particularly with respect to magnesium and manganese - favors precipitation of coarse equant calcites from saline fluids. Sodium concentrations in the acid-soluble fraction exhibit a small, but noticeable, increase at the shelf margin (Fig. 5.27). Limestones from Cedar Springs all have <200 ppm sodium, while equivalent facies from Red House Branch sometimes have concentrations above 300 ppm. Veizer et al. (1977) found that hypersaline and open marine facies are well separated at ca. 230 ppm sodium. Shelf margin facies not originally deposited in hypersaline environments still have concentrations above this value. This suggests diagenetic enrichment of certain intervals by brines with high dissolved Na contents.

Timing of deep-burial diagenesis. Determination of the absolute timing of burial diagenesis is usually accomplished by comparing the formation temperatures of respective authigenic phases with the basin's thermal history ascertained from burial curves. Cercone (1987) offers a detailed example of these techniques in bracketing the age of late diagenesis. Accurate temperatures of phases can be attained from formation temperatures of solid inclusions

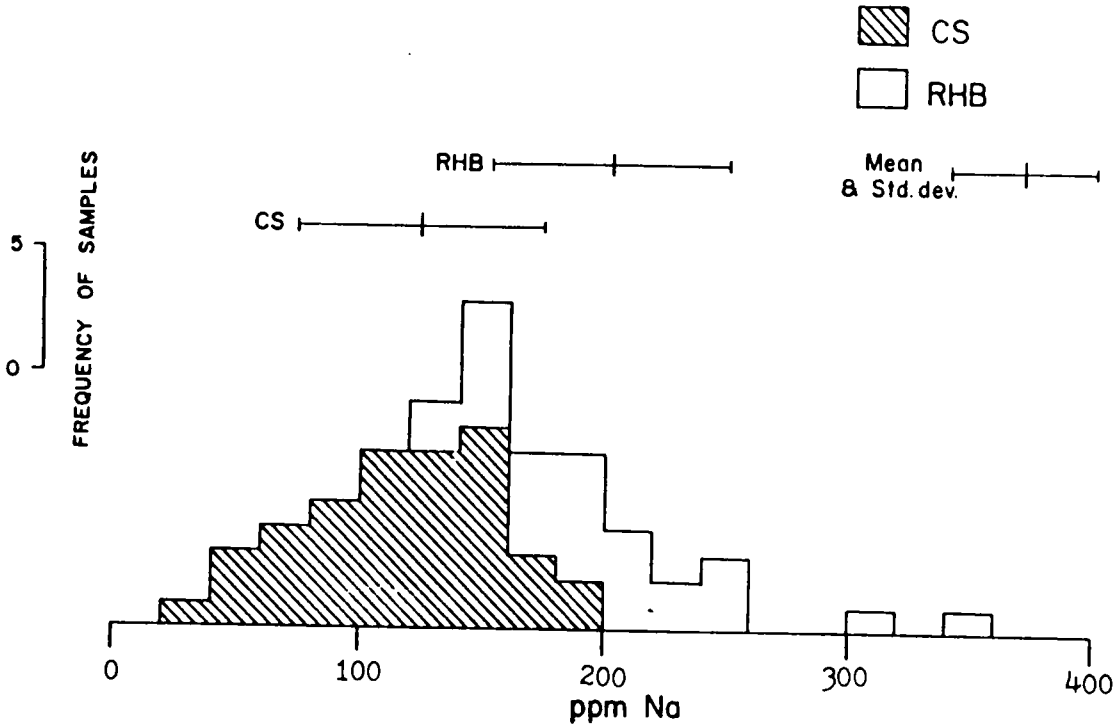


Figure 5.27. Frequency histogram showing bulk sodium concentrations of shelf-marginal limestones.

(e.g., pyrobitumen) and/or homogenization temperatures of fluid inclusions. Recent experimental work, however, has shown measured values may actually represent maximum burial, not origination, temperatures because of inclusion stretching during burial (Prezbindowski and Larese, 1987). Such stretching of inclusions in calcites would be likely in areas such as the Valley and Ridge where strata have experienced both depositional and tectonic loading. The majority of the error in determining the time of deep burial diagenesis is related to uncertainties in selecting an appropriate geothermal gradient. Measured gradients in sedimentary basins range from 15-35 degrees C per kilometer, with 25 degrees C per kilometer oftentimes cited as a "normal value" for passive margins. There is also the potential for the gradient to increase in response to changes in ambient heat flow, or decrease by introduction of cooler, near-surface waters (Choquette and James, 1987). In the absence of alternative dating methods, the time range determined by the above method represents only a rough first-order approximation.

The pre-tectonic burial history of Middle Ordovician and younger strata in northeastern Tennessee (Fig. 5.28) was ascertained using the method outlined by Waples (1980). (Compacted thicknesses of sedimentary units are listed in Table 5.5) The use of compacted thickness values and

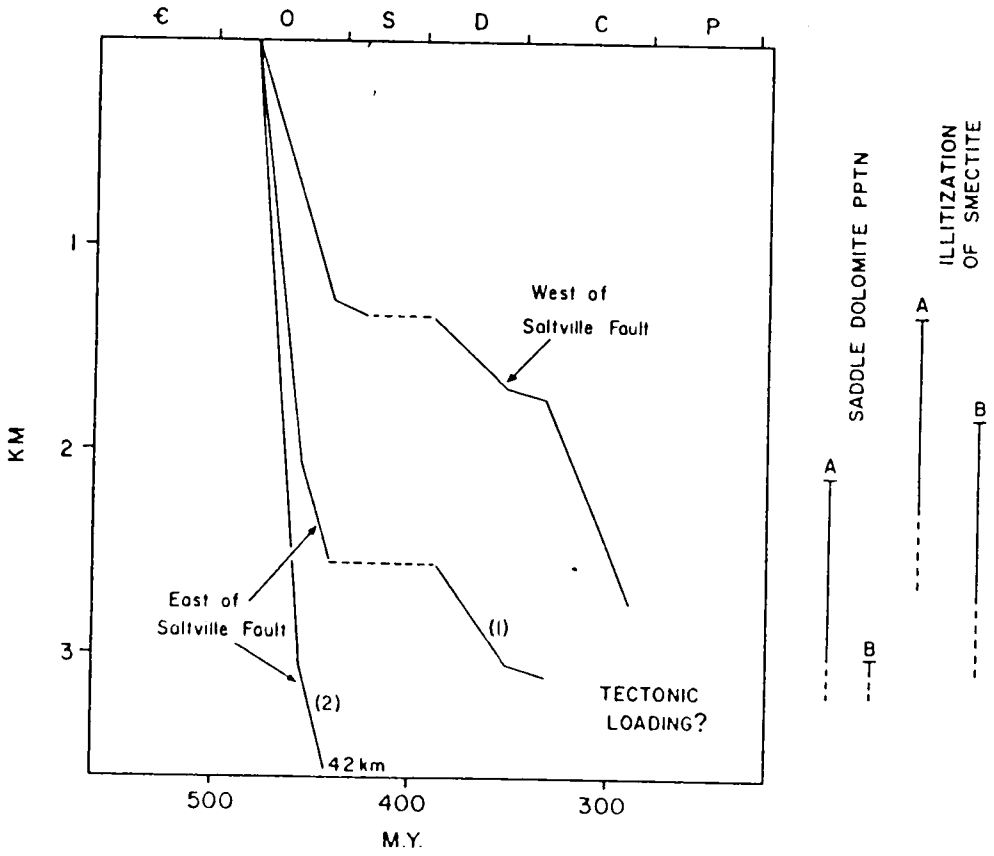


Figure 5.28. Burial history of Middle Ordovician shelf and basinal strata using compacted stratigraphic thicknesses of exposed Paleozoic rocks (see Table 5.5). The earliest occurrence of P,T-dependent diagenetic processes (baroque dolomite precipitation and smectite-illite conversion) are marked using geothermal gradients of (A) 35 ^{o}C/km, and (B) 25 ^{o}C/km.

TABLE 5.5

STRATIGRAPHIC UNITS AND THEIR RESPECTIVE THICKNESSES USED IN CONSTRUCTING BURIAL CURVES

West of Saltville Fault		East of Saltville Fault		
			(1)*	(2)*
Crooked Fork Gp. Crab Orchard Mtn. Gp. Gizzard Gp. Pennington Fm.	1000+m			
Newman Fm.	50 m	Newman Fm.	50 m	50 m
Grainger Fm.	150 m	Grainger Fm.	300 m	300 m
Chattanooga Fm.	200 m	Chattanooga Fm.	200 m	200 m
UNCONFORMITY				
Clinch Fm.	70 m	UNCONFORMITY		
Juniata Fm.	120 m			
Martinsburg Fm.	550 m	Martinsburg Fm.	550 m	550 m
Chickamauga Gp.	600 m	Bays Fm.	250 m	300 m
		Sevier Fm.	1500 m	2500 m
		Blockhouse Fm.	100 m	200 m
		Whitesburg Fm.	100 m	25 m
		Lenoir Fm.	50 m	25 m

* (1) = slope area; (2) = basinal area.

possibility of erosion means the constructed curves represent minimum burial values during most of the Paleozoic. Separate histories were determined for strata southeast and northwest of the Saltville Fault because of variations in subsidence and sedimentation across the region during the Middle Ordovician. Two areas southeast of the Saltville are differentiated: 1)slope areas, and 2)basin areas.

Precipitation of saddle dolomite, and smectite-illite conversion to some degree, can be used to constrain the maximum time of deep burial diagenesis commensurate with expulsion of brines from the shale basin. Radke and Mathis (1980) indicate the probable formation temperature of saddle dolomite is >100 degrees C. The transformation of expandable smectite to nonexpandable illite begins at approximately 70 degrees C (Burst, 1969; Hower et al., 1976; Boles and Franks, 1979). The fact that illitization preceded the precipitation of saddle dolomite again suggests the former contributed ions to the eventual dolomite-forming brines. Absence of dolomite from fractures restricts the time of fluid migration to pre-deformation (if not earlier). This evidence indicates a geothermal gradient between 25-35 degrees C per kilometer. Based on these gradients, basinal fluids would have reached the necessary temperatures from a period ranging from the late Ordovician to perhaps as late

as the Devonian. Brines migrating to shallower depths would have experienced only a minor decrease in temperature due to water's high thermal capacity, provided these strata were not in communication with recharging surface waters. The proposed time range is slightly earlier than ages cited by Grover and Read (1983) for brine migration in contemporaneous strata of southwestern Virginia. In the Virginia sequence, the basinal equivalents are thinner, so that burial temperatures would have been reached at a later time.

The youngest time of deep burial diagenesis cannot be ascertained without temperature data for fracture-filling equant calcites or ages of stylolites truncating these early fracture sets. However, this diagenetic stage must have ended before the initiation of Alleghanian deformation in the Pennsylvanian.

CHAPTER 6

SUMMARY AND CONCLUSIONS

1. Grain textures observed under SEM and trace element (Sr,Mg) compositions favor a (magnesian) calcite-dominated precursor for Middle Ordovician shelf micrites, as opposed to the aragonite-dominated precursors which dominate altered Quaternary sediments. An originally calcitic mineralogy may contribute to the formation of finely crystalline, early diagenetic dolomites in tidal flat sequences by providing an autochthonous source of Mg ions. This potential magnesium contribution should be considered when evaluating the origin of Phanerozoic platform dolostones and dolomitic limestones.

2. Deep-water hemipelagites of the Whitesburg Formation consisted of shelf-derived magnesian calcite mud. However, these deposits are enriched in strontium relative to contemporaneous shallow water micrites, indicating an alternative stabilization pathway during burial diagenesis. The higher Sr/Mg ratios for deep water facies are the result of selective adsorption-desorption of ions by argillaceous sediments. Mineralogical interpretations reached solely on

the basis of geochemical data, without any consideration of the sequence's diagenetic history, may be incorrect and should be avoided in future studies.

3. Comparative petrogenesis of grains allowed for reasonable interpretation of the original mineralogy of both skeletal and non-skeletal allochems in the Middle Ordovician Chickamauga Group and equivalents. Using constituent analyses and the above mineralogic interpretations, shelf and basinal facies consisted predominately of magnesian calcite (>80%) with co-equal proportions of aragonite and calcite. Shelf-wide mineralogical variations observed in modern environments are undetectable in this Early Paleozoic setting.

4. The presence of synsedimentary cements (fibrous-bladed calcite, microdolomite-bearing echinoderm overgrowth calcite, microcrystalline calcite) causes only minimal change in the location of "bulk sediment" fields with respect to the three carbonate polymorphs. The relative abundance of these originally magnesian calcite cements in the onlap sequence produces a minor shift in the shelf-margin facies toward the magnesian calcite apex.

5. Multivariate cluster analysis of combined lithologic

and geochemical data allowed for the recognition of six(6) groupings, which are interpreted as geochemical facies. The degree of similarity between samples comprising each facies shows considerable variation. In general, tidal flat and open marine, shallow subtidal lithofacies containing minor admixed terrigenous clastic material (Facies I, II, and V) possess greater similarity than both shelf and basinal lithofacies associated with abundant terrigenous sediments (Facies III, IV, and VI). The differences with respect to the presence/absence of terrigenous clastics suggests either these sediments selectively interact with carbonates during diagenesis, and/or geochemical conditions in the respective depositional environments exhibit significant fluctuation, thus affecting the availability of certain trace constituents for incorporation in carbonate minerals.

6. Previous studies which have recognized certain trace elements as being facies specific have oftentimes tried to interpret the variations in terms of the primary mineralogy of carbonate sediments. The existence of analogous patterns in this Early Paleozoic sequence indicates that other factors - especially geochemical reactions associated with argillaceous sediments and "openness" of the diagenetic system - may be more important in controlling the elemental concentrations within a

specific facies. However, the original mineralogy did provide an underlying control on the concentration of some elements (e.g., Sr and Mg) in limestones deposited in both the shelf and basin.

7. Shallow to intermediate burial diagenesis of Whitesburg calcisiltites produced element compositions distinct from other deep water allochthonous sediments that underwent lithification while exposed on the seafloor. Compositional variations present at different scales reflect organic matter decomposition and ion exchange reactions in shales which influenced pore water chemistries during carbonate lithification. Unlithified shallow-water ramp/shelf sediments drowned by formation of the Sevier foredeep basin offered permeable conduits for migration of early compaction-driven fluids expelled from overlying slope sediments. The introduction of these diagenetic fluids is reflected by both unique cement types, and highly enriched iron and manganese in the carbonate fraction. Such geochemically anomalous intervals at limestone-shale contacts may provide a chemostratigraphic fingerprint in sequences where metal-bearing hardgrounds are absent due to shorter lag times between drowning and renewed sedimentation.

8. Holston lithofacies (and some portions of the more shelfward Rockdell) were in periodic contact with shelf-directed waters that represent a mixing of oxygen-rich and subthermocline, oxygen-poor water masses by internal tides and Kelvin waves. Movement of these "mixed currents" allowed for the precipitation of syndepositional Fe-Mn oxides/oxyhydroxides. Oxide crusts on allochems and cavity walls oftentimes possess a serrate morphology indicating some degree of carbonate dissolution in association with this early diagenetic event. The timing of calcium carbonate removal with respect to Fe-Mn deposition is equivocal; however, lack of solutional fabrics in other grains suggests undersaturation may have been related to lowered alkalinity in chemical microenvironments associated with oxide/oxyhydroxide precipitation. Basinal shales also influenced diagenesis of contemporaneous shelf limestones during deep burial. The sporadic occurrence of saddle dolospar, ferroan to nonferroan, coarsely crystalline equant calcite cement, and authigenic quartz in shelf facies immediately west-northwest of the Sevier Shale point to the movement of warm, saline brines through relatively porous intervals in response to regional fluid potential gradients. Dissolved constituents requisite for these diagenetic products were probably provided by depth-related reactions involving smectitic clays.

LIST OF REFERENCES

LIST OF REFERENCES

Adams, J. A. S., and Weaver, C. E., 1958, Thorium-to-uranium ratios as indicators of sedimentary processes: example of concept of geochemical facies: Am. Assoc. Petroleum Geologists Bull., v. 42, p. 387-430.

Ahr, W. M., 1973, The carbonate ramp: an alternative to the shelf model: Trans. Gulf Coast Assoc. of Geol. Soc., v. 23, p. 221-225.

Al-Aasm, I. S., and Veizer, J., 1982, Chemical stabilization of low-Mg calcite: an example of brachiopods: Jour. Sed. Petrology, v. 52, p. 1101-1109.

Alberstadt, L. P., 1973, Depositional environments and origin of the fine-grained limestones of the Bigby-Cannon Formation (middle Ordovician), Central Basin, Tennessee: Jour. Sed. Petrology, v. 43, 621-633.

Asreen, R. C., 1985, Stratigraphy, petrology and depositional environments of the Middle Ordovician Upper Lenoir through Lower "Bays" Formations near Calhoun, Tennessee: unpubl. M.S. thesis, The Univ. of Tennessee, Knoxville, 201 p.

Badiozamani, K., 1973, The Dorag dolomitization model - application to the Middle Ordovician of Wisconsin: Jour. Sed. Petrol., v. 43, p. 965-984.

Baker, P. A., Gieskes, J. M., and Elderfield, H., 1982, Diagenesis of carbonates in deep-sea sediments - evidence from Sr/Ca ratios and interstitial dissolved Sr2+ data: Jour. Sed. Petrol., v. 52, p. 71-82.

Ball. M. M., Shinn, E. A., Stockman, K. W., 1967, The geologic effects of hurricane Donna in south Florida: Jour. Geology, v. 75, p. 583-597.

Bath, A. H., 1977, Experimental observation of exchange of Rb and Sr between clays and solution: Proc. 2th Internat. Symposium on Water-Rock Interaction (Strasbourg, August 17-25, 1977), p. 244-249.

Bathurst, R. G. C., 1958, Diagenetic fabrics in some British Dinantian limestones: Liverpool Manchester Geol. Jour., v. 2, p. 11-36.

_____, 1966, Boring algae, micrite envelopes and lithification of molluscan biosparites: Geol. Jour., v. 5, p. 15-32.

_____, 1970, Problems of lithification in carbonate muds: Geologists' Assoc. Proc., v. 81, p. 429-440.

_____, 1975, Carbonate Sediments and Their Diagenesis: Oxford-New York, Elsevier, 658 p.

Beales, F. W., 1965, Diagenesis in pelletted limestones, IN Pray, L. C., and Murray, R. C., eds., Dolomitization and Limestone Diagenesis, A Symposium: Soc. Econ. Paleon. Mineral. Spec. Publ. 13, p. 49-70.

Bencini, A., and Turi, A., 1974, Mn distribution in the Mesozoic carbonate rocks from Lima Valley, northern Appennines: Jour. Sed. Petrol., v. 44, p. 774-782.

Benedict, G. L., 1980, Stop 6: Outer shelf margin-upper slope transition zone in the Lenoir and Whitesburg Formations, IN Walker, K. R., Broadhead, T. W., and Keller, F. B., eds., Middle Ordovician carbonate shelf to deep water deposition in the Southern Appalachians: The Univ. of Tenn., Knoxville, Dept. Geol. Sci. Studies in Geology, No. 4, p. 69-73.

_____, and Walker, K. R., 1978, Paleobathymetric analysis in Paleozoic sequences and its geodynamic significance: Am. Jour. Sci., v. 278, p. 579-607.

Benson, L. V., 1974, Transformation of a polyphase sedimentary assemblage into a single phase rock: a chemical approach: Jour. Sed. Petrol., v. 44, p. 123-135.

Bergstrom, S. M., and Carnes, J. B., 1985, Conodont biostratigraphy of the Lower Middle Ordovician Chickamauga Group at Thorn Hill and Evans Ferry, IN Walker, K. R., ed., The Geologic History of the Thorn Hill Paleozoic section (Cambrian-Mississippian), eastern Tennessee: The Univ. of Tenn., Knoxville, Dept. of Geol. Sci. Studies in Geology, No. 10, p. 51-59.

Berner, R. A., 1966, Chemical diagenesis of some modern carbonate sediments: Am. Jour. Sci., v. 264, p. 1-36.

_____, 1971, Principles of Chemical Diagenesis: New York, McGraw-Hill, 240 p.

_____, 1980, Early Diagenesis: A Theoretical Approach: Princeton NJ, Princeton Univ. Press, 241 p.

_____, 1981, A new geochemical classification of sedimentary environments: Jour. Sed. Petrology, v. 51, p. 359-365.

Bethke, C. M., 1985, A numerical model of compaction-driven groundwater flow and heat transfer and its application to the paleohydrology of intracratonic sedimentary basins: Jour. Geophys. Res., v. 90, p. 6817-6828.

Biddle, K. T., 1983, Girvanella oncoids from Middle to Upper Triassic allochthonous boulders of the Dolomite Alps, northern Italy, IN Peryt, T. M., ed., Coated Grains: Berlin Heidelberg, Springer-Verlag, p. 390-397.

Billings, G. L., and Ragland, P. C., 1968, Geochemistry and mineralogy of the Recent reef and lagoonal sediments south of Belize (British Honduras): Chem. Geology, v. 3, p. 135-153.

Boardman, M. R., and Neumann, A. C., 1984, Sources of periplatform sediment to Northwest Providence Channel, Bahamas: Jour Sed. Petrol., v. 54, p. 1110-1123.

_____, _____, Baker, P. A., Dulin, L. A., Kenter, R. J., Hunter, G. E., Kiefer, K. B., 1986, Banktop responses to Quaternary fluctuations in sea level recorded in periplatform sediments: Geology, v. 14, p. 28-31.

Boggild, O. B., 1930, The shell structure of the mollusks: Kgl. Danske Videnskab. Selskab. Mat. Fys. Medd., v. 9, p. 231-325.

Bohm, L., Futterer, D., Kaminski, E., 1978, Algal calcification in some Codiaceae (Chlorophyta) ultrastructure and location of skeletal deposits: Jour. Phycol., v. 14, p. 486-493.

Boles, J. R., and Franks, S. G., 1979, Clay diagenesis in Wilcox sandstones of southwest Texas: implications of smectite diagenesis on sandstone cementation: Jour. Sed. Petrology, v. 49, p. 55-70.

Bolye, E. A., 1983, Manganese carbonate overgrowths on foraminifera tests: Geochim. Cosmochim. Acta, v. 47, p. 1815-1819.

Bosence, D. W. J., Rowlands, R. J., and Quine, M. L., 1985, Sedimentology and budget of a Recent carbonate mound, Florida Keys: Sedimentology, v. 32, p. 317-343.

Brand, U., 1982, Mineralogy and chemistry of the Lower Pennsylvanian Kendrick fauna, eastern Kentucky: Chem. Geology, v. 32, p. 1-16.

_____, and Veizer, J., 1980, Chemical diagenesis of a multicomponent carbonate system - 1: Trace elements: Jour. Sed. Petrology, v. 50, p. 1219-1236.

_____, and _____, 1983, Origin of coated grains: Trace element constraints, IN Peryt, T. M., ed., Coated Grains: Springer-Verlag, Berlin-New York, p. 9-26.

Breland, F. C., 1980, Stratigraphic, paleoenvironmental, and echinoderm distributional patterns in an unfaulted Middle Ordovician (Chickamauga Group) shelf-edge to on-shelf transect in East Tennessee: unpubl. PhD. dissertation, The Univ. of Tennessee, Knoxville, 217 p.

Broecker, W. S., and Takahashi, T., 1966, Calcium carbonate precipitation on the Bahamas Banks: Jour. Geophys. Res., v. 71, p. 1575-1602.

Burst, J. R., 1969, Diagenesis of Gulf Coast clayey sediments and its possible relationships to petroleum migration: Am. Assoc. Petroleum Geologists Bull., v. 53, p. 73-93.

Burton, E. A., and Walter, L. W., 1987, Relative precipitation rates of aragonite and Mg calcite from seawater: Temperature or carbonate ion control?: Geology, v. 15, p. 111-114.

Busenburg, E, and Plummer, L. N., 1985, Kinetic and thermodynamic factors controlling the distribution of SO4 and Na+ in calcites and selected aragonites: Geochim. Cosmochim. Acta, v. 49, p. 713-725.

Cadot, H. M., Van Schmus, W. R., and Kaesler, R. L., 1972, Magnesium in calcite of marine Ostracoda: Geol. Soc. Am. Bull., v. 83, p. 3519-3522.

Cantrell, D. L., 1982, Anatomy, diagenesis and geochemistry of a Middle Ordovician oolite shoal, eastern Tennessee: unpubl. M.S. thesis, The Univ. of Tennessee, Knoxville, 153 p.

Carballo, J. D., Land, L. S., and Miser, D. E., 1987, Holocene dolomitization of supratidal sediments by active tidal pumping, Sugarloaf Key, Florida: Jour. Sed. Petrol., v. 57, p. 153-165.

Carter, J. G., 1980, Environmental and biological controls of bivalve shell mineralogy and microstructure, IN Rhoads, D. C., and Lutz, R. A., eds., Skeletal Growth of Aquatic Organisms: New York, Plenum Press, p. 69-113, 645-673.

_____, and Clark, G. R., 1985, Classification and phylogenetic significance of molluscan shell microstructure, IN Broadhead, T. W., ed., Mollusks - Notes for a Short Course: The Univ. of Tenn., Dept. Geol. Sci. Studies in Geology, No. 13, p. 50-71.

Cayeux, L., 1935, Les Roches Sedimentaries de France; Roches Carbonatees: Paris, Masson, 463 p.

Cercone. K. R., and Lohmann, K., 1987, Late burial diagenesis of Niagaran (Middle Silurian) pinnacle reefs in Michigan Basin: Am. Assoc. Petroleum Geologists Bull., v. 71, p. 156-166.

Chave, K. E., 1954, Aspects of the biogeochemistry of magnesium. 1. Calcareous marine organisms: Jour. Geology, v. 62, p. 266-283.

Chave, K. E., 1964, Skeletal durability and preservation, IN Imbrie, J., and Newell, N., eds., Approaches to Paleoecology: Wiley and Sons, New York, p. 377-387.

Chester, R., 1965, Geochemical criteria for differentiating reef and non-reef facies in carbonate rocks: Am. Assoc. Petroleum Geologists Bull., v. 49, p. 258-276.

Choquette, P. W., and James, N. P., 1987, Diagenesis in limestones - 3. The deep burial environment: Geosci. Canada, v. 14, p. 3-35.

Cloud, P. E., 1962, Environment of calcium carbonate deposition west of Andros Island, Bahamas: U. S. Geol. Surv. Prof. Pap. 350, p. 1-138.

Coniglio, M., and James, N. P., 1985, Calcified algae as sediment contributors to Early Paleozoic limestones: evidence from deep-water sediments of the Cow Head Group, western Newfoundland: Jour. Sed. Petrol., v. 55, p. 746-754.

Cook, H. E., Hine, A.C., and Mullins, H.T., eds., 1983, Platform Margin and Deep Water Carbonates: Soc. Econ. Paleon. Mineralog. Short Course 12.

_____, Zemmels, I., and Matti, J. C., 1974, X-ray mineralogy data, eastern Indian Ocean--Leg 27, Deep Sea Drilling Project, IN Veevers, J., Heirtzler, J. R., et al., Initial Reports of the Deep Sea drilling Project Vol. 27: Washington D. C., U.S. Govt. Printing Office, p. 535-548.

_____ , and Mullins, H. T., 1983, Basin margin environment, IN Scholle, P. A., Bebout, D. G., and Moore, C H., eds., Carbonate Depositional Environments: Am. Assoc. Petroleum Geologists Memoir 33, p. 539-618.

Cooper, B. N., 1945, Industrial limestones and dolomites in Virginia: Clinch Valley district: Virginia Geol. Surv. Bull. 66, 137 p.

Cristil, A. I., 1985, Analysis of the Upper Lenoir and Holston Formations deposited along a Middle Ordovician shelf reentrant, Rutledge Pike locality, Knoxville, Tennessee: unpubl. M.S. Thesis, The Univ. of Tennessee, Knoxville, 151 p.

Curtis, C. D., 1978, Possible links between sandstone diagenesis and depth-related geochemical reactions occurring in enclosing mudrocks: Jour. Geol. Soc. London, v. 135, p. 107-117.

_____, Coleman, M. L., and Love, L. G., 1986, Pore water evolution during sediment burial from isotopic and mineral chemistry of calcite, dolomite and siderite: Geochim. Cosmochim. Acta, v. 50, p. 2321-2334.

Czerniakowski, L. A., Lohmann, K. C., and Wilson, J. L., 1984, Closed-system marine burial diagenesis: isotopic data from the Austin Chalk and its components: Sedimentology, v. 31, v. 863-877.

Davies, P. J., 1972, Trace element distribution in reef and subreef rocks of Jurassic age in Britian and Switzerland: Jour. Sed. Petol., v. 42, p,4. 183-194.

Dravis, J., 1979, Rapid and widespread generation of Recent oolitic hardgrounds on a high energy Bahamian platform, Eleuthera Bank, Bahamas: Jour. Sed. Petrol. v. 49, p. 195-208.

Drever, J. I., 1971, Early diagenesis of clay minerals, Rio Ameca Basin, Mexico: Jour. Sed. Petrol., v. 41, p. 982-994.

Dunoyer de Segonzac, G., 1970, The transformation of clay minerals during diagenesis and low-grade metamorphism: a review: Sedimentology, v. 15, p. 281-346.

Enkeboll, R. H., 1981, Petrology and provenance of sands and gravels from the Middle American Trench and trench slope, southwestern Mexico and Guatemala, IN Watkins, J. S., Moore, J. C., et al., Initial Reports of the Deep Sea Drilling Project, Volume 66: Washington D. C., U. S. Gov. Printing Office, p. 521-530.

Enos, P., and Freeman, T., 1979, Lower Cretaceous peritidal limestones at 2700-m depth, Blake nose, Atlantic Ocean: Geology, v. 7, p. 83-87.

Fischer, A. G., Honjo, S., and Garrison, R. E., 1967, Electron Micrographs of Limestones: Princeton, N.J., Princeton Univ. Press, 141 p.

Flajs, G., 1977, Skeletal structures of some calcifying algae, IN Flugel, E., ed., Fossil Algae - Recent Results and Developments: New York Berlin, Springer-Verlag, p. 225-231.

Focke, J. W., and Gebelein, C. D., 1978, Marine lithification of reef rock and rhodolites at a fore-reef slope locality (50m) off Bermuda: Geologie en Mijnbouw, v. 57, p. 163-171.

Folk, R. , 1962, Spectral subdivision of limestone types, IN Ham, W. E., ed., Classification of Carbonate Rocks: Am. Assoc. Petroleum Geologists Memoir 1, p. 62-84.

_____, 1965, Some aspects of recrystallization in ancient limestones, IN Pray, L. C., and Murray, R. C., eds., Dolomitization and Limestone Diagenesis: a Symposium: Soc. Econ. Paleon. Mineralog. Spec. Publ. 13, p. 14-48.

_____, and Robles, R., 1964, Carbonate sands of Isla Perez, Alacran reef complex, Yucatan: Jour. Geology, v. 72, p. 255-292.

Forelich, P. E., Klinkhammer, G. P., Bender, M. L., Leudtke, N. A., Heath, G. R., Cullen, D., Dauphin, P., Hammond, D., Hartman, B., and Maynard, V., 1979, Early oxidation of organic matter in pelagic sediments of the eastern equatorial Atlantic: suboxic diagenesis: Geochim. Cosmochim. Acta, v. 43, p. 1075-1090.

Foscolos, A. E., and Powell, T. G., 1979, Mineralogical and geochemical transformation of clays during burial diagenesis (catagenesis): relation to oil generation, IN Mortland, M. M., and Farmer, V. C., eds., International Clay Conference 1978: New York-Amsterdam-Oxford, Elsevier, p. 261-270.

Frank, J. R., Carpenter, A. B., and Oglesby, T. W., 1982, Cathodoluminescence and composition of calcite cements in the Taum Sauk Limestone (Upper Cambrian), southeast Missouri: Jour. Sed. Petrol., v. 52, p. 631-638.

Freeman-Lynde, R. P., Whitley, K. F., and Lohmann, K. C., 1986, Deep-marine origin of equant spar cements in Bahama escarpement limestones: Jour. Sed. Petrol., v. 56, p. 799-811.

Friedman, G. M., 1968, Geology and geochemistry of reefs, carbonate sediments, and waters, Gulf of Aqaba (Elat), Red Sea: Jour. Sed. Petrol., v. 38, p. 895-919.

Garrels, R. M., and Christ, C. L., 1965, Solutions, Minerals and Equilibria: Harper, New York, 450 p.

Gebelein, C. D., and Hoffman, P., 1971, Algal origin of dolomite lamination in stromatolitic limestone: Jour. Sed. Petrol., v. 41, p. 603-613.

Gervitz, J. L., and Friedman, G. M., 1966, Deep-sea carbonate sediments of the Red Sea and their implications on marine lithification: Jour. Sed. Petrol., v. 36, p. 143-151.

Gillot, J. E., 1969, Study of the fabric of fine-grained sediments with the scanning electron microscope: Jour. Sed. Petrol., v. 39, p. 90-105.

Ginsburg, R. N., Marszalek, D. S., and Schneidermann, N., 1971, Ultrastructure of carbonate cements in a Holocene algal reef of Bermuda: Jour. Sed. Petrol., v. 41, p. 472-482.

Given, R. K., and Wilkinson, B. H., 1985, Kinetic control of morphology, composition, and mineralogy of abiotic sedimentary carbonates: Jour. Sed. Petrol., v. 55, p. 109-119.

Gomberg, D. N., and Bonatti, E., 1970, High-magnesian calcite: leaching of magnesium in the deep sea: Science, v. 168, p. 1451-1452.

Grim, R. E., 1968, Clay Mineralogy: New York, McGraw-Hill, 596 p.

Grover, G., and Read, J. F., 1978, Fenestral and associated vadose diagenetic fabrics of tidal flat carbonates, Middle Ordovician New Market Limestone, southwestern Virginia: Jour. Sed. Petrol., v. 48, p. 453-473.

_____, and _____, 1983, Paleoaquifer and deep-burial-related cements defined by regional cathodoluminescent patterns, Middle Ordovician carbonate, Virginia: Am. Assoc. Petroleum Geologists Bull., v. 67, p. 1275-1303.

Hall, G. M., and Amick, H. C., 1934, The section on the west side of Clinch Mountain, Tennessee: Tenn. Acad. Sci. Jour., v. 9. p. 157-168.

Hallam, A., and O'Hara, M. J., 1962, Aragonitic fossils in the Lower Carboniferous of Scotland: Nature, v. 195, p. 273-274.

Hardie, L. A., 1987, Dolomitization: a critical view of some current views: Jour. Sed. Petrol., v. 57, p. 166-183.

Heckel, P. H., 1983, Diagenetic model for carbonate rocks in Midcontinent Pennsylvanian eustatic cyclothems: Jour. Sed. Petrol., v. 53, p. 733-759.

Hem, J. D., 1972, Chemical factors that influence the availability of iron and manganese in aqueous systems: Geol. Soc. Am. Bull., v. 83, p. 443-450.

Hesse, R., 1986, Early diagenetic pore water/sediment interaction: modern offshore basins: Geoscience Canada, v. 13, p. 165-196.

Hirst, D. M., and Nicholls, G. D., 1958, Techniques in sedimentary geochemistry, 1. Separation of detrital and non-detrital fractions of limestones: Jour. Sed. Petrol., v. 28, p. 468-481.

Honjo, S., and Tabuchi, H., 1970, Distribution of some minor elements in carbonate rocks, 1: Pacific Geology, v. 2, p. 41-79.

Hower, J., Eslinger, E. V., Hower, M. E., Perry, E. A., 1976, Mechanism of burial and metamorphism of argillaceous sediment: 1. Mineralogical and chemical evidence: Geol. Soc. Am. Bull., v. 87, p. 725-737.

Husseini, S. I., and Matthews, R. K., 1972, Distribution of high-magnesium calcite in lime muds of the Great Bahama Bank: diagenetic implications: Jour. Sed. Petrol., v. 42, p. 179-182.

Illing, L. V., 1954, Bahamian calcareous sands: Am. Assoc. Petroleum Geologists Bull., v. 38, p. 1-95.

Ingram, R. L., 1954, Terminology for the thickness of stratification and parting units in sedimentary rocks: Geol. Soc. Am. Bull., v. 65, p. 937-938.

Irwin, H., Curtis, C., and Coleman, M., 1977, Isotopic evidence for source of diagenetic carbonates formed during burial of organic-rich sediments: Nature, v. 269, p. 209-213.

Jackson, M. L., 1969, Soil chemical analysis - Advanced course: Univ. of Wisconsin Press, Madison, 895 p.

James, N. P., Ginsburg, R. N., Marszalek, D. S., and Choquette, P. W., 1976, Facies and fabric specificity of early subsea cements in shallow Belize (British Hondorous) reefs: Jour. Sed. Petrol., v. 46, p. 523-544.

_____, and Ginsburg, R. N., 1979, The Seaward Margin of Belize Barrier and Atoll Reefs: Internat. Assoc. Sedimentologists Spec. Publ. 3, 191 p.

_____, and Klappa, C. F., 1983, Petrogenesis of early Cambrian reef limestones, Labrador, Canada: Jour. Sed. Petrol., v. 53, p. 1051-1096.

_____, and Choquette, P. W., 1984, The seafloor diagenetic environment: Geoscience Canada, v. 10, p. 162-179.

Jernigan, D. G., 1987, Comparative diagenetic histories of the Holston and Rockdell formations, Middle Ordovician of northeastern Tennessee: unpubl. M.S. thesis, The Univ. of Tennessee, Knoxville, 243 p.

Jones, K., and Hirst, D. M., 1972, The distribution of barium, lead and zinc in the Lower and Middle Magnesian Limestone of County Durham, Great Britian: Chem. Geology, v. 10, p. 223-236.

Kahle, C. F., 1965, Possible roles of clay minerals in the formation of dolomite: Jour. Sed. Petrol., v. 35, p. 448-453.

Kearns, C., Hurley, N. F., and Playford, P. E., 1986, Marine diagenesis in Devonian reef complexes of the Canning Basin, western Australia, IN Schroeder, J. H., and Purser, B. H., eds., Reef Diagenesis: Berlin Heidelberg, Springer-Verlag, p. 357-380.

Kendall, C. G. StC., and Schlager, W., 1981, Carbonates and relative changes in sea level: Mar. Geology, v. 44, p. 181-212.

Klappa, C. F., 1978, Biolithogenesis of Microcodium: elucidation: Sedimentology, v. 25, p. 489-522.

Lahann, R. W., 1980, Smectite diagenesis and sandstone cement: the effect of reaction temperature: Jour. Sed. Petrol., v. 50, 755-760.

Land, L. S., 1967, Diagenesis of skeletal carbonates: Jour. Sed. Petrol., v. 37, p. 914-930.

_____, 1985, The origin of massive dolomite: Jour. Geol. Educa., v. 33, p. 112-125.

_____, and Goreau, T. F., 1970, Submarine diagenesis of Jamacian reefs: Jour. Sed. Petrol., v. 40, p. 457-462.

_____, Beherns, E. W., and Frishman, S. A., 1979, The ooids of Baffin Bay, Texas: Jour. Sed. Petrol., v. 49, p. 1269-1278.

_____, and Moore, C. H., 1980, Lithification, micritization and syndepositional diagenesis of biolithites on the Jamaican Island slope: Jour. Sed. Pettrol., v. 50, p. 357-370.

Lasemi, Z., and Sandberg, P. A., 1984, Transformation of aragonite-dominated lime muds to microcrystalline limestones: Geology, v. 12, p. 420-423.

Lees, A., 1975, Possible influence of salinity and temperature on modern carbonate shelf sedimentation: Mar. Geology, v. 19, p. 159-198.

Lindholm, R. C., 1969, Carbonate petrology of the Onondaga Limestone (Middle Devonian), New York: a case for calsiltite: Jour. Sed. Petrol., v. 39, p. 268-275.

Lindstrom, M., 1979, Probable sponge borings in Lower Ordovician limestone of Sweden: Geology, v. 7, p. 152-155.

Lobo, C. F., and Osborne, R. H., 1973, The American Upper Ordovician standard, XVIII: investigation of micrite in typical Cincinnatian limestones by means of scanning electron microscopy: Jour. Sed. Petrol., v. 43, p. 478-483.

Logan, B. W., Harding, J. L., Ahr, W. A., Williams, J. D., and Snead, R. G., 1969, Carbonate sediments and reefs, Yucatan shelf, Mexico: Am. Assoc. Petroleum Geologists Memoir 11, p. 1-196.

_____, and Semeniuk, V., 1976, Dynamic metamorphism; processes and products in Devonian carbonate rocks, Canning Basin, Western Australia: Geol. Soc. Australia Spec. Publ. 6, 138 p.

Lohmann, K. C., and Meyers, W. J., 1977, Microdolomite inclusions in cloudy prismatic calcites: a proposed criterion for for high-magnesian calcites: Jour. Sed. Petrol., v. 47, p. 1078-1088.

Longman, M. W., 1977, Factors controlling the formation of microspar in the Bromide Formation: Jour. Sed. Petrol., v. 47, p. 347-350.

_____, 1980, Carbonate diagenetic textures from near-surface diagenetic environments: Am. Assoc. Petroleum Geologists Bull., v. 64, p. 461-487.

Lorens, R. B., 1981, Sr, Cd, Mn, and Co distribution coefficients in calcite as a function of calcite precipitation rate: Geochim. Cosmochim. Acta, v. 45, p. 553-561.

Loucks, R. G., and Folk, R. L., 1976, Fanlike rays of former aragonite in Permian Capitan Reef pisolite: Jour. Sed. Petrol., v. 46, p. 483-485.

Lowenstam, H. A., 1954, Factors affecting the aragonite/calcite ratios in carbonate-secreting marine organisms: Jour. Geology, v. 62, p. 284-322.

_____, and Epstein, 1957, On the origin of sedimentary aragonite needles of the Great Bahama Bank: Jour. Geology, v. 65, p. 364-375.

McFarran, E. F., Lishka, R. J., and Parker, J. H., 1970, Criterion for judging acceptability of analytical methods: Anal. Chem., v. 42, p. 358-365.

McHargue, T. R., and Price, R. C., 1982, Dolomite from clay in argillaceous or shale-associated marine carbonates: Jour. Sed. Petrol., v. 52, p. 873-886.

McKee, E. D., and Gutschick, R. C., 1969, Histroy of the Redwall Limestone of northern Arizona: Geol. Soc. Am., Memoir 114, 726 p.

McGill, M. M., 1982, Study of diagenesis of a portion of the Holston Formation: paragenesis of cements and evaluation of geochemistry: unpubl. M.S. thesis, The Univ. of Tennessee, Knoxville, 103 p.

MacLintock, C., 1967, Shell structure of the Patteloid and Bellerophonotid gastropods (Mollusca): Peabody Museum Natural Hist., Yale Univ., Bull., v. 22, p. 1-140.

Macintyre, I. G., 1977, Distribution of submarine cements in a modern Caribbean fringing reef, Galeta Point, Panama: Jour. Sed. Petrol., v. 47, p. 503-516.

Mack, G. H., 1985, Provenance of the Middle Ordovician Blount clastic wedge, Georgia and Tennessee: Geology, 13, p. 299-302.

Macqueen, R. W., Ghent, E. D., and Davies, G. R., 1974, Magnesium distribution in living and fossil specimens of the echinoid Peronella lesueuri Agassiz, Shark Bay, Western Australia: Jour. Sed. Petrol., v. 44, p. 60-69.

Majewske, O. P., 1969, Recognition of Invertebrate Fossil Fragments in Rocks and Thin Sections: Leiden, Brill, 101 p.

Magara, K., 1976, Water expulsion from clastic sediments during compaction - directions and volumes: Am. Assoc. Petroleum Geologists Bull., v. 60, p. 543-553.

Majid, A. H., and Veizer, J., 1986, Deposition and chemical diagenesis of Tertiary carbonates, Kirkuk Oil Field, Iraq: Am. Assoc. Petroleum Geologists Bull., v. 70, p. 898-913.

Marshak, S., and Engelder, T., 1985, Development of cleavage in limestones of a fold-thrust belt in eastern New York: Jour. Structural Geology, v. 7, p. 345-359.

Marshall, J. F., 1985, Cross-shelf and facies related variations in submarine cementation in the central Great Barrier Reef: Proc. 5th Internat. Coral Reef Congr., v. 3, p. 221-226.

Martin, G. D., Wilkinson, B. H., and Lohmann, K. C., 1986, The role of skeletal porosity in aragonite neomorphism - Strombus and Montastrea from the Pleistocene Key Largo Limestone, Florida: Jour. Sed. Petrol., v. 56, p. 194-203.

Mattes, B. W., and Mountjoy, E. W., 1980, Burial dolomitization of the Upper Devonian Miette buildup, Jasper National Park, Alberta, IN Zenger, D. H., Dunham, J. B., and Ethington, R. L., eds., Concepts and Models of Dolomitization: Soc. Econ. Paleon. Mineralog. Spec. Publ. 28, p. 259-297.

Matthews, R. K., 1966, Genesis of Recent lime mud in southern British Honduras: Jour. Sed. Petrol., v. 36, p. 428-454.

Maynard, J. B., 1982, Extension of Berner's "new geochemical classification of sedimentary environments" to ancient sediments: Jour. Sed. Petrol., v. 52, p. 1325-1331.

Mazzullo, S. J., 1980, Calcite pseudospar replacive of marine acicular aragonite, and implications for aragonite cement diagenesis: Jour. Sed. Petrol., v. 50, 409-422.

_____, Reid, A. M., and Gregg, J. M., 1987, Dolomitization of Holocene Mg-calcite supratidal deposits, Ambergris Cay, Belize: Geol. Soc. Am. Bull., v. 98, p. 224-231.

Metcalfe, S. J., 1974, Acid-insoluble residues in Chickamauga equivalents (Middle Ordovician) in East Tennessee--an aid to paleogeographic reconstruction: unpubl. M.S. thesis, The Univ. of Tennessee, Knoxville, 64 p.

Meyers, W. J., 1980, Compaction in Mississippian skeletal limestones, southwestern New Mexico: Jour. Sed. Petrol., v. 50, p. 457-474.

Miller, J., 1986, Facies relationships and diagenesis in Waulsortian mudmounds from the Lower Carboniferous of Ireland and N. England, IN Schroeder, J. H., and Purser, B. H., eds., Reef Diagenesis: Berlin-Heidelberg, Springer-Verlag, p. 311-335.

Milliman, J. D., 1966, Submarine lithification of carbonate sediments: Science, v. 153, p. 994-997.

_____, 1974, Marine Carbonates, Berlin, Springer, 375 p.

Misik, M., 1971, Observations concerning calcite veinlets in carbonate rocks: Jour. Sed. Petrol., v. 41, p. 450-460.

Moore, C. H., 1973, Intertidal carbonate cementation, Grand Cayman, West Indies: Jour. Sed. Petrol., v. 43, p. 591-602.

_____, 1985, Upper Jurassic subsurface cements: a case history, IN Schneidermann, N., and Harris, P. M., eds., Carbonate Cements: Soc. Econ. Paleon. Mineralog. Spec. Publ. 36, p. 291-308.

_____, and Druckman, Y., 1981, Burial diagenesis and porosity evolution, Upper Jurassic Smackover, Arkansas and Louisiana: Am. Assoc. Petroleum Geologists Bull., v. 65, p. 597-628.

Moore, G. F., 1979, Petrography of subduction zone sandstones from Nias Island, Indonesia: Jour. Sed. Petrol., v. 49, p. 71-84.

Moore, N. K., 1977, Distribution of the benthic algal flora in Middle Ordovician carbonate environmental units of the southern Appalachians, IN Ruppel, S. C., and Walker, K. R., eds., The Ecostratigraphy of the Middle Ordovician of the Southern Appalachians (Kentucky, Tennessee, and Virginia), U.S.A.: A Field Excursion: The Univ. of Tenn., Dept. Geol. Sci. Studies in Geology, No. 77-1, p. 18-29.

_____, 1978, Taxonomy and paleoenvironmental distribution of the benthic algal flora fbrom Middle Ordovician carbonate rocks of East Tennessee: unpubl. PhD. dissertation, The Univ. of Tennessee, Knoxville, 148 p.

Moore, R. C., ed., 1965, Treatise on Invertebrate Paleontology, Part H, Brachiopoda: Geol. Soc. Am. and Univ. of Kansas Press, 521 p.

Morrow, D. W., 1983, Dolomite-Part 2. Dolomitization models and ancient dolostones: Geosci. Canada, v. 9, p. 93-107.

Morse, J. W., Zullig, J. J., Bernstein, L. D., Millero, F. J., Milne, P., Mucci, A., and Choppin, G. R., 1985, Chemistry of calcium carbonate-rich shallow water sediments in the Bahamas: Am. Jour. Sci., v. 285, p. 147-185.

Moshier, S. O., and McManus, K. M., 1986, Textural evolution during experimental lime-mud diagenesis (abs.): Am. Assoc. Petroleum Geologists Bull, v. 70, p. 623-624.

Moss, T., 1981, A comparative study of the trace element distribution in limestones, dolostones and breccias in the Upper Knox Group of the Copper Ridge zinc district, East Tennessee: unpubl. M.S. thesis, The Univ. of Tennessee, Knoxville, 174 p.

Muller, G., and Friedman, G. M. (eds.), 1968, Recent Developments in Carbonate Sedimentology in Central Europe: Berlin, Springer, 255 p.

Mullins, H. T., and Neumann, A. C., 1979, Deep carbonate bank margin structure and sedimentation in the northern Bahamas, IN Doyle, L., and Pilkey, O. H., eds., Geology of Continental Slopes: Soc. Econ. Paleon. Mineralog. Spec. Publ. 27, p. 165-192.

_____, _____, Wilber, R. J., and Boardman, M. R., 1980, Nodular carbonate sediment on Bahamian slopes: possible precursors to nodular limestones: Jour. Sed. Petrol., v. 50, p. 117-131.

_____, Wise, S. W., Gardulski, A. F., Hinchley, E. J., Masters, P. M., and Siegel, D. I., 1985, Shallow subsurface diagenesis of Pleistocene periplatform ooze; northern Bahamas: Sedimentology, v. 32, p. 473-494.

Nelsen, J. E., and Ginsburg, R. N., 1986, Calcium carbonate production by epibionts on Thalassia in Florida Bay: Jour. Sed. Petrol., v. 56, p. 622-628.

Neumann, A. C., Gebelein, C. D., and Scoffin, T. P., 1970, The composition, structure and erodability of subtidal mats, Abaco, Bahamas: Jour. Sed. Petrol., v. 40., p. 274-297.

_____, and Land, L. S., 1975, Lime mud deposition and calcareous algae in the Bight of Abaco, Bahamas: a budget: Jour. Sed. Petrol., v. 45, p. 763-786.

Neumann, R. B., 1955, Middle Ordovician rocks of Tellico-Sevier belt, eastern Tennessee: U. S. Geol. Surv. Prof. Paper 274-F, p. 141-177.

Nicholls, G. D., 1967, Trace elements in sediments: an assessment of their possible utility as depth indicators: Mar. Geology, v. 5, p. 539-555.

Oldershaw, A. E., and Scoffin, T. P., 1967, The source of ferroan and non-ferroan calcite cements in the Halkin and Wenlock Limestones: Geol. Jour., v. 5, p. 309-320.

Parker, W. C., Ragland, P. C., and Textoris, D. A., 1985, Controls on trace elements in the Ordovician Black River Group, New York, U.S.A.: Chem. Geology, v. 53, p. 83-94.

Parrish, J. T., Zeigler, A. M., and Humphreville, R. G., 1983, Upwelling in the Paleozoic Era, IN Thiede, J., and Suess, E., eds., Coastal Upwelling: Its Sediment Record: NATO Conf. Series, IV - Marine Sciences, v. 10B, p. 553-578.

Pilkey. O. H., and Rucker, J. B., 1966, Mineralogy of Tongue of the Ocean's sediment: Jour. Mar. Res., v. 24, p. 276-285.

_____, and Blackwelder, B. W., 1968, Mineralogy of the sand size carbonate fraction of some Recent marine terrigenous and carbonate sediments: Jour. Sed. Petrol., v. 38, p. 799-810.

Pingitore, N. E., 1976, Vadose and phreatic diagenesis: processes, products and their recognition in corals: Jour. Sed. Petrol., v. 46, p. 985-1006.

_____, 1978, The behavior of Zn2+ and Mn2+ during carbonate diagenesis; theory and applications: Jour. Sed. Petrol., v. 48, p. 799-814.

_____, 1982, The role of diffusion during carbonate diagenesis: Jour. Sed. Petrol., v. 52, p. 27-39.

Podhalanska, T., 1984, Microboring assemblage in Lower/Middle Ordovician limestones from northern Poland: N. Jb. Geol. Palaont. Mh., v. 32, p. 497-511.

Popp, B. N., Anderson, T. F., and Sandberg, P. A., 1986, Textural, elemental, and isotopic variations among constituents in Middle Devonian limestones, North America: Jour. Sed. Petrol., v. 56, p. 715-727.

Prezbindowski, D. R., 1985, Burial cementation - is it important? A case study, Stuart City Trend, South Central Texas, IN Schneidermann, N., and Harris, P. M., eds., Carbonate Cements: Soc. Econ. Paleon. Mineralog. Spec. Publ. 36, p. 241-264.

_____, and Larese, R. E., 1987, Experimental stretching of fluid inclusion in calcite - implications for diagenetic studies: Geology, v. 15, p. 333-336.

Prouty, C. E., 1946, Lower Middle Ordovician of southwest Virginia and northeast Tennessee: Am. Assoc. Petroleum Geologists Bull., v. 30, p. 1140-1191.

Purdy, E. G., 1963, Recent calcium carbonate facies of the Great Bahama Bank. 1. Petrography and reaction groups: Jour. Geology, v. 71, p. 334-355.

Purser, B. H., 1969, Syn-sedimentary marine lithification of Middle Jurassic limestones in the Paris Basin: Sedimentology, v. 12, p. 205-230.

Radke, B. M., and Mathis, R. L., 1980, On the formation and occurrence of saddle dolomite: Jour. Sed. Petrol., v. 50, p. 1149-1168.

Raup, D. M., 1966, The endoskeleton of the echinoderm, IN Boolootian, R. A., ed., Physiology of Echinodermata: New York, Wiley-Interscience, p. 379-395.

Read, J. F., 1980, Carbonate ramp-to-basin transitions and foreland basin evolution, Middle Ordovician, Virginia Appalachians: Am. Assoc. Petroleum Geologists Bull., v. 64, p. 1575-1612.

_____, 1982, Carbonate platforms of passive (extensional) continental margins: types, characteristics and evolution: Tectonophys., v. 81, p. 195-212.

Reeder, R. J., 1983, Crystal chemistry of the rhombohedral carbonates, IN Reeder, R. J., ed., Carbonates: Mineralogy and Chemistry, Reviews in Mineralogy 11: Washington D.C., Mineral. Soc. Am., p. 1-47.

Reijers, T. J. A., 1984, Devonian carbonate facies patterns in the Dinant Synclinorium, Belgium: Geologie en Mijnbouw, v. 63, p. 19-29.

Richter, D. K., and Fuchtbauer, H., 1978, Ferroan calcite replacement indicates former magnesian calcite skeletons: Sedimentology, v. 25, p. 843-860.

Richter, F. M., and DePaolo, D. J., 1987, Numerical models for diagenesis and the Neogene Sr isotopic evolution of seawater from DSDP Site 590B: Earth Planetary Sci. Letters, v. 83, p. 27-38.

Riding, R., 1977, Calcified Plectonema (blue-green algae), a recent example of Girvanella from Aldabra Atoll: Paleontology, v. 20, p. 33-46.

Riva, J., 1974, A revision of some Ordovician graptolites in eastern North America: Paleontology, v. 17, p. 1-40.

Robertson, C. E., 1965, Experimental consolidation of carbonate mud (abs.), IN Pray, L. C., and Murray, R. C., eds., Dolomitization and Limestone Diagenesis, A Symposium: Soc. Econ. Paleon. Mineralog. Spec. Publ. 13, p. 170.

Rodgers, J., 1953, Geologic map of East Tennessee with explanatory text: Tenn. Div. Geology Bull., v. 58, p. 64-96.

Rudwick, M. J. S., 1970, Living and Fossil Brachiopods: London, Hutchinson, 199 p.

Ruppel, S. C., 1979, The stratigraphy, carbonate petrology and depositional environments of the Chickamauga Group (Middle Ordovician) of northern East Tennessee: unpubl. PhD. dissertation, The Univ. of Tennessee, Knoxville, 231 p.

_____, and Walker, K. R., eds., 1977, The ecostratigraphy of the Middle Ordovician of the Southern Appalachians (Kentucky, Tennessee, Virginia) U.S.A.: an excursion: The Univ. of Tenn., Knoxville, Dept. of Geol. Sci. Studies in Geology No. 1, 171 p.

_____ , and _____, 1982, Sedimentology and distinction of carbonate buildups: Middle Ordovician, East Tennessee: Jour. Sed. Petrol., v. 52, p. 1055-1071.

_____, and _____, 1984, Petrology and depositional history of a Middle Ordovician carbonate platform: Chickamauga Group, northeastern Tennessee: Geol. Soc. Am. Bull., v. 95, p. 568-583.

Russell, K. L., 1970, Geochemistry and halmyrolysis of clay minerals, Rio Ameca, Mexico: Geochim. Cosmochim. Acta, v. 34, p. 893-907.

Ryland, J. S., 1970, Bryozoans: London, Hutchinson, 175 p.

Saller, A. H., 1986, Radiaxial calcite in Lower Miocene strata, subsurface Enewetak Atoll: Jour. Sed. Petrol., v. 56, p. 743-762.

Sandberg, P. A., 1975, Bryozoan diagenesis: bearing on the nature of the original skeleton of rugose corals: Jour. Paleo., v. 49, p. 587-606.

_____, 1983, An oscillating trend in Phanerozoic non-skeletal carbonate mineralogy: Nature, v. 305, p. 19-22.

_____, 1985, Aragonite cements and their occurrence in ancient limestones, IN Schneidermann, N., and Harris, P. M., eds., Carbonate Cements: Soc. Econ. Paleon. Mineralog. Spec. Publ. 36, p. 33-57.

Sayles, F. L., and Mangelsdorf, P. C., 1977, The equilibration of clay minerals with seawater: exchange reactions: Geochim. Cosmochim. Acta, v. 41, p. 951-960.

_____, and _____, 1979, Cation-exchange characteristics of Amazon River suspended sediment and its reaction with seawater: Geochim. Cosmochim. Acta, v. 43, p. 767-779.

Scherer, M., 1975, Cementation and replacement of Pleistocene corals from the Bahamas and Florida: diagenetic influence of non-marine environments: Neues Jahrb. Geol. Palaont. Abh., v. 149, p. 259-285.

Schlanger, W., 1980, Mesozoic calciturbidites in Deep Sea Drilling Project Hole 416A -- recognition of a drowned carbonate platform, IN Lancelot, Y., Winterer, E. L. et al., Initial Reports of the Deep Sea Drilling Project Vol. 50: Washington, D.C., U. S. Govt. Printing Office, p. 733-749.

_____, and James, N. P., 1978, Low-magnesian calcite limestones forming at the deep-sea floor, Tongue of the Ocean, Bahamas: Sedimentology, v. 25, p. 675-702.

Schmidt, G. W., 1973, Interstitial water composition and geochemistry of deep Gulf Coast shales and sandstones: Am. Assoc. Petroleum Geologists Bull., v. 57, p. 321-337.

Scholle, P. A., 1971, Diagenesis of deep-water carbonate turbidites, Upper Cretaceous Monte Antola Flysch, northern Apennines, Italy: Jour. Sed. Petrol., v. 41, p. 233-250.

_____, and Halley, R. B., 1985, Burial diagenesis: out of sight, out of mind!, IN Schneidermann, N., and Harris, P. M., eds., Carbonate Cements: Soc. Econ. Paleon. Mineralog. Spec. Publ. 36, p. 309-334.

Schroeder, J. H., 1973, Submarine and vadose cements in Holocene Bermuda cup reefs: Geol. Rundschau, v. 61, p. 708-730.

Scotese, C. R., Bambach, R. K., Barton, C., Van der Voo, R., and Ziegler, A. M., 1979, Paleozoic base maps: Jour. Geology, v. 87, p. 217-277.

Sellwood, B. W., 1978, Shallow-water carbonate environments, IN Reading, H. G., ed., Sedimentary Environments and Facies: New York, Elsevier, p. 259-314.

Shanmugam, G., and Benedict, G. L., 1978, Fine-grained carbonate debris flow, Ordovician basin margin, Southern Appalachians: Jour. Sed. Petrol., v. 48, p. 1233-1240.

_____, and Walker, K. R., 1980, Sedimentation, subsidence, and evolution of a foredeep basin in the Middle Ordovician, Southern Appalachians: Am. Jour. Sci., v. 280, p. 479-496.

_____, and _____, 1983, Anatomy of the Middle Ordovician Sevier Shale basin, eastern Tennessee: Sed. Geology, v. 34, p. 315-337.

_____, and Benedict, G. L., 1983, Manganese distribution in the carbonate fraction of shallow and deep marine lithofacies, Middle Ordovician, eastern Tennessee: Sed. Geology, v. 35, p. 159-175.

_____ , Walker, K. R., and Lash, G. G., 1985, Comment on "Provenance of the Middle Ordovician Blount clastic wedge, Georgia and Tennessee": Geology, v. 13, p. 889-890.

Shinn, E. A., 1969, Submarine lithification of Holocene carbonate sediments in the Persian Gulf: Sedimentology, v. 12, p. 109-144.

_____, 1975, Polygonal cement sutures from the Holocene: a clue to recognition of submarine diagenesis (abs.): Am. Assoc. Petroleum Geologists - Soc. Econ. Paleon. Mineralog. Annual Mtg. Abstr., v. 2, p. 68.

_____, 1983, Recognition and economic significance of ancient carbonate tidal flats - a comparison of modern and ancient examples, IN Scholle, P. A., Bebout, D. G., and Moore, C. H., eds., Carbonate Depositional Environments: Am. Assoc. Petroleum Geologists Mem. 33, p. 171-210.

_____, and Robbin, D. M., 1983, Mechanical and chemical compaction in fine-grained, shallow-water limestones: Jour. Sed. Petrol., v. 53, p. 595-618.

Sickafoose, D. K., 1979, Ecostratigraphy of the Lower Middle Ordovician and paleoecology of Portfieldian and Wildernessian biotas at Evans Ferry, Tennessee: unpubl. M.S. thesis, The Univ. of Tennessee, Knoxville, 185 p.

Siegel, F. R., 1961, Variations in Sr/Ca ratios and Mg contents in Recent carbonate sediments of the northern Florida Keys area: Jour. Sed. Petrol., v. 31, p. 336-342.

Simonson, J. C. B., 1985, The stratigraphy, carbonate petrology, depositional environments, and paleoecology of the Middle Ordovician Moccasin Formation near Thorn Hill, Tennessee: unpubl. M.S. thesis, The Univ. of Tennessee, Knoxville, 279 p.

Sippel, R. F., and Glover, E. D., 1965, Structures in carbonate rocks made visible by luminescence petrography: Science, v. 150, p. 1283-1287.

Sorby, H. C., 1879, On the structure and origin of limestones: Quart. Jour. Geol. Soc. London, v. 35, p. 56-95.

Sperber, C. M., Wilkinson, B. H., and Peacor, D. R., 1984, Rock composition, dolomite stoichiometry, and rock/water reactions in dolomitic carbonate rocks: Jour. Geology, v. 92, p. 609-622.

Srodon, J., 1979, Correlation between coal and clay diagenesis in the Carboniferous of the Upper Silesian Coal Basin, IN Mortland, M. M., and Farmer, V. C., International Clay Mineral Conference 1978: New York-Amsterdam-Oxford, Elsevier, p. 251-260.

Stanley, S. M., 1966, Paleoecology and diagenesis of Key Largo Limestone, Florida: Am. Assoc. Petroleum Geologists Bull., v. 50, p. 1927-1947.

Stehli, F. G., 1956, Shell mineralogy of Paleozoic invertebrates: Science, v. 123, p. 1031-1032.

_____, and Hower, J., 1961, Mineralogy and early diagenesis of carbonate sediments: Jour. Sed. Petrol., v. 31, p. 358-371.

Steinen, R. P., 1978, On the diagenesis of lime mud: scanning electron microscopic observations of surface material from Barbados, W. I.: Jour. Sed. Petrol., v. 48, p. 1139-1148.

_____, 1982, SEM observations on the replacement of Bahaman aragonitic mud by calcite: Geology, v. 10, p. 471-475.

Stockman, K. W., Ginsburg, R. N., and Shinn, E. A., 1967, The production of lime mud by algae in south Florida: Jour. Sed. Petrol., v. 37, p. 633-648.

Stueber, A. M., Pushkar, P., and Hetherington, E. A.., 1984, A strontium isotopic study of Smackover brines and associated solids, southern Arkansas: Geochim. Cosmochim. Acta, v. 48, p. 1637-1649.

Stumm, W., and Morgan, J. J., 1981, Aquatic Chemistry: New York, John Wiley and Sons, 780 p.

Suchecki, R. K., and Hubert, J. F., 1984, Stable isotopic and elemental relationships of ancient shallow-marine and slope carbonates, Cambro-Ordovician Cow Head Group, Newfoundland: implications for fluid flux: Jour. Sed. Petrol., v. 54, p. 1062-1080.

Sundby, B., Anderson, L. G., Hall, P. O. J., Iverfeldt, A., Rutgers van der Loeff, M. M., and Westerlund, S. F. G., 1986, The effect of oxygen on the release and uptake of cobalt, manganese, iron and phosphate at the sediment-water interface: Geochim. Cosmochim. Acta, v. 50, p. 1281-1288.

Sweet, W. C., and Bergstrom, S. M., 1976, Conodont biostratigraphy of the Middle and Upper Ordovician of the United States midcontinent, IN Bassett, M. G., ed., The Ordovician System: proceedings of Paleontological Assoc. symposium, Birmingham, England: Cardiff, Univ. of Wales Press, p. 121-151.

Taggart, M. S., and Kaiser, A. D., 1960, Clay mineralogy of Mississippi River deltaic sediments: Geol. Soc. Am. Bull., v. 71, p. 521-530.

Talbot, M. R., 1971, Calcite cements in the Corallian beds (Upper Oxfordian) of southern England: Jour. Sed. Petrol., v. 41, p. 261-273.

Teichert, C., 1958, Concepts of facies: Am. Assoc. Petroleum Geologists Bull., v. 42, p. 2718-2744.

Teigler, D. J., and Towe, K. M., 1975, Microstructure and composition of the trilobite exoskeleton: Fossils and Strata 4, p. 137-149.

Thompson, R. O. R. Y., and Golding, T. J., 1981, Tidally induced 'upwelling' by the Great Barrier Reef: Jour. Geophys. Res., v. 86, p. 6517-6521.

Till, R., 1968, Some aspects of the geochemistry of Recent Bahamian carbonate sediments from the Bimini Lagoon: unpubl. PhD. dissertation, Univ. of Sheffield, England, 166 p.

Toomey, D. F., and Klement, K. W., 1966, A problematical micro-organism from the El Paso group (Lower Ordovician) of West Texas: Jour. Paleo., v. 40, p. 1304-1311.

Toth, J., 1970, Relation between electric analogue patterns of groundwater flow and accumulation of hydrocarbons: Can. Jour. Earth Sci., v. 7, p. 988-1007.

Towe, K. M., 1967, Echinoderm calcite: single crystal or polycrystalline aggregate: Science, v. 157, p. 1048-1050.

_____, and Hemleben, C., 1976, Diagenesis of magnesian calcite: evidence from miliolacean foraminifera: Geology, v. 4, p. 337-339.

Tucker, M. E., 1973, Sedimentology and diagenesis of Devonian pelagic limestones (Cephalopodenkalk) and associated sediments of the Rhenohercynian Geosyncline, West Germany: Neus. Jahb. Geol. Palaont. Abh., v. 142, p. 320-350.

_____, 1981, Sedimentary Petrology: An Introduction: New York Toronto, John Wiley and Sons, 252 p.

Tudhope, A. W., and Risk, M. J., 1985, Rate of dissolution of carbonate sediments by microboring organisms, Davies Reef, Australia: Jour. Sed. Petrol., v. 55, p. 440-447.

Van der Plas, L., and Tobi, A. C., 1965, A chart for judging the reliability of point count results: Am. Jour. Sci., v. 263, p. 87-90.

Veizer, J., 1983, Chemical diagenesis of carbonates: theory and application of trace element technique: Soc. Econ. Paleont. Mineralog. Short Course No. 10, p. 3-1 to 3-100.

_____, and _____, 1974, Strontium as a tool in facies analysis: Jour. Sed. Petrol., v. 44, p. 93-115.

_____, Lemieux, J., Jones, B., Gibling, M. R., and Savelle, J., 1977, Sodium: paleosalinity indicator in ancient rocks: Geology, v. 5, p. 177-179.

_____, _____, _____, _____, and _____, 1978, Paleosalinity and dolomitization of a Lower Paleozoic carbonate sequence, Somerset and Prince of Wales Islands, Arctic Canada: Can. Jour. Earth Sci., v. 15, p. 1448-1461.

Von Engelhardt, W., and Gaida, K. H., 1963, Concentration changes of pore solutions during the compaction of clay sediments: Am. Assoc. Petroleum Geologists Bull., v. 33, p. 919-930.

Wada, H., Niitsuma, N., Nagasawa, K., Okada, H., 1981, Deep sea carbonate nodules from the Middle America Trench area off Mexico, Deep Sea Drilling Project Leg 66, IN Watkins, J. C., Moore, J. C., et al., Initial Reports of the Deep Sea Drilling Project, Vol. 66: Washington D. C., U.S. Govt. Printing Office, p. 453-474.

Wagner, P.D., and Matthews, R. K., 1982, Porosity preservation in the Upper Smackover (Jurassic) carbonate grainstone, Walker Creek Field, Arkansas: response to paleophreatic lenses to burial processes: Jour. Sed. Petrol., v. 52, p. 3-18.

Walker, K. R., and Benedict, G. L., 1980, Slope facies of the Whitesburg Formation and overlying basinal pelagic shales of the Blockhouse Formation near Silver City, Tennessee, IN Walker, K. R., Broadhead, T. W., and Keller, F. B., eds., Middle Ordovician Carbonate Shelf to Deep Water Basin Deposition in the Southern Appalachians: The Univ. Of Tenn., Knoxville, Dept. Geol. Sci. Studies in Geology No. 4, p. 81-85.

_____, Broadhead, T. W., and Keller, F. B., 1980, Middle Ordovician Carbonate Shelf to Deep Water Basin Deposition in the Southern Appalachians: The Univ. of Tenn., Knoxville, Dept. Geol. Sci. Studies in Geology No. 4, 120 p.

_____, Jernigan, D. G., and Weber, L. J., 1985, Diagenetic environments of syntaxial cement formation as a function of geologic age (abs.): Geol. Soc. Am. Abst. with Progr., v. 17, No. 7, p. 742.

_____, _____, and Stienhauff, D. M., 1986, Fluid-flow timing and pathway predition across carbonate shelf margins: the Lower Paleozoic of the Southern Appalchians as a natural laboratory, IN Rifts, Ramps, Reefs and Royalites: West Virginia Geological and Economic Survey, Cir. C-40, p. 105-118.

Waples, D. W., 1980, Time and temperature in petroleum formation - application of Lopatin's method to petroleum exploration: Am. Assoc. Petroleum Geologists Bull. v. 64, p. 916-926.

Wedekind, J. E., 1986, The stratigraphy, depositional environments, bryozoan paleoecology and taphonomy of the middle Chickamauga Group near Thorn Hill, Grainger County, Tennessee: unpubl. M.S. thesis, The Univ. of Tennessee, Knoxville, 179 p.

Wedephol, K. H., 1978, Handbook of Geochemistry, Vol. II: Berlin-Heidelberg- New York, Springer-Verlag.

Weiss, E. A., 1981, Environmental sedimentology of the Middle Ordovician and paleoecology of a portion of the Witten Formation at Solway, Tennessee: unpubl. M.S. thesis, The Univ. of Tennessee, Knoxville, 229 p.

White, A. F., 1977, Sodium and potassium coprecipitation in aragonite: Geochim. Cosmochim. Acta, v. 41, p. 613-625.

_____, 1978, Sodium coprecipitation in calcite and dolomite: Chem. Geology, v. 23, p. 65-72.

Wiggins, W. D., 1986, Geochemical signatures in carbonate matrix and their relation to deposition and diagenesis, Pennsylvanian Marble Falls Limestone, central Texas: Jour. Sed. Petrol., v. 56, p. 771-783.

Wilkinson, B. H., 1979, Biomineralization, paleoceanography, and the evolution of calcareous marine organisms: Geology, v. 7, p. 425-427.

_____, and Landing, E., 1978, "Eggshell diagenesis" and primary radial fabric in calcite ooids: Jour. Sed. Petrol., v. 48, p. 1129-1138.

_____, Janecke, S. U., and Brett, C. E., 1982, Low-magnesian calcite cement in Middle Ordovician hardgrounds from Kirkfield, Ontario: Jour. Sed. Petrol., v. 52, p. 47-57.

_____, Buczynski, C., and Owen, R. M., 1984, Chemical control of carbonate phases: implications from Upper Pennsylvanian calcite-aragonite ooids of southeastern Kansas: Jour. Sed. Petrol., v. 54, 932-947.

_____, Smith, A. L., and Lohmann, K. C., 1985, Sparry calcite marine cement in Upper Jurassic Limestones of southeastern Wyoming, IN Schneidermann, N., and Harris, P. M., eds., Carbonate Cements: Soc. Econ. Paleont. Mineralog. Spec. Publ. 36, p. 169-184.

Wilson, J. L., 1975, Carbonate Facies in Geologic History: Berlin-New York, Springer-Verlag, 471 p.

Winland, H. D., 1968, The role of high Mg calcite in the preservation of micrite envelopes and textural features of aragonite sediments: Jour. Sed. Petrol., v. 38, 1320-1325.

Wolanski, E., and Pickard, G. L., 1983, Upwelling by Internal tides and Kelvin waves at the continental shelf break on the Great Barrier Reef: Aust. Jour. Mar. Res., v. 34, p. 65-80.

Wood, A., 1942, The algal nature of the genus Koninckopora Lee; its occurrence in Canada and western Europe: Quart. Jour. Geol. Soc. London, v. 98, p. 205-221.

Wong, P. K., and Oldershaw, A., 1981, Burial cementation in the Devonian, Kaybob Reef Complex, Alberta, Canada: Jour. Sed. Petrol., v. 51, p. 507-520.

Woronick, R. E., and Land, L. S., 1985, Late burial diagenesis, Lower Cretaceous Pearsall and Lwer Glen Rose formations, south Texas, IN Schneidermann, N., and Harris, P. M., eds., Carbonate Cements: Soc. Econ. Paleon. Mineralog. Spec. Publ. 36, p. 265-275.

Wray, J. C., 1977, Calcareous Algae: New York-Amsterdam-Oxford, Elsevier, 185 p.

Wright, V. P., 1981, Ultrastructure and early diagenesis of the Visean alga Koninckopora: Paleo., v. 24, p. 185-94.

APPENDICES

APPENDIX A

DESCRIPTIONS OF STRATIGRAPHIC SECTIONS

Explanatory Note

The following descriptions of stratigraphic sections are presented with the base of the section first (Post-Knox unconformity) and the top of the section last. Because of the nature of this study and the fact that each section has previously been studied, formations were divided into gross stratigraphic units. Sample locations are listed in meters above the unconformity. For sections in which detailed lithologic descriptions exist, samples are grouped based on the previous work. Underlining indicates samples chosen for petrographic and/or bulk geochemical analysis. All thin sections produced for this study are in the Ordovician collections of the Department of Geological Sciences, The University of Tennessee, Knoxville, Tennessee.

Measurement Conventions

The following bed thickness and grain size conventions were used in each of the stratigraphic section descriptions. Bed thickness conventions (in metric units) are based on Ingram (1954).

Bed Thickness

Very thick bedded.....greater than 1.0 m.

Thick bedded.....0.3 - 1.0 m.

Medium bedded.....0.1 - 0.3

Thin bedded.....0.03 - 0.1 m.

Very thin bedded.....0.01 - 0.03 m.

Thick laminated.....0.003 - 0.01 m.

Thin laminated.....less than 0.003 m.

Grain size

Coarse grained.....grains easily identifiable with the naked eye (approximately >1 mm)

Medium grained.....grains visible but not identifiable with the naked eye (approximately 0.25-1 mm)

Fine grained.....grains only visible with a hand lens (approximately 0.1-0.25 mm).

Very fine grained.....individual grains not visible with a hand lens (approximately <0.1 mm)

Localities and Description of Measured Sections

Locality N1. Cedar Springs Church Section

Along and in fields west of Cedar Springs Church road approximately 4.8 km. northeast of Thorn Hill, Tennessee on State Rte. 131. Section begins just off an unmarked gravel road leading to a barn. Post-Knox unconformity is poorly exposed in the fields. Unit numbers in the first column are from this study; numbers in the second column are from Ruppel (1979). Sample code: CS.

Unit #	Unit # Ruppel	Unit Thk(m)	Cumul. Thk(m)	
				KNOX GROUP
				Unconformity
				CHICKAMAUGA GROUP
1	1-2	1.7	1.7	Five Oaks Formation(Blackford Member). Thin bedded, light to medium gray, very fine grained limestone to dolomitic limestone. Birdseye vugs are common.
	1-2			Samples: CS 1 (1.4 m.); CS 2 (0.8 m.)
2	3-19	18.5	20.2	Five Oaks Formation. Thin to medium bedded, light to medium gray, fine to very fine grained limestone to dolomitic limestone. Beds occasionally have internal laminations. Scalloped erosional surfaces and birdseye vugs are present in some beds. Macrofossils limited to molluscan and arthropod debris. Sharp contact with overlying unit.
	3-11			Samples: CS 3 (4.7 m.); CS 4

				(6.0 m.); CS 5 (7.4 m.); CS 6 (8.3 m.).
	12-16			Samples: CS 7 (11.8 m.): CS 8 (12.6 m.).
	17-19			Samples: CS 9 (16.1 m.); CS11 (18.8 m.).
3	20-35	84.2	104.4	Lincolnshire Formation. Thin to thick bedded, gray to white to red, fine to coarse grained limestone. Certain intervals weather to a nodular appearence. Stromatolites (LLH-type) present at the base of the unit. Macrofossils include abundant bryozoan and echinoderm debris, algae, arthropods and molluscs and brachiopods. Gradational contact with the overlying unit.
	20-21			Samples: CS 10 (21.5 m.); CS 12 (24.3 m.); CS 13 (24.9 m.); CS 14 (25.6 m.); CS 15 (29.0 m.).
	22-27			Samples: CS 16 (32.0 m.); CS 17 (36.4 m.); CS 18 (43.1 m.); CS 19 (44.9 m.); CS 20 (51.1 m.); CS 22 (57.3 m.).
	28-35			Samples: CS 23 (59.6 m.); CS 24 (62.3 m.); CS24' (63.5 m.); CS 25 (65.8 m.); CS 26 (64.8 m.); CS 27 (67.1 m.); CS 28 (74.7 m.); CS 29 (78.5 m.); CS 30 (88.3 m.); CS 31 (92.0 m.); CS 32 (94.5 m.); CS 33 (96.4 m.); CS 35 (97.4 m.); CS 36 (102.1 m.).
4	36-44	93.9	198.3	Rockdell Formation. Lower portion consists of light to medium gray, fine to medium grained limestone with abundant clay partings, producing a nodular appearance. The remainder consists of white to brownish gray, medium to coarse grained limestone intermixed with reddish to greenish gray, fine to very fine grained

	limestone. Two lithologies intertongue to form a thick bedded sequence. Macrofossils include abundant ramose and encrusting bryozoans, echinoderms, brachiopods and arthropods. Sharp contact with overlying unit.
36	Samples: CS 37 (104.7 m.); CS 38 (108.4 m.)
37	Samples: CS 39 (110.2 m.)
38-39	Samples: CS 40 (115.3 m.); CS 41 (119.3 m.); CS 42 (124.0 m.); CS 43 (121.2 m.); CS 44 (126.5 m.).
40-41	Samples: CS 45 (135.4 m.); CS 46 (157.8 m.); CS 47 (148.5 m.).
42-44	Samples: CS 48 (155.8 m.); CS 49 (157.8 m.); CS 50 (163.7 m.); CS 51 (162.8 m.); CS 52 (165.3 m.); CS 53 (171.2 m.); CS 54 (176.3 m.); CS 55 (180.9 m.); CS 56 (183.5 m.); CS 57 (192.7 m.); CS 58 (187.5 m.); CS 59 (191.1.m.) CS 60 (195.9 m.); CS 60' (195.9 m.).

Benbolt Formation

Locality N2. Red House Branch Section

Along the east and west banks of Red House Branch which flows northward from Cherokee Lake. Section begins approximately 150 yards up the embayment on the east side and continues on the west bank. Sporadic exposures of the Post-Knox unconformity occur along the east bank. Strata are overturned with dip varying from 30 to 60 degress southeast. Unit numbers in the first column are from this study; numbers in the second column are from Ruppel (1979). Sample code: RHB.

Unit #	Unit # Ruppel	Unit Thk(m)	Cumul. Thk(m)	
				KNOX GROUP
				Unconformity
				CHICKAMAUGA GROUP
1	1	5.2	5.2	Five Oaks Formation. Thick bedded, medium gray, fine to very fine grained limestone to dolomitic limestone. Planar to scalloped erosional surfaces and birdseye vugs present. Sparsely fossiliferous. Sharp contact with overlying unit.
	1			Samples: RHB 1 (1.2 m.); RHB 2 (3.0 m.); RHB 3 (4.8 m.).
2	2	15.0	20.2	'Lenoir Formation'. Medium to thick bedded, dark gray, fine grained limestone. Abundant clay partings/stylolites which preferentially weather out. Abundant macrofossils that include molluscan and arthropod debris, brachiopods and bryozoans. Algae present in the lower portion of the unit. Domal stromatoporoids occur approximately 11 m. above the unconformity. Very sharp contact with the overlying unit.
	2			Samples: RHB 4 (6.6 m.); RHB 5 (9.7 m.); RHB 6 (13.0 m.); RHB 7 (16.3 m.); RHB 8 (17.0 m.).
3	3-8	221.5	241.7	Holston Formation. Thick bedded, red to gray to white, medium to coarse grained limestone with

				patches of brick red, fine to very fine grained limestone and stromatactic limestone in the lower portion of the unit. Medium to coarse grained limestones tend to be cross-bedded and contain abundant echinoderm and bryozoan debris. Fine grained limestones form irregular patches that are intermixed with the other lithotype, and contain abundant encrusting bryozoans and sediment-filled cavities. Gradational contact with the overlying unit.
	3			Samples: RHB 9 (25.7 m.); RHB 10 (30.8 m.); RHB 11 (34.3 m.).
	4			Samples: RHB 12 (39.6 m.); RHB 17 (48.8 m.).
	5			Samples: RHB 18 (53.0 m.); RHB 19 (55.3 m.); RHB 20 (58.5 m.); RHB 21 (61.0 m.); RHB 22 63.2 m.); RHB 23 (74.0 m.); RHB 24 (79.5 m.); RHB 25 (83.3 m.).
	6			Samples: RHB 26 (112.6 m.); RHB 27 (121.0 m.).
	7			Samples: RHB 28 (127.0 m.); RHB 29 (129.0 m.); RHB 30 (129.8 m.).
	8			Samples: RHB 31 142.7 m.); RHB 32 179.8 m.); RHB 33 (181.8 m.); RHB 34 (182.8.m.); RHB 35 (192.0 m.); RHB 36 (198.8 m.).
4	9-10	42.3	284.0	'Rockdell Formation'. Mixture of cream to medium gray, medium to coarse grained limestone and greenish to reddish gray, fine to very fine grained limestone. Two lithologies form a thick bedded sequence. Stromatactis build-ups occur near the top

			of the unit. Echinoderms and bryozoans are the dominant macrofossils in both lithologies. Sharp contact with the overlying unit.
			9 Samples: RHB 37 (247.2 m.); RHB 38 (247.8 m.).
			10 Samples: RHB 39 (258.0 m.); RHB 40 (260.0 m.); RHB 41 (264.0 m.); RHB 42 (270.0 m.); RHB 43 (271.5 m.); RHB 44 (276.0 m.); RHB 45 (279.0 m.); RHB 46 (280.0 m.); RHB 47 (283.0 m.).
			Benbolt Formation

Locality N3. St. Clair Section.

Exposures in the field and abandoned quarry on the southeast side of State Route 66, approximately 0.8 km. northeast of St. Clair. Unit numbers and lithologic descriptions from Ruppel (1979). Sample code: STC.

Unit # Ruppel	Unit Thk(m)	Cumul. Thk(m)	
			KNOX GROUP
			Contact Unexposed
1	6.2	6.2	Lenoir Formation (Mosheim Member). Medium gray, fine to very fine grained limestone. Occasional birdseye vugs present. Sparsely fossiliferous. Samples: STC 2 (0.5 m.); STC 3 (5.8 m.).
2	112.8	119.0	Lenoir Formation ('Main Body'). Dark gray, fine to medium grained argillaceous limestone. Nodular bedded

			as a result of microstylolite swarms/clay partings. Algal oncoids abundant in the lower 40 m. of the unit; other macrofossils include echinoderm debris, brachiopods, arthropods, bryozoans, molluscs and sponges. Biotic diversity and abundance decrease upwards. Sharp contact with the overlying unit. Samples: STC 4 (16.3 m.); STC 5 (22.5 m.); STC 6 (30.6 m.); STC 7 (40.5 m.); STC 8 (45.0 m.); STC 9 (51.0 m.); STC 10 (58.0 m.); STC 11 (66.0 m.); STC 12 (83.0 m.); STC 13 (87.4 m.); STC 14 (99.3 m.); STC 15 (106.4 m.).
3	11.4	130.4	Blockhouse Formation. Dark brownish gray, fissile, unfossiliferous clay shale. No samples.
4	3.0	133.4	Blockhouse Formation (cont'd.). Nodular bedded, dark gray, fine to medium grained fossiliferous limestone. Macrofossils include echinoderm and bryozoan debris. Samples: STC 16 (130.7 m.); STC 17 (132.0 m.).
5			Blockhouse Formation (cont'd.). Clay shale, same as unit 3.

Locality N4. Silver City Section.

Exposures in lea on the south side of unmarked county road, opposite the Post Office at Silver City, approximately 2.5 km. northeast of abandoned Tennessee State Fish Hatchery. Section begins approximately 20 yards south of the county road. Post-Knox unconformity is poorly exposed at this locality. Sample code: SC.

Unit #	Unit Thk(m)	Cumul. Thk(m)	
			KNOX GROUP
			Contact Unexposed
1	20.4	20.4	Lenoir Limestone (Mosheim Member). Thin to thick bedded, medium gray, fine to very fine grained limestone. Birdseye vugs and vertical burrows common. Thin intraclastic layers present near the base. Abundant stylolites and bed-normal calcite veinlets. Sparsely fossiliferous, with macrofossils restricted to molluscan and arthropod debris. Sharp contact with overlying unit. Samples: SC 1 (0.5 m.); SC 2 (3.2 m.); SC 3 (5.9 m.); SC 4 (8.3 m.); SC 5 (12.5 m.); SC 6 (14.1 m.); SC 7 (15.9 m.); SC 8 (18.6 m.); SC 9 (15.2 m.).
2	30.8	51.2	Lenoir Formation ('Main Body'). Nodular bedded, dark gray, fine to medium grained argillaceous limestone. Weathers to a cobbly appearence

			characteristic of this portion of the Lenoir. Planar scour surfaces present in the lower portion of the unit. Abundant algal oncoids present in the lower portion of the unit (Asbury Member?). Macrofossils include molluscs, arthropods, bryozoans, brachiopods and echinoderm debris. Sharp contact with the overlying unit. Samples: SC 10 (21.2.m.); SC 11 (26.5 m.); SC12 (28.4 m.); SC13 (30.3 m.); SC14 (29.0 m.); SC 15 (34.0 m.); SC16 (38.4 m.); SC17 (50.5 m.).
3	107.4	158.6	Whitesburg Formation. Thin bedded, dark gray to black, fine grained limestone intercalated with poorly exposed dark gray to black, graptolitic, calcareous shale. Lower bedding contacts of limestones typically planar although some possess load casts. No visible grading within individual limestone beds. Macrofossils are rare and limited to trilobites, graptolites and inarticulate brachiopods. Sharp contact with the overlying unit. Samples: SC 18 (53.6 m.); SC 19 (59.1 m.); SC 20 (69.2 m.); SC 21 (74.5 m.); SC 22 (82.8 m.); SC 23 (92.0 m.); SC 24 (108.6 m.); SC 25 (114.4 m.); SC 26 (121.9 m.); SC 27 (128.2 m.); SC 28 (137.8 m.); SC 29 (143.3 m.); SC 30 (150.3 m.).
4	5.4	164.0	Blockhouse Formation. Black, fissile, graptolitic clay shale.

			No samples.
5	0.7	164.7	Blockhouse Formation (cont'd.). Single bed of black, fine to coarse grained, fossiliferous limestone which forms a resistant ledge traceable for several tens of meters along strike. Macrofossils include trilobite and molluscan debris, and echinoderms. Samples: SC 31 (164.2 m.); SC 32 (164.5 m.).
6			Blockhouse Formation (cont'd.). Black clay shale, same as Unit 4.

Locality S1. Solway Bridge Section.

Exposures in cementary northwest and pasture southeast of Bethel Valley Road near the intersection of this road with State Route 62, approximately 1 km. northwest of Solway, Tennessee. Section begins on the northwest side of the road. Post-Knox unconformity is unexposed at this locality. Unit numbers in the first column are from this study; numbers in the second column are from Weiss (1981). Lithologic descriptions are from Weiss (1981). Sample code: SB.

Unit #	Unit # Weiss	Unit Thk(m)	Cumul. Thk(m)	
				KNOX GROUP
				Contact Unexposed
				CHICKAMAUGA GROUP
1	1	3.5	3.5	Blackford Formation. Nodular bedded, brownish to dark gray, fine to coarse grained, cherty limestone. Algal oncoids present. Macrofossils include molluscs, bryozoans, arthropod and echinoderm debris. Gradational contact with the overlying unit.
	1			No samples.
2	2-3	35.5	39.0	Blackford Formation (cont'd.). Thin laminated to thin bedded, red to greenish gray, quartzose, dolomitic limestone. Sedimentary structures include mudcracks, burrows and cross-lamination. No visible macrofossils. Contact with the overlying unit is unexposed.
	2-3			Samples: SB 1 (6.2 m.); SB 2 (7.5 m.); SB 3 (17.2 m.); SB 4 (21.7 m.); SB 5 (23.2 m.); SB 6 (27.4 m.); SB 7 (32.9 m.); SB 8 (35.7 m.); SB 9 (37.8 m.).
3	4-5	47.0?	86.0?	Lincolnshire Formation (Eidson Member). Thin to medium bedded, medium to dark gray, fine to coarse grained, cherty limestone. Macrofossils include echinoderm and molluscan debris, and bryozoans. Contact with the overlying unit is unexposed.
	4-5			Samples: SB 10 (66.2 m.); SB 11 (68.0 m.); SB 12 (72.5

				m.).
4	6	31.0?	117.0?	Lincolnshire Formation (Hogskin Member). Wavy to nodular bedded, gray to yellowish brown, fine to coarse grained argillaceous limestone. Numerous shale partings separating limestone beds. Diverse macrofossils that include brachiopods, bryozoans, molluscs, echinoderms and arthropods; algal oncoids also present. Contact with the overlying unit is unexposed.
	6			Samples: SB 13 (94.2 m.).
5	7-9	25.0?	142.0?	Benbolt Formation. Thin to medium to nodular bedded, dark gray to yellowish green, fine to coarse grained, argillaceous limestone with minor shale interbeds. Macrofossils in limestones include brachiopods, molluscs, echinoderms and arthropods; algal oncoids also present. Shales are unfossiliferous.
	7			No samples.
	8			Samples: SB 14 (131.6 m.).
	9			Samples: SB 15 (133.4 m.); SB 16 (135.0 m.).
6	10	13.0?	155.0?	Benbolt Formation (cont'd.). Thin bedded, dark gray, medium to coarse grained limestone. Scattered shale laminae present. Fossils include brachiopods, bryozoans and echinoderm debris.
	10			Samples: SB17 (149.7 m.); SB 18 (150.0 m.).
7	11-13	52.0?	207.0	Benbolt Formation (cont'd.). Laminated to thin bedded, brownish yellow to reddish

			and greenish gray, fine grained, slightly argillaceous limestone and dolomitic limestone. Birdseye vugs, burrow mottling and mudcracks present at certain intervals. No macrofossils visible. Sharp contact with overlying unit.
			11 Samples: SB 19 (161.9 m.); SB 20 (163.7 m.).
			12-13 Samples: SB 21 (186.4 m.); SB 22 (187.7 m.); SB 23 (190.3 m.); SB 24 (197.0 m.); SB 25 (198.5 m.); SB 26 (201.7 m.).
			Wardell Formation.

Locality S2. Martin Mill Pike Section.

Exposures are along and east of Martin Mill Pike, approximately 3.2 km. south of the intersection with John Sevier Hwy. Section begins in lea east of the road, south of the abandoned cabin. Post-Knox unconformity is unexposed. Sample code: MM.

Unit #	Unit Thk(m)	Cumul. Thk(m)	
			KNOX GROUP
			Contact Unexposed
1	25.0	25.0	Lenoir Formation (Mosheim Member). Medium to thick bedded, light to medium gray, fine to very fine grained dolomitic limestone. Birdseye vugs abundant. No visible macrofossils. Sharp contact with the overlying unit.

			Samples: MMa (2.2 m.); MMb (5.7 m.); MMc (11.8 m.); MMd (13.7 m.); MMe (15.5 m.).
2	20.6	45.6	Lenoir Formation ('Main Body'). Thick bedded, dark gray, fine to medium bedded limestone. Algal oncoids abundant in the lower 10 meters. Macrofossils include echinoderm and arthropod debris, and nautiloids. Very sharp contact with the overlying unit. Samples: MM 1' (30.6 m.); MM 2' (32.4 m.); MM 1 (34.0 m.); MM 3' (38.8 m.); MM 2 (39.5 m.); MM 3 (43.3 m.).
3	64.4	110.0	Whitesburg Formation. Thin bedded, black, fine grained limestone intercalated with dark gray calcareous graptolitic shales. Lower contacts of limestone beds are planar; no grading was observed. Bed-normal calcitic veinlets are present in some beds. Macrofossils in shales are restricted to rare graptolites and inarticulate brachiopods. Gradational contact with the overlying unit. Samples: MM 4 (45.9 m.); MM 5 (66.1 m.); MM 6 (78.2 m.); MM 7 (87.8 m.); MM 8 (99.4 m.).
4	24.3	134.3	Lenoir Formation. Generally thin to medium bedded, dark gray, fine grained, sparsely fossiliferous limestone. Shale partings/laminae typically occur between limestone beds, giving the unit an appearance similar to the underlying unit.

			Macrofossils are relatively more abundant than the underlying unit and include arthropods and brachiopods. Gradational contact with the overlying unit. Samples: MM 10 (120.0 m.); MM 11 (132.0 m.); MM 12 (121.5 m.); MM 13 (125.8 m.).
5	52.2	186.5	Lenoir Formation ('Main Body'). Nodular bedded, medium to dark gray, argillaceous limestone. Fossils include brachiopods, arthropod and echinoderm debris; algae are present in the upper portion of the unit. Contact with the overlying unit is unexposed. Samples: MM 14 (134.5 m.); MM 15 (137.0 m.); MM 16 (149.0 m.); MM 17 (162.2 m.); MM 18 (173.0 m.); MM 19 (182.3 m.).
6			Holston Formation. Very thick to thick bedded, white to pinkish, coarse grained, fossiliferous limestone. No samples.

Locality S3. Douglas Lake Section.

Exposures are approximately 1 km. east of the U.S. Highway 25/70 bridge at the east side of parking area for the public boat dock, approximately 2 km. east of Dandridge Tennessee. Sample code: DL.

Unit #	Unit Thk(m)	Cumul. Thk(m)	
			KNOX GROUP
			Unconformity
1	1.7	1.7	Lenoir Formation (Douglas Lake Member). Thin to medium bedded, brown to tan, quartzose sandstone. Vertical and horizontal burrows, and cross-lamination common. No visible macrofossils. Samples: DL 2 (0.5 m.).
2	5.9	7.6	Lenoir Formation ('Main Body'). Thin to thick bedded, medium gray, fine to medium grained limestone. Occasional wispy clay laminations which become more abundant upwards through the unit. Abundant macrofossils that include echinoderm debris, bryozoans, brachiopods and algae. Samples: DL 3 (4.2 m.); DL 4 (5.7 m.); DL 5 (6.0 m.); DL 6 (7.0 m.).
3	15.6	23.2	Lenoir Formation ('Main Body' cont'd.). Nodular bedded, medium gray, fine grained, argillaceous limestone. Rare thin beds of medium grained limestone in the lower portion of the unit. Abundant macrofossils including sponges, brachiopods and echinoderm debris. Samples: DL 7 (9.6 m.); DL 8 12.1 m.); DL 9 (14.5 m.); DL 10 (17.0 m.); DL 11 (17.8 m.); DL 12 (20.9 m.).
4	1.9	25.1	Lenoir Formation ('Main Body' cont'd.). Thin to

			medium bedded, dark gray, fine grained limestone. Less nodular than the underlying unit, although wispy argillaceous laminations are present. Macrofossils include algae, brachiopods, bryozoans and echinoderm debris. Samples: DL 13 (24.9 m.).
5	0.6	25.7	Whitesburg Formation. Black, fissile shale. No samples.
6	2.7	28.4	Whitesburg Formation (cont'd.). Thin to medium bedded, black, fine grained limestone. Metal oxide staining, especially in the upper portion of the unit. Abundant macrofossil debris that includes nautiloid cephalopods. Samples: DL 14 (25.8 m.); DL 15 (26.4 m.).
7	1.0	29.4	Whitesburg Formation (cont'd.). Thin to medium bedded, medium gray to red, medium to coarse grained limestone. Bidirectional cross laminations present in the upper portion. Reddish color corresponds to metal-rich zones that are more resistant than associated limestone. Fossils include echinoderm debris, bryozoans and brachiopods. Samples: DL 16 (28.9 m.); DL 17 (29.3 m.).
8	100+	130+	Whitesburg Formation (cont'd.). Thin bedded, black, fine grained limestone intercalated with dark gray to black, calcareous shale. Faint

parallel laminations are present in flaggy limestone beds. Lower and upper contacts of limestones planar to slightly undulose. No visible macrofossils. Samples: DL 18 (37.9 m.); DL 19 (43.9); DL 20 (46.9 m.); DL 21 (48.4 m.); DL 22 (58.8 m.); DL 23 (65.9 m.); DL 24 (77.8 m.); DL 25 (80.8 m.); DL 26 (82.2 m.); DL 27 (105.8 m.); DL 28 (119.4 m.).

APPENDIX B

PROCEDURE FOR ATOMIC ABSORPTION ANALYSIS OF LIMESTONES, ALLOCHEMS AND MATRIX

Lithologies selected for bulk chemical analysis were sampled by cutting 3 to 4 cubes approximately one centimeter square from representative portions of a slab. Care was taken to avoid sampling areas containing stylolites and bed-normal calcite veinlets. Allochem and matrix separates were obtained by either cutting the desired sub-sample from the rock, or by coring with a stainless steel drill bit mounted in a Jensen vertical milling machine. Samples obtained by cutting were ground on all surfaces to remove surface contamination, washed throughly with deionized water, and dried. Pieces were then crushed in a porcelain mortar and pestle to finer than 60 mesh (<250 microns).

The laboratory procedure is summarized in Figure B.1. A randomly selected portion of the powder was weighed on a Mettler Balance. Initial weights of bulk, 'micro-bulk', allochem and matrix samples are given in Table B.1. Carbonate minerals were brought into solution by adding an appropriate volume of 25% (v/v) glacial acetic acid. Digestion times ranged from 12 to 24 hours at room temperature. After dissolution the mixture was filtered once through a Whatman fine porosity filter paper, and the filtrate collected in a 100 ml volumetric flask. The insoluble residue was washed once with acid, dried and the filter paper re-weighed. The weight of residue was subtracted from the initial weight to determine the weight

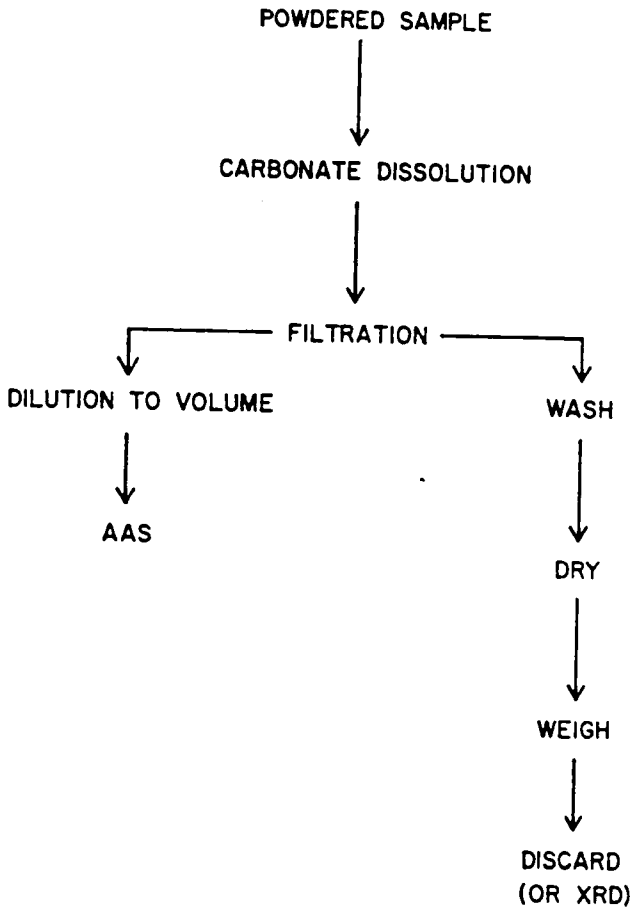


Figure B.1. Simplified flow diagram showing laboratory sample processing scheme.

TABLE B.1

SAMPLE WEIGHTS PRIOR TO ACID DISSOLUTION

Sample Type	Approx. weight of sample
Bulk	1.00 + 0.01 g
Micro-bulk	0.1-0.2 +0.001 g
Allochems, Matrix	0.1 + 0.001 g

of sample in solution. The filtrate solution was precisely brought to volume with 25% (v/v) glacial acetic acid.

The elements Mn, Fe, Na, Zn, and Mg were analyzed on a Varian AA-475 atomic absorption spectrophotometer using an air-acetylene flame, and Sr using a nitrous oxide-acetylene flame; see Cantrell (1982, Table B.2) for a summary of other analytical conditions. All element concentrations were determined using the analytical curve technique. After setting the operating conditions for a given element, absorbances of prepared standard solutions of known concentration were measured and values plotted on an absorbance vs. concentration graph. Each sample solutions was then analyzed, and its concentration determined graphically from the working curve. Absorbance readings were between 0.1 and 0.8 to minimize errors using this method. Actual concentrations for the sample (C) were calculated using the equation:

$$C = cVD/W,$$

where c = measured concentration, V = sample volume (100 ml), D = dilution factor and W = weight of sample in solution. Potassium was added as an ionization buffer to both calibration and unknown solutions for Sr, Na, and Mg determinations; lanthanium was added as a releasing agent to calibration and unknown solutions for Mg determinations.

The accuracy of the analytical procedure, as compared

TABLE B.2

SUMMARY OF TRACE ELEMENT DATA AND METHOD ACCEPTABILITY

Element	Certified Analysis	This Study* Mean(std. dev.)	Total Error
Fe	1923 ppm	1110 (11)	43%-Acceptable
Mn	194 ppm	145 (1)	27%-Acceptable
Na	148 ppm	207 (1)	42%-Acceptable
Sr	245 ppm	285 (6)	17%-Excellent
Mg	2533 ppm	1900 (90)	32%-Acceptable

* Means and standard deviations are for five replicate analyses of the limestone standard.

The accuracy of the analytical procedure, as compared with selected values from N.B.S. 1a (argillaceous limestone) reference standard (SRM #20234), are presented in Table B.2. The total error is defined as (McFarran, et al., 1970)

$$\frac{[\text{True value} - \text{mean of replicate analyses} + 2(\text{std. dev. of replicate analyses})] \times 100}{\text{True value}}$$

Using acceptiblility criteria of McFarren, et al. (1970), the analytical method is acceptable for all elements. However, the error in some instances is relatively high, and for Fe approaches the upper limit of acceptibility (50%). Moss (1981) suggests the large errors are probably an artifact of different sample preparation techniques. Analyses of the N.B.S. standard were done after dissolution with concentrated HCl. Such an acid treatment, in place of acetic acid, would attack the argillaceous (clay) fraction of the sample (Hirst and Nichols, 1958) and add certain elements to the analyte solution.

Results derived from carbonate shelf, ramp and slope facies are listed on the following four pages. Elemental geochemistry of skeletal allochems is given in Table B.3. The mean sample precision in relative percent for elements are: Mn, 3.1; Fe, 3.5; Na, 3.2; Sr, 5.7; Mg, 3.8; Zn, 8.6.

Atomic absorption analyses of bulk rock samples

Sample	Sr	Mn	Fe	Na	Mg	Zn
CS1	204	26	256	51	2950	8
CS2	195	16	276	33	3450	8
CS3	385	39	718	111	15200	5
CS4	178	25	816	50	14200	10
CS5	200	22	500	52	5000	8
CS7	184	109	874	90	7520	6
CS8	176	79	448	29	2500	12
CS9	231	60	430	86	3310	6
CS10	206	241	395	56	3990	9
CS12	309	336	436	65	3180	8
CS13	145	464	625	55	2670	12
CS15	165	800	446	40	2480	12
CS16	138	715	1440	46	4100	13
CS17	215	1100	1090	82	6580	28
CS19	273	676	548	152	3590	16
CS20	185	1080	738	92	3000	12
CS22	198	413	788	61	3170	23
CS24	171	349	923	140	2560	15
CS25	202	929	786	169	4210	5
CS26	223	313	370	154	2300	42
CS27	176	485	915	169	3910	19
CS30	156	143	354	64	2480	12
CS31	159	119	370	85	2780	10
CS32	210	113	389	86	2910	5
CS33	219	114	445	85	3190	5
CS35	194	92	588	155	3030	21
CS36	194	190	724	98	4140	7
CS37	158	140	628	121	4490	8
CS38	488	298	595	110	4960	9
CS40	180	176	1250	112	12100	6
CS41	229	161	982	125	6320	7
CS42	336	140	860	110	5760	7
CS43	174	155	1060	107	4590	7
CS44	376	118	1080	242	4310	9
CS45	197	121	829	109	6550	5
CS49	280	132	508	164	3050	8
CS51	188	190	492	130	3440	9
CS52	206	205	779	142	4290	5
CS53	160	260	780	117	3290	7
CS54	153	195	1250	113	6330	8
CS55	150	204	527	128	3570	5
CS57	217	236	333	148	2560	5
CS58	165	167	463	109	2730	6
CS59	134	244	609	159	2750	6
CS60I	138	285	672	186	2580	10
CS60II	170	324	596	98	2290	5
RHB1	290	41	239	181	4680	8
RHB2	242	39	241	137	3370	5
RHB3	280	31	243	168	4670	5
RHB4	250	73	793	178	41100	4
RHB5	286	57	329	173	13800	5
RHB6	293	52	334	158	10200	7
RHB8	303	92	238	202	4670	7
RHB9	148	111	203	138	1880	5
RHB10	145	98	176	148	1720	5

Sample	Sr	Mn	Fe	Na	Mg	Zn
RHB12	240	356	619	158	2770	9
RHB17	187	327	202	206	2320	6
RHB18	152	168	304	186	1850	6
RHB19	222	158	392	217	2550	4
RHB21	149	225	383	309	2160	4
RHB22	164	163	495	205	1960	7
RHB23	164	336	1030	183	7290	6
RHB24	185	160	322	194	2570	7
RHB25	161	232	526	174	3220	6
RHB27	165	162	389	183	1760	6
RHB28	207	296	398	241	2830	19
RHB29	171	248	366	146	2200	6
RHB30	134	252	405	176	2030	5
RHB31	146	140	1400	189	5290	5
RHB32	125	99	510	218	2320	9
RHB33	144	67	332	202	2330	5
RHB34	149	123	1060	202	2940	7
RHB35	127	103	1040	160	3030	6
RHB36	146	122	1240	180	5490	5
RHB37	125	117	436	140	1840	4
RHB39	157	183	919	159	1580	5
RHB40	167	153	545	240	1750	4
RHB41	187	193	1110	232	1950	7
RHB42	201	162	480	351	2690	11
RHB43	190	155	440	180	2320	4
RHB45	194	122	308	259	2090	5
RHB46	211	153	414	163	2210	4
RHB47	175	204	552	244	1670	4
STC2	523	47	491	165	11500	0
STC3	763	87	318	0	6130	0
STC4	753	49	237	0	5670	0
STC5	800	102	483	0	3660	0
STC6	787	109	525	0	3930	0
STC7	599	113	793	0	4320	0
STC8	618	113	916	0	5500	0
STC9	592	104	953	0	5660	0
STC10	934	182	1740	141	3330	0
STC11	1000	332	2690	0	2890	0
STC12	1110	373	2070	0	3240	0
STC13	1050	251	1990	0	2730	0
STC14	857	309	1740	0	0	0
STC15	1180	303	1320	0	3350	0
STC16	1060	8	1660	174	4520	0
STC17	1280	785	2990	126	3740	0
SC1	240	64	565	92	9460	6
SC2	228	38	588	121	6300	6
SC4	299	36	600	91	7030	7
SC5	240	45	527	94	5090	6
SC7	279	53	435	103	5860	5
SC9	382	71	791	69	6110	5
SC10	334	161	718	142	8450	7
SC11	360	149	610	131	5150	7
SC14	339	230	552	181	4420	7
SC15	363	555	1200	137	3540	10
SC16	369	876	2940	260	2990	10
SC17	413	720	6370	141	6890	16

Sample	Sr	Mn	Fe	Na	Mg	Zn
SC18	583	164	833	96	2240	11
SC19	743	257	1150	111	2780	16
SC20	722	233	1180	114	2700	7
SC22	591	260	1210	116	3400	8
SC23	627	269	1030	133	2760	13
SC24	906	549	1640	124	2690	22
SC26	878	737	1607	134	2680	8
SC27	957	997	1960	124	3220	11
SC29	836	859	5300	139	3010	9
SC30	504	721	866	112	3690	8
SC31	455	325	1450	220	5040	9
SC32	488	331	1340	109	3410	10
SB2	302	497	630	317	2960	25
SB3	365	484	702	435	2590	29
SB4	404	525	635	329	3230	15
SB5	462	524	671	322	3440	11
SB6	553	550	707	328	3610	14
SB7	367	532	623	439	3440	11
SB8	304	694	700	234	3130	8
SB9	334	442	848	307	3090	13
SB10	629	200	1210	111	3510	30
SB11	569	107	422	97	4630	5
SB12	470	102	500	111	6040	5
SB13	442	286	667	123	3720	17
SB14	561	330	1380	131	4230	9
SB15	612	273	1060	103	4240	9
SB16	852	362	2070	90	4530	8
SB17	330	267	1010	125	3620	8
SB18	423	304	1140	154	4460	9
SB19	469	423	3110	128	7360	7
SB20	349	464	2080	172	4490	32
SB21	322	294	1810	185	3940	14
SB22	348	180	1190	121	4040	7
SB23	338	276	1350	152	4820	6
SB24	296	168	966	151	6110	6
SB25	297	248	1480	84	5340	4
SB26	427	483	1340	179	3610	10
MMA	216	49	490	194	6720	13
MMB	184	53	752	83	12500	6
MMD	202	59	1040	147	16300	7
MME	230	52	718	101	10300	6
MM1'	411	1240	4600	158	4530	6
MM2'	475	1340	6770	152	4530	9
MM1	385	1750	6880	203	10070	5
MM3'	479	1050	7890	171	7980	7
MM2	487	1210	8760	228	8200	7
MM3	320	264	5980	246	5980	8
MM4	395	165	689	411	3590	3
MM5	711	166	1390	180	3630	7
MM6	1030	202	887	242	5930	5
MM7	921	237	1090	267	4770	9
MM8	909	271	2130	241	18500	10
MM10	662	410	1640	211	3610	13
MM11	1220	458	2910	275	3820	9
MM12	1730	454	2760	264	7390	9
MM15	615	556	1710	247	3940	7
MM16	610	671	3030	252	8230	10
MM18	863	559	2480	248	4040	7

Sample	Sr	Mn	Fe	Na	Mg	Zn
DL1	441	51	150	33	1550	12
DL3	369	188	229	100	3930	7
DL4	375	236	528	95	4170	20
DL5	356	286	404	101	4140	6
DL6	446	226	306	104	4740	6
DL7	480	231	241	104	3790	6
DL8	510	231	309	121	4970	10
DL9	561	338	500	102	3940	8
DL10	390	395	670	80	4880	9
DL11	396	410	650	76	3800	5
DL12	400	658	1640	79	4430	5
DL13	525	1120	4500	103	4080	4
DL14	645	1160	13300	160	6080	6
DL15	673	1570	14200	192	5290	9
DL16	650	621	31900	95	8960	7
DL17	528	560	11200	94	5480	9
DL18	570	240	2700	67	2700	5
DL19	583	276	2810	110	2280	6
DL20	528	185	1810	90	2310	8
DL22	525	180	2040	92	2050	7
DL23	582	156	1740	99	2440	8
DL24	662	219	2170	85	2350	8
DL25	490	176	1830	85	2190	7
DL26	630	223	2230	102	2430	6
DL27	568	185	1680	97	2220	7
DL28	575	213	1780	95	2320	6

TABLE B.3

TRACE ELEMENT COMPOSITION OF ORDOVICIAN SKELETAL ALLOCHEMS

Skeletal Allochem	wt% Mg	ppm Sr	ppm Mn
Girvanella oncoid	0.215	148	63
	0.151	114	50
	0.191	139	59
Solenopora	0.124	148	40
	0.190	196	160
	0.140	113	777
Bryozoa			
A. preserved fabric	0.206	155	553
	-	148	254
	0.205	140	296
	0.185	181	294
	0.193	196	215
	0.215	158	679
	0.226	150	520
	0.257	195	819
B. replacement-cement mosaic	-	217	144
	0.273	175	254
	0.158	147	162
	0.136	140	154
	0.300	149	173
	0.152	139	139
	0.246	129	124
	0.168	109	733
	0.249	163	524
	0.238	148	246
	0.283	164	247
Echinoderm	0.219	119	48
	0.277	176	74
	0.208*	149*	69*

* = composite sample.

APPENDIX C

DERIVATION OF STRONTIUM AND MAGNESIUM CONCENTRATIONS FOR LIME MUDS AND THEIR LITHIFICATION PRODUCTS

Micrite

Since the original lime muds resulted from the breakdown of skeletal particles, the initial step is to identify as nearly as possible all potential mud-contributing organisms. Petrographic analysis of over 200 samples from shelf facies revealed the following preserved biota:

Calcite -- echinoderms, bryozoans, arthropods, rhodophyte algae, chlorophyte algae (codiaceans), articulate brachiopods, Nuia.

Aragonite -- chlorophyte algae (dasyclads), nicholsonellid bryozoans, molluscs.

Other organisms not preserved as allochems may have also contributed particles to this sediment fraction in addition to those listed above. This bias introduces some uncertainty in the subsequent analysis; however, its significance on the trends produced can only be accessed by studies of modern shallow-water environments.

Determination of mud geochemistry is a two-step process: (1)approximate the proportion of each biotic group to its respective end member; (2)calculate the whole-sediment composition based on the contribution and biogeochemistry of each group. Bryozoans and echinoderms

were the dominant calcite-secreting organisms. Calcareous algae, brachiopods and arthropods were subordinate in subtidal shelf facies during Chickamauga deposition (see Ruppel and Walker, 1984). The element composition of the calcite precursor was calculated assuming the following relative proportions:

echinoderms : bryozoans : arthropods : chlorophytes: rhodophytes : brachiopods 30 : 30 : 15 : 10 : 15 : 0.

Thus, the calcite-precursor trend actually represents the probable element composition of an original mud consisting of 100% magnesian calcite. Aragonite-secreting organisms were minor contributors to shelf sediments. Since molluscs are not major lime-mud producers on modern carbonate platforms, aragonitic muds would only contain algal and bryozoan components. For simplicity, we will assume these muds would have contained both groups in a 1 : 1 ratio.

Strontium, magnesium and calcium concentrations of extant, warm-water species from each taxon (excluding Nuia) are listed in Table C.1. The composition of codiacean algae is based on equilibrium precipitation of calcite from modern sea water, because analyses of living species could not be found. These values are probably comparable with Ordovician chlorophytes due to their passive mode of calcification.

TABLE C.1

MINERALOGY AND ELEMENTAL COMPOSITION OF MUD-CONTRIBUTING MARINE ORGANISMS

Taxon	wt%Ca	wt%Mg	ppm Sr	Mineralogy
Green Algae	40.0	0.10	8800	Aragonite
	34.0	7.60	1000	Calcite
Red Algae	31.6	4.10	2800	Calcite
Bryozoans	39.2	0.25	8500	Aragonite
	36.1	2.50	2200	Calcite
Arthropods	38.7	1.20	4200	Calcite
Echinoderms	34.5	3.00	2400	Calcite

Concentrations for codiacean green algae discussed in text. Mg concentrations from Veizer (1984), except for arthropods which is from Cadot et al. (1972). Ca concentrations are from Milliman (1974); Sr concentrations from Veizer (1984).

The arthropod component is dominated by trilobites which precipitated magnesian calcite cuticles. Magnesium concentrations for this group correspond to magnesium-rich portions of tropical marine ostracodes analyzed by Cadot, et al. (1972); strontium and calcium concentrations are representative of living marine ostracodes. Using these data, concentrations for calcite and aragonite end-member muds are given below.

Calcite-dominated:	35.7 wt. % Ca
	3.20 wt. % Mg
	2530 ppm Sr.
Aragonite-dominated:	36.6 wt. % Ca
	.175 wt. % Mg
	8650 ppm Sr

Mud lithification, like the stabilization of allochems, is typically accomplished in a system characterized by a low solute index. During shallow meteoric diagenesis, the bulk of the Sr, Mg and Ca ions within pore fluids at the reaction sites are derived from the equilibrating metastable phase. Using the Berthelot-Nernst distribution law and rearranging terms, we obtain the relation

$$(m_T/m_{Ca})_{cal} = K^{T}_{cal} \times (m_T/m_{Ca})_{soln}$$

Assuming the concentration of major and trace elements in reaction zones adjacent to diagenetic calcites are largely

governed by the precursor mineral phase, the ratio (m_T/m_{Ca}) is equal to $(m_T/m_{Ca})_{calcite}$ [or $(m_T/m_{Ca})_{aragon.}$]. Based on this characterization of the diagenetic system, the above relation may be expressed as

$$ppm\ T_{cal} = K^T_{cal} \times ppm\ T_{mud} \times ppm\ Ca_{cal} / ppm\ Ca_{mud}$$

where:

T_{cal} = Sr, Mg conc. in diagenetic calcite

T_{mud} = Sr, Mg conc. in original mud

Ca_{cal}/Ca_{mud} = Ca ratio, sediment and diagenetic calcite

Assuming Ca_{cal} = 38.0 wt. %, and 0.05 and 0.06 for the partition coefficients for Sr and Mg, respectively, the final concentrations after meteoric diagenesis are given below.

CALCITE: Mg = .06 x 32,000 x 380,000/357,000
= 2040 ppm.

Sr = .05 x 2530 x 380,000/357,000
= 135 ppm.

ARAGONITE: Mg = .06 x 1750 x 380,000/366,000
= 109 ppm.

Sr = .05 x 8650 x 380,000/366,000
= 449 ppm.

Calcisiltite.

Evaluation of sediment-producing biota, together with sedimentologic and diagenetic processes suggests that slope calcisiltites resulted from the trituration of echinoderm debris. Whereas contributions from several groups had to be considered in generating the equilibration trends for micrites, a single higher taxon appears to have formed the silt-sized sediments, thus simplifying the process. Mean concentrations of cations in extant echinoderms are: Ca, 34.5 wt. %; Mg, 3.28 wt. %; Sr, 2200 ppm. Using the previous equations together with the same assumptions concerning the magnitude of the partition coefficient and Ca concentration in diagenetic calcite, trace element concentrations after meteoric diagenesis are given below.

$$Mg = .06 \times 32{,}800 \times 380{,}000/345{,}000$$
$$= 2170 \text{ ppm.}$$

$$Sr = .05 \times 2200 \times 380{,}000/345{,}000$$
$$= 121 \text{ ppm.}$$

APPENDIX D

X-RAY DIFFRACTION ANALYSIS OF SHALES

Calcareous shales from the Whitesburg Formation at the Martin Mill Pike and Douglas Lake sections were sampled for x-ray diffraction analysis. Approximately 10-15 grams of unweathered sample was ground to less than 50 mesh using a porcelain mortar and pestle. The carbonate fraction was removed from all samples (except DL-S3) using the technique of Jackson (1969): 30 minute treatments with a buffered sodium acetate-acetic acid solution at 60 degrees C. There was no evidence of carbonate reaction after three treatments. The remaining fraction was washed and centrifuged, then dried at 75 degrees C for approximately 5 hours. Six to eight grams of either the acid-treated or untreated sample was suspended in 1000 ml of deionized water. After successive settling intervals, the <5 micrometer size fraction was pipetted into a beaker and allowed to settle. At least one elutriated slide was prepared from this size fraction for XRD analysis. Samples were analyzed on a Norelco diffractometer using filtered CuK radiation. Samples were run untreated, solvated with ethylene glycol, and heated for one hour at 550 degrees C. A portion of the <5 m fraction of DL-S1 was saturated with 1 N KCl to identify mixed-layer chlorite minerals.

Table D.1 lists the interpreted mineralogy for each sample. A "-" separating two minerals represents a mixed-layer species.

TABLE D.1

SUMMARY OF MINERALOGICAL DATA ON SEVIER BASIN SHALES

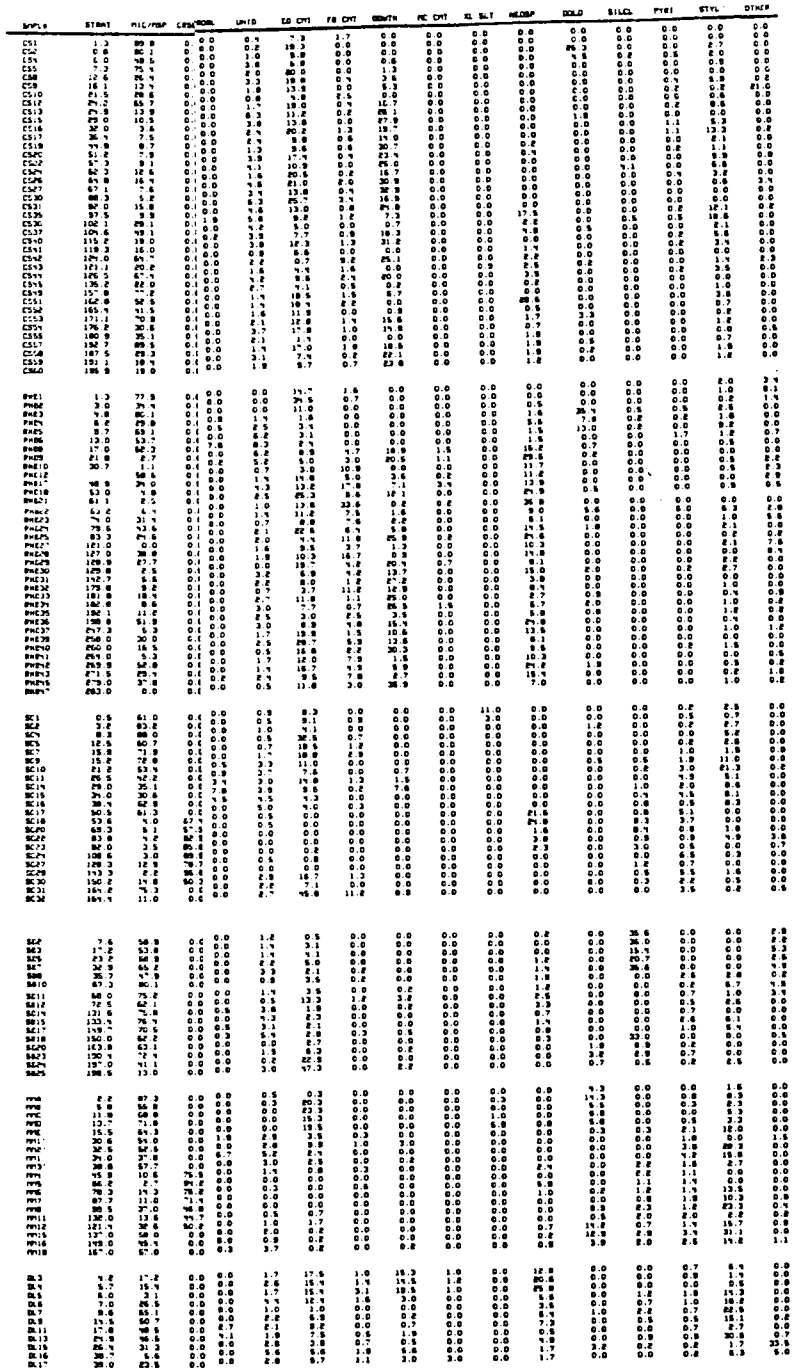
Sample	Mineralogy
DL-S1	Chlorite-Smectite, Illite, Quartz
DL-S2	Chlorite-Smectite, Illite, Quartz, Feldspar
DL-S3	Chlorite, Illite, Kaolinite, Quartz Calcite
MM-S1	Illite-Smectite, Illite, Kaolinite, Quartz, Feldspar
MM-S2	Illite-Smectite, Illite, Quartz
MM-S3	Illite-Smectite, Illite, Kaolinite, Quartz, Feldspar
MM-S4	Chlorite-Smectite, Illite, Kaolinite, Quartz, Feldspar

APPENDIX E

CONSTITUENT PARTICLE ANALYSIS

Volume percentages of depositional and diagenetic constituents obtained by point count analysis are given in the following data.

Volume pei diagenetic constituents



APPENDIX F

INTERPRETED ORIGINAL SEDIMENT MINERALOGY

The inferred primary bulk sediment mineralogies (excluding synsedimentary cements) for shelf/ramp and slope carbonate facies are given in the following data. Based on thin section petrography, all skeletal allochems were monomineralic and composed of the polymorph given in Table 3.5. (Since no distinction was made between originally calcite and Mg-calcite ostracode carapaces during constituent analysis, 50% were assumed to have been calcite and 50% Mg-calcite.) Micrite, microspar neomorphic after micrite and micrite-composed allochems (pellets, intraclasts) were assumed to have the following mineralogy: 80% Mg-calcite, 10% calcite, 10% aragonite. Peloids resulting from the micritization of skeletal grains were assumed to have been originally magnesian calcite.

Interpreted original mineralogy of Middle Ordovician limestones

SHELF MARGIN SUBTIDAL

Sample	Mg Cal	Arag	Cal
RHB12	77	15	8
RHB17	83	11	6
RHB18	90	9	1
RHB21	90	9	1
RHB22	83	12	5
RHB23	84	8	8
RHB24	85	9	6
RHB25	88	7	5
RHB27	87	13	0
RHB28	86	8	6
RHB30	98	1	1
RHB31	88	11	1
RHB32	96	2	2
RHB33	93	3	4
RHB34	88	10	2
RHB35	92	6	2
RHB36	85	8	7
RHB37	97	2	1
RHB39	86	8	6
RHB40	85	11	4
RHB41	95	4	1
RHB42	82	11	7
RHB43	84	8	8
RHB45	87	7	6
RHB47	98	0	2

SLOPE/BASIN

Sample	Mg Cal	Arag	Cal
SC18	100	0	0
SC20	98	1	1
SC22	100	0	0
SC23	100	0	0
SC24	100	0	0
SC27	98	1	1
SC29	100	0	0
SC30	93	2	5
SC31	80	13	7
MM4	98	1	1
MM5	100	0	0
MM6	98	1	1
MM7	98	1	1
MM8	92	4	4

TIDAL FLAT

Sample	Mg Cal	Arag	Cal
CS1	80	10	10
CS2	80	10	10
CS4	80	10	10
CS5	80	10	10
CS8	86	7	7
CS9	87	6	7
RHB1	80	10	10
RHB2	80	10	10
RHB3	80	10	10
SC1	80	10	10
SC2	80	10	10
SC4	80	10	10
SC5	80	10	10
SC7	80	10	10
SC9	80	10	10
SB23	80	10	10
SB24	80	10	10
SB25	78	10	12
MMa	79	11	10
MMb	80	10	10
MMc	80	10	10
MMd	80	10	10
MMe	80	10	10

SHELF SUBTIDAL

Sample	Mg Cal	Arag	Cal
CS10	91	4	5
CS13	91	5	4
CS15	94	2	4
CS16	96	3	1
CS17	93	4	3
CS19	97	1	2
CS20	97	1	2
CS22	91	7	2
CS24	95	2	3
CS26	88	6	6
CS27	90	2	8
CS30	95	4	1
CS31	94	3	3
CS35	92	5	3
CS37	85	7	8
CS41	90	6	4
CS42	83	10	7
CS43	90	6	4
CS44	84	8	8
CS45	92	4	4
CS49	81	10	9
CS51	83	9	8
CS53	82	9	9
CS54	89	5	6
CS55	87	6	7
CS57	79	10	11
CS58	89	5	6
CS59	93	3	4
CS60	88	7	5
RHB4	79	13	8
RHB6	82	9	9
RHB8	82	9	9
SC10	84	7	9
SC11	85	7	8
SC14	90	5	5
SC15	89	5	6
SC16	84	8	8
SB10	81	9	10
SB11	80	11	9
SB12	82	9	9
SB14	81	9	10
SB15	81	9	10
SB17	82	9	9
MM15	78	9	13
MM16	82	9	9
MM18	83	8	9
DL3	84	7	9
DL4	92	4	4
DL5	85	5	10
DL6	83	6	11
DL7	81	9	10
DL9	80	10	10
DL11	83	8	9
DL13	86	7	7

VITA

Robert Eric Johnson was born in Pittsburgh, Pennsylvania on January 27, 1959. He attended secondary school in the Washington D.C. area and graduated from Gaithersburg High School in June 1977. The following September he matriculated at Montgomery College, but after one year was tired of Maryland and transferred to Rutgers College (New Jersey) where he received a Bachelor of Arts degree in Geology in 1981. In the Fall of 1981 he accepted a teaching assistantship at The University of Tennessee, Knoxville and began studies toward a Master's degree. During his first year, the faculty offered him the opportunity to by-pass the Master's degree and enter the doctoral program at the University of Tennessee, Knoxville. He was awarded his PhD. in March 1987.

The author is a member of Sigma Xi, the Society of Economic Paleontologists and Mineralogists, and Geological Society of America. Mr. Johnson is presently seeking gameful employment in America's capitalistic economic system.